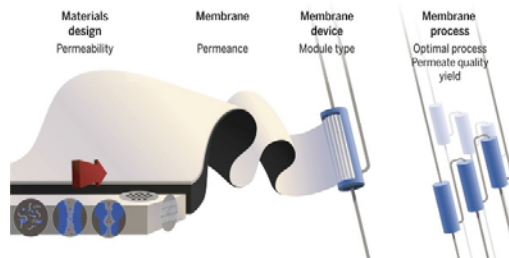
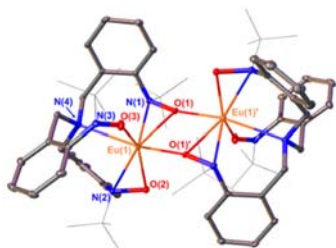


Representative 3D trajectory of a bovine serum albumin molecule near a modified fused silica surface

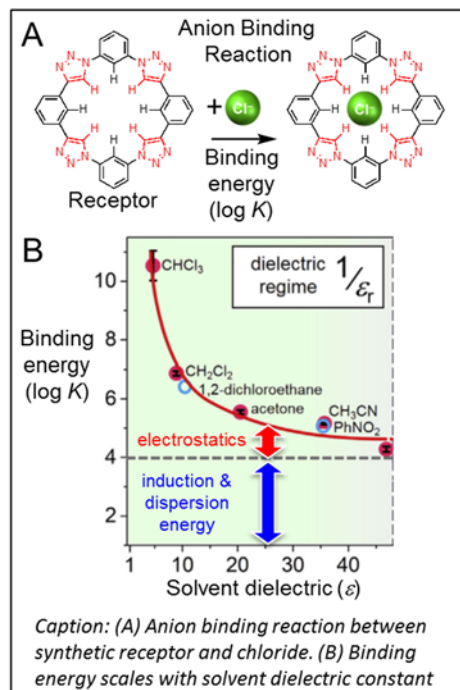
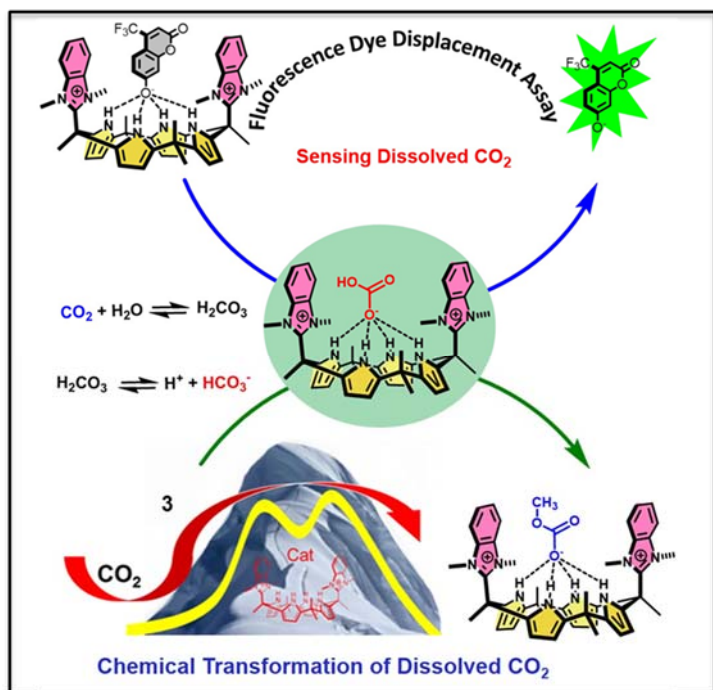


U.S. DEPARTMENT OF  
**ENERGY**

Office of  
Science



**2018 Separation Science PI Meeting**  
Gaithersburg Marriot Washingtonian Center  
Gaithersburg, MD  
February 6-7, 2018



Caption: (A) Anion binding reaction between synthetic receptor and chloride. (B) Binding energy scales with solvent dielectric constant

Program and Abstracts for the

# 2018 BES/Separation Science Research PI Meeting



U.S. DEPARTMENT OF  
**ENERGY**

Office of  
Science

Gaithersburg Marriott Washingtonian Center  
Gaithersburg, Maryland  
February 6-7, 2018

The research grants and contracts described in this document are supported by the U.S. Department of Energy, Office of Science/Basic Energy Sciences, as part of the Separation Science Program within the Chemical Sciences, Geosciences and Biosciences Division.

## FOREWORD

This abstract booklet provides a record of the 2018 U.S. Department of Energy (DOE) contractors' meeting in Separation Science. This meeting, held at the Marriott Washingtonian Hotel in Gaithersburg, Maryland on February 6-7, 2018, is sponsored by the Chemical Sciences, Geosciences and Biosciences Division of the Office of Basic Energy Sciences (BES). The objective of this meeting is to provide a fruitful environment in which principal investigators (PIs) within the BES/Separation Science (SEP) Program will present and exchange information about their current research activities, will build collaborations among research groups with mutually reinforcing strengths, will identify current needs of the research community, and will focus on opportunities for future research directions. The agenda has an invited plenary talk from Prof. David Scholl, Georgia Institute of Technology, oral presentations by a number of the PIs, as well as an evening poster session. In this way, all PIs within the BES/SEP Program will present their most recent work funded by the program. With ample time for discussion and interactions, we emphasize that this is an informal meeting for exchange of information and building of collaborations; it is not a review of researchers' achievements or a forum to specifically choose future directions for the program.

We appreciate the privilege of serving as the managers of this research program within DOE/BES. The best part of this job is learning about the PIs' achievements, and sharing in the excitement of the research of the many sponsored scientists and students whose names appear on the scientific papers listed in the following pages. We hope that this meeting will enhance your research efforts and will nurture future collaborations and initiatives.

We thank all of the PIs whose dedication and innovation have advanced separation science research, and made this meeting possible and productive. We also hope that all of the PIs will build on their successes that we can then discuss when we assemble for our next PI meeting.

Finally, we thank Diane Marceau of the BES/Chemical Sciences, Geosciences and Biosciences Division, and Connie Lansdon of the Oak Ridge Institute for Science and Education for their important contributions to the technical and logistical features of this meeting.

Philip Wilk and Chuck Peden, Program Managers  
Separation Science Program - Office of Basic Energy Sciences - U.S. Department of Energy

# 2018 Separation Science PI Meeting

February 6-7, 2018

Marriott Washingtonian, Gaithersburg, MD

## Monday Afternoon, February 5

2:00 – 5:00 p.m. **Registration**

## Tuesday Morning, February 6

7:30-8:30 a.m. **Breakfast**

### **OPENING SESSION**

Session Chairs: **Philip Wilk and Charles Peden**

8:30-8:50 am Welcoming remarks  
**Philip Wilk and Charles Peden**, DOE/BES/Separation Science Program

8:50-9:10 am BES Update  
**Bruce Garrett**, Director, DOE/BES/Chemical Sciences, Geosciences and Biosciences Division

### **PLENARY SESSION I**

Session Chair: **TBD**

9:10-10:00 am Expanding the Chemical Palette for Adsorption-Base Separations  
**David Sholl**, Georgia Institute of Technology

10:10-10:20 am **Coffee Break**

### **PI SESSION I**

Session Chair: **TBD**

10:20-10:50 am Title: Binding Anions Selectively with Modular Receptors, and Releasing them with Light  
**Presenter – Amar Flood**, Indiana University

10:50-11:20 am Title: “Modular Approaches to Contemporary Complexants for Separations”  
**Presenter – Jesse Carrick**, Tennessee Technological University

11:20am-11:50pm Title: “Lattice Dynamics of Flexible Framework Structures: Insights from Inelastic Neutron Scattering (INS)”  
**Presenter – Nancy Ross**, Virginia Polytechnic Institute and State University

11:50-1:30 pm **Working Lunch**

**Tuesday Afternoon, February 6**

**PI SESSION II**

Session Chair: **TBD**

1:30-2:00 pm Title: “Multiscale Simulation of Acidic Solutions in Complex Environments, and their Implications for Understanding Transport and Separations”  
**Presenter – Gregory Voth**, University of Chicago

2:00-2:30 pm Title: “The Role of Inner- and Outer-Sphere Interactions in the Selective Extraction of Metal Ions”  
**Presenter – Vyacheslav Bryantsev**, Oak Ridge National Laboratory

2:30-3:00 pm Title: “The Interfacial Chemistry of Solvent Extraction: Predictive Insight into Mechanisms and Kinetic Regimes for Actinide Separations”  
**Presenter – Aurora Clark**, Washington State University

3:00-3:20 pm **Coffee Break**

**PI SESSION III**

Session Chair: **TBD**

3:20-3:50 pm Title: “Hierarchically Functional Iptycene-containing Polymers for Advanced Membrane Applications”  
**Presenter – Ruilan Guo**, Notre Dame University

3:50-4:20 pm Title: “Coordination-Chemistry-Derived Materials Featuring Nanoscale Porosity and Selective Chemical Separation”  
**Presenter – Joseph Hupp**, Northwestern University

4:20-4:50 pm Title: “Porous Liquids: Emerging Media for Gas Separation and Storage”  
**Presenter – Sheng Dai**, Oak Ridge National Laboratory

4:50-7:00 pm            **Dinner (on your own)**

**Tuesday Evening, February 6**

7:00-8:30 pm            **Poster Session**

**Wednesday Morning, February 7**

7:30-8:30 am            **Breakfast**

**PI Session IV**  
Session Chair: **TBD**

8:30-9:00 pm            Title: “Molecular-Level Investigation of Diffusion Behaviors within  
Cylindrical Nanoscale Pores”  
**Presenter – Takashi Ito**, Kansas State University

9:00-9:30 pm            Title: “Single-Molecule Resolution of Surface Interactions and  
Dynamics”  
**Presenter – Daniel Schwartz**, University of Colorado

9:30-10:00 pm            Title: “Microscopy Methods for Investigating Separation Processes within  
Porous Particles”  
**Presenter – Joel Harris**, University of Utah

10:00-10:20 am            **Coffee Break**

**PI SESSION V**  
Session Chair: **TBD**

10:20-10:50 am            Title: “Combined Capture and Conversion of CO<sub>2</sub>”  
**Presenter – David Heldebrant**, Pacific Northwest National Laboratory

10:50-11:20 am            Title: “Highly Selective Ion Transport through Ion-Exchange Membranes  
Coated with Polyelectrolyte Multilayers”  
**Presenter – Merlin Bruening**, Notre Dame University

11:20-11:50 am            Title: “Exploiting Insertion Processes for Continuous Membrane-Free Ion  
Separations”  
**Presenter – Richard Crooks**, University of Texas

11:50-1:10 pm      **Working Lunch**

**Wednesday Afternoon, February 7**

**PI SESSION VI**  
Session Chair: **TBD**

1:10-1:40 pm      Title: “Tailoring High Performance Carbon Molecular Sieve Membranes for Energy Intensive Separations”  
**Presenter – William Koros**, Georgia Institute of Technology

1:40-2:10 pm      Title: “pKa Dependent Facilitated Transport of CO<sub>2</sub> across Hyperthin Polyelectrolyte Multilayers”  
**Presenter – Steven Regen**, Lehigh University

2:10-2:40 pm      Title: “Design and Study of Hybrid Polyimide-Ionene Architectures for Membrane Separations”  
**Presenter – Jason Bara**, University of Alabama

2:40-3:00 pm      Closing Remarks  
**Wilk, Peden**

3:00 pm              **Adjourn**

## Poster Session – Tuesday, February 6, 2018

Jared Anderson, AMES  
Georges Belfort, RPI  
Paul Bohn, Notre Dame  
Jeff Davis, Univ. Maryland  
Vanda Glezakou, PNNL  
Santa Jansone-Popova, ORNL  
De-en Jiang, UC Riverside  
Grant Johnson, PNNL  
Brian Long, Univ. Tennessee  
Bruce Moyer, ORNL  
Alexandra Navrotsky, UC Davis  
Eric Schelter, Univ. Pennsylvania  
Mark Schlossman, Univ. Illinois, Chicago  
Jonathan Sessler, Univ. Texas  
Emily Smith, AMES  
Brian Woodfield, BYU  
Alla Zelenyuk, PNNL

# TABLE OF CONTENTS

TITLE PAGE .....	i
FOREWORD .....	ii
AGENDA .....	iii
TABLE OF CONTENTS .....	viii
ABSTRACTS .....	1
<b><u>Plenary Session Abstract</u></b>	
<i>Computational Separation Science</i>	
David Scholl (Georgia Institute of Technology) .....	3
<b><u>Principal Investigator Abstracts</u></b>	
<b><u>Oral Sessions</u></b>	
<i>Binding Anions Selectively with Modular Receptors and Releasing them with Light</i>	
Amar H. Flood (Indiana University).....	5
<i>Modular Approaches to Contemporary Complexants for Separations</i>	
Jesse D. Carrick (University of Alabama) .....	8
<i>Lattice Dynamics of Flexible Framework Structures: Insights from Inelastic Neutron Scattering (INS)</i>	
Nancy L. Ross (Virginia Tech) .....	10
<i>Proton Solvation and Transport in Acidic Solutions and Complex Materials</i>	
Gregory A. Voth (University of Chicago).....	14
<i>Understanding Liquid:Liquid Interfacial Structure in Non-Ideal Systems</i>	
Aurora E. Clark (Washington State University).....	18
<i>The Role of Inner- and Outer-Sphere Interactions in the Selective Extraction of Metal Ions</i>	
Vyacheslav S. Bryantsev (Oak Ridge National Laboratory).....	22
<i>Hierarchically Functional Iptycene-containing Polymers for Advanced Membrane Applications</i>	
Ruilan Guo (University of Notre Dame) .....	30
<i>Coordination-Chemistry-Derived Materials Featuring Nanoscale Porosity and Selective Chemical Separation</i>	
Joseph T. Hupp (Northwestern University) .....	36
<i>Fundamental Studies of Novel Separations</i>	
Sheng Dai (Oak Ridge National Laboratory) .....	37
<i>Diffusion and Partitioning Behavior of Fluorescent Single Molecules within Surfactant-Filled Cylindrical Silica Nanopores</i>	
Takashi Ito (Kansas State University).....	40

<i>Single-Molecule Resolution of Surface Interactions and Dynamics</i> Daniel K. Schwartz (University of Colorado).....	45
<i>Microscopy Methods for Investigating Separation Processes within Porous Particles</i> Joel M. Harris (University of Utah) .....	49
<i>Understanding Reactive Separations of CO<sub>2</sub></i> David J. Heldebrant (Pacific Northwest National Laboratory).....	53
<i>Electrically Driven Ion Separations in Permeable Membranes</i> Merlin L. Bruening (University of Notre Dame).....	59
<i>Exploiting Insertion Processes for Continuous Membrane-free Ion Separations</i> Richard M. Crooks (University of Texas, Austin).....	64
<i>Tailoring High Performance Carbon Molecular Sieve Membranes for Energy Intensive Separations</i> William J. Koros (Georgia Institute of Technology) .....	68
<i>Influence of Pendant Group Basicity on the Facilitated Transport of CO<sub>2</sub> across Hyperthin Polyelectrolyte Multilayers</i> Steven L. Regen (Lehigh University) .....	73
<i>Design and Study of Hybrid Polyimide-Ionene Architectures for Membrane Separations</i> Jason E. Bara (University of Alabama) .....	77
<b><u>Poster Session</u></b>	
<i>Elucidating the Role of Spatial and Chemical Inhomogeneity in Separations Processes</i> Jared Anderson (AMES Laboratory).....	82
<i>ARGET ATRP Grafting on Membranes: Predictive Tool and Characterization</i> Georges Belfort (Rensselaer Polytechnic Institute).....	84
<i>Nanoscale Coupling of Transport and Chemical Reactivity</i> Paul W. Bohn (University of Notre Dame).....	88
<i>Self-Assembled Ionophores in Water: Supramolecular Hydrogels and Membrane Transporters</i> Jeffrey T. Davis (University of Maryland).....	92
<i>Atomic-level description of separations phenomena using multi-scale models</i> Vassiliki-Alexandra Glezakou (Pacific Northwest National Laboratory).....	94
<i>New Ionic Covalent Organic Framework (iCOF) for Selective Cr(VI) Removal</i> Santa Jansone-Popova (Oak Ridge National Laboratory) .....	96
<i>Computational Insight into Novel Membranes and Sorbents for Gas Separations</i> De-en Jiang (University of California, Riverside).....	97
<i>Interfacial Structure and Dynamics in Ion Separations</i> Grant E. Johnson (Pacific Northwest National Laboratory).....	99
<i>Investigations into the Gas Separation Performance of Siloxane-Substituted Polynorbornene Membranes</i> Brian K. Long (University of Tennessee) .....	104

<i>The Eleven Ways to Use Host-Guest Chemistry to Extract Aqueous Ions</i> Bruce A. Moyer (Oak Ridge National Laboratory) .....	109
<i>Experimental and Theoretical Evaluation of the Thermodynamic Stability of True MOF Polymorphs Explains their Mechanochemical Interconversions</i> Alexandra Navrotsky (University of California, Davis) .....	111
<i>Developing Metal- and Ligand-Redox Properties in New Separations Methods for Rare Earth Elements</i> Eric J. Schelter (University of Pennsylvania) .....	114
<i>A nanoscale view of assisted ion transport across the liquid-liquid interface</i> Mark L. Schlossman (University of Illinois, Chicago) .....	118
<i>Ion Pair Receptors and Extractants</i> Jonathan L. Sessler (University of Texas, Austin).....	122
<i>Chemical Analysis of Nanodomains</i> Emily A. Smith (AMES Laboratory).....	126
<i>Heat Capacity and Thermodynamic Functions of Crystalline and Amorphous Forms of the MOF Zinc 2-Ethylimidazolate, Zn(EtIm)<sub>2</sub></i> Brian F. Woodfield (Brigham Young University) .....	134
<i>Interfacial Structure and Dynamics in Ion Separations: Separation Phenomena in Nanostructured Materials</i> Alla Zelenyuk (Pacific Northwest National Laboratory).....	137
<b>LIST OF PARTICIPANTS</b> .....	138

# **ABSTRACTS**

# **Plenary Session Abstract**

**Expanding the Chemical Palette for Adsorption-Base Separations**

David S. Sholl  
School of Chemical & Biomolecular Engineering,  
Georgia Institute of Technology, Atlanta, GA 30332

**Presentation Abstract**

The majority of research literature on chemical separations focuses on a relatively small collection of chemicals. In many ways this is appropriate because of the dramatic economic and environmental impacts of these species. The space of possible chemicals, however is vast; Carl Sagan's famous "billions and billions" is many orders of magnitude too small for chemical space. I will discuss early steps towards methods that may eventually allow rapid development of adsorbent-based separations for a diverse range of molecules drawn from a broad chemical space. Time permitting, I will also discuss recent attempts to quantify reproducibility of experimental data in adsorption, a topic that brings up wide-ranging issues in forming connections between basic discovery-oriented science and the practical application of materials in real-world separations.

# **Tuesday PI**

# **Oral Presentations**

## Binding Anions Selectively with Modular Receptors and Releasing them with Light

Amar H. Flood, Yun Liu, Arkajyoti Sengupta, Fred Parks, Sydney Stutsman, and Krishnan Raghavachari

Department of Chemistry, Indiana University

### Presentation Abstract

Anions play critical roles in human biology and chemical processes. For these reasons, mastering ways to manipulate their availability across many environments will have far-reaching consequences. We are using supramolecular chemistry for this task by taking advantage of triazole-based receptors (Figure 1) that are easy to make and modify. Triazoles (colored red in Figure 1a) are amide isosteres that bind anions using strong, yet non-traditional, CH hydrogen bonds. Taking inspiration from biology's halorhodopsin, a new class of light-active foldamers has been created that make use of the photoisomerizable azobenzenes (colored blue in Figure 1b). The foldamers can catch and release chloride with affinity swings of up to 84-fold to regulate its concentration. We then move out of organic solvents, again taking biology's lead, to tackle one of the grand challenges in host-guest chemistry: Extracting highly-hydrated chloride ions from aqueous solutions. We were the first to discover protein-like driving forces can take over when the foldamers intertwine into a duplex (Figure 1c) to extract hydrophilic chloride ions from semi-aqueous solutions. Ultimately, the formation cooperativity of the duplex and the encapsulated microenvironment it creates are believed to be key to functionality. We address these questions and the related fundamental science to provide the understanding needed for computer-aided receptor designs of receptors for ion extraction.

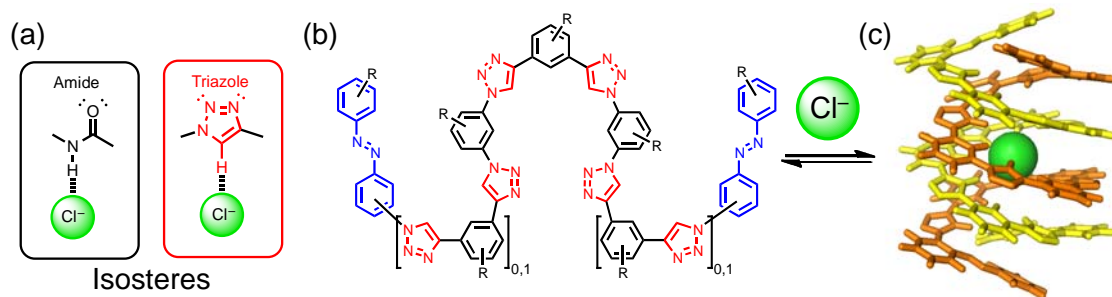


**Figure 1.** (a) Triazoles are the basis for binding anions and (b) for preparing the photoactive foldamers that (c) can wrap up chloride ions.

### DE-SC0002728: Binding Anions Selectively with Modular Triazolophanes and Releasing them with Light

**PI:** Amar H Flood, CoPI Krishnan Raghavachari

**Graduate Students:** Yun Liu, Arkajyoti Sengupta, Fred Parks

**Undergraduate Student:** Sydney Stutsman

## RECENT PROGRESS

### *Anion Binding in Solution: Beyond the Electrostatic Regime*

A fundamental understanding of how synthetic receptors bind anions is essential for managing salts during nuclear power production. However, the limited understanding of solvent effects in ion recognition leads to a persistent blind spot that prevents effective receptor design. We experimentally discovered an underlying dependence of anion binding energy on solvent dielectric constant. We found this relationship by measuring how chloride binds to macrocyclic receptors across the widest range of solvents examined to date. Solvent weakens binding energy by screening electrostatic interactions. In solvents even as non-competitive for anion binding as dichloromethane, electrostatics no longer governs affinity; the role of electrostatics gets increasingly weaker thereafter. Density functional theory helped us understand this dependence. Our theory-backed model accurately predicts chloride binding energies in solvents like 1,2-dichloroethane and benzonitrile (PhNO<sub>2</sub>), which are used as mimics to study liquid-liquid extractions in the nuclear fuel cycle. This model offers a general foundation for anion recognition and the basis for computer-aided receptor design.

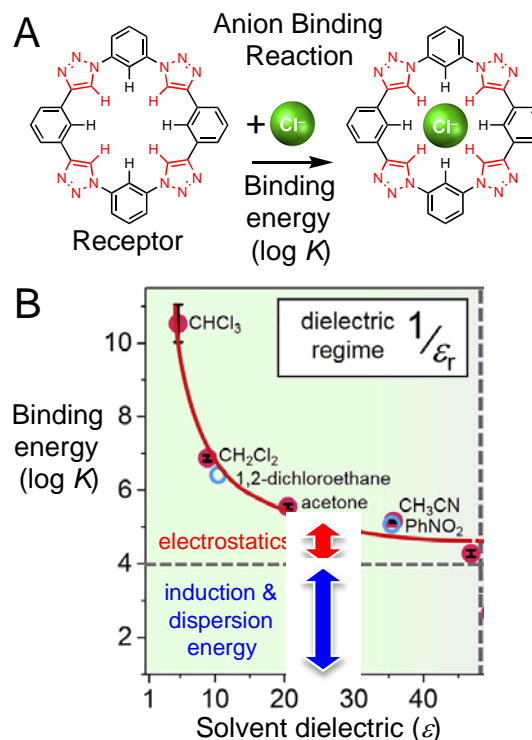


**Figure 1.** (A) Anion binding reaction between synthetic receptor and chloride. (B) Binding energy scales with solvent dielectric constant

### *Anion Binding by Receptors: Beyond the Electrostatic Regime*

When we examined the factors controlling stabilization of anions inside authentic receptors, we discovered that the driving forces are significantly different from expectations based on small molecules. In small molecules, hydrogen bonding to anions has been deconvoluted into its contributions. It is found that electrostatics scales with total binding energy because the sum of dispersion and induction attractions is offset by exchange repulsions. When those same small hydrogen bonding molecules are unified in a larger receptor architecture, however, the expectations set by the small molecules no longer hold. Rather, electrostatics lowers in relative importance, while induction and dispersion grow. This emerges naturally from the distance dependence of hydrogen bonding together with the

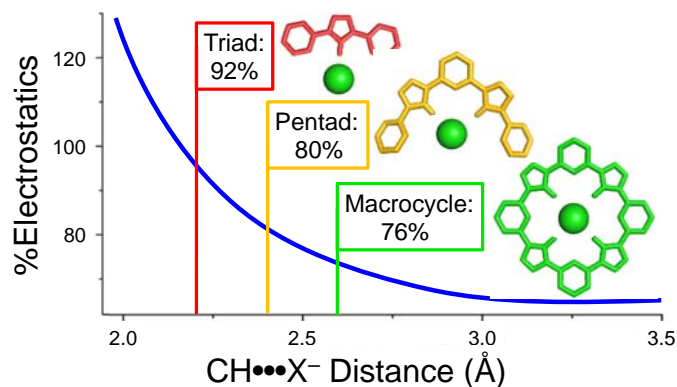


**Figure 2.** The contribution of electrostatics to the hydrogen bond stabilization of anion-receptor complexes decreases as the size of the molecule increases.

fact that many hydrogen-bonding contacts cooperate to extend the hydrogen bond lengths. On the basis of this new understanding we generated a new predictive model.

***Anion Selectivity in Photoactive Aryl-triazole Foldamers: Is it better to bind or release?***

Removal of anions from nuclear waste is a major hurdle for safe and sustainable energy production. To this end, switchable receptors to bind and release guests offer new ways to remove ions. Despite new examples, the rules governing the bind-release selectivity have not been addressed. We use aryl-triazole foldamers to bind and release anions by controlling the helix-coil transition with azobenzene photoswitches. We provide an examination of the widest range of anions (11) to determine selectivity rules. We found an interesting correlation in selectivity of anion affinity swing rationalized from helix and coil conformations of the receptor. When helical, selectivity is sharp and determined by size (strong to weak affinity) while random coils have flat selectivity (medium affinity). This leads to the unusual outcome seen with  $\text{PF}_6^-$ , that instead of the bind-release cycle correlating with helix-coil, we see the inverse correlation with coil-helix.

**Publications Acknowledging this Grant in 2015 – present**

(I) *Exclusively funded by this grant;*

1. Qiao, B.; Sengupta, A.; Liu, Y.; McDonald, K. P.; Pink, M.; Anderson, J.; Raghavachari, K.; Flood, A. H., Electrostatic and Allosteric Cooperativity in Ion-pair Binding: A Quantitative and Coupled Experiment-Theory Study with Aryl-Triazole-Ether Macrocycles, *J. Am. Chem. Soc.* **2015**, *137*, 9746–9757
2. Dobscha, J. R.; Liu, Y.; Flood, A. H., Shape-persistent Anion Receptors. In *Comprehensive Supramolecular Chemistry II*; Elsevier, **2016**
3. Liu, Y.; Sengupta, A.; Raghavachari, K.; Flood, A. H., Anion binding in solution: Beyond the electrostatic regime, *Chem* **2017**, *3*, 411-427. *Cover Art*
4. Sengupta, A.; Liu, Y.; Flood, A. H.; Raghavachari, K., Anion Binding by Receptors: Beyond the Electrostatic Regime, *submitted*

## Modular Approaches to Contemporary Complexants for Separations

Jesse D. Carrick,<sup>†</sup> Cory A. Hawkins,<sup>†</sup> David A. Dixon<sup>‡</sup>

<sup>†</sup>Tennessee Technological University, <sup>‡</sup>The University of Alabama

### Presentation Abstract

Closure of the nuclear fuel cycle is contingent, in part, on the development of effective separations processes for the selective removal of desired radionuclides from used nuclear fuel allowing for further transmutation. Liquid-liquid separation techniques involving multidentate, soft Lewis basic donors have demonstrated significant promise in recent decades. Identification of improved complexants and related scaffolds for separations is predicated on efficient synthetic methodology for the construction of novel species devised from computational theory or experimentally observed results. The evaluation of structure-activity relationships for the production of more efficacious complexants can inform fundamental understanding of separations processes and narrow current outstanding knowledge gaps. Work in this laboratory has focused on developing methods to allow for the diversification of resident molecular functionality in a convergent manner by employing modular concepts in concert with metal-mediated coupling strategies to heteroaromatic synthons to afford complexants with potential for improved performance in separation science. Recent efforts have afforded access to functionalized constructs for use in liquid-liquid separations. Utilization of the Sonogashira coupling to 3-(6-bromo-pyridin-2-yl)-5,6-diphenyl-[1,2,4]triazine complexant scaffolds affords a unified strategy for diversification into symmetric and unsymmetric multidentate structures. Preliminary methodology development and initial separations data will be presented.

### 0000228927: Modular Approaches to "Click" Complexants for Chemosselective Minor Actinide Separations

**PI:** Jesse D. Carrick, Cory A. Hawkins (Co-PI), David A. Dixon (Co-PI)

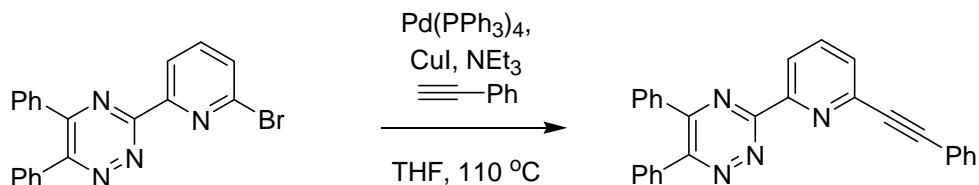
**Postdoc(s):** Dr. Sauradip Chaudhuri

**Student(s):** Daniel A. Flatt,<sup>†</sup> Steven J. Laxton,<sup>†</sup> Kyle R. Lyons,<sup>†</sup> Gabrielle Waters<sup>†</sup>

**Affiliations(s):** *(include only if different from above)*

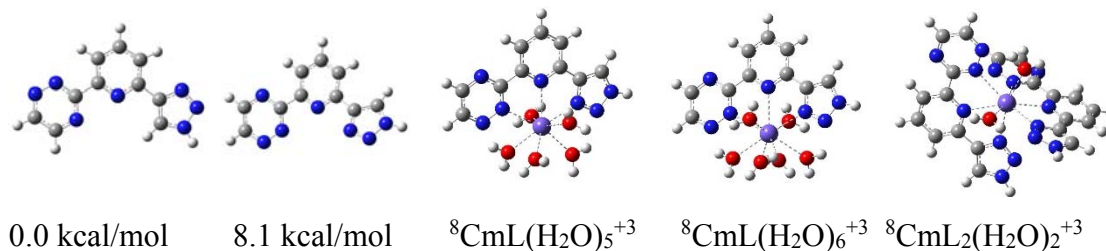
## RECENT PROGRESS

### *Sonogashira Coupling of 3-(6-bromo-pyridin-2-yl)-5,6-diphenyl-[1,2,4]triazine*



Preliminary proof of concept data has been obtained towards the production of alkynyl cross-coupling products of Br-MTPs. This synthon presents a substantive point of initiation towards the production of numerous multidentate heteroaromatic structures including 1,2-pyrazoles and related structures which are currently being investigated.

Electronic structure calculations on the ligands and their binding to An(III) have been initiated. The ligand must undergo conformational changes to bind the An(III). The reactions for the ligands displacing H<sub>2</sub>O are being studied.



### **Publications Acknowledging this Grant 9/2017 – present**

Lambert, A. E.; Carrick, J. D. Diversification of 6-bromo-2-substituted pyridine derivatives via Suzuki-Miyaura cross-coupling. *Journal of Heterocyclic Chemistry* **2017**, Submitted 11/16/17.

**Lattice Dynamics of Flexible Framework Structures:  
Insights from Inelastic Neutron Scattering (INS)**

Nancy L. Ross  
Department of Geosciences, Virginia Tech

**Presentation Abstract**

Porous frameworks such as metal-organic frameworks (MOFs) form the chemical and structural basis for critical technologies in separations, catalysis, nuclear waste containment, and biomedical applications. Despite impressive advances in the development of MOFs, the relationship between the structural topology of the framework and energetics of their formation and stability remain poorly understood. Inelastic Neutron Scattering (INS) provides a powerful method to address this by determining the full lattice vibrational spectrum from which the thermodynamic driving forces, including entropic factors, can be determined. In this study, INS spectra for a set of zeolitic imidazolate framework (ZIF) polymorphs synthesized by mechanochemistry were measured on the spectrometer, SEQUOIA, at the Spallation Neutron Source (Oak Ridge National Laboratory). The INS spectra of these complex materials display many similarities above 50 meV, but major differences are observed at low energies, especially below 20 meV. These low-frequency vibrations are critical as they control the thermodynamic stabilities of the polymorphs and reveal the dynamics of the open framework. Work is in progress to determine whether these vibrations are correlated with physical phenomena such as gate-opening and pore-breathing mechanisms, and / or shear-induced phase transitions that signify the onset of structural instability. The results from this study have immense broader impact as they will contribute to our fundamental knowledge relating structures of MOFs with their lattice dynamics, energetics and entropies, thus elucidating the energy landscape of this exciting class of novel microporous framework materials.

.....  
**DE-SC0016448: The Energetics and Dynamics of Flexible Frameworks and Molecular Confinement**

**PI:** Nancy L. Ross

**Research associate:** Jing Zhao

**Postdoc:** Wenlin Chen (joining group in Jan. 2018)

**RECENT PROGRESS**

Ross's team has begun studying, by inelastic neutron scattering, the lattice dynamics and thermodynamic stabilities of a series of ZIF polymorphs synthesized via a mechanochemical route by Tomislav Friscic of McGill University. A proposal submitted for beam time at the Spallation Neutron Source at Oak Ridge National Laboratory (ORNL) in April 2017 was successful. INS experiments were completed in September and November 2017 on beamline SEQUOIA with

collaborator, A.I. Kolesnikov of ORNL. The INS spectra of the three polymorphs of  $\text{Zn}(\text{EtIm})_2$  with RHO, analcime (ANA), and beta-quartz topologies (QTZ), shown in Figure 1, display many interesting features. While the INS spectra are virtually identical above 50 meV, the polymorphs differ substantially in lattice vibrations below 20 meV. These low-frequency vibrations are important as they control the thermodynamic stabilities of the polymorphs and reveal the dynamics of the open framework. They are therefore expected to shed light on B. Woodfield's (BYU) low-temperature heat capacity results. Postdoc, Dr. Wenlin Chen, will be joining the group in Jan. 2018 and will complete *ab initio* DFT calculations to elucidate the nature of the low-energy modes and physical phenomena such as gate-opening and pore-breathing mechanisms, as well shear-induced phase transitions and the onset of structural instability. This work is in progress and is expected to be submitted to the *J. Am. Chem. Soc.* in 2018.

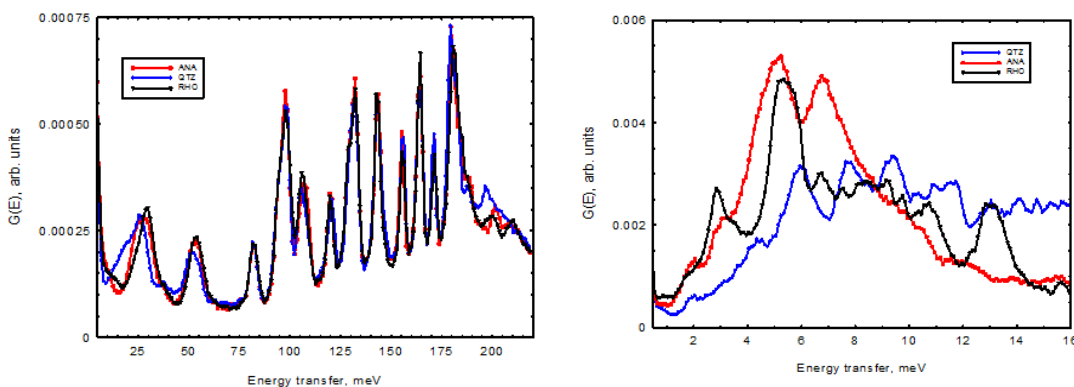


**Figure 1.** INS spectra  $\text{Zn}(\text{EtIm})_2$  polymorphs (RHO, ANA and QTZ) from 0–225 meV (left) and below 20 meV (right).

In parallel with the INS studies, the Ross group has been exploring the stability of ZIFs and MOFs at high pressure using Raman spectroscopy. The spectra shown at room pressure in Figure 2, show good agreement with the INS spectra.

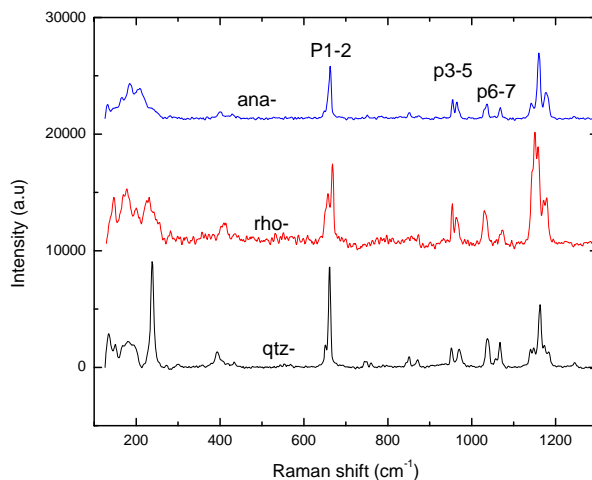


**Figure 2.** Raman spectra of  $\text{Zn}(\text{EtIm})_2$  polymorphs (RHO, ANA and QTZ) at room pressure.

Distinct changes in the spectra of the polymorphs are observed at high pressure indicating possible phase transitions to new structures. Figure 3, follows the strong peak at  $670\text{ cm}^{-1}$  in all three

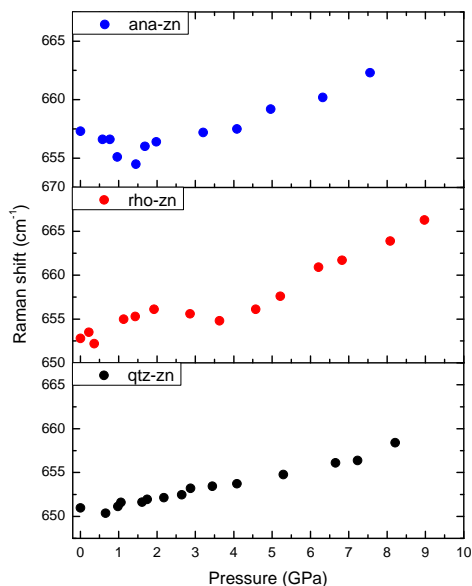


**Figure 3.** Variation of peak near  $670\text{ cm}^{-1}$  for  $\text{Zn}(\text{EtIm})_2$  polymorphs (RHO, ANA and QTZ).

polymorphs. In ANA and RHO, the mode shows softening between 1 bar and 1.5 GPa and 0.5 GPa, respectively, before increasing to a plateau to 4 GPa before increasing steeply at higher pressure. The changes in the QTZ polymorph are more subtle but a slight softening in the mode is observed near 0.7 GPa, reaching plateau up to ca. 5 GPa and increasing a greater rate at pressures above 6 GPa. The trends are fully reversible suggesting that the changes are related to a “flexing” of the framework. This is a common response to pressure observed in inorganic tetrahedral framework structures such as zeolites and feldspars. There are additional high-pressure Raman spectroscopic experiments are being carried out on cation-exchanged zeolites from the Navrotsky group. The results gathered in this study will be combined with structural studies at high pressure using neutron and X-ray diffraction methods. It will provide a comprehensive high-pressure study relating structure to lattice vibrations and polymorphic stability in MOFs that will be submitted for publication in 2018.

This research is part of a collaborative project involving A. Navrotsky (UC Davis) and B. Woodfield (BYU) to understand the energetics and dynamics of flexible frameworks and molecular confinement. Navrotsky’s group has begun studying, by solution calorimetry, the energetics of the ZIF polymorphs studied with INS. They have provided the first combined experimental and theoretical evaluation of how differences in ligand structure and framework topology affect the relative stabilities of isocompositional (i.e. true polymorph) metal-organic frameworks (MOFs). Solution calorimetry and periodic DFT calculations were used to analyze thermodynamics of two families of topologically-distinct polymorphs of zinc zeolitic imidazolate frameworks (ZIFs) based on 2-methyl- and 2-ethylimidazolate linkers, demonstrating a correlation between measured thermodynamic stability and density, and a pronounced effect of the ligand substituent on their stability. The results also show that thermodynamic stability of a given ZIF does not depend on the choice of synthetic method, and that mechanochemical syntheses and transformations of ZIFs are consistent with Ostwald’s rule of stages and proceed toward thermodynamically increasingly stable, more dense phases. Thus grinding, rather than creating more metastable phases by the added mechanical energy, enables the system to overcome kinetic barriers and form more stable denser MOF structures. Therefore a rich landscape of polymorphs closely spaced in energy becomes accessible. These studies are being extended to ZIFs with modified linkers to separate out effects of porosity and chemistry.

The Woodfield group has measured the low-temperature heat capacities of four of these ZIF polymorphs. The results show several interesting features. First, the heat capacities (and standard

entropies at 298 K) are significantly different, indicating that the polymorphs differ substantially in lattice vibrations and/or defects. These differences are far more pronounced than those seen in earlier studies on silica zeotype polymorphs. Second, all of the samples exhibit gaps in the phonon spectra at low temperatures. This was expected as it is common for porous frameworks, e.g. zeolites, and is now confirmed for MOFs. Third, all the samples exhibit a broad Cp anomaly centered around 200 K. At first, it was thought this was a Schottky anomaly, but no suitable Schottky model was found that could fit the data. The data were also fit to other lattice models, but currently nothing has been found that is physically reasonable. We are now in the process of synthesizing, characterizing, and then measuring the heat capacity of a series of model imidazole and Zn-amine compounds that we can use as a non-framework model for the heat capacity of ZIFs. The non-framework model will be used as a baseline to subtract out the phonon modes unique to these MOF materials and then explore whether this behavior is unique or general.

.....

**Publications Acknowledging this Grant**

Work in progress.

## Proton Solvation and Transport in Acidic Solutions and Complex Materials

Gregory A. Voth

Department of Chemistry and James Franck Institute, The University of Chicago

### Presentation Abstract

The DOE-supported research in the Voth group focuses on understanding the nature of proton transport in complex systems such as proton exchange membranes (PEMs). The most unique aspect of this research is the development and implementing of a novel reactive molecular dynamics methodology. In this approach, covalent bonds can dynamically break and form, allowing us to accurately treat the proton hopping process essential to capturing the physics of proton transport. The Voth group has applied this method to proton exchange membrane systems, providing insight into their proton transport mechanism. We have found that protons can diffuse most rapidly in the water-rich regions, but that protons actually spend so little time in such regions that transport along the hydrophobic – hydrophilic interface controls the membrane performance. In addition, the group has worked to increase understanding of acidic solutions, developing methods for simulating and interpreting experimental infrared vibrational spectroscopy for excess protons (acidic solutions). The group has also implemented novel tools for developing proton transport reactive MD models using a relative entropy minimization scheme.

### DE-SC0005418: Computer Simulation of Proton Transport in Fuel Cell Membranes

**Postdoc:** Chris Arntsen

**Students:** Paul Calio, Zhefu Li

### RECENT PROGRESS

#### *Reactive Molecular Dynamics for Acidic Systems*

We have most recently developed a novel multiscale reactive molecular dynamics (MS-RMD) model by utilizing relative entropy minimization (REM) (see Fig. 1a). With REM, we are able to develop reactive hydrated excess proton models which faithfully reproduce the free energy barrier along the proton transfer coordinate between water molecules and other key properties such as the radial distribution functions of the same system treated at a higher level of theory (in this case, experimentally biased *ab initio* molecular dynamics, which naturally includes reactivity).

#### *Unraveling the Spectroscopy of Acidic Solutions*

In addition to generating improved hydrated proton models, we have developed several tools to facilitate an in-depth interpretation of experimental infrared vibrational spectroscopy for acidic solutions, as implemented in the Tokmakoff group at the University of Chicago and elsewhere. We developed a spectroscopic model which couples MS-RMD simulation with electronic structure

calculations of protonated water clusters. With this, we are able to decompose spectral contributions from the hydrated proton Eigen complexes, Zundel complexes, and solvating water (a representative solvation structure is shown in Fig. 1b). This modeling proves that IR spectroscopy can indeed distinguish different protonated water species within the bulk phase.

### ***Exploration of Catalyst Layers in Thin Film PEMs***

In order to better understand the influence of catalyst layers on thin film of PEMs, we also constructed systems on model metal surfaces. As the hydrophobicity/hydrophilicity can have a significant impact on proton transport of a PEM, we varied the relative strength of interaction between the surface and the hydrophobic and hydrophilic groups in our simulations. There are various proposed morphologies for PEMs, though we have shown in previous work that bundle morphologies agree most with experimental water self-diffusion constants. We therefore performed MS-RMD simulation on PEM systems in the bundle morphology at various surface hydrophobicity and hydration level. In order to decompose the effect of morphology, we also performed identical simulations on systems having random morphology.

The simulations yielded several interesting results. First, water network formation is highly dependent on hydrophobicity of the catalyst surface (an example system is shown in Fig. 1c). In the most hydrophobic surface, the PEM/catalyst interface region is comprised nearly entirely of polymer atoms (either from the backbone or from the regions of the side chain near the backbone). Conversely, at the most hydrophilic surfaces, the interface region contains a robust water layer in which many hydronium ions and charged sulfonate groups also reside.

We also found that for systems with increased hydrophilic surfaces, there is a decrease in proton diffusion, despite the robust water layer formed. This is a result of the increased concentration of charged sulfonate groups in this region, to which hydronium ions have a strong electrostatic attraction. This is consistent with our previous work that showed morphologies in which hydronium molecules spend less time in the first solvation shell of the sulfonate groups resulted in higher proton diffusion constants.

### ***Effects of Applied Electric Field***

We have also begun to investigate the effects of applied electric fields on the proton transport in PEMs. Due to the potential difference between electrodes, electric fields may enhance proton transport, especially in ultrathin inter-electrode electrochemical cells where the double layers of the electrodes overlap. Thus, we have begun simulations of a random morphology of Nafion PEM, varying the strength of the electric field to understand the electric field's impact on PEM systems at the atomistic level.

In our previous work, we discovered an excess proton hopping mechanism in which the protons are passed between adjacent sulfonate groups of a PEM. Consistent with this proposed mechanism, we find that increasing the voltage 1) increases proton transport, 2) increases the probability of finding sulfonates within a shorter distance from each other, and 3) increases the probability of finding the hydrated excess proton associated with more sulfonates. This gives rise to the idea that although electric fields enhance proton transport by adding an external force, the sulfonate groups are also very active in the proton transport through these PEMs.

In the future, we will also study these E-field, thin film layer, and other effects for novel PEM materials, e.g., having alternating side chain lengths (Fig. 1d).

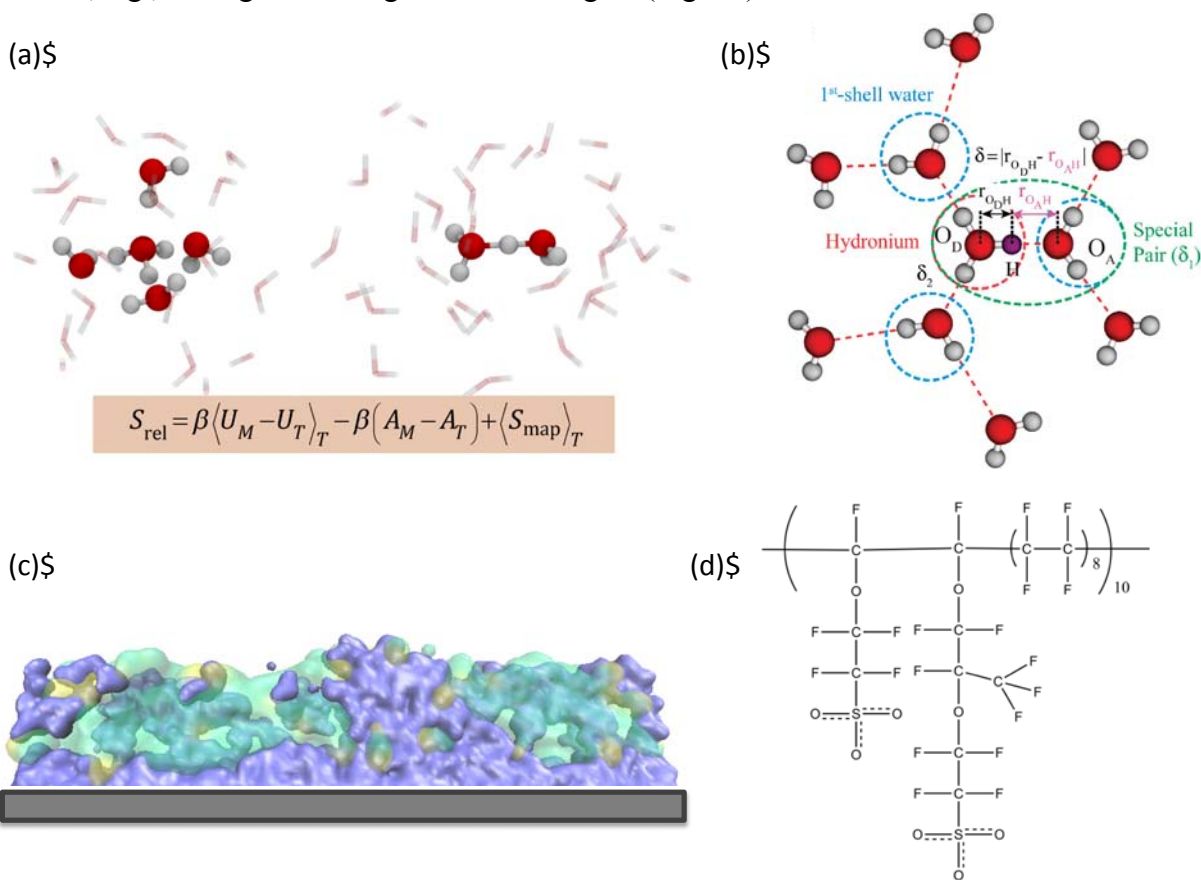


**Figure 1.** (a) Snapshots of Eigen ( $\text{H}_9\text{O}_4^+$ ) and Zundel ( $\text{H}_5\text{O}_2^+$ ) cations from *ab initio* MD (AIMD) simulation used in the relative entropy minimization (REM) methodology. (b) Solvation structure of hydrated excess proton in water. Decomposing of vibrational modes in such a system is difficult due to the complexity of the structure. (c) Snapshot of a proton exchange membrane (PEM) at the surface of an electrode. Water and hydronium ions are rendered blue, polymer atoms are rendered green, and sulfonate groups are rendered yellow. (d) Chemical structure of novel PEM which contains adjacent, uneven sidechains. The short side chain is the side chain found in the perfluorosulfonic acid Hyflon, and the long side chained is the side chain found in the perfluorosulfonic acid Nafion.

### Publications Acknowledging this Grant in 2015 – present

1. Tse, Y.-L. S.; Knight, C.; Voth, G. A. An Analysis of Hydrated Proton Diffusion in *Ab Initio* Molecular Dynamics. *J. Chem. Phys.* **2015**, *142*, 014104(1-13).

2. Liu, S.; Voth, G. A. Mesoscale Study of Proton Transport in Proton Exchange Membranes: Role of Morphology. *J. Phys. Chem. C* **2015**, *119*, 1753–1762.
3. Biswas, R.; Tse, Y. -L. S.; Tokmakoff, A.; Voth, G. A. Role of Pre-Solvation and Anharmonicity in Aqueous Phase Hydrated Proton Solvation and Transport. *J. Phys. Chem. B* **2016**, *120*, 1793–1804.
4. Savage, J.; Voth, G. A. Proton Solvation and Transport in Realistic Proton Exchange Membrane Morphologies. *J. Phys. Chem. C* **2016**, *120*, 3176–3186.
5. Arntsen, C.; Savage, J.; Tse, Y. -L. S.; Voth, G. A. Simulation of Proton Transport in Proton Exchange Membranes with Reactive Molecular Dynamics. *Fuel Cells*. **2016**, *16*, 695-703.
6. Biswas, R.; Carpenter, W.; Voth, G. A.; Tokmakoff, A. Molecular Modeling and Assignment of IR Spectra of the Hydrated Excess Proton in Isotopically Dilute Water *J. Chem. Phys.* **2016**, *145*, 154504(1-12).
7. Biswas, R.; Carpenter, W.; Fournier, J. A.; Voth, G. A.; Tokmakoff, A. IR Spectral Assignments for the Hydrated Excess Proton in Liquid Water. *J. Chem. Phys.* **2017**, *146*, 154507(1-11).
8. Arntsen, C.; Chen, C.; Voth, G. A. Reactive Molecular Dynamics Models from *Ab Initio* Molecular Dynamics Data Using Relative Entropy Minimization. *Chem. Phys. Lett.* **2017**, *683*, 573-578.
9. Biswas, R.; Voth, G. A. Role of Solvation Structure in the Shuttling of the Hydrated Excess Proton. *J. Chem. Sci.* **2017**, *129*, 1045–1051.
10. Chen, C.; Arntsen, C.; Voth, G. A. Development of Reactive Force Fields Using *Ab Initio* Molecular Dynamics Simulation Minimally Biased to Experimental Data. *J. Chem. Phys.* **2017**, *147*, 161719(1-7).

**The Role of Inner- and Outer-Sphere Interactions  
in the Selective Extraction of Metal Ions**

Vyacheslav S. Bryantsev, Ross J. Ellis, Alexander S. Ivanov, Santanu Roy,  
Laetitia H. Delmau, Bruce A. Moyer  
Oak Ridge National Laboratory, Chemical Sciences Division

**Presentation Abstract**

Our overarching research goal is to develop a rational basis for ligand design in separating ions using selective liquid-liquid extraction. Structural and thermodynamic factors governing the formation of extraction complexes provide the basis for fundamental understanding of ion recognition in extractive experiments and guiding ligand design. Due to a multitude of effects that manifest beyond the primary coordination shell, current computational models at best can only reproduce the trends in the biphasic extraction of ions, but not the absolute values of thermodynamic parameters. A combination of extended X-ray absorption spectroscopy (EXAFS), density functional theory (DFT), and classical molecular dynamics (MD) simulations can provide unique structural information on the inner- and, to some extent, outer-sphere coordination environment around a metal ion in solution. Our results show how outer-sphere lanthanide chloride and nitrate ion clusters are assembled in hydrocarbon solutions during the extraction with diglycolamide ligands, elucidating new strategies for controlling ion-cluster extraction. Toward rationalizing and predicting selectivity for size-based separation of lanthanides, we will discuss the impact of counterions and water in the outer sphere on the predicted selectivity trend for lanthanides with diglycolamide ligands and develop a hypothesis as to why this class of ligands shows a characteristic nonlinear trend in lanthanide selectivity. Based on the structural information from EXAFS and DFT, we will show how a dramatic change in selectivity for actinides over lanthanides can be achieved with polyazine extractants by replacing organic solvent with ionic liquid. In another example, we will compare the hydration structure and water-exchange dynamics around  $\text{Cs}^+$  and  $\text{Fr}^+$  cations and rationalize the difference in the free energy of partitioning of  $\text{Cs}^+$  and  $\text{Fr}^+$  in water-organic solvent systems using DFT and the Born model.

**Principles of Chemical Recognition and Transport in Extractive Separations  
Field Work Proposal ERKCC08**

**PI:** Bruce A. Moyer

**Co-PIs:** Vyacheslav Bryantsev, Radu Custelcean, Santa Jansone-Popova

**Postdoc(s):** Neil J. Williams, Alexander S. Ivanov

**Student(s):** Charles A. Seipp (graduated)

## RECENT PROGRESS

### Sterically-directed assembly of outer-sphere ion clusters

Outer-sphere ion clusters are inferred in many important natural and technological processes, but their mechanisms of assembly and solution structures are difficult to define. A remarkably symmetric complex of lanthanides with three molecules of the well-known oxygen-donor extractant TODGA, N,N,N,N-tetra(n-octyl)diglycolamide, was characterized using a complimentary combination of DFT, MD simulations, and EXAFS (Figure 2). The clusters are assembled through steric and electrostatic forces, with the chloride anions residing in equidistant ‘clefts’ between coordinating diglycolamide ligands in positions that satisfy both repulsive and attractive ion-ion interactions. The apparent host-guest chemistry demonstrated in the sterically-directed association of ions into a tight, outer-sphere cluster helps to explain the effectiveness of this highly successful extractant ligand class, elucidating new strategies for controlling ion cluster assembly and extraction. This study provides new insights into controlling the weak forces involved in outer-sphere ion clustering in liquid-liquid extraction systems, which underpins important technological processes that rely on ion separation.

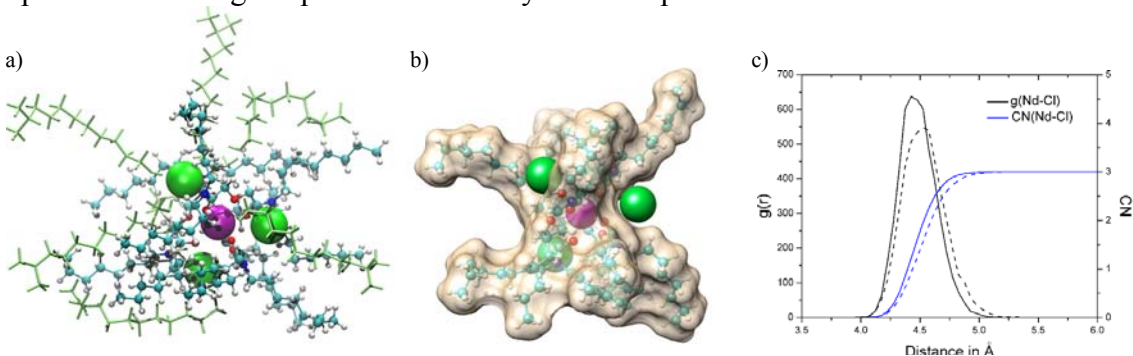


**Figure 1.** (a) Snapshot of the  $[Nd(TODGA)_3]^{3+}(Cl^-)_3$  complex with phase-modifier molecules (isodecanol) in dodecane from classical MD simulations. (b) Solvent-accessible surface representation of  $[Nd(TODGA)_3]^{3+}(Cl^-)_3$  showing the chloride ion locations in hydrophobic clefts between the TODGA ligands. (c) Radial distribution function ( $g(r)$ ; black curve, left axis) and its integration (coordination number, CN; blue curve, right axis) of  $Cl^-$  anions around  $Nd^{3+}$  hydrocarbon solvent (solid lines) and hydrocarbon solvent in the presence of 30% isodecanol phase modifiers (dashed lines).

### Capping the calix around Cs(I) in toluene solution

The role of solvent in molecular recognition systems is under-researched and often ignored, especially when the solvent is considered “non-interacting”. Likewise, there is limited understanding of how solvents influence the coordination structure, which might be different from that of the crystalline solid, where packing forces and long-range electrostatics are often the most important contributions to structure. The EXAFS measurements and simulations were used to elucidate the coordination environment around cesium(I) in calix[4]pyrrole-toluene solution (Figure 3). Unlike in crystal structures, the Cs(I) does not form contact ion pairs with an anion, but rather sits snugly in the C4P ‘cup’, and the open face interacts with aromatic solvent molecules through additional cation- $\pi$  interactions. Our results elucidate the importance of cation- $\pi$  interactions in solvation of receptor-bound cations and show how “non-interacting” solvents like toluene may influence recognition more than previously thought.

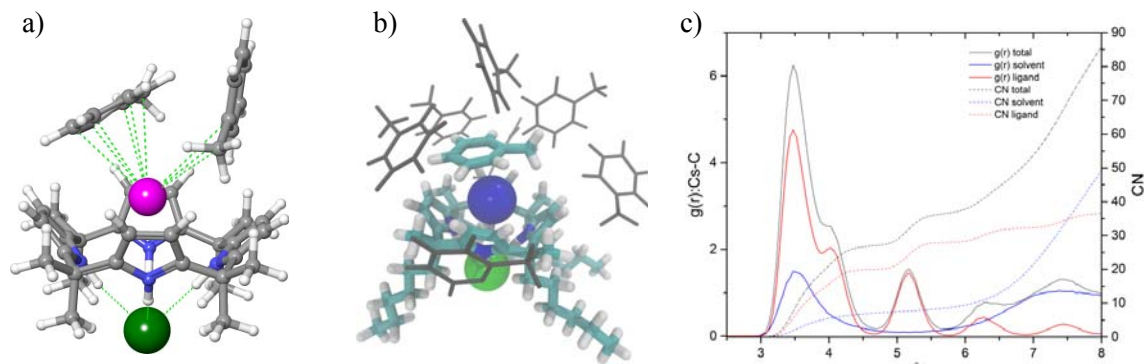


**Figure 2.** (a) DFT-optimized structure of the Cs-C4P-Br complex in the presence of two solvent (toluene) molecules. (b) Snapshot of the lipophilic Cs-C4P<sup>L</sup>-Br complex in toluene from classical MD simulations (central panel). (c) Radial distribution function of carbon atoms around Cs<sup>+</sup> ( $g(r)$ , left axis) and its integration (coordination number, CN, right axis) for the Cs-C4P<sup>L</sup>-Br complex in toluene obtained from classical MD simulations.

### Simple Guanidinium Motif for the Selective Binding and Extraction of Sulfate

It is shown that a simple guanidinium molecule binds sulfate selectively in methanol/water solution, and a synthesized lipophilic analog permits the selective extraction of sulfate from aqueous sodium chloride into 1,2-dichloroethane. This receptor, N,N'-bis(2-pyridyl)guanidinium, features a rigid pseudo-bicyclic conformation in binding anions in the solid state. It selectively binds sulfate in 10% water/90% MeOD-D4 solutions with stepwise  $\log K_1$  and  $\log K_2$  values of  $3.78 \pm 0.12$  and  $2.10 \pm 0.23$ , respectively. DFT calculations were performed to predict the conformational preferences of guanidinium receptors upon anion coordination in solution. The guanidinium was found to be 55 times stronger than the control nonbinding anion exchanger Aliquat 336, suggesting that the hydrogen-bond-donating ability and stronger Coulombic stabilization enhance the selectivity of the guanidinium receptor for the charge-dense sulfate anion. With further development of the synthesis chemistry, the N,N'-bis(2-pyridyl)guanidinium group could become a central part of more complicated and more potent receptors in the future.

### Characterization of coordination environment around Eu(III)/Am(III) complexed to bis-triazine phenanthroline in [C<sub>4</sub>mim][NTf<sub>2</sub>]

As an example of synergy with other BES programs at ORNL (Sheng Dai, ERKCT08), a remarkable capability of 2,9-bis(triazine)-1,10-phenanthroline (BTPhen) extractant to achieve highly efficient partitioning of Am(III) from Eu(III) upon dissolution in the ionic liquid [C<sub>4</sub>mim][NTf<sub>2</sub>] was reported, exceeding the best performance for traditional approaches using organic solvents by over 40 times. In order to provide a rationale for enhanced Am(III) over Eu(III) selectivity in the ionic liquid solvent compared to traditional organic solvents, characterization of coordination environment was performed using a combination of the X-ray absorption spectroscopy (XAFS) and DFT calculations. DFT calculations were used to investigate whether the nitrates, hydroxide, and ionic liquid directly interact with the extracted metal. XAFS used DFT-generated structures to fit experimental data, revealing that unlike a 2:1 ligand:metal complex in the organic phase, where one nitrate can enter the inner sphere of the complex and adopt a chelate coordination mode, a tightly-bound coordinating water molecule was found in a complex formed in ionic liquid (Figure 1). DFT results indicate that substitution of bidentate nitrate in organic

solvent by H<sub>2</sub>O in [C<sub>4</sub>mim][NTf<sub>2</sub>] leads to a shorter average metal ion-ligand bond distance and a stronger ligand binding, which could in turn lead to a higher selectivity for Am(III) over Eu(III).

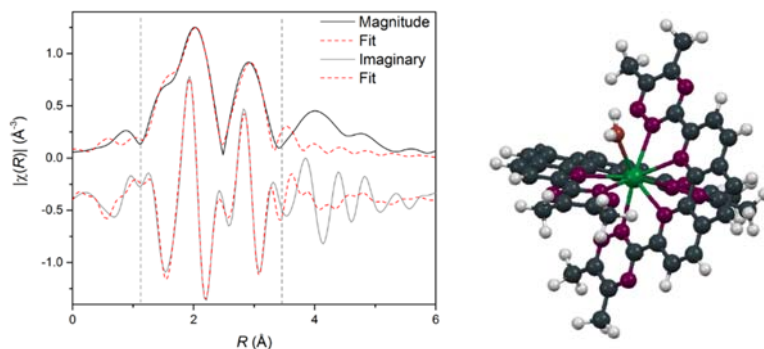


**Figure 3.** Fourier transform of the Eu L<sub>III</sub>-edge EXAFS spectrum (left) with accompanying fit afforded by the [Eu(BTPhen)<sub>2</sub>(H<sub>2</sub>O)]<sup>3+</sup> model from DFT (right).

### Selective Crystallization of Anion-Water Clusters with Self-Assembled Guanidines

We have discovered a new approach to aqueous anion separation based on selective crystallization of anion-water clusters with bis-guanidinium ligands self-assembled in situ by condensation of aminoguanidinium salts with simple dialdehydes such as glyoxal or terephthaldehyde. The resulting bis-iminoguanidinium (BIG) cations form extremely insoluble salts with tetrahedral oxoanions like sulfate, thus providing a simple and effective separation approach for this class of anions via crystallization. Single-crystal X-ray diffraction analyses showed the sulfate anions crystallized as extended [SO<sub>4</sub>(H<sub>2</sub>O)<sub>5</sub><sup>2-</sup>]<sub>n</sub> or discrete [(SO<sub>4</sub>)<sub>2</sub>(H<sub>2</sub>O)<sub>4</sub>]<sup>4-</sup> sulfate-water clusters, (Figure 4). The exceptionally low aqueous solubilities of these sulfate salts, comparable to SrSO<sub>4</sub> or BaSO<sub>4</sub>, were rationalized based on the favorable stacking of the rigid and planar BIG cations, and the reduced dehydration penalty of the sulfate-water clusters compared to the naked sulfate anion. Another important factor appears to be the entropically favorable release of solvent water molecules from the strongly hydrated sulfate anions, and from the planar and hydrophobic BIG cations. The real-world utility of this crystallization-based approach to sulfate separation was demonstrated by removing more than 99% of sulfate from seawater in a single step, which has the potential to mitigate scale problems in oil field operations.

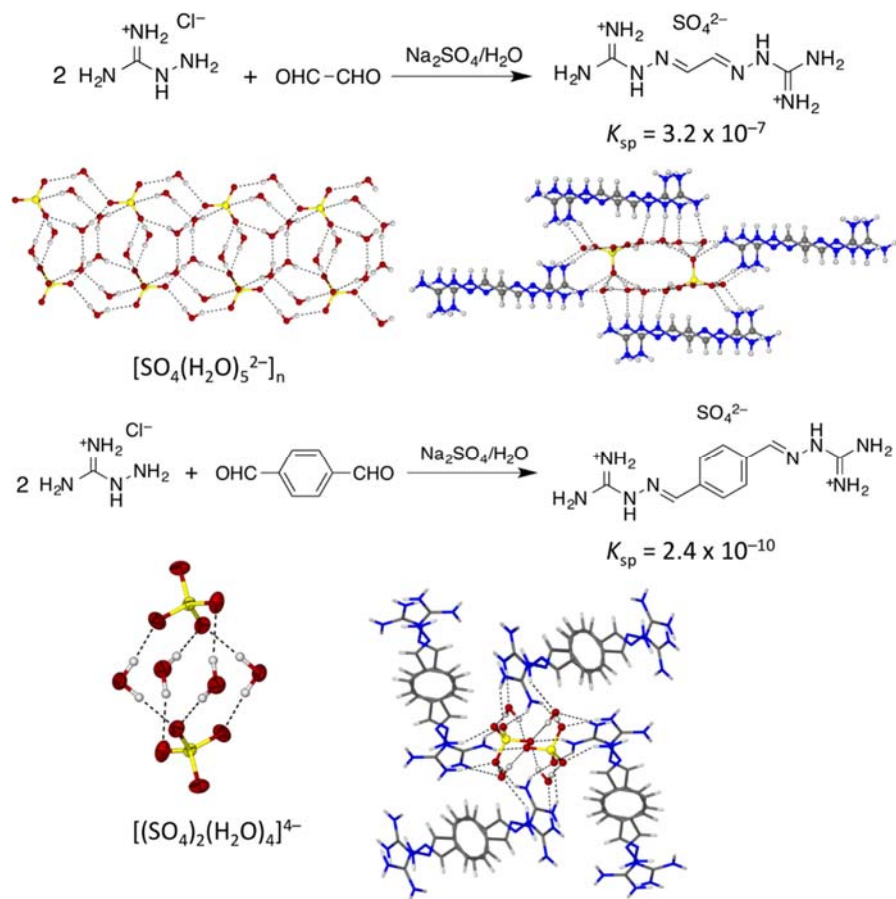


**Figure 4.** Selective crystallization of sulfate-water clusters with BIG ligands.

### CO<sub>2</sub> Capture from Ambient Air by Crystallization with a Guanidine Sorbent

Imine condensation of 2,6-pyridinedialdehyde with aminoguanidinium resulted in a bis-guanidine ligand capable of capturing atmospheric CO<sub>2</sub> as a crystalline carbonate salt of very low aqueous solubility. Single-crystal X-ray and neutron diffraction analyses revealed the presence of extended  $[\text{CO}_3(\text{H}_2\text{O})_4]^{2-}$  clusters hydrogen-bonded tightly inside the crystal by the guanidinium groups (Figure 5). The bound CO<sub>2</sub> can be released by relatively mild heating of the crystals at 80-120 °C, which regenerates the BIG ligand quantitatively. Thus, this crystallization-based approach offers the prospect for effective and economical carbon capture technologies

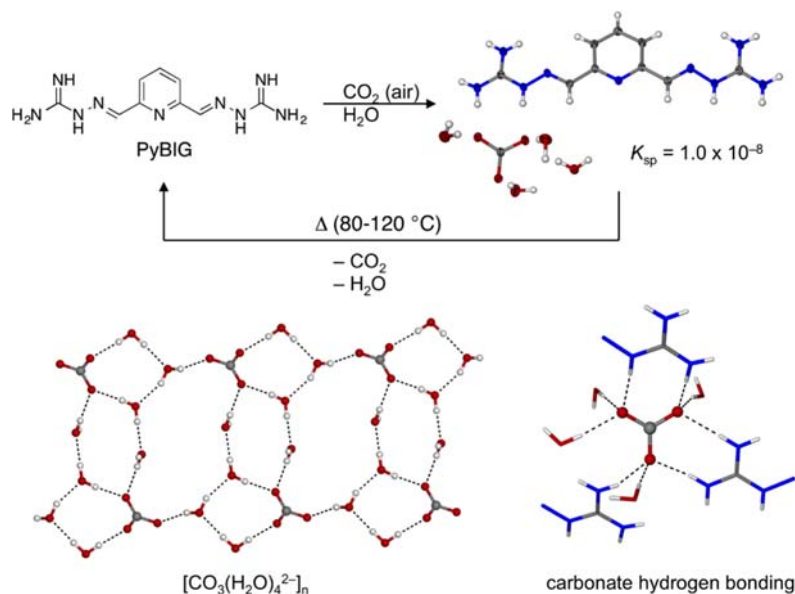


**Figure 5.** *CO<sub>2</sub> capture from ambient air by carbonate crystallization with a BIG ligand.*

### New Ionic Covalent Organic Framework (iCOF) for Selective Cr(VI) Removal

Selective chromium(VI) oxoanion removal has been demonstrated using a novel ionic covalent organic framework (iCOF). The ionic groups in this material are symmetrically positioned on the edges of the hexagonal pores, thus forming one-dimensional channels functionalized with anion-binding groups running throughout the three-dimensional superstructure (Figure 6). The monovalent anions in iCOF readily and quantitatively undergo exchange with the divalent oxoanions at close to neutral pH value, suggesting excellent accessibility of the cationic sites in the porous framework. Moreover, Cr(VI) oxoanions are selectively removed by iCOF in the presence of a variety of other tetrahedral oxoanions (e.g, sulfate and selenate). In a single treatment with iCOF, Cr(VI) concentration in aqueous solution is lowered from 1 ppm to 10 ppb level, which is an order of magnitude lower than the current US Environmental Protection Agency maximum contaminant level for total chromium of 100 ppb.

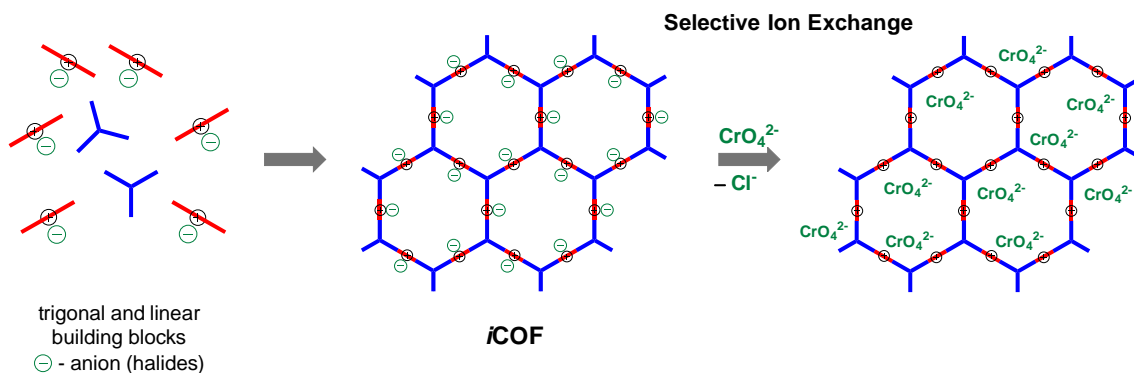


**Figure 6.** *Schematic representation of the synthesis of iCOF and ion exchange process.*

## Publications Acknowledging this Grant in 2015 – present

### (I) Exclusively funded by this grant;

1. Custelcean, R.; Williams, N. J.; Seipp, C. A. Aqueous Sulfate Separation by Crystallization of Sulfate–Water Clusters. *Angew. Chem., Int. Ed.* **2015**, *54* (36), 10525-10529.
2. Seipp, C. A.; Williams, N. J.; Bryantsev, V. S.; Custelcean, R.; Moyer, B. A. A Conformationally Persistent Pseudo-bicyclic Guanidinium for Anion Coordination as Stabilized by Dual Intramolecular Hydrogen Bonds. *RSC Advances* **2015**, *5*, 107266–107269.
3. Custelcean, R.; Williams, N. J.; Seipp, C. A.; Ivanov, A.; Bryantsev, V. S. Aqueous Sulfate Separation by Sequestration of  $[(\text{SO}_4)_2(\text{H}_2\text{O})_4]^{4-}$  Clusters within Highly Insoluble Imine-Linked Bis-Guanidinium Crystals. *Chem.-Eur. J.* **2015**, *1997-2003*.
4. Williams, N. J.; Bryantsev, V. S.; Custelcean, R.; Seipp, C. A.; Moyer, B. A.  $\alpha,\alpha',\alpha'',\alpha'''$ -Meso-Tetrahexyltetramethyl-Calix[4]Pyrrole: An Easy-to-Prepare, Isomerically Pure Anion Extractant with Enhanced Solubility in Organic Solvents. *Supramol. Chem.* **2016**, *28*, 176-187.
5. Ellis, R. J. Acid-Switched Eu(III) Coordination Inside Reverse Aggregates: Insights into a Synergistic Liquid-Liquid Extraction System. *Inorg. Chim. Act.* **2016**, *460*, 159-164.
6. Seipp, C. A.; Williams, N. J.; Custelcean, R. Sulfate Separation by Selective Crystallization with a Bis-Iminoguanidinium Ligand. *J. Vis. Exp.* **2016**, *115*, e54411.
7. Seipp, C. A.; Williams, N. J.; Kidder, M.; Custelcean, R. Effective CO<sub>2</sub> Capture from Ambient Air via Crystallization with a Guanidine Sorbent. *Angew. Chem., Int. Ed.* **2017**, *56* (4), 1042-1045.
8. Seipp, C. A.; Williams, N. J.; Bryantsev, V. S.; Moyer, B. A. A Simple Guanidinium Motif for the Selective Binding and Extraction of Sulfate. *Sep. Sci. Technol.* **2017**, *Online Only*, DOI: 10.1080/01496395.2017.1318922.
9. Ellis, R. J.; Reinhart, B.; Williams, N. J.; Moyer, B. A.; Bryantsev, V. S. Capping the Calix: How Toluene Completes Cesium(I) Coordination with Calix[4]pyrrole. *Chem. Commun.* **2017**, *53* (41), 5610-5613.

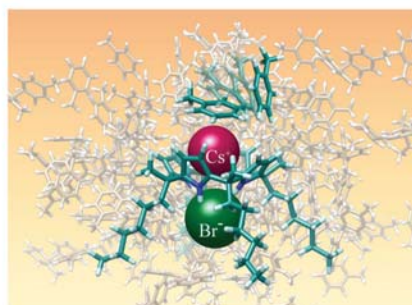
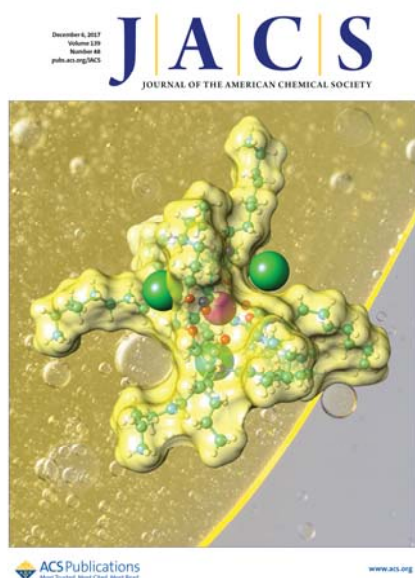
### (II) Jointly funded by this grant and other grants with leading intellectual contribution from this grant;

10. Tai, S.; Williams, N. J.; Carrick, J. D. Synthesis of Bis-1,2,4-triazines via Telescoped Condensation of [1,10]-Phenanthroline-2,9-dicarbonitrile with Aromatic 1,2-Dicarbonyls. *J. Heterocycl. Chem.* **2016**, *53* (1), 307-312.
11. Ellis, R. J.; Doidge, E. D.; Carson, I.; Takser, P.A.; Morrison, C. A.; Love, J. B. A Simple Primary Amide for the Selective Recovery of Gold from Secondary Resources. *Angew. Chem., Int. Ed.* **2016**, *55* (40), 12436-12439.
12. Williams, N. J.; Dehaut, J.; Bryantsev, V. S.; Luo, H.; Abney, C. W.; Dai, S. Selective Separation of Americium from Europium Using 2,9-Bis(triazine)-1,10-phenanthrolines in Ionic Liquids: A New Twist on an Old Story. *Chem. Commun.* **2017**, *53*, 2744-2747.
13. Jia, C.; Custelcean, R.; Wu, B. Highly Selective Binding of Choline by a Biomimetic Triple Anion Helicate. *Nat. Commun.* **2017**, *8* (1), 1-8.
14. Brigham, D.; Ivanov, A.; Moyer, B. A.; Delmau, L.; Bryantsev, V. S.; Ellis, R. J. Trefoil-shaped outer-sphere ion clusters mediate lanthanide(III) ion transport with diglycolamide ligands. *J. Am. Chem. Soc.* **2017**, *139*, 17350-17358.

### (III) Jointly funded by this grant and other grants with relatively minor intellectual contribution from this grant;

15. Sefat, A. S.; Li, L.; Cao, H.; McGuire, M. A.; Sales, B. C.; Custelcean, R.; Parker, D. S. Anomalous Magneto-Elastic and Charge Doping Effects in Thallium-doped BaFe<sub>2</sub>As<sub>2</sub>. *Sci. Rep.* **2016**, *6*, 21660.

## Journal Covers in 2017

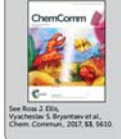


Outstanding research from Dr. Ella, Dr. Bryntseva, and co-authors at the Oak Ridge National Laboratory, USA, Argonne National Laboratory, USA, and University of Tennessee, Knoxville, USA

Capping the calix: how toluene completes cesium(I) coordination with calix[4]pyrene

EXAFS measurements and molecular simulations reveal a surprising interaction between the toluene solvent and the open face of the Cs(I) cation coordinated to calix[4]pyrene, with additional  $\pi$ - $\pi$  interactions that allow toluene to 'cap-the-calix'. The results show how 'non-interacting' solvents may not be as 'innocent' in ion recognition as previously assumed.

As featured in:



rsc.li/chemcomm  
Registered charity number: 207890

## Understanding Liquid:Liquid Interfacial Structure in Non-Ideal Systems

Aurora E. Clark

Department of Chemistry, Washington State University, Pullman, Wa 99164

### Presentation Abstract

In recent years advanced experimental and computational methods have begun to probe the underlying structure and dynamics directly at the liquid:liquid interface. This talk will detail key concepts as well as recent computational research regarding the physico-chemical characteristics of solvents and solutes directly within the phase boundary. This includes characterization of the capillary wave front at the phase boundary and its influence upon successive layers moving into the bulk solution, as well as the nuanced but impactful effects of surfactants upon hydrogen bonding and the geometric configurations adopted by interfacial surfactant molecules. Collaborative research that leverages vibrational sum frequency generation to understand interfacial structure will also be discussed.

**Grant or FWP Number:** Interfacial chemistry of actinide solvent extraction

**Postdoc(s):** Michael Servis

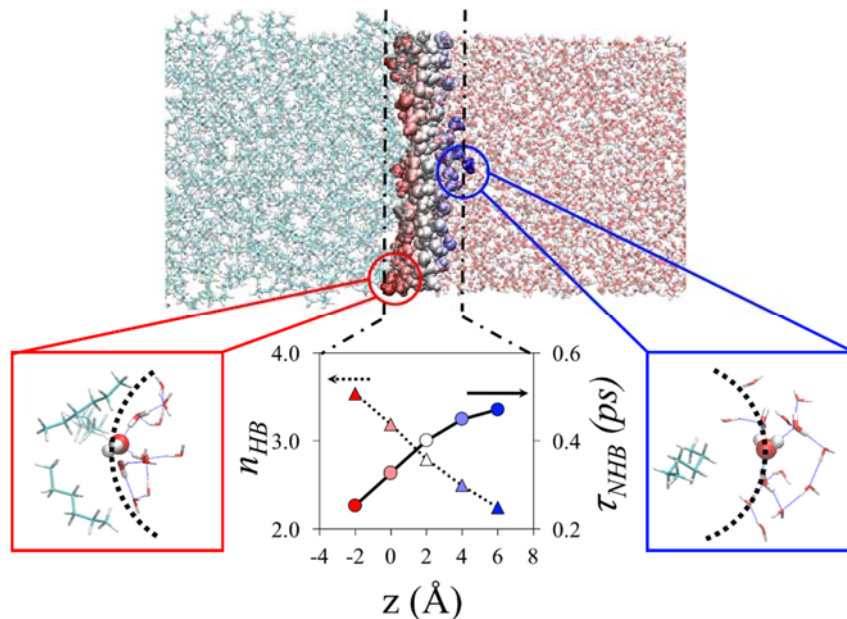
**Student(s):** Tiecheng Zhou, Alex McCue

### RECENT PROGRESS

#### *Interfacial Structure and Dynamics in Complex Aqueous:Organic Phase Boundaries.*

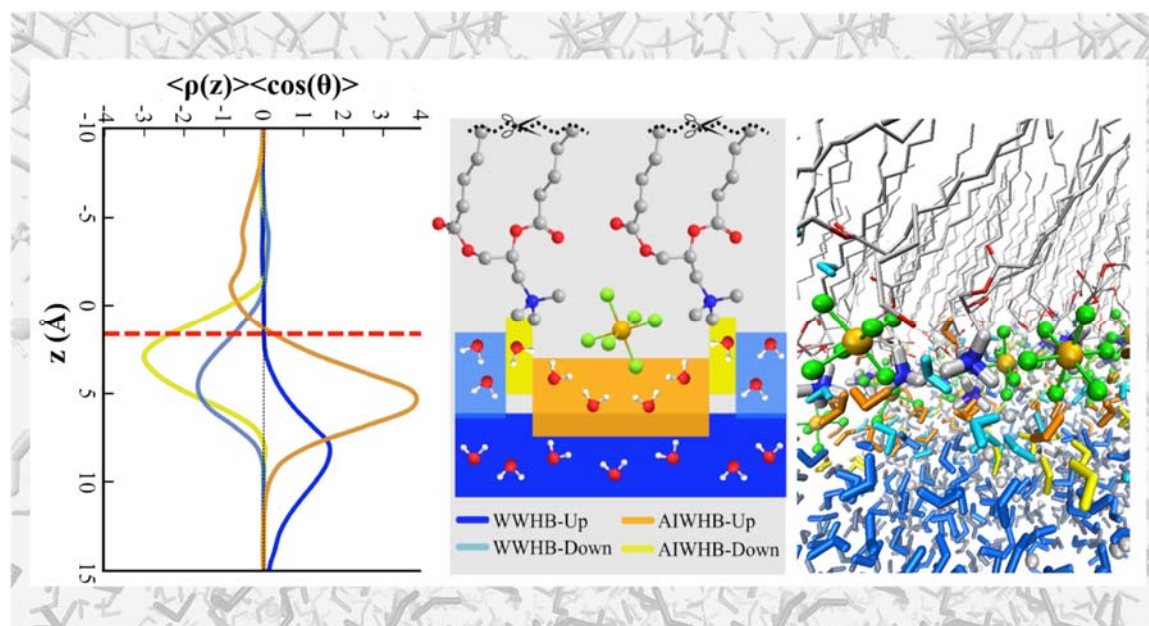
The structural and dynamic perturbations of the interfacial water molecules have been studied at different locations within the surface capillary waves. From both the structural and dynamic properties analyzed, it is found that these interfacial water molecules dominate the perturbations within the interfacial region, which can extend deep into the water phase relative to the Gibbs dividing surface. Of more importance, is the demonstration of structural and dynamic heterogeneity of the interfacial water molecules at the capillary wave front, as indicated by the dipole orientation and the structural and dynamic behavior of hydrogen bonds and their networks (Figure 1). Heterogeneity within the capillary wave may be highly relevant to kinetically driven processes at the interfaces, for example transport or chemical reactions that depend upon solvent organizations and dynamics (e.g. dissociative metal-ligand complexation reactions).

**Figure 1.** Side-on view of truly interfacial H<sub>2</sub>O at the water:hexane interface, with waters that are at the crest of the capillary wave (facing more waters) distinguished from those waters at the trough of the capillary wave (facing more hexane) and the differences in their number of hydrogen bonds and hydrogen bond lifetime.



This work has been followed by a highly successful collaboration with staff scientists at Argonne National Laboratory, led by Ahmet Uysal (Heavy Element Program). This work recognizes that water molecules form an ordered hydrogen-bonded network in a thin interfacial layer at the air/water interface. The extent of this orientational order is enhanced with the introduction of an electric field, for instance by a Langmuir monolayer with a charged headgroup on the water surface. When ions are adsorbed at the interface, they shield the water molecules from the electric field and disturb or destroy the water ordering in an ion specific way. However, a qualitatively different interfacial water structure as a result of the adsorbed ions has not previously been observed. Using surface sensitive vibrational sum frequency generation (VSFG) spectroscopy, we show that  $\text{PtCl}_6^{2-}$  ions, in concentrated LiCl solutions, eliminate the VSFG signal from the interfacial water-water hydrogen-bonding (WWHB) network and induce a unique, weakly hydrogen-bonded oriented water structure (Figure 2). Polarization dependent measurements and molecular dynamics (MD) simulations further elucidated the characteristics of this newly observed interfacial water structure, and the structural details of chlorometalate adsorption. Specifically, the addition of  $\text{PtCl}_6^{2-}$  causes two major changes to the VSFG spectra: the WWHB signal disappears, and the anion induced water hydrogen bond (AIWHB) signal appears. First, consider the disappearance of the WWHB signal. The addition of  $\text{I}^-$  to a DPTAP sub-phase produced the same VSFG observation, and was attributed to  $\text{I}^-$  adsorbing close to the DPTAP monolayer and completely screening water from the surface charge. The MD results confirm that  $\text{PtCl}_6^{2-}$  adsorbs close to the interface, but also suggests that the WWHB environment is significantly structured, in contrast to what would be assumed from previous  $\text{I}^-$  studies.

**Figure 2.** Dipole orientation (left), a simplified representation of the water structures MD predicts (middle), an actual MD snapshot of the differently oriented waters (right). The plot is the product of the average water number density ( $\langle\rho(z)\rangle$ ) and the average water orientation ( $\langle\cos(\theta)\rangle$ ) – where  $\theta$  is the angle between the water dipole vector and the surface normal – vs the z-dimension coordinate ( $z(\text{\AA})$ ).  $z(0)$  is the average position of the DPTAP N atoms, and the green dashed line is the average Pt position. MD plots 4 water sub-ensembles: (blue) water interacting with both  $\text{N}^+$  and  $\text{PtCl}_6^{2-}$ , (peach) water only interacting with  $\text{N}^+$ , (grey) water only interacting with  $\text{PtCl}_6^{2-}$ , and (yellow) water not interacting with  $\text{N}^+$  or  $\text{PtCl}_6^{2-}$ .



## Publications Acknowledging this Grant in 2015 – present

### (I) Exclusively funded by this grant;

1) Ghadar, Y.; Christiansen, S. L.; Clark, A. E. *Fluid Phase Equilibria*, **2016**, 407, 126-134. *Invited article – special issue Aqueous Solutions: Bulk Fluids and Interfaces.*

2) Clark, A. E.; Samuels, A.; Wisuri, K.; Landstrom, S.; Saul, T. *Inorganic Chemistry*, **2015**, 54, 6216-6225.

3) Ghadar, Y.; Parmar, P.; Samuels, A.; Clark, A. E. *Journal of Chemical Physics*, **2015**, 142, 104707.

4) Parmar, P.; Samuels, A.; Clark, A. E. *Journal of Chemical Theory and Computation*, **2015**, 11, 55-63.

### (II) Jointly funded by this grant and other grants with leading intellectual contribution from this grant;

5) Rock, W.; Qiao, B.; Zhou, T.; Clark, A. E.; Uysal, A. *Journal of Physical Chemistry Letters*, **2018**, submitted.

6) Zhou, T.; McCue, A.; Ghadar, Y.; Bako, I.; Clark, A. E. *Journal of Physical Chemistry B*, **2017**, *121*, 9052-9062.

7) Freiderich, J.; Burn, A.; Leigh, M.; Nash, K.; Clark, A. E. *Inorganic Chemistry*, **2017**, *56*, 4788-4795.

8) Kelley, M. P., Yang, P.; Clark, S. B.; Clark, A. E. *Inorganic Chemistry*, **2016**, *55*, 4992-4999.

9) Kelley, M.; Donley, A.; Clark, S.; Clark, A. E. *Journal of Physical Chemistry B* **2015**, *119*, 15652-15661.

*(III) Jointly funded by this grant and other grants with relatively minor intellectual contribution from this grant;*

10) Kelley, M. P.; Davis, A.; Clowers, B.; Clark, A. E.; Clark, S. B. *The Analyst*, **2017**, *142*, 4468-4475.

11) Hayes, T. R.; Bottorff, S. C.; Slocumb, W. S.; Barnes, C. L.; Clark, A. E.; Benny, P. D. *Dalton Transactions*, **2017**, *46*, 1134-1144

## Hierarchically Functional Iptycene-containing Polymers for Advanced Membrane Applications

Ruilan Guo

University of Notre Dame, Department of Chemical and Biomolecular Engineering

### Presentation Abstract

Polymeric membranes with good chemical, mechanical, and thermal stability in the process environment are needed in many emerging energy and environment technologies, ranging from membranes for gas separation, water purification, to clean energy production. This talk presents our recent efforts of developing a new membrane platform based on iptycene-containing polymers, with an emphasis on their uses as gas separation membranes and polyelectrolyte membranes (PEMs) for fuel cell. The rich structural hierarchy and chemistry versatility of iptycenes offer great opportunities for generating well-defined yet tailorable microstructures and introducing supramolecular interaction which synergistically lead to intriguing membrane properties. Two representative series of iptycene-based polymers, developed for gas separation membranes and PEM membranes, respectively, will be discussed. In particular, iptycene-based (i) microporous gas separations membranes with superior size sieving ability and (ii) nanostructured, multiblock copolymer PEMs for fuel cell applications will be presented. The discussion will focus on the macromolecular design motifs and the fundamental relationships between exquisitely tuned microstructures and macroscopic membrane properties for these innovative polymers.

### DE-SC0010330: Design, Synthesis and Characterization of Triptycene-Containing Macromolecules with Hierarchically Controlled Architectures as Functional Membrane Materials for Energy Applications

**Postdoc(s):** Shuangjiang Luo

**Student(s):** Jennifer Weidman, Greg Kline, Joseph Aboki

### RECENT PROGRESS

***Fundamental structure-property relationship of iptycene-based polyimides.*** We have developed two new synthesis strategies of iptycene monomers to identify the effects of key structure parameters on gas transport properties in iptycene-polyimides: (1) backbone linkage geometry, i.e., 1,4-*para*, 1,4-*ortho* and 2,6-*para* (**Figure 1a**); and (2) backbone rigidity by eliminating flexible ether linkages, i.e., 1,4-*direct* (**Figure 1b**). Microstructure and fractional free volume (FFV) analysis showed that the triptycene connection did not play a significant role, as 1,4-*para* and 2,6-*para* were nearly identical in FFV. Conversely, the *ortho* geometry has 20% lower FFV than the *para* geometry, suggesting more compact chain packing of the *ortho* structure. Correspondingly, the 1,4-*ortho* polyimide has the expectedly lowest permeability. While having the same overall FFV, the 2,6-*para* polymer

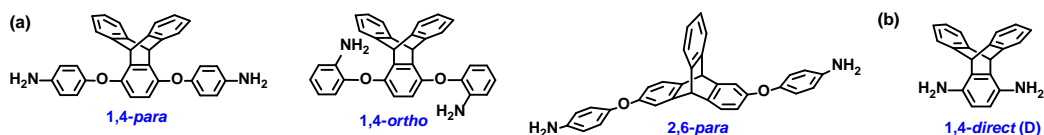


**Figure 1.** Structures of new triptycene monomers for the polyimides synthesis.

displays lower permeabilities than the 1,4-*para*, suggesting different microcavity size distribution between the two linkage geometries. While large variation in permeability is seen across the isomeric series, the selectivities are less sensitive to backbone geometry suggesting that the size sieving ability of triptycene-polyimides is governed largely by the intrinsic internal free volume elements of the triptycene moiety. Chain rigidity effect has been studied by preparing a highly sterically-hindered 1,4-*direct* diamine (**Figure 1b**) without flexible ether linkages such that imide rings are directly linked to rigid triptycene skeleton. Copolyimides were prepared with various 1,4-*direct* content to adjust the chain rigidity. The FFV shows a strong dependence on the composition and chain rigidity. Increasing the 1,4-*direct* content increases the FFV, i.e., the copolymer with the highest 1,4-*direct* content has the highest FFV and permeabilities. The copolyimides also show increased selectivities as more 1,4-*direct* units are included making the separation performance laterally approaching the upper bounds (**Figure 2**). This desirable trend is mainly due to the increase in diffusivity selectivity as revealed by analyzing diffusivity and solubility coefficients.

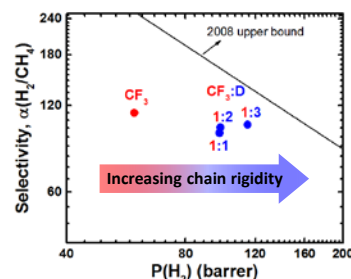


**Figure 2.** Chain rigidity effect on membrane performance.

**Triptycene-based polybenzoxazole (PBO) membranes.** We have successfully introduced for the first time the triptycene structure into PBO structures (also known as TR polymers). In particular, triptycene-based PBOs (TPBOs) were prepared via thermal treatment of *ortho*-functional triptycene-polyimide precursors with systematically varied composition to investigate how the microporosity and gas transport properties are altered by the precursor composition and *ortho*-functionality (**Figure 3**). The composition was adjusted by varying the molar ratio between triptycene-dianhydride and 6FDA (i.e., 0.25, 0.5, 0.75 and 1.0); the *ortho*-functionality of the precursors was altered by using different imidization method (thermal imidization for -OH groups and chemical imidization for acetate groups). All polyimides were fully imidized with target composition and *ortho*-functionality, which were then thermally converted to corresponding TPBOs following the

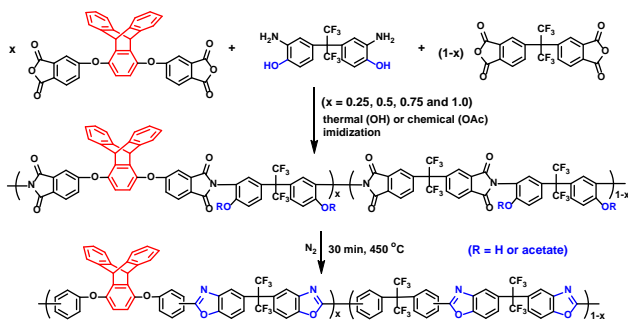


**Figure 3.** Preparation of triptycene-based PBOs.

same protocol (pretreated at 300 °C for 2 h and then 450 °C for 0.5 h in N₂). The completeness of the imide-to-benzoxazole conversion was confirmed by the structural changes using FTIR and weight loss measurements. The PBOs prepared from chemical imidized precursor showed the largest inter-chain spacing; the inter-chain spacing increased consistently with the

increase in the molar content of triptycene unit, suggesting the effective roles of triptycene units and bulky *ortho* group in chain packing disruption and microporous structure construction. Pure gas permeation results revealed that these TPBO films have extraordinarily high permeability and high selectivity for a wide range of gas pairs, such as H<sub>2</sub> separation (H<sub>2</sub>/N<sub>2</sub>, H<sub>2</sub>/CH<sub>4</sub>), air separation (O<sub>2</sub>/N<sub>2</sub>) and natural gas purification (CO<sub>2</sub>/CH<sub>4</sub>). All TPBOs exceed the 2008 upper bounds for these separations (**Figure 4**), with TPBO-1.0 and TPBO-Ac-1.0 exceeding the 2015 upper bound for H<sub>2</sub>/N<sub>2</sub> and H<sub>2</sub>/CH<sub>4</sub> separations.

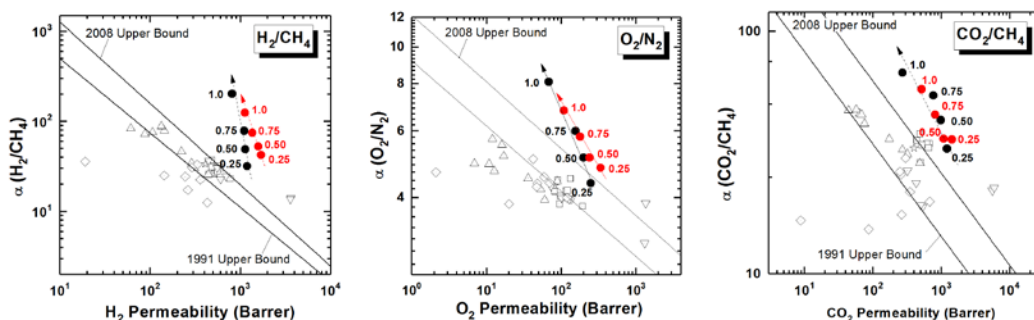


**Figure 4.** Representative upper bound plots for TPBO-OH-x (●) and TPBO-Ac-x (●) films.

***Semi-interpenetrating polymer network (S-IPN) membranes for CO<sub>2</sub> separations.*** We

have developed a new design strategy of S-IPNs membranes based on triptycene-containing polyimides entwined by crosslinked PEO networks to address the issue of weak mechanical stability of pure PEO-based membranes. The S-IPNs are consisted of crosslinked PEO networks penetrated by triptycene-based linear (co)polyimides. Six S-IPNs (**Figure 5**) were prepared to identify the effects of the composition and microstructure. Maintaining the same overall PEO content of ~70 wt%, the PEO networks are varied in crosslink density by crosslinking 600 or 2000 g/mol PEO oligomers; the linear polyimides used include either a homopolyimide (0 wt% PEO) or a PEO-*co*-imide copolymer of 24 or 34 wt% PEO. The S-IPNs are named as S-*x*-*y*, where “S” signifies S-IPN, “*x*” is the PEO weight content (wt%) in the linear polyimide component and “*y*” is the MW of PEO oligomers (600 or

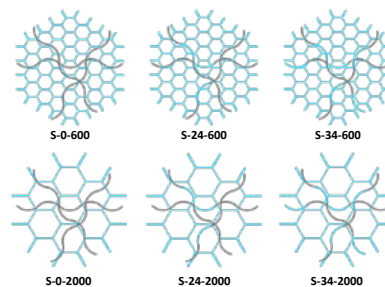


**Figure 5.** Schematics of S-IPNs. (blue: PEO network and segment; gray: linear polyimide chains)

2000) used for crosslinking. All S-IPNs are amorphous rubbery materials with degradation temperature above 300 °C. The S-IPN membranes showed significantly improved mechanical properties relative to crosslinked pure PEO membranes. For example, the tensile strength of the S-0-2000 membrane is ~ 6 times of the corresponding PEO2000 network film. Simultaneously, a significant enhancement in the ductility was also achieved. The gas permeability-selectivity tradeoff plots for CO<sub>2</sub>/H<sub>2</sub> are presented in **Figure 6**. All S-IPNs show plasticization-enhanced separation performance in that both gas

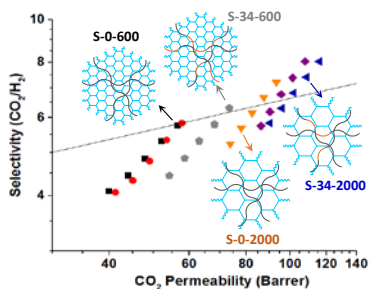


**Figure 6.** CO<sub>2</sub>/H<sub>2</sub> upper bound plot of S-IPN films (Five feed pressures at 3, 6, 10, 13, 17 bar).

permeability and selectivity increase with increasing the feed pressure, which is a known phenomenon for PEO-rich membranes. While all S-IPNs have similar overall PEO content, the separation performance showed large variations across the S-IPN composition. S-IPNs with a low crosslink density (PEO2000 network) outperform the ones with a high crosslink density (PEO600 one) due to a more loose chain packing. For the S-IPNs having the same PEO network, incorporating PEO sequences in the linear copolyimides improves the separation performance, due to greatly enhanced connectivity of CO<sub>2</sub>-philic PEO domains.

**Nanophase separated multiblock copolymer PEMs for fuel cell.** We have extended the iptycene concept to the synthesis of poly(arylene ether sulfone) multiblock copolymers as polyelectrolyte membranes (PEMs) for fuel cell. The idea is to exploit the supramolecular interlocking interaction of triptycene units to suppress excessive water swelling of PEMs while simultaneously promoting ion conductivity. Triptycene units are introduced into the hydrophobic blocks which are coupled with fully sulfonated hydrophilic blocks to form multiblock copolymers with alternating hydrophilic-hydrophobic sequences (**Figure 7**). The block length was controlled by offsetting the stoichiometry of the monomers in polycondensation to produce telechelic oligomers of 5000, 7000, 10000 and 15000 g/mol.

Correspondingly, multiblock copolymers produced with different block length combination were named as BPS100-TRP0-x-y (x and y are the MWs of each blocks).

While water uptake (wt%) showed a monotonically increasing trend with increasing the block length as expected, ranging from 49% in 5K-5K sample to 105% in 15K-15K one, the volume swelling ratio displayed an unusual trend which is first increasing and then decreasing with block length. Comparing to other non-triptycene 15K-15K multiblock copolymers, BPSH100-TRP0-15K-15K has significantly reduced water swelling with similarly high water uptake (**Figure 8**). These results confirm that the supramolecular interlocking interaction induced by the triptycene units is highly effective in restrict water swelling. Membrane morphology analysis by AFM and SAXS shows distinct nanophase separated structure (**Figure 8**). In particular, the 15K-15K film has a clear lamellar morphology with nanophase separated “fingerprint-type” structure such that the connectivity of hydrophilic domains is greatly improved leading to its excellent proton conductivity of 150 mS/cm (25 °C in liquid water).

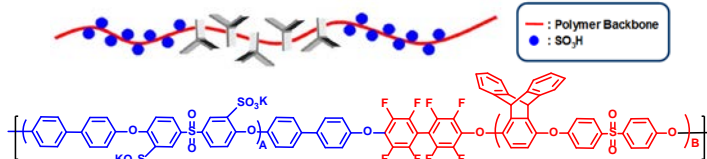


**Figure 7.** Schematics of BPS100-TRP0 multiblock copolymers with alternating hydrophilic-hydrophobic blocks

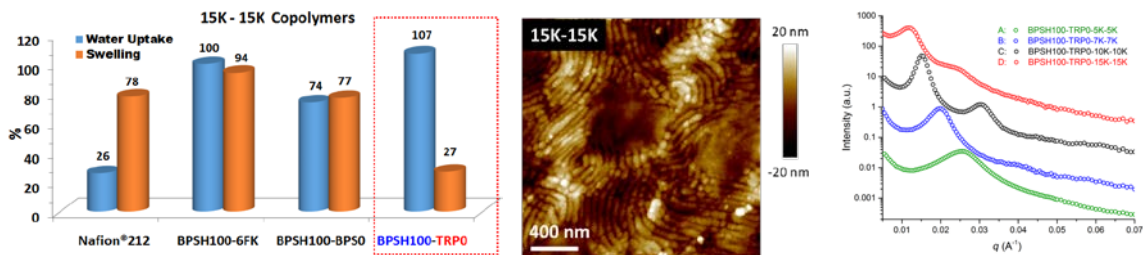


**Figure 8.** Left: Triptycene-containing 15K-15K multiblock copolymer shows significantly suppressed water swelling; middle: AFM height image shows periodic lamellar structure for 15K-15K film; right: SAXS profiles confirm a lamellar organization of the nanophase-separated domains in these triptycene-containing multiblock copolymers.

## Publications Acknowledging this Grant in 2015 – present

### (I) Exclusively funded by this grant;

1. Luo, S.; Zhang, Q.; Bear, T.K.; Curtis, T.E.; Roeder, R.K.; Doherty, C.M.; Hill, A.J.; Guo, R. Triptycene-containing Poly(benzoxazole-co-imide) Membranes with Enhanced Mechanical Strength for High-Performance Gas Separation. *Journal of Membrane Science*, **2017**, in revision.
2. Aboki, J.; Jing, B.; Luo, S.; Zhu, Y-X.; Zhu, L.; Guo, R. Highly Proton Conducting Polyelectrolyte Membranes with Unusual Water Swelling Behavior Based on Triptycene-containing Poly(arylene ether sulfone) Multiblock Copolymers. *ACS Applied Materials and Interfaces*, **2017**, accepted (DOI: 10.1021/acsami.7b13542).
3. Kline, K. G.; Zhang, Q.; Weidman, J. R.; Guo, R. PEO-rich Semi-Interpenetrating Polymer Networks (s-IPNs) for CO<sub>2</sub> Separation, *Journal of Membrane Science*, **2017**, *544*, 143-150.
4. Kline, K. G.; Weidman, J. R.; Zhang, Q.; Guo, R. Studies of the Synergistic Effects of Crosslink Density and Crosslink Inhomogeneity on Crosslinked PEO Membranes for CO<sub>2</sub>-selective Separations. *Journal of Membrane Science*, **2017**, *544*, 25-34.
5. Kushwaha, A.; Dose, M. E.; Luo, S.; Freeman, B. D., Guo, R. Polybenzoxazole-based Gas Separation Membranes Prepared from the blends of API and PHA. *Separation and Purification Technology*, **2017**, *184*, 384–393.
6. Luo, S.; Liu, J.; Lin, H.; Kazanowska, B.; Hunckler, M. D.; Roeder, R. K.; Guo, R. Preparation and gas transport properties of triptycene-containing polybenzoxazole (PBO)-based polymers derived from thermal rearrangement (TR) and thermal cyclodehydration (TC) processes. *Journal of Materials Chemistry A*, **2016**, *4*, 17050–17062.
7. Luo, S.; Wiegand, J. R.; Gao, P.; Doherty, C. M.; Hill, A. J.; Guo, R. Molecular Origin of Fast and Selective Gas Transport in Pentriptycene-containing Polyimide Membranes. *Journal of Membrane Science*, **2016**, *518*, 100–109.
8. Luo, S.; Wiegand, J. R.; Kazanowska, B.; Gao, P.; Doherty, C. M.; Konstas, K.; Hill, A. J.; Guo, R. Finely Tuning the Free Volume Architecture in Iptycene-containing Polyimides for Highly Selective and Fast Hydrogen Transport. *Macromolecules*, **2016**, *49*(9), 3395–3405.
9. Luo, S.; Stevens, K. A.; Park, J-S.; Moon, J. D.; Liu, Q.; Freeman, B. D.; Guo, R. Highly CO<sub>2</sub>-selective Gas Separation Membranes Based on Segmented Copolymers of Poly(ethylene oxide) Reinforced with Pentriptycene-containing Polyimide Hard Segments. *ACS Applied Materials & Interfaces*, **2016**, *8*(3), 2306–2317.
10. Luo, S.; Liu, Q.; Zhang, B.; Wiegand, J. R.; Freeman, B. D.; Guo, R. Pentriptycene-based polyimides with hierarchically controlled molecular cavity architecture for efficient membrane gas separation. *Journal of Membrane Science*, **2015**, *480*, 20–30.

### (II) Jointly funded by this grant and other grants with leading intellectual contribution from this grant;

1. (*Invited*) Weidman, J. R.; Luo, S.; Breier, J. M.; Buckley, P.; Gao, P.; Guo, R. Triptycene-Based Copolyimides with Tailored Backbone Rigidity for Enhanced Gas Transport (Special Issue of “*Porous Polymers*”), *Polymer*, **2017**, *126C*, 314-323.
2. (*Invited*) Weidman, J. R.; Guo, R. The Use of Iptycenes in Rational Macromolecular Design for Gas Separation Membrane Applications (Special Issue of “*2017 Class of Influential Researchers*”), *Industrial & Engineering Chemistry Research*, **2017**, *56(15)*, 4220–4236.
3. (*Invited and highlighted in cover page*) Weidman, J. R.; Luo, S.; Zhang, Q.; Guo, R. Structure Manipulation in Triptycene-Based Polyimides through Main Chain Geometry Variation and Its Effect on Gas Transport Properties (Special Issue of “*Best Presentation of ACS 2016 Philadelphia*”), *Industrial & Engineering Chemistry Research*, **2017**, *56(7)*, 1868–1879.
4. Weidman, J. R.; Luo, S.; Doherty, C. M.; Hill, A. J.; Gao, P.; Guo, R. Analysis of Governing Factors Controlling Gas Transport Through Fresh and Aged Triptycene-based Polyimide Films. *Journal of Membrane Science*, **2017**, *522*, 12–22.

(III) *Jointly funded by this grant and other grants with relatively minor intellectual contribution from this grant;*

**Joseph T. Hupp**

**DE-FG02-08ER15967: Coordination-Chemistry-Derived Materials Featuring Nanoscale Porosity and Selective Chemical Separation**

No extended abstract available.

## Fundamental Studies of Novel Separations

Sheng Dai, Principal Investigator

Co-PIs: De-en Jiang and Shannon Mahurin

Research Team: Jinshui Zhang (ORNL former postdoc), Ziqi Tian (UCR former postdoc); Jennifer Schott (UTK graduate student), Song Wang (UCR graduate student), Nicole Onishi (UCR graduate student); Weihong Wu (UCR visiting student), Peipei Li (ORNL visiting student)

Overall research goals: The overarching goal of this program is to investigate fundamental issues of chemical separations by nanostructured architectures and unconventional media that selectively bind and/or transport target molecular species via tailored interactions. Currently, the systems of study include novel nanoporous materials and porous ionic liquids with a focus on separation of energy-relevant gaseous species.

### Significant achievements in 2016-2018:

(1) We pioneered the development of porous liquids as unique separation media. The structural characteristics and adsorption properties were investigated. We further examined these novel nanostructured liquids with intrinsic porosity for membrane gas transport.

(2) We continued our innovation in synthesis methodologies for novel mesoporous carbons, porous organic polymers, and functionalized ionic liquids. Their gas-separation performances were evaluated and gas uptake and diffusivity were computationally simulated to establish a structure-property relationship.

(3) We demonstrated from simulations that an ion-gated graphene membrane comprising a monolayer of ionic liquid coated porous graphene can dynamically modulate the pore size to achieve selective gas separation. This approach enables the otherwise non-selective large pores on the order of 1 nm in size to be selective for gases of three to four angstroms in diameter.

### Science objectives for 2018-2019:

Examine gas transport properties of porous ionic liquids and polymer membranes by combining carbon nano-shells with a viscous ionic liquid and measuring permeability and selectivity.

Neutron scattering will be explored as methods to correlate structure and transport properties of gas adsorption and diffusion in ionic liquids and carbon materials.

Design and simulate porous liquids based on cage compounds and deep eutectic solvents.

Develop advanced pore-size control concepts in ultrathin membranes made of graphene layers and ionic liquids.

### Selected references to work supported by this project 2016-2018:

Tian, Z. Q.; Mahurin, S. M.; Dai, S.; Jiang, D. E. Ion-Gated Gas Separation through Porous Graphene. *Nano Lett.* **2017**, *17*, 1802-1807.

Tao, D. J.; Chen, F. F.; Tian, Z. Q.; Huang, K.; Mahurin, S. M.; Jiang, D. E.; Dai, S. Highly Efficient Carbon Monoxide Capture by Carbanion-Functionalized Ionic Liquids through C-Site Interactions. *Angew. Chem.-Int. Edit.* **2017**, *56*, 6843-6847

Li, P. P.; Schott, J. A.; Zhang, J. S.; Mahurin, S. M.; Sheng, Y. J.; Qiao, Z. A.; Hu, X. X.; Cui, G. K.; Yao, D. D.; Brown, S.; Zheng, Y. P.; Dai, S. Electrostatic-Assisted Liquefaction of Porous Carbons. *Angew. Chem.-Int. Edit.* **2017**, *56*, 14958-14962.

Zhang, J. S.; Schott, J. A.; Li, Y. C.; Zhan, W. C.; Mahurin, S. M.; Nelson, K.; Sun, X. G.; Paranthaman, M. P.; Dai, S. Membrane-Based Gas Separation Accelerated by Hollow Nanosphere Architectures. *Adv. Mater.* **2017**, *29*, 1603797.

- Zhu, X.; Tian, C. C.; Do-Thanh, C. L.; Dai, S. Two-Dimensional Materials as Prospective Scaffolds for Mixed-Matrix Membrane-Based CO<sub>2</sub> Separation. *ChemSusChem* **2017**, *10*, 3304-3316.
- Zhu, X.; Ding, S. M.; Abney, C. W.; Browning, K. L.; Sacci, R. L.; Veith, G. M.; Tian, C. C.; Dai, S. Superacid-promoted synthesis of highly porous hypercrosslinked polycarbazoles for efficient CO<sub>2</sub> capture. *Chem. Commun.* **2017**, *53*, 7645-7648.
- Zhang, P. F.; Zhang, J. S.; Dai, S. Mesoporous Carbon Materials with Functional Compositions. *Chem.-Eur. J.* **2017**, *23*, 1986-1998.
- Zhang, P. F.; Wang, L.; Yang, S. Z.; Schott, J. A.; Liu, X. F.; Mahurin, S. M.; Huang, C. L.; Zhang, Y.; Fulvio, P. F.; Chisholm, M. F.; Dai, S. Solid-state synthesis of ordered mesoporous carbon catalysts via a mechanochemical assembly through coordination cross-linking. *Nat. Commun.* **2017**, *8*, 15020.
- Zhang, P. F.; Dai, S. Mechanochemical synthesis of porous organic materials. *J. Mater. Chem. A* **2017**, *5*, 16118-16127.
- Yang, D. Z.; Han, Y. L.; Qi, H. B.; Wang, Y. B.; Dai, S. Efficient Absorption of SO<sub>2</sub> by EmimCl-EG Deep Eutectic Solvents. *ACS Sustain. Chem. Eng.* **2017**, *5*, 6382-6386.
- Wu, W. H.; Tian, Z. Q.; Wang, S.; Peng, C. J.; Liu, H. L.; Dai, S.; Jiang, D. E. Design of Calix-Based Cages for CO<sub>2</sub> Capture. *Ind. Eng. Chem. Res.* **2017**, *56*, 4502-4507.
- Wang, S.; Tian, Z. Q.; Dai, S.; Jiang, D. E. Optimal Size of a Cylindrical Pore for Post-Combustion CO<sub>2</sub> Capture. *J. Phys. Chem. C* **2017**, *121*, 22025-22030.
- Shan, W. D.; Zhang, P. F.; Yang, S. Z.; Zhu, H. Y.; Wu, P. W.; Xing, H. B.; Dai, S. Sustainable synthesis of alkaline metal oxide-mesoporous carbons via mechanochemical coordination self-assembly. *J. Mater. Chem. A* **2017**, *5*, 23446-23452.
- Huang, Y. J.; Cui, G. K.; Zhao, Y. L.; Wang, H. Y.; Li, Z. Y.; Dai, S.; Wang, J. J. Preorganization and Cooperation for Highly Efficient and Reversible Capture of Low-Concentration CO<sub>2</sub> by Ionic Liquids. *Angew. Chem.-Int. Edit.* **2017**, *56*, 13293-13297.
- Zhu, X.; Tian, C. C.; Veith, G. M.; Abney, C. W.; Dehaut, J.; Dai, S. In Situ Doping Strategy for the Preparation of Conjugated Triazine Frameworks Displaying Efficient CO<sub>2</sub> Capture Performance. *J. Am. Chem. Soc.* **2016**, *138*, 11497-11500.
- Zhu, W. S.; Gao, X.; Li, Q.; Li, H. P.; Chao, Y. H.; Li, M. J.; Mahurin, S. M.; Li, H. M.; Zhu, H. Y.; Dai, S. Controlled Gas Exfoliation of Boron Nitride into Few-Layered Nanosheets. *Angew. Chem.-Int. Edit.* **2016**, *55*, 10766-10770.
- Tian, Z. Q.; Dai, S.; Jiang, D. E. Site Partition: Turning One Site into Two for Adsorbing CO<sub>2</sub>. *J. Phys. Chem. Lett.* **2016**, *7*, 2568-2572.
- Sheng, Y. J.; Chen, Q. B.; Yao, J. Y.; Lu, Y. X.; Liu, H. L.; Dai, S. Guest-Induced Breathing Effect in a Flexible Molecular Crystal. *Angew. Chem.-Int. Edit.* **2016**, *55*, 3378-3381.
- Nelson, K. M.; Mahurin, S. M.; Mayes, R. T.; Williamson, B.; Teague, C. M.; Binder, A. J.; Baggetto, L.; Veith, G. M.; Dai, S. Preparation and CO<sub>2</sub> adsorption properties of soft-templated mesoporous carbons derived from chestnut tannin precursors. *Microporous Mesoporous Mat.* **2016**, *222*, 94-103.
- Meng, B.; Li, H. Y.; Mahurin, S. M.; Liu, H. L.; Dai, S. Hyper-crosslinked cyclodextrin porous polymer: an efficient CO<sub>2</sub> capturing material with tunable porosity. *RSC Adv.* **2016**, *6*, 110307-110311.
- Li, X. F.; Chi, M. F.; Mahurin, S. M.; Liu, R.; Chuang, Y. J.; Dai, S.; Pan, Z. W. Graphitized hollow carbon spheres and yolk-structured carbon spheres fabricated by metal-catalyst-free chemical vapor deposition. *Carbon* **2016**, *101*, 57-61.
- Li, H. Y.; Meng, B.; Chai, S. H.; Liu, H. L.; Dai, S. Hyper-crosslinked beta-cyclodextrin porous polymer: an adsorption-facilitated molecular catalyst support for transformation of water-soluble aromatic molecules. *Chem. Sci.* **2016**, *7*, 905-909.
- Jin, T.; Xiong, Y.; Zhu, X.; Tian, Z. Q.; Tao, D. J.; Hu, J.; Jiang, D. E.; Wang, H. L.; Liu, H. L.; Dai, S. Rational design and synthesis of a porous, task-specific polycarbazole for efficient CO<sub>2</sub> capture. *Chem. Commun.* **2016**, *52*, 4454-4457.
- Jiang, F.; Jin, T.; Zhu, X.; Tian, Z. Q.; Do-Thanh, C. L.; Hu, J.; Jiang, D. E.; Wang, H. L.; Liu, H. L.; Dai, S. Substitution Effect Guided Synthesis of Task-Specific Nanoporous Polycarbazoles with Enhanced Carbon Capture. *Macromolecules* **2016**, *49*, 5325-5330.
- Chen, F. F.; Huang, K.; Zhou, Y.; Tian, Z. Q.; Zhu, X.; Tao, D. J.; Jiang, D. E.; Dai, S. Multi-Molar Absorption of CO<sub>2</sub> by the Activation of Carboxylate Groups in Amino Acid Ionic Liquids. *Angew. Chem.-Int. Edit.* **2016**, *55*, 7166-7170.

# **Wednesday PI Oral Presentations**

**Diffusion and Partitioning Behavior of Fluorescent Single Molecules within Surfactant-Filled Cylindrical Silica Nanopores**

Takashi Ito, Ruwandi Kumarasinghe, and Daniel A. Higgins  
Department of Chemistry, Kansas State University

**Presentation Abstract**

Molecular confinement within nanoscale pores plays an essential role in size-selective chemical separations and stereoselective catalytic reactions. Previously, we measured the dynamic behavior of single perylene diimide (PDI) molecules confined to surfactant- and solvent-filled silica nanopores of cylindrical geometry and uniform diameters (~ 4 nm). However, it was challenging to identify the exact diffusion pathways of these solute molecules within the pores. The nanopores have multiple possible pathways, including along the nonpolar micelle cores formed from the surfactants and the hydrophilic interfaces along the silica pore walls. Here, we use a polarity-sensitive fluorescent dye, Nile Red (NR), as a model hydrophobic solute to identify its diffusion pathway in the silica nanopores. NR fluorescence dramatically shifts to a longer wavelength in polar environments, as explained by Lippert-Mataga theory. The local polarity around NR molecules within individual pores is determined at the single-molecule level by recording fluorescence videos simultaneously in two different spectral bands. These measurements show that 1D-diffusing NR molecules are located in very nonpolar regions. Meanwhile, single-molecule emission polarization measurements reveal that 1D-diffusing NR molecules are tightly confined to nanoscale pathways. The accessible diameter of the pores, estimated from the maximum wobbling angle exhibited by NR, is about 1 nm, close to that of the PDI molecules in our previous reports. These results indicate that hydrophobic molecules diffuse along the nonpolar cores of the surfactant micelles within the silica nanopores. These measurements help clarify the molecular-level origins of the unique selectivity afforded by nanoporous materials in separations and catalysis, and thus will aid in the engineering of improved nanoporous materials.

**DE-SC0002362: SISGR: Molecular-Level Investigations of Diffusion Behavior within Cylindrical Nanoscale Pores**

**PI:** Takashi Ito, **Co-PI:** Daniel A. Higgins

**Students:** Dr. Khanh-Hoa Tran-Ba, Dr. Seok Chan Park, Dr. Hao Xu, Dol Raj Sapkota, Ruwandi Kumarasinghe, Govinda Ghimire, Herman Coceancigh, Zeinab Harandizadeh

**RECENT PROGRESS**

*Ensemble and Single-Molecule Diffusion Measurements within Identical Regions of Nanostructured Materials<sup>2</sup>*

The permeability of a nanoporous material is conventionally assessed using flux data obtained from a large number of solute molecules permeating across the overall material. However, these ensemble-averaged data are not suitable to evaluate the intrinsic permeability of the nanopores due to the presence of (sub-)μm-scale material heterogeneity (*e.g.*, tortuosity, defects). Recently, we have demonstrated ensemble and single-molecule diffusion measurements within identical μm-scale sample regions using two different fluorescence microscopy techniques, and evaluated the contribution of material heterogeneity to overall permeability. Our samples comprised a thin film of polystyrene-*block*-poly(ethylene oxide) (PS-*b*-PEO) incorporating aligned cylindrical PEO microdomains (*ca.* 30 nm in diameter). We investigated the diffusion of fluorescent molecules (sulforhodamine B, SRB) within the cylindrical nanostructures using both fluorescence recovery after photobleaching (FRAP) and single-molecule tracking (SMT) methods, without changing the measurement position (**Figure 1**). FRAP provided the ensemble diffusion direction ( $\overline{\theta}_{FRAP}$ ) and diffusion coefficient ( $D_{FRAP}$ ) across the entire focal depth (**Table 1**), in addition to the long-range (> 100 μm) microdomain connectivity, which is challenging to obtain using SMT. SMT provided the diffusion direction ( $\theta_{SMT}$ ) and diffusion coefficient ( $D_{SMT}$ ) of individual molecules across the entire film thickness. The consistency between FRAP data ( $\overline{\theta}_{FRAP}$  and  $D_{FRAP}$ ) and the average of the SMT data ( $\overline{\theta}_{SMT}$  and  $\overline{D}_{SMT}$ , **Table 1**) indicates the presence of well-aligned and defect-free cylindrical microdomains on length scales > 100 μm. The diffusion coefficients reflect the SRB permeability of the PEO microdomains.

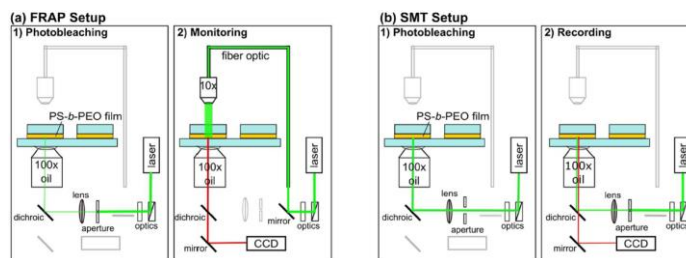


**Figure 1.** Experimental setups for (a) FRAP and (b) SMT measurements at an identical location.

**Table 1. Comparison between FRAP and SMT Data Measured at Identical Sample Areas in a Thin PS-*b*-PEO Film.**

Position	$\overline{\theta}_{FRAP}$ (°)	$\overline{\theta}_{SMT}$ (°)	$D_{FRAP}$ (μm <sup>2</sup> /s)	$\overline{D}_{SMT}$ (μm <sup>2</sup> /s)
$x = 0$ mm	$0 \pm 1$	$0 \pm 4$	$1.0 \pm 0.3$	$1.0 \pm 1.2$
$x = 0.5$ mm	$-2 \pm 1$	$2 \pm 16$	$1.5 \pm 0.7$	$1.1 \pm 1.1$

### ***Diffusion and Partitioning Behavior of Single Fluorescent Molecules within Surfactant-Filled Cylindrical Silica Nanopores***<sup>3,4</sup>

Selectivity and efficiency in chemical separations and catalysis with nanoporous materials are controlled by the mass transport, adsorption/desorption and partitioning of solute molecules within the nanoscale pores that incorporate distinct chemical environments. Such dynamic processes have conventionally been discussed on the basis of ensemble-averaged data obtained from a large number of molecules in different nanoscale environments. However, extensive averaging prevents the investigation of detailed molecular-level behavior in heterogeneous media. Single-molecule tracking (SMT) and related methods provide a means to visualize the motions of individual fluorescent solute molecules in different nanoscale environments. Previously, we employed SMT to study the diffusional behavior of individual molecules confined to cylindrical surfactant-filled silica nanopores (4-10 nm in diameter). Both cetyltrimethylammonium bromide (CTAB) and Pluronic surfactants were employed as pore templates. We established the means to quantitatively evaluate the morphologies, dimensions and permeability of the nanopores from SMT data. In addition, we assessed the average orientation and orientational wobbling behavior of single molecules diffusing along CTAB-filled cylindrical silica nanopores via single-molecule emission

polarization (SMEP) measurements. Results from SMEP measurements suggested that hydrophobic PDI molecules were confined to nanoscale pathways that were much smaller (*ca.* 1 nm) than the silica pore diameter (*ca.* 4 nm). We postulated that the hydrophobic dye molecules were confined to the nonpolar cores of the CTAB micelles as they diffused within the pores.

Recently, we worked to identify the diffusion pathway of hydrophobic solute molecules in the CTAB-filled silica nanopores. These studies used a solvatochromic dye, Nile Red, NR. NR exhibits a red-shift in its fluorescence emission with increasing polarity of the surrounding environment (**Figure 2**). The local polarity around the NR molecules was determined by recording the fluorescence intensity in two different spectral bands ( $580 \pm 20$  nm and  $625 \pm 20$  nm; **Figure 2**). The emission intensities in these bands,  $I_{580}$  and  $I_{625}$ , were then used to determine the dielectric constant,  $\epsilon$ , of the environment around each molecule using the following equation:

$$E \equiv \frac{I_{625} - I_{580}}{I_{625} + I_{580}} = K \left( \frac{\epsilon - 1}{2\epsilon + 1} \right) + C$$

In this equation,  $K$  and  $C$  are determined from standard solutions of known  $\epsilon$  such as mixtures of *n*-hexane and ethanol. **Figure 3a** shows single-molecule tracking data simultaneously recorded in the two spectral bands. The  $E$  values obtained from individual 1D-diffusing molecules (**Figure 3b**) indicate that the majority of the NR molecules were in nonpolar environments with  $\epsilon$  close to that of *n*-hexane. Meanwhile, SMEP images (**Figure 4a**) indicate that the 1D-diffusing NR molecules were also oriented along the long axis of the CTAB-filled silica nanopores, as was also observed for PDI molecules. The wobbling angle from SMEP data gave a pathway diameter of *ca.* 1 nm for 1D-diffusing NR molecules, suggesting that the hydrophobic solute molecules were confined to the nonpolar micelle cores (**Figure 4b**).

We have also compared the diffusional behavior of PDI molecules having different charges in flow-aligned cylindrical silica nanopores filled with Pluronic F127 (*ca.* 10 nm in diameter). We showed that uncharged PDI molecules partitioned to and diffused along the cylindrical surfactant-filled nanopores, whereas charged PDI molecules could pass through defects in the silica pore wall (**Figure 5**), suggesting they were present in more hydrophilic regions near the pore walls.

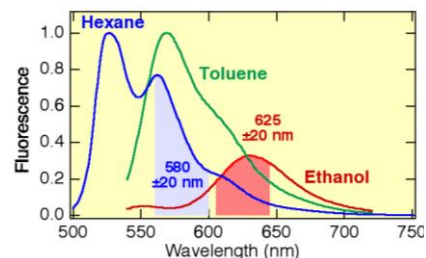


**Figure 2.** Fluorescence spectra of NR in different solvents. Two spectral bands represent those monitored in single-molecule experiments.

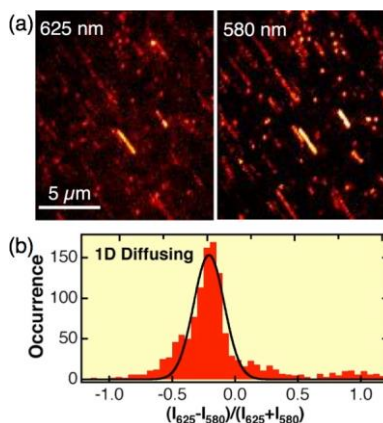


**Figure 3.** (a) Z-projection images of single NR molecules recorded at the two spectral bands. (b) Distribution of  $E$  for 1D-diffusing molecules.

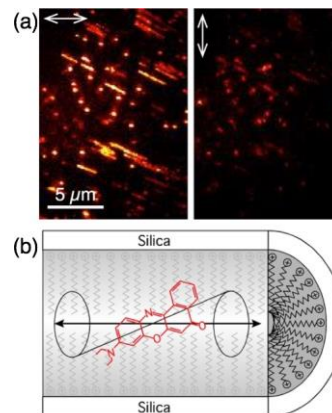


**Figure 4.** (a) Z-projection SMEP images of single NR molecules acquired for the orthogonal emission polarizations. (b) Schematic illustration of a NR molecule in a CTAB-filled silica nanopore.

## Molecular Diffusion and Distribution in Organic Nanotubes<sup>5,7</sup>

An in-depth understanding of molecular partitioning and diffusion in nanoporous media is crucial to the design of better chemical separation membranes. However, it is often challenging to assess molecular behavior in such chemically heterogeneous systems. In this study, two-color fluorescence imaging methods were used to study the distribution and diffusion behavior of polarity-sensitive fluorescent molecules in individual synthetic organic nanotubes. These nanotubes, originally designed as a drug delivery vehicle, are self-assembled from bolaamphiphile surfactants (**Figure 6**).

The nanotubes were employed as nearly ideal models of nanoporous materials due to their uniform inner pore diameter (10 nm), well-defined cylindrical structure, and known chemical characteristics, with amine and glucose groups on their inner and outer surfaces, respectively, and hydrocarbon chains in between. NR and its hydroxylated derivative (NR-OH) were used as polarity-sensitive fluorescent dyes to investigate their distribution and diffusion in ethanol-filled nanotubes. Imaging fluorescence correlation spectroscopy (imaging-FCS) employing videos recorded in two spectral bands ( $580 \pm 20$  and  $625 \pm 20$  nm) was employed to determine the location and diffusion coefficient of NR and NR-OH in local regions of individual nanotubes. Two-color fluorescence images of individual nanotubes (**Figure 7**) showed that NR-OH was located in more polar regions than NR. The imaging-FCS results suggested that diffusion of NR-OH was significantly slower than that of NR. These observations reflect the presence of NR-OH near the nanotube surfaces, likely due to hydrogen bonding interactions with the amine and glucose groups.

Recently, we have systematically investigated the diffusion of anionic fluorescent molecules (SRB) within organic nanotubes under different aqueous environments (pH, electrolyte concentrations) using imaging-FCS. We have found that SRB molecules diffuse via a desorption-mediated diffusion mechanism controlled by coulombic interactions with the inner amine-terminated surface of an organic nanotube.

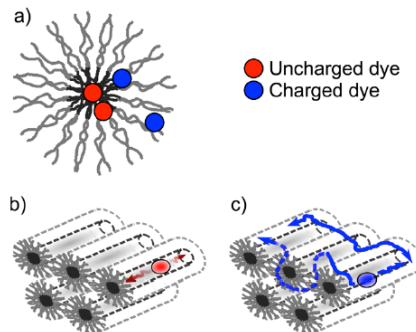


**Figure 5.** (a) Estimated preferential locations of PDI molecules; diffusion (b) in a hydrophobic core and (c) across hydrophilic corona regions.

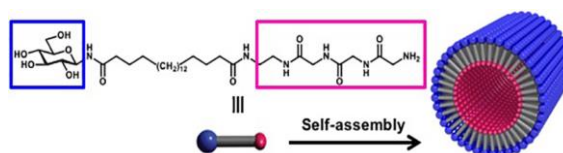


**Figure 6.** Schematic illustration of an organic nanotube used in this study.

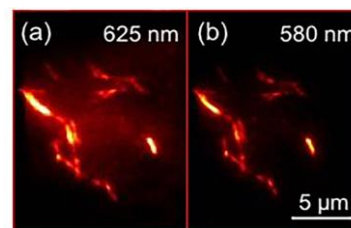


**Figure 7.** Two color fluorescence images showing NR-doped nanotubes at (a) 625 nm and (b) 580 nm.

## Publications Acknowledging this Grant in 2015 – present

### (I) Exclusively funded by this grant:

1. Higgins, D. A.; Park, S. C.; Tran-Ba, K.-H.; Ito, T. Single-Molecule Investigations of Morphology and Mass Transport Dynamics in Nanostructured Materials. *Annu. Rev. Anal. Chem.* **2015**, *8*, 193-216.
2. Tran-Ba, K.-H.; Higgins, D. A.; Ito, T. Fluorescence Recovery After Photobleaching and Single-Molecule Tracking Measurements of Anisotropic Diffusion within Identical Regions of a Cylinder-Forming Diblock Copolymer Film. *Anal. Chem.* **2015**, *87*, 5802-5809.
3. Park, S. C.; Ito, T.; Higgins, D. A. Dimensionality of Diffusion in Flow-Aligned Surfactant-Templated Mesoporous Silica: A Single Molecule Tracking Study of Pore Wall Permeability. *J. Phys. Chem. C* **2015**, *119*, 26101-26110.
4. Kumarasinghe, R.; Higgins, E. D.; Ito, T.; Higgins, D. A. Spectroscopic and Polarization-Dependent Single-Molecule Tracking Reveal the One-Dimensional Diffusion Pathways in Surfactant-Templated Mesoporous Silica. *J. Phys. Chem. C* **2016**, *120*, 715-723.
5. Xu, H.; Nagasaka, S.; Kameta, N.; Masuda, M.; Ito, T.; Higgins, D. A. Imaging Fluorescence Correlation Spectroscopy Studies of Dye Diffusion in Self-Assembled Organic Nanotubes. *Phys. Chem. Chem. Phys.* **2016**, *18*, 16766-16774.
6. Sapkota, D. R.; Tran-Ba, K.-H.; Elwell-Cuddy, T.; Higgins, D. A.; Ito, T. Single-Molecule Tracking Study of the Permeability and Transverse Width of Individual Cylindrical Microdomains in Solvent-Swollen Polystyrene-*block*-Poly(ethylene oxide) Films. *J. Phys. Chem. B* **2016**, *120*, 12177-12183.
7. Xu, H.; Nagasaka, S.; Kameta, N.; Masuda, M.; Ito, T.; Higgins, D. A. Spectroscopic Imaging Studies of Nanoscale Polarity and Mass Transport Phenomena in Self-Assembled Organic Nanotubes. *Phys. Chem. Chem. Phys.* **2017**, *19*, 20040-20048.

### (II) Jointly funded by this grant and other grants with leading intellectual contribution from this grant:

1. Ghimire, G.; Yi, Y.; Derylo, M. A.; Baker, L. A.; Ito, T. Electron Propagation within Redox-Active Microdomains in Thin Films of Ferrocene-Containing Diblock Copolymers. *Langmuir* **2015**, *31*, 12307-12314.
2. Kisley, L.; Brunetti, R.; Tauzin, L. J.; Shuang, B.; Yo, X.; Kirkemide, A. W.; Higgins, D. A.; Weiss, S.; Landes, C. F. Characterization of Porous Materials by Fluorescence Correlation Spectroscopy Super-resolution Optical Fluctuation Imaging. *ACS Nano* **2015**, *9*, 9158-9166.
3. Sun, X.; Xie, J.; Xu, J.; Higgins, D. A.; Hohn, K. L. Single-Molecule Studies of Acidity Distributions in Mesoporous Aluminosilicate Thin Films. *Langmuir* **2015**, *31*, 5667-5675.
4. Ghimire, G.; Coceancigh, H.; Yi, Y.; Ito, T. Electrochemical Characterization and Catalytic Application of Gold-Supported Ferrocene-Containing Diblock Copolymer Thin Films in Ethanol Solution. *ACS Appl. Mater. Interfaces* **2017**, *9*, 2906-2913.
5. Coceancigh, H.; Tran-Ba, K.-H.; Siepser, N.; Baker, L. A.; Ito, T. Longitudinally Controlled Modification of Cylindrical and Conical Track-Etched Poly(ethylene terephthalate) Pores Using Electrochemically-Assisted Click Reaction. *Langmuir* **2017**, *33*, 11998-12006.

### (III) Jointly funded by this grant and other grants with relatively minor intellectual contribution from this grant:

1. Collinson, M. M.; Higgins, D. A. Organosilane Chemical Gradients: Progress, Properties, and Promise. *Langmuir* **2017**, *33*, 13719-13732.
2. Li, Z.; Ashraf, K. M.; Collinson, M. M.; Higgins, D. A. Single Molecule Catch and Release: Potential-Dependent Plasmid DNA Adsorption along Chemically Graded Electrode Surfaces. *Langmuir* **2017**, *33*, 8651-8662.

## Single-Molecule Resolution of Surface Interactions and Dynamics

Daniel K. Schwartz  
University of Colorado Boulder

### Presentation Abstract

The dynamic behavior of molecules and nanoparticles in confined environments, such as at interfaces and within porous materials, lead to complex and highly-varied phenomena, where heterogeneity may arise from spatial variation of the material/interface itself, from structural configurations (i.e. conformation, orientation, aggregation state, etc.), or temporally, through inhomogeneous dynamic behavior. In order to capture relevant information about these complex dynamics, we have developed highly multiplexed single-molecule/single-nanoparticle tracking methods that are capable of acquiring  $>10^5$  trajectories in a given experiment; automated unbiased data analysis methods are used to interpret these large data sets. One specific discovery that was enabled by these methods involves the intermittent motion (i.e. “hopping diffusion”) of molecules at liquid-solid interfaces, which has been described within the context of a continuous time random walk (CTRW) model. CTRW-based “search” processes are widely predicted to exhibit improved efficiency compared with Brownian searches, we have found that enhanced interfacial transport is responsible for intermolecular interactions and associations that lead to surface layer formation, and for enhanced binding efficiency between “searching” adsorbates and surface binding sites. Recent work in our lab has extended the tracking methods to acquire fully 3D trajectories, enabling tracking of individual molecules and nanoparticles in complex environments, including porous media. Results will be shown that provide new insights into the transport of nanoparticles within inverse opals and polymeric ultrafiltration membranes.

### Surface Functionality and Reactivity Using Single Molecule Probes

**Postdoc(s):** Dapeng Wang (2016-2017), Mark Kastantin (2015)

**Student(s):** Gregory Morrin (2017), Haichao Wu (2017), Yu Cai (2016)

### RECENT PROGRESS

#### 3D Tracking in Confined Environments

We have developed methods to study the 3D motion of nanoparticles and molecules near surfaces and within the void space of porous materials using double-helix point-spread-function (DH-PSF) imaging. Temporal sequences of images are acquired, and trajectories linked, providing long-duration 3D trajectories for tens of thousands of particles or molecules simultaneously. Trajectories are subjected to statistical analyses, including multivariate machine-learning analytic approaches, e.g. to identify time intervals where particles are in confined/retained vs. freely diffusing “states”.

### *DH-PSF with Variable-Angle Illumination Epifluorescence Microscopy*

We demonstrated that the signal-to-noise ratio (SNR) and three-dimensional localization precision of a double helix point spread function (DH-PSF) were greatly improved by applying variable-angle illumination epifluorescence microscopy.

### *Three-Dimensional Tracking of Interfacial Hopping Diffusion*

Theoretical predictions have suggested that molecular motion at interfaces may be dominated by “hops” through the adjacent liquid phase, where the molecule re-adsorbs after a given hop according to a probabilistic “sticking coefficient”. Here, we used 3D single molecule tracking to explicitly visualize this process for a macromolecular probe at solid/liquid interfaces that exerted varying electrostatic interactions.

### *Nanoparticle diffusion within inverse opals*

3D diffusion of nanoparticle probes was observed within a model porous material, an inverse opal, comprising an interconnected network of hexagonally close packed spherical cavities. Each nanoparticle trajectory was analyzed to determine its dwell time within each cavity to determine comprehensive escape-time distributions as a function of size of the channels connecting the cavities.

### **Molecular Transport in Complex Interfacial Environments**

Our studies of molecular motion at solid/liquid interfaces have described the transport in the context of a continuous time random walk (CTRW) process, in which diffusion switched between desorption-mediated “flights” (i.e. hopping) and surface-adsorbed waiting-time intervals during which the molecules were either immobilized or engaged in slow 2D diffusive motion. We recently extended this work to include interfacial transport under more complex conditions, where the surface itself exhibited some degree of fluidity and/or where molecules were increasingly crowded at the interface.

### *Three Distinct Regimes in Polymer Surface Crowding Dynamics*

Single-molecule tracking was used to characterize the dynamics of PEG polymer on a hydrophobic surface as the concentration was systematically increased over 4 orders of magnitude from dilute surface coverage to well above monolayer coverage. We observed three characteristic regimes of dynamic behavior as a function of concentration, as evidenced by multiple statistical analyses. The Site-Blocking regime was characteristic of very dilute concentrations and exhibited faster dynamics as strong-adsorption sites were blocked. Subsequently, the Crowding regime was distinguished by increasingly sub-diffusive behavior as a function of coverage. Finally, the Brush regime occurred at higher coverage, and exhibited faster dynamics with increasing concentration.

### *Diffusion at Fluid Interfaces Encodes Information about Molecular Conformation*

Here we employed a macromolecular probe, a cadherin ectodomain that is known to change its flexibility as a function of solution conditions, to understand how the viscous coupling of a macromolecule to a vicinal fluid interface (a supported lipid bilayer) influences motion, and how this viscous coupling is related to molecular conformation. Rigid probe molecules exhibited a “fast” diffusion coefficient that was identical to that of individual lipid molecules in the bilayer. Under conditions where the probe was more flexible, individual trajectories were temporally heterogeneous, exhibiting alternating periods of fast and slow diffusion. These observations suggested that more flexible molecules alternated between upright and lying-down conformations, where the latter interacted with more lipid molecules and experienced greater viscous drag.

### Single Molecule Probes of Surface Chemistry

A longstanding goal of this research program has been to develop methods that use dynamic and spectral properties of individual probe molecules to obtain local nanoscale information about the chemical properties of materials interfaces.

#### *Nanoscale Hydrophobic Regions in a Polymer Brush*

We developed a novel single-molecule fluorescent probe that identified local regions on the basis of hydrophobicity. This allowed us to characterize the structural heterogeneity of a complex polymer material, PEG brushes, which are ubiquitous due to their extraordinary non-fouling character. It has been hypothesized that there may be a trade-off between the most adsorption-resistant brushes (at high grafting density), and less hydrophobic brushes. We correlated the effects of grafting density with local brush hydrophobicity by exploiting the solvatochromic properties of an environmentally sensitive dye (nitrobenzoxadiazole) with Mapping using Accumulated Probe Trajectories (MAPT). The results showed an increase in local nanoscale hydrophobic regions with grafting density, supporting the hypothesis that increased grafting density leads to the formation of poorly hydrated niches within the overall hydrophilic brush.

### **Publications Acknowledging this Grant in 2015 – present**

#### *(I) Exclusively funded by this grant:*

J. N. Mabry and D. K. Schwartz, "Tuning the Flight Length of Molecules Diffusing on a Hydrophobic Surface", *J. Phys. Chem. Letters*, **6**, 2065-2069 (2015).

M. J. Skaug and D. K. Schwartz, "Tracking Nanoparticle Diffusion in Porous Filtration Media", *Industrial and Engineering Chemical Research*, **54**, 4414-4419 (2015).

N. Nelson and D.K. Schwartz, "Unbiased Clustering of Molecular Dynamics for Spatially-Resolved Analysis of Chemically Heterogeneous Surfaces", *Langmuir*, **31**, 6099-6106 (2015).

J.N. Mabry, M. Kastantin, and D.K. Schwartz, "Capturing Conformation-Dependent Molecule-Surface Interactions when Surface Chemistry Is Heterogeneous", *ACS Nano*, **9**, 7237-7247 (2015).

D. Wang, R. Hu, M.J. Skaug, and D.K. Schwartz, "Temporally anti-correlated motion of nanoparticles at a liquid interface", *J. Phys. Chem. Letters*, **6**, 54-59 (2015).

D. Wang, A. Agrawal, A. Williams, R. Piestun, D.K. Schwartz, "Enhanced Information Content for Three-Dimensional Localization and Tracking Using the Double-Helix Point Spread Function with Variable-Angle Epifluorescence Microscopy", *Applied Physics Letters*, **110**, 211107 (2017).

D. Wang, H. Wu, D.K. Schwartz, "Three-Dimensional Tracking of Interfacial Hopping Diffusion", *Physical Review Letters*, **119**, 268001 (2017).

#### *(II) Jointly funded by this grant and other grants with leading intellectual contribution from this grant:*

S. Chakraborty, N. Nelson, and D.K. Schwartz, "Anisotropic Molecular Hopping at the Solid-Nematic Interface", *Soft Matter*, **11**, 7712-7716 (2015).

D. Wang, C. He, M.P. Stoykovich, D.K. Schwartz, "Nanoscale Topography Influences Polymer Surface Diffusion", *ACS Nano*, **9**, 1656-1664 (2015).

M.J. Skaug, L. Wang, Y. Ding, and D.K. Schwartz, “Hindered Nanoparticle Diffusion and Void Accessibility in a Three-Dimensional Porous Medium”, *ACS Nano*, **9**, 2148-2156 (2015).

Blake B. Langdon, Mark Kastantin, Daniel K. Schwartz, “Surface Chemistry Influences Fibrinogen Self-association”, *Biomacromolecules*, **16**, 3201-3208 (2015).

D. Wang, R. Hu, J.N. Mabry, D.T. Wu, K. Koynov, and D.K. Schwartz, “Scaling of Polymer Dynamics at an Oil-Water Interface in Regimes Dominated by Viscous Drag and Desorption-Mediated Flights”, *J. Am. Chem. Soc.*, **137**, 12312-12320 (2015).

D. Wang, H.-Y. Chin, C. He, M. P. Stoykovich, and D. K. Schwartz, “Polymer Surface Transport is a Combination of In-Plane Diffusion and Desorption-Mediated Flights”, *ACS Macro Letters*, **5**, 509-514 (2016); doi:10.1021/acsmacrolett.6b00183.

Y. Cai, N. Shashikanth, D.E. Leckband, and D.K. Schwartz, “Cadherin Diffusion in Supported Lipid Bilayers Exhibits Dynamic Heterogeneity”, *Biophys J*, **111**, 2658–2665 (2016).

*(III) Jointly funded by this grant and other grants with relatively minor intellectual contribution from this grant:*

B.B. Langdon, R. Mirhossaini, I. Sriram, J. Mabry, A. Lajmi, Y. Zhang, O.J. Rojas, D.K. Schwartz, “Single-molecule resolution of protein dynamics on polymeric membrane materials: The roles of spatial and population heterogeneity”, *ACS Applied Materials and Interfaces*, **7**, 3607-3617 (2015).

## Microscopy Methods for Investigating Separation Processes within Porous Particles

Joel M. Harris, Jay P. Kitt, and David A. Bryce  
University of Utah – Department of Chemistry  
Salt Lake City, UT 84112

### Presentation Abstract

In the development of new separation media, it is critical to understand how their interface composition and structure relate to their functioning for selective solute retention. Confocal Raman microscopy has been adapted to examining the interior surfaces of porous chromatographic silica particles, reporting information on the structure of the stationary phase and its interactions with solute molecules. The spatial resolution of the confocal collection optics can selectively probe the internal composition of an *individual* porous particle, yielding quantitative information on populations of molecules on their pore surfaces. The technique is an *in situ* method, so that interfacial structure and composition can be monitored as conditions are varied. In addition, the spatially-resolved kinetics of solute exchange can be measured within a single particle under high solute-retention conditions. We apply this methodology to studies of the assembly of hybrid-lipid bilayers onto C<sub>18</sub> silica surfaces, which can be used for assessing the lipid-membrane affiliation of analytes from their retention on these model lipid-membrane phases. Raman spectroscopy provides insight into conformations of the grafted alkyl chains and the acyl chains of the lipid monolayer, and how these conformations change with surface composition and temperature, leading to control of solute retention. Assembly of symmetrical supported-lipid bilayers onto bare silica and cyano-derivatized surfaces is also being investigated, and the structures of these sorbent phases and their retention of model solutes are being compared with the hybrid C<sub>18</sub>-lipid phases.

### DE-FG03-93ER14333: Analytical Spectroscopy Methods for Liquid/Solid Interfaces

PI: Joel M. Harris

Postdocs: Jay P. Kitt

Students: David A. Bryce, Maryam Zare, Grant Myres, Zin (Kristy) Wen

Visiting Faculty: Carol Korzeniewski, Texas Tech University

### RECENT PROGRESS

*Probing the interior surface chemistry of porous particles.* Most practical applications of liquid/solid interfaces to chemical separations, including extraction, chromatography, and environmental remediation, are carried out in porous media. The high specific surface area of porous materials makes them challenging to investigate because most of the surface area lies within the interior making it inaccessible to traditional surface-selective spectroscopies. With DOE support, the Harris lab has pioneered the use of confocal Raman microscopy to probe the interior composition and interface structure of individual porous particles, providing vibrational spectra from sampled volumes within particles smaller than 1 fL.

The resolution and efficiency of separations are significantly impacted by the kinetics of partitioning and transport into the interior of porous particles. To understand these kinetics, measurements of within-particle molecular transport were carried out using confocal Raman microscopy to probe the time-dependent accumulation of a model solute, pyrene, from an aqueous mobile phase *into the center of individual porous silica particles* modified with n-alkyl chains. The measured time constants for pyrene accumulation were much slower than diffusion-limited transport of solute in solution to the particle surface. Furthermore, accumulation into the center of the particle did not show a time-lag characteristic of slow-diffusion to the particle center. The exponential rise of pyrene concentration was consistent with first-order Langmuir adsorption kinetics at low surface coverages. The linear dependence of the time-constant on particle radius indicated an adsorption barrier near the outer boundary of the particle, where the accumulation rate depends on flux across the boundary (proportional to the particle area) to satisfy the within-particle capacity at equilibrium (proportional to the particle volume). Pyrene accumulation kinetics into the porous material, expressed as a heterogeneous rate constant, were nearly 50-times faster than the pyrene adsorption rate at a planar n-alkane-functionalized silica surface, demonstrating the impact of multiple surface encounters within the porous structure producing much greater capture efficiency compared to a planar surface. The methodology developed here is label-free and applicable to *in-situ* investigations of accumulation kinetics within nearly any porous sorbent or selective-binding material.

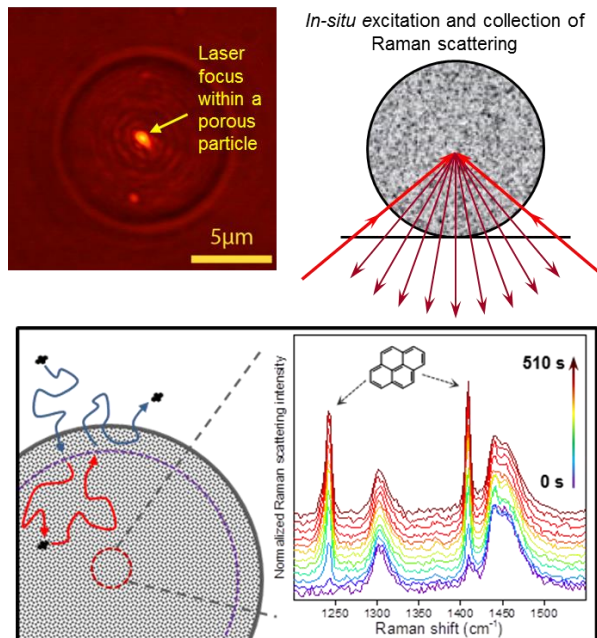


Figure 1. Raman scattering collected from within a 10- $\mu\text{m}$   $\text{C}_{18}$  silica particle. Time-resolved measurements of pyrene accumulation into the particle center

**Octanol-water hydrophobicity measurements in fL volumes.** The hydrophobicity of organic compounds that governs extraction efficiency into non-polar media is generally specified by octanol-water partitioning. Traditional methods for measuring octanol-water partition coefficients ( $K_{ow}$ ), require hours for equilibration and large volumes of a sample solution, which have led to development of smaller-scale methods for measuring  $K_{ow}$ . With DOE-support, we have reduced the receiver volume of octanol-water partitioning measurements from the previous small-scale state-of-the-art by six-orders-of-magnitude to the femtoliter scale, by using a single octanol-filled reversed-phase, octadecylsilane-modified ( $\text{C}_{18}$ -silica) chromatographic particle as a collector. Partitioning was measured *in-situ* within the pore-confined octanol phase using confocal Raman microscopy. Equilibration times are fast ( $< 1$  minute) because molecular diffusion is efficient over distance scales of micrometers. The demonstrated amount of analyte needed to carry out a measurement is extremely small, *less than 50 fmol*, a useful attribute for acquiring  $K_{ow}$  data on small quantities of unstable, environmentally sensitive, or toxic compounds.

**Developing separations based on biological membrane affinity.**

Octanol-water partition coefficients report the hydrophobicity of compounds relevant to their partitioning between water and bulk organic phases. Partitioning into octanol is not an ideal model for assessing the environmental impact and bioactivity of fossil fuel contaminants and their byproducts and their interactions with the environment which derives from interactions of molecules with the lipid membranes of cells. A novel approach to separations based on lipid-membrane affinity is to employ a hybrid-lipid bilayer supported on the interior surfaces of porous particles. Hybrid bilayers, produced through the self-assembly of a phospholipid monolayer on n-alkane-modified surfaces within porous silica particles, have been used in chromatographic retention studies of small molecules. Despite their application as separation media, the structure of hybrid-bilayers in chromatographic silica was unknown. To address this question, we employed confocal-Raman microscopy to investigate the structure of hybrid-phospholipid bilayers in C18-modified, porous-silica chromatographic particles. The surface-density of lipid in the hybrid bilayer, ordering of *both* C-18 and lipid acyl chains upon bilayer formation, and decoupling of C<sub>18</sub> methylene C-H vibrations by deuterated-lipid acyl chains all suggest an interdigitated acyl-chain structure. Simultaneous melting of both layers was consistent with this structure, where immobility of surface-grafted C<sub>18</sub>-chains lowers cooperativity and increases the melting transition compared to a vesicle bilayer.

A unique means of controlling the structure of a hybrid-bilayer stationary phase can be realized through a simple variation in temperature. Lipid bilayers undergo large changes in acyl-chain conformation when passing through their main phase transition. The gel-to-liquid crystalline phase transition we observe in hybrid-lipid bilayers in porous silica disrupts the all-trans conformations of the lipid-acyl and C<sub>18</sub> chains, producing a disordered phase dominated by gauche defects. We have discovered that this change in stationary-phase structure impacts solute retention, controlled by small 10 to 15°C changes in temperature across the melting phase transition. The disordering of acyl-chains as the hybrid lipid bilayer melts is accompanied by a nearly 10-fold decrease in concentration of pyrene partitioned into the hybrid bilayer, proportional to the loss of trans-character of the acyl chains (see Figure 3). Current research is directed toward the assembly of

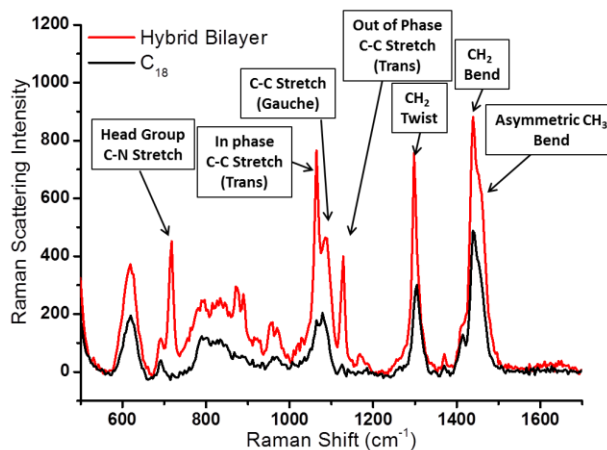


**Figure 2.** Raman scattering from a single C<sub>18</sub> silica particle prior to (black) and following (red) assembly of a hybrid-lipid bilayer at a C<sub>18</sub> interface.

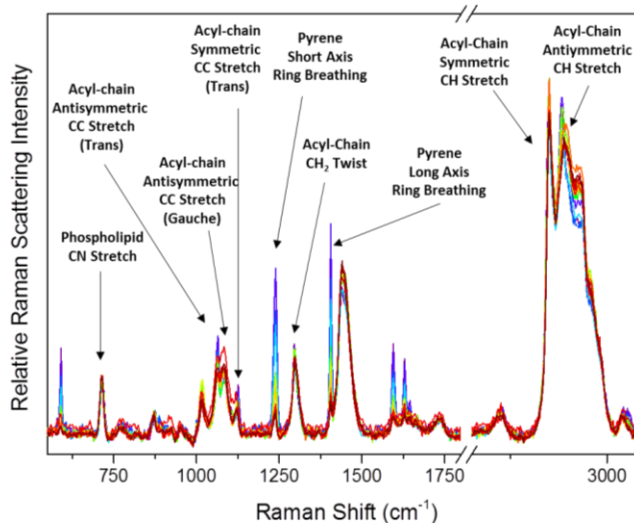


**Figure 3.** Intraparticle Raman spectra of a hybrid bilayer from 15°C (violet) to 40°C (red) in equilibrium with

1 0-μM nrvrene: changes in bilayer structure correlate with

more authentic (symmetrical) supported-lipid bilayers onto bare silica and cyano-derivatized surfaces. The structures of these biomimetic lipid phases and their retention of model solutes are being compared with the hybrid C<sub>18</sub>-lipid phases. Mixed surfactant analogs of hybrid-lipid bilayers are also being investigated.

### **Publications acknowledging this grant in 2015 – present**

1. Kitt, J. P.; Bryce, D. A.; Harris, J. M. Spatial Filtering of a Diode Laser Beam for Confocal Raman Microscopy. *Applied Spectroscopy* **2015**, *69* (4), 513-517. (I)
2. Kitt, J. P.; Harris, J. M. Confocal Raman Microscopy for in Situ Measurement of Octanol–Water Partitioning within the Pores of Individual C<sub>18</sub>-Functionalized Chromatographic Particles. *Analytical Chemistry* **2015**, *87* (10), 5340-5347. (I)
3. Kitt, J. P.; Bryce, D. A.; Harris, J. M. Calorimetry-Derived Composition Vectors to Resolve Component Raman Spectra in Phospholipid Phase Transitions. *Applied Spectroscopy* **2016**, *70* (7), 1165-1175. (I)
4. Kitt, J. P.; Harris, J. M. Confocal Raman Microscopy of Hybrid-Supported Phospholipid Bilayers within Individual C<sub>18</sub>-Functionalized Chromatographic Particles. *Langmuir* **2016**, *32* (35), 9033-9044. (I)
5. Bryce, D. A.; Kitt, J. P.; Harris, J. M. Confocal Raman Microscopy Investigation of Molecular Transport into Individual Chromatographic Silica Particles. *Analytical Chemistry* **2017**, *89* (5), 2755-2763. (I)
6. Kitt, J. P.; Bryce, D. A.; Minter, S. D.; Harris, J. M. Raman Spectroscopy Reveals Selective Interactions of Cytochrome c with Cardiolipin That Correlate with Membrane Permeability. *Journal of the American Chemical Society* **2017**, *139* (10), 3851-3860. (I)
7. Korzeniewski, C.; Liang, Y.; Zhang, P.; Sharif, I.; Kitt, J. P.; Harris, J. M.; Hamrock, S. J.; Creager, S. E.; DesMarteau, D. D. Vibrational Spectroscopy for the Determination of Ionizable Group Content in Ionomer Materials. *Applied Spectroscopy* **2018**, *72* (1), 141-150. (I)
8. Bukola, S.; Liang, Y.; Korzeniewski, C.; Harris, J. M.; Creager, S. Selective proton/deuteron transport through Nafion | graphene | Nafion sandwich structures at very high current density. *Journal of the American Chemical Society* **2018**, submitted, in review. (III)
9. Bryce, D. A.; Kitt, J. P.; Harris, J. M. Confocal-Raman Microscopy Characterization of Supported Phospholipid Bilayers Deposited on the Interior Surfaces of Chromatographic Silica. *Journal of the American Chemical Society* **2018**, submitted, in review. (I)

(I) Exclusively funded by this grant.

(II) Jointly funded by this grant and other grants with leading intellectual contribution from this grant.

(III) Jointly funded by this grant and other grants with relatively minor intellectual contribution from this grant.

## Understanding Reactive Separations of CO<sub>2</sub>

David J. Heldebrant,<sup>1\*</sup> Deepika Malhotra,<sup>1</sup> Jotheeswari Kothandaraman,<sup>1</sup> Trent Graham,<sup>4</sup> Roger Rousseau,<sup>1</sup> Vanda Glezakou,<sup>1</sup> Mal-soon Lee,<sup>1</sup> Xiao-Ying Yu,<sup>1</sup> Johnny Saavedra Lopez<sup>1</sup>, Leo Bañuelos,<sup>2</sup> Robert Dalglish,<sup>3</sup> Tom Headen.<sup>3</sup>

1. Pacific Northwest National Laboratory, 2. University of Texas, El Paso  
3. ISIS, Oxford, UK, 4. Washington State University

### Presentation Abstract

Nature has long performed “reactive separations,” where both the capture and subsequent conversion are performed in synergistic, concerted steps. Humans treat CO<sub>2</sub> capture and conversion as two distinctive energy-intensive steps, though ironically the same chemicals that are used in capture can also be used in conversion. Thus, the aim of this work is to learn how to perform synergistic capture and conversion in the same solvent using the same chemicals. Switchable ionic liquids (SWILs) which are promising solvents used for CO<sub>2</sub> capture, coincidentally are comprised of chemicals that promote catalytic reduction of CO<sub>2</sub> to methanol. We describe here, a combination of experimental and theoretical approaches used to characterize the newly discovered heterogeneous, mesoscopic structure distinctive to SWILs. The dynamic structure, *i.e.* the gradient changes in disparate (ionic/non-ionic) micro-domains within structure impacts the physical and thermodynamic properties of the fluid, notably the movement and reactivity of CO<sub>2</sub> for both the capture and conversion steps. We first focus on characterizing the mesoscopic structure and speciation of the fluid to learn how the solvent’s mesoscopic structure originates and how this dynamic structure controls reactivity of CO<sub>2</sub>. We then focus on governing the reactivity of the chemically complexed CO<sub>2</sub> by distinct changes in the electrophilicity (hydride acceptor strength) of the CO<sub>2</sub> captured in solution. The two synergistic thrusts include:

- Experimental/theoretical studies to characterize the mesoscopic structure by mapping the speciation and orientation of alkylcarbonates (complexed CO<sub>2</sub>) compared to un-reacted solvent. The molecular reorganization in the fluid provides a platform to study *how* CO<sub>2</sub> dissolution and diffusion occurs to shed light on the how CO<sub>2</sub> is fixated in solution. Studies here are performed to characterize the dynamic molecular reorganization as a function of CO<sub>2</sub> loading to learn how the solvent’s structure impacts the solvent properties that control CO<sub>2</sub> uptake.
- Experimental studies to determine the correlation between the mesoscopic SWIL structure, electronic properties, and CO<sub>2</sub> (conversion) reactivity with a focus on defining the catalyst’s location and structure inside the SWIL ionic domains. We aim to obtain direct observations of the interactions between alkylcarbonates and catalysts as well as a thorough evaluation of the impact of alkylcarbonate electrophilicity on CO<sub>2</sub> hydrogenation.

**FWP 67038, Pacific Northwest National Laboratory**  
**Title: Early Career: Combined Capture and Conversion of CO<sub>2</sub>**

**PI:** Dr. David J. Heldebrant<sup>a,b</sup>

**Postdoc(s):** Dr. Jotheeswari Kothandaraman<sup>a</sup>, Dr. Johnny Saavedra Lopez<sup>a</sup>

**Student(s):** Trent Graham<sup>b</sup>

**Affiliations(s):** Pacific Northwest National Laboratory,<sup>a</sup> Washington State University<sup>b</sup>

## RECENT PROGRESS

### *Mesoscopic Ordering and Impacts on CO<sub>2</sub> Diffusion*

To first learn how CO<sub>2</sub> moves into and ultimately through capture solvents, we focused on characterizing the mesoscopic 3-dimensional structure of CO<sub>2</sub> capture solvent as a function of CO<sub>2</sub> loading. The goal was to learn insights into what the solvent's molecular structure is, and observe any mesoscopic changes in structure or ordering at varied CO<sub>2</sub> loadings. This will allow us to determine how CO<sub>2</sub> enters, diffuses through, and ultimately reacts with the solvent molecules. We began probing solvent's Structure using PNNL's 3D Time of Flight Mass Spectrometry (ToF-SIMS) capability.

We performed the first known 2-dimensional and 3-dimensional chemical speciation of a water-lean CO<sub>2</sub> capture solvent. Our analysis focused on IPADM-2-BOL CO<sub>2</sub> capture solvent (Figure 1), which has been shown to be an energetically promising solvent. We chose mass-spectrometry as a measurement tool because it enables us to differentiate between the CO<sub>2</sub>-free and CO<sub>2</sub>-rich regions in the fluid and confirm the binding mechanism and stoichiometry of CO<sub>2</sub> fixation (Figure 2). Using PNNL's unique

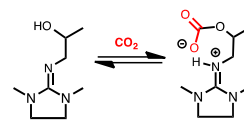


**Figure 1.** CO<sub>2</sub> fixation by IPADM-2-BOL.

microfluidic SALVI microfluidic capability, we have the ability to perform speciation studies in 2

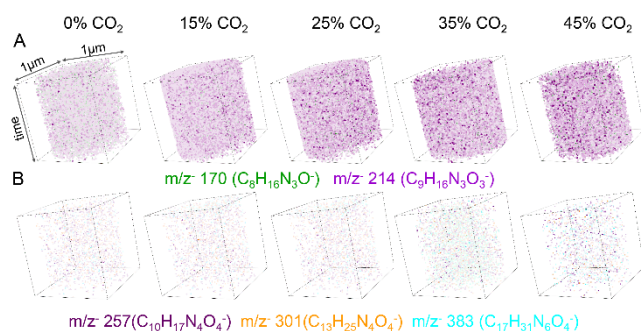


**Figure 2.** 3D overlay images of selected m/z peaks.

and 3-dimensions in a liquid sample, identifying m/z peaks for IPADM-2-BOL and IPADM-2-BOL-CO<sub>2</sub>, confirming the CO<sub>2</sub>-bound molecule was zwitterionic. This confirms our hypothesized 1:1 CO<sub>2</sub> binding mechanism even though IPADM-2-BOL is fully saturated with CO<sub>2</sub> at a mole fraction of 0.5. This validates previous hypotheses and thermodynamic models that had

predicted a different 1:1 binding mechanism compared to the conventional 2:1 carbamate binding mode expected by total gravimetric CO<sub>2</sub> uptake.

Constructing the 2D and 3D chemical mapping validated the predicted mesoscale molecular structure as first predicted by Liauw and our own molecular dynamic simulations. The heterogeneity in the solvent was found to be comprised of disparate regions of IPADM-2-BOL coexisting with clusters of zwitterionic (IPADM-2-BOL-CO<sub>2</sub>). We had previously calculated a mesoscopic structure for IPADM-2-BOL that had nanometer sized clusters of zwitterions at CO<sub>2</sub>

loadings up to 15%. Increasing CO<sub>2</sub> loading from mole fractions 0.15 through 0.45, the clusters did not grow in size, but the concentration and distribution of the clusters in solution increased, again matching theoretical predictions. We also found evidence of aggregation of the clusters into >500 nm spheres that were composed of many independent clusters, suggesting more complexity of the mesoscopic structure than previously thought.

### ***Evidence of a Glass Transition Using Inelastic and Small Angle Neutron Scattering.***

We began to look deeper into the mesoscopic structure, more specifically to probe the size and shape of the clusters and their subsequent aggregation. We reached out to our collaborators and procured beam time at ISIS to perform inelastic neutron scattering and small angle neutron scattering on IPADM-2-BOL. We used the LARMOR and NIMROD instruments to collect data on the size, shape and distribution functions of IPADM-2-BOL and the IPADM-2-BOL-CO<sub>2</sub> zwitterion. Experiments were performed at CO<sub>2</sub> loadings ranging from mole fractions between 0 and 0.5 at temperatures ranging from 20-100 °C. Selective isotopic enrichment of the IPADM-2-BOL molecule was performed to provide contrast and a higher signal to noise.

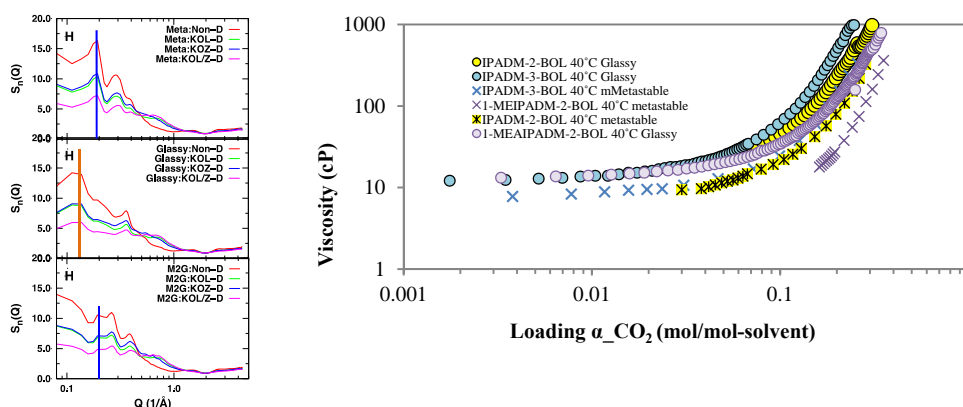


**Figure 3.** A) Comparison of Small Angle Neutron Scattering (SANS) showing differences between glassy and metastable states of IPADM-2-BOL. B) Measured glassy and metastable viscosities of three SWIL derivatives.

Neutron scattering and diffraction studies showed the presence of 2-5 nm oblong clusters that are present at any temperature and at any CO<sub>2</sub> loading above zero. The scattering experiments confirmed that clusters form, which we believe to be comprised of dimers or tetramers of IPADM-2-BOL-CO<sub>2</sub> zwitterions. Further analysis showed that the clusters did not increase in size or change shape with increases in CO<sub>2</sub> loading or temperature, matching the ToF-SIMs data. Neutron diffraction experiments showed the temperature dependent flocculation of the clusters into >500 nm spherical aggregates, which was comprised of many independent clusters of zwitterions. The 500 nm aggregates were found to dissociate back into the 2-5 nm clusters, suggesting this aggregation is reversible like a flocculation. Theoretical calculations had previously predicted the transition of IPADM-2-BOL into a “glassy state” (Figure 3A) which was subsequently confirmed with viscosity measurements, where these fluids exhibit two different viscosity profiles at the same CO<sub>2</sub> loading and temperature (colored X’s VS circles, Figure 3B). We attribute this reversible aggregation as the root cause for the formation of the glassy state, which we have observed in different chemistries of CO<sub>2</sub> capture solvents, suggesting this phenomenon may be universal. We conclude that the high viscosities in water-lean solvents could be abated if aggregation could be stopped.

We hypothesized that CO<sub>2</sub> is able to dissolve in low-polarity non-ionic regions of the SWIL rather than the polar ionic regions. Here, CO<sub>2</sub> could readily diffuse in the CO<sub>2</sub>-free IPADM-2-BOL (Figure 4, teal) domains and immediately react rather than diffusing into the polar, viscous CO<sub>2</sub>-bound domains (Figure 4, purple). In IPADM-2-BOL and other alkanolguanidines, the unreacted pores or channels will always be present as these solvents are saturated with CO<sub>2</sub> at a mole fraction of 0.5, leaving half of the solvent un-reacted. To test this hypothesis, we have started CO<sub>2</sub> diffusion measurements using <sup>13</sup>C 2-D NMR to determine which domain CO<sub>2</sub> diffuses through.

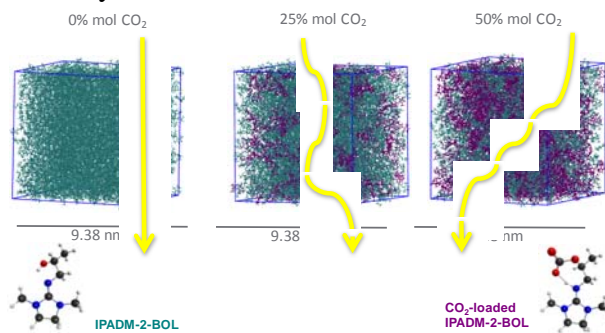


**Figure 4.** Proposed diffusion pathways (yellow) of CO<sub>2</sub> through SWILs at varied loadings.

### Conversion of ‘Captured’ CO<sub>2</sub>

We began to study the reactivity of chemically complexed CO<sub>2</sub> in solution. As indicated before, the same alcohol/non-nucleophilic bases that are used in capture are also used to promote the conversion of CO<sub>2</sub>. Jessop and Noyori were the first to notice the addition of alcohols and bases promoted the homogeneous hydrogenation of CO<sub>2</sub> to formate.<sup>(1)</sup> It is not by coincidence that alcohols and bases promote this reaction as both reagents produce anionic carboxylates (carbamates, alkylcarbonates) which (while negatively charged) may be electrophilic enough to be reduced by catalysts to formate and subsequently to methanol. We had previously shown that CO<sub>2</sub> capture solvents that are comprised of alkylcarbonates and carbamates exhibit different reactivity than neutral CO<sub>2</sub>.<sup>(2)</sup> These carboxylates were found to directly coordinate to molecular catalysts and undergo an inner-sphere reduction mechanism to formate, which is in contrast to hydrogenations of neutral CO<sub>2</sub> which proceeds via an outer-sphere mechanism. Formate can then undergo thermal condensation to a formate ester or formamide intermediate, which can be reduced to methanol (Figure 5), though literature reports cite the need for Lewis acid/base sites to drive the final hydrogenation.<sup>(3)</sup>

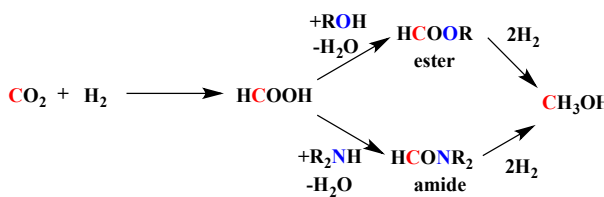


**Figure 5.** Routes to make methanol

We hypothesized that the reactive pathways demonstrated through homogeneous catalysts would be available to heterogeneous catalysts as the hydrogenations to methanol have been shown to be catalytic with respect to solvent.<sup>(3)</sup> Further, the solid-support can provide Lewis acid/base sites required for the final hydrogenation of formate esters or formamides to methanol. The challenge is that CO<sub>2</sub> hydrogenations using heterogeneous catalysts are often performed in the gas phase at high T (>250 C) and P (>50 bar) using synthesis gas mixture (H<sub>2</sub>/CO<sub>2</sub>/CO). Thus, it was unclear if catalysis could be performed in the condensed-phase, with lower temperature and pressures compared to what is typically required in a gas-phase reaction.

We started screening condensed-phase hydrogenations of alkylcarbonates and carbamates using the commercial Cu/ZnO/Al<sub>2</sub>O<sub>3</sub> catalyst (Table 1).<sup>(4)</sup> Our results showed that in the absence of solvent, there is no hydrogenation of CO<sub>2</sub> at 170 °C, 50 bar, which was expected because gas phase hydrogenations require higher temperature and pressure to proceed.<sup>(5)</sup> We then screened

amine bases, finding that 1° and 2° amines such as ethylene diamine and dibutylamine were hydrogenated to their respective formamides, but were unable to continue to methanol. This result indicates that the formamide route (Figure 4, bottom) may not be feasible under these conditions, which we attribute to the low hydride acceptor strength (low electrophilicity) of formamides compared to that of formate esters. Tertiary amines were found to be non-reactive, as were alcohols, though a 1:1 combination of 3° amines and alcohols produced methanol at 2% conversion with respect to NEt<sub>3</sub>, suggesting the reaction proceeds via the formate ester route (Figure 5, bottom). Changing the ratio of base to alcohol influenced the conversion to methanol. If the ratio of amine to alcohol was 10:1, the conversion of methanol is poor, whereas a ratio of 1:10 enables a 100% conversion to methanol with respect to amine. It is possible that excess amine could passivate the catalyst surface and limiting the reaction. Conversely, the polarity of the solvent could be impacting the conversion, as amines are non-polar whereas an excess of alcohol would be very polar and able to solvate polar transition states and charged intermediates common to CO<sub>2</sub> hydrogenations. Excess alcohol would also promote the thermal esterification (C-O cleavage) to produce formate ester. Gas chromatographic analysis of the gas mixture only showed traces of methane and CO in addition to excess H<sub>2</sub> and CO<sub>2</sub>. Under optimal conditions, the amount of produced methanol never surpassed the amount of amine used regardless of time suggesting equilibrium had been reached. We attribute this to the production of water, which along with unreacted CO<sub>2</sub> would form carbonic acid, which would neutralize the base and prevent formate production. Higher turnovers and yields could be achieved by performing hydrogenations away from equilibrium by using a continuous flow cell, where the water and methanol could be removed and the NEt<sub>3</sub> and ethanol could be reused. We conclude that the catalytic hydrogenation from CO<sub>2</sub> to methanol is feasible using CO<sub>2</sub> capture solvents, highlighting the synergies between capture and conversion.

**Table 1. Catalytic hydrogenations**

Entry	Cat.	CO <sub>2</sub> :H <sub>2</sub> (50 bar)	Promoter	T (°C)	HCOO <sup>-</sup> (%) <sup>a</sup>	HCOOR (%) <sup>a</sup>	N-CHO (%) <sup>a</sup>	MeOH (%) <sup>a</sup>
1	Cu/ZnO/Al <sub>2</sub> O <sub>3</sub>	1:1.5	Ethylenediamine	170	-	-	7%	-
2	Cu/ZnO/Al <sub>2</sub> O <sub>3</sub>	1:1.5	NEt <sub>3</sub>	170	trace	-	-	-
3	Cu/ZnO/Al <sub>2</sub> O <sub>3</sub>	1:1.5	NEt <sub>3</sub> : EtOH	170	trace	trace	-	2%
4	Cu/ZnO/Al <sub>2</sub> O <sub>3</sub>	1:1.5	EtOH	170	-	-	-	-
5	Cu/ZnO/Al <sub>2</sub> O <sub>3</sub>	1:1.5	NEt <sub>3</sub> : EtOH <sup>c</sup>	170	-	-	-	-
6	Cu/ZnO/Al <sub>2</sub> O <sub>3</sub>	1:1.5	NEt <sub>3</sub> : EtOH <sup>d</sup>	170	3%	trace	-	100%
7 <sup>b</sup>	Cu/ZnO/Al <sub>2</sub> O <sub>3</sub>	1:1.5	NEt <sub>3</sub> : EtOH <sup>d</sup>	170	3%	1%	-	76%

<sup>a</sup>%yield with respect to amine, reaction time=16 h; <sup>b</sup>reaction time=48h, longer reaction time lead to slow decomposition of methanol to ethylacetate, <sup>c</sup>10:1 amine to alcohol, <sup>d</sup>1:10 amine to alcohol.

## References:

- 1) *Chem. Rev.*, **1995**, 95, 259–272. 2) *Green. Chem.* **2016**, 18, 4871-4874. 3) *Angew. Chem. Int. Ed.* **2012**, 124 (30), 7617-7620, *J. Am. Chem. Soc.* **2016**, 138 (3), 778-781. 4) *Appl. Catal.* **1988**, 36, 1. 5) *Science* **2012**, 336, 893–897.

## Publications Acknowledging this Grant in 2015 – present

### Sole funding by this grant:

- 1) Heldebrant, D. J.\*; Koech, P. K.; Glezakou, V. A. “Water-Lean Solvents for Post-Combustion CO<sub>2</sub> Capture: Fundamentals, Uncertainties, Opportunities and Outlook.” Thematic Issue on CCS: *Chem. Rev.*, **2017**, *117*, 14, 9594–9624.
- 2) Lao, D. B., Galagan, B. R., Linehan, J. C., Heldebrant, D. J. \* “The steps of activating a prospective CO<sub>2</sub> hydrogenation catalyst with combined CO<sub>2</sub> capture and reduction,” *Green. Chem.* **2016**, *18*, 4871-4874.
- 3) Kothandaraman, J., Dagle, R., Dagle, V., Heldebrant, D. J. \* “Condensed-Phase Hydrogenation of CO<sub>2</sub> to Methanol.” *In Preparation*, **2018**
- 4) Malhotra, D., Cantu, D., Lee, M.S., Rousseau, R., Glezakou, V. A., Heldebrant, D. J.\*, Headen, T., Jones, M. O. “Characterization of CO<sub>2</sub> Capture Fluids Using Total Neutron Scattering.” *In Preparation*, **2018**.
- 5) Yao, J., Yu, X. Y., Lao, D. B., Zhu, Z., Heldebrant, D. J.\* “Influence of mesoscopic solvent structure on facilitated CO<sub>2</sub> transport in Switchable Ionic Liquids.” *In Preparation*, **2018**.

### Co-funding by this grant:

- 6) Yao, J., Yu, X. Y., Lao, D. B., Zhu, Z., Nune, S. K., Ma, X., Heldebrant, D. J.\* “Two Coexisting Liquid Phases in Switchable Ionic Liquids.” *Phys. Chem. Chem. Phys.*, **2017**, *19*, 22627—22632i.
- 7) Grubel, K., Heldebrant, D. J.\*, Bays, J. T. “Octane on Demand: On-Board Separation of Oxygenates from Gasoline.” *In Preparation*, **2018**.

## Electrically Driven Ion Separations in Permeable Membranes

Merlin L. Bruening,<sup>a,b</sup> Andriy Yaroschuk,<sup>c</sup> Nicholas White,<sup>d</sup> Yan Zhu,<sup>d</sup> Muhammad Ahmad,<sup>b</sup>  
Maria Misovich<sup>d</sup> and Liu Yang<sup>b</sup>

<sup>a</sup>University of Notre Dame, Department of Chemical and Biomolecular Engineering

<sup>b</sup>University of Notre Dame, Department of Chemistry

<sup>c</sup>Polytechnic University of Catalonia – Barcelona Tech, Department of Chemical Eng.

<sup>d</sup>Michigan State University, Department of Chemistry

### Presentation Abstract

Although ion-exchange membranes exhibit high selectivities between cations and anions, modest selectivities among cations or among anions limit the applications of these materials in ion separations. This project explores modification of ion-exchange membranes with polyelectrolyte multilayers to dramatically enhance selectivity among cations or anions. Remarkably, adsorption of polyelectrolyte multilayers on Nafion and Fujifilm cation-exchange membranes yields  $\text{Li}^+/\text{Co}^{2+}$ ,  $\text{K}^+/\text{La}^{3+}$ , and  $\text{K}^+/\text{Mg}^{2+}$  selectivities  $>1000$ , whereas the corresponding selectivities of bare membranes are around 2. New anion-exchange membranes coated with polyelectrolyte films show similarly remarkable  $\text{Cl}^-/\text{SO}_4^{2-}$  selectivities. Moreover, in Donnan dialysis through modified membranes  $\text{K}^+/\text{Li}^+$  selectivities are  $>50$ , demonstrating remarkable discrimination even among monovalent ions. Low partition coefficients for divalent or highly hydrated monovalent ions such as  $\text{Li}^+$  may lead to space-charge regions in membranes and give unusual trends in mass transfer resistances as a function of the thickness of ultrathin barrier layers. Although surface charge likely plays an important role in membrane selectivity, even at ionic strengths  $>0.1$  M, monovalent/divalent ion selectivities remain above 1000. In ED, as the applied current density increases above a limiting value, the  $\text{K}^+/\text{Mg}^{2+}$  selectivities of coated membranes decrease from  $>1000$  to 22 and current efficiency decreases. Water-splitting at overlimiting currents likely leads to a local pH increase close to the membrane surface and alters film permeability or allows passage of  $\text{Mg}(\text{OH})_x$  species to decrease selectivity. Future work aims to increase limiting currents and better understand the mechanisms behind the high selectivities of polyelectrolyte multilayers.

**DE-SC0017618 and DE-FG02-98ER14907: Electrically Driven Ion Separations in Permeable Membranes**

**Student(s):** Muhammad Ahmad, Liu Yang, and Chao Tang

## RECENT PROGRESS

### *Development of Highly Selective Cation-exchange Membranes*

Our initial studies of ion-exchange membranes demonstrated unprecedented  $K^+/Mg^{2+}$  electro dialysis (ED) selectivities after coating Nafion with multilayer films containing protonated poly(allylamine) (PAH) and poly(styrene sulfonate) (PSS).<sup>5</sup> More recently we reported similarly high  $Li^+/Co^{2+}$  and  $K^+/La^{3+}$  selectivities.<sup>2</sup> Figure 1 shows an example of highly selective electro dialysis using a source phase containing 0.01 M  $LiNO_3$  and 0.01 M  $Co(NO_3)_2$ . Cations migrate across the  $(PAH/PSS)_5PAH$ -modified membrane to the receiving phase, and the ion fluxes are proportional to the slopes in Figure 1. Based on the flux ratios, the  $Li^+/Co^{2+}$  selectivity is only 0.66 for the bare Nafion membrane and  $>1500$  for the coated membrane. Interestingly, in ED with PSS-terminated coatings ( $(PAH/PSS)_5$  films), the  $Li^+/Co^{2+}$  selectivity is only 24. Thus, positively-charged terminal layers are likely essential for achieving extreme selectivities among monovalent and divalent cations. Nevertheless, even at source-phase  $LiNO_3$  and  $Co(NO_3)_2$  concentrations of 0.1 M, where one would expect significant charge screening, the selectivity remains  $>1000$ .

The high cost of Nafion membranes may preclude their use in many applications. Thus, we also coated less expensive Fujifilm cation-exchange membranes with  $(PAH/PSS)_5PAH$  films and achieved  $K^+/Mg^{2+}$  selectivities  $>1000$ .<sup>1</sup> Nevertheless, one drawback in the use of PAH/PSS films is a relatively low limiting current due to the low diffusion permeability of the coatings. Poly(diallyldimethylammonium) (PDADMAC)/PSS films swell strongly in water, which should lead to a relatively high diffusion permeability. Membranes coated with  $(PDADMAC/PSS)_5PDADMAC$  films retain a  $K^+/Mg^{2+}$  selectivity  $>1000$ , and their use increases current efficiency to 80%, whereas membranes coated with PAH/PSS films show a current efficiency of only 60%.

Most recently, we began investigating selectivities among monovalent cations in both Donnan dialysis (DD) and ED. In DD through cation-exchange membranes, diffusion of cations from the source to the receiving phase couples with cation diffusion from the receiving to the source phase. Initial experiments examined DD using a source phase containing 0.01 M  $LiNO_3$  and 0.01 M  $KNO_3$  and a receiving phase of 0.02 M  $NaNO_3$ . With bare Nafion membranes, such experiments lead to a  $K^+/Li^+$  selectivity of 1.8, but coating of Nafion with  $(PAH/PSS)_5PAH$  films increases this selectivity to 10.5. This is surprising because the aqueous electrophoretic mobility of  $K^+$  is only

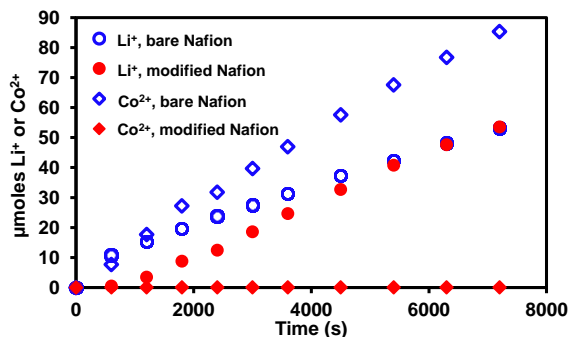


*Figure 1. Moles of  $Li^+$  and  $Co^{2+}$  in the receiving phase as a function of time during ED (current density of  $0.63 \text{ mA cm}^{-2}$ ) through bare Nafion membranes (open blue symbols) or Nafion coated with a  $(PAH/PSS)_5PAH$  film (filled red symbols). The source phase initially contained 0.01 M  $LiNO_3$  and 0.01 M  $Co(NO_3)_2$ , and the receiving phase was initially 0.01 M  $HNO_3$ . The membrane area was  $3.14 \text{ cm}^2$ .*

twice that of  $\text{Li}^+$ . Moreover, when the source phase contains 0.01 M  $\text{HNO}_3$  along with 0.01 M  $\text{LiNO}_3$  and 0.01 M  $\text{KNO}_3$ , the  $\text{K}^+/\text{Li}^+$  selectivity of the coated membrane increases to 69. Figure 2 demonstrates the selectivity in one DD experiment. Interestingly, in these experiments the  $\text{K}^+$  flux is greater than the proton flux, even though the aqueous mobility of protons is 5 times that of  $\text{K}^+$  ions. We surmise that the high selectivity in these membranes occurs due to selective partitioning into the polyelectrolyte film and hopping between ion-exchange sites. In ED with the same source phases as in Figure 2, the  $\text{K}^+/\text{Li}^+$  selectivity of the coated membrane is only 7.3, but this is still significantly higher than the selectivity of 1.9 for bare Nafion.

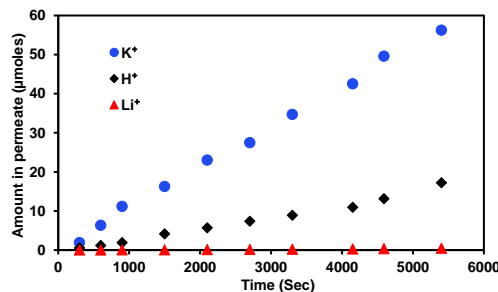


**Figure 2.** Moles of  $\text{K}^+$ ,  $\text{H}^+$ , and  $\text{Li}^+$  in the receiving phase as a function of time during DD through Nafion coated with a  $(\text{PAH}/\text{PSS})_5\text{PAH}$  film (filled symbols). The source phase initially contained 0.01 M  $\text{KNO}_3$ , 0.01 M  $\text{LiNO}_3$  and 0.01 M  $\text{HNO}_3$ , and the receiving phase was initially 0.02 M  $\text{NaNO}_3$ . The membrane area was  $3.14 \text{ cm}^2$ .

### Highly Selective Anion-exchange Membranes

Coating anion-exchange membranes with polyelectrolyte multilayers also yields highly selective transport. Figure 3 shows the total moles of  $\text{Cl}^-$  and  $\text{SO}_4^{2-}$  in the receiving phase as a function of time during 120 min of ED from a source phase containing 0.01 M  $\text{NaCl}$  and 0.01 M  $\text{Na}_2\text{SO}_4$ . Bare membranes show high passages of both  $\text{Cl}^-$  and  $\text{SO}_4^{2-}$ , and the average  $\text{Cl}^-/\text{SO}_4^{2-}$  selectivity of the unmodified membrane is only 1.3. However, after coating both sides of the Fujifilm membranes with  $(\text{PSS}/\text{PAH})_5\text{PSS}$  films, the  $\text{SO}_4^{2-}$  flux decreases to nearly undetectable levels and the  $\text{Cl}^-$  flux increases, giving rise to a remarkable  $\text{Cl}^-/\text{SO}_4^{2-}$  selectivity around 180. This value is much higher than the typical selectivities of  $<3$  for anion-exchange membranes and indicates that polyelectrolyte films fully cover the surface of Fujifilm anion-exchange membranes. Notably, selectivity is much lower when coating with  $(\text{PSS}/\text{PAH})_6$  films that terminate in a polycation, suggesting that electrostatic exclusion of  $\text{SO}_4^{2-}$  plays a major role in these separations. However, the  $\text{Cl}^-/\text{SO}_4^{2-}$  selectivity is still 50 in 0.1 M salt solutions, showing that charge screening does not greatly alter transport. Current work focuses on better understanding the mechanisms of selective ion transport.

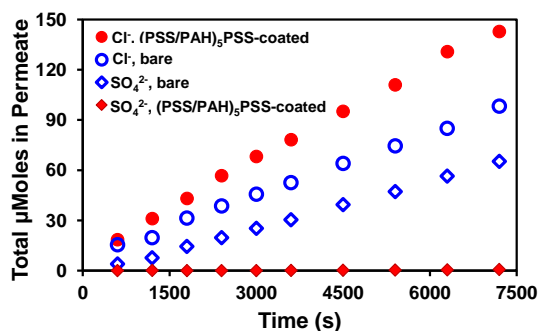


**Figure 3.** Amounts of  $\text{Cl}^-$  (triangles) and  $\text{SO}_4^{2-}$  (squares) in the receiving phase vs time during ED with a source phase containing 0.01 M  $\text{NaCl}$  and 0.01 M  $\text{Na}_2\text{SO}_4$ . The open blue and filled red symbols represent ED through bare and  $(\text{PSS}/\text{PAH})_5\text{PSS}$ -coated membranes, respectively, at a current density of  $0.63 \text{ mA cm}^{-2}$ . The receiving phase initially contained 0.01 M  $\text{Na}_2\text{CO}_3$ . The membrane area was  $3.14 \text{ cm}^2$ .

### Modelling Ion Transport

*Nonelectroneutrality in Barrier Layers.* Commercial reverse osmosis (RO) and nanofiltration (NF) membranes contain ultrathin barrier layers on porous supports.<sup>24</sup> The barrier layer selectively passes water (relative to salts or small molecules), while the thick support provides strength. Although solution-diffusion models of salt transport through barriers assume electroneutrality,

with ultrathin skins and low ion partition coefficients, space-charge regions may occupy most of the layer. We examined theoretically the implications of nonelectroneutrality on salt transport.<sup>4</sup>

Both immobile external surface charge and unequal cation and anion solvation energies in the barrier layer can give regions with excess mobile charge, and the size of these regions increases with decreasing feed concentrations and ion partition coefficients. Figure 4a shows the ion concentration profile in a membrane where the intrinsic partition coefficient, ( $\Gamma_i^{int}$ ) the partition coefficient with no electrical potential difference between the solution and the membrane, is low for the cation. The low cation solubility in the barrier gives a negatively charged region with a low cation concentration. The space charge creates a gradient of electrical potential between the solution and the membrane interior (Figure 4b), and for this case the potential difference leads to nearly equal cation and anion concentrations only in the center of the membrane (Figure 4a).

The low cation concentration in the space-charge region dramatically affects the resistance to salt transport,  $R_s$ , which we define in Eq(1), where  $\Delta c_s$  is the salt concentration difference between the feed and permeate solutions and  $j_s$  is the salt flux.

$$R_s \equiv \frac{\Delta c_s}{j_s} \quad (1)$$

Figure 5 shows how  $R_s$  varies with the barrier-layer thickness and the partition coefficient for the cation. As expected, lower partition coefficients lead to higher resistances. Moreover, the y-intercepts of the dashed lines in Figure 5 represent the additional resistance due to the depletion regions in membranes with half-thicknesses  $> \sim 30$  nm. Even for these relatively thick membranes, the space-charge region significantly increases resistance.

The ideal membrane should have a high value of  $R_s$  and a low hydraulic resistance to achieve high salt rejections at a fixed transmembrane pressure drop. For a specific barrier-layer material, the hydraulic resistance increases approximately linearly with thickness. In contrast, as the barrier-layer thickness increases,  $R_s$  initially rises rapidly and then plateaus or peaks and finally increases slowly. Thus, for the conditions in Figure 5 the highest ratios of  $R_s$  to hydraulic resistance will occur at half-thicknesses  $< 5$  nm, and these membranes should show the highest rejections at a given pressure. Further increasing the membrane half-thickness beyond  $\sim 10$  nm may even decrease  $R_s$ . Although the ideal membrane should have a total thickness  $< 10$  nm (half layer thickness  $< 5$  nm), total thicknesses of 20 nm will still produce high rejections, but further increases in thickness will decrease NF rejection for a given transmembrane pressure drop primarily because of decreases in volume flow. This may have significant implications for salt transport across cell membranes where the barrier layer thickness is only a few nm.

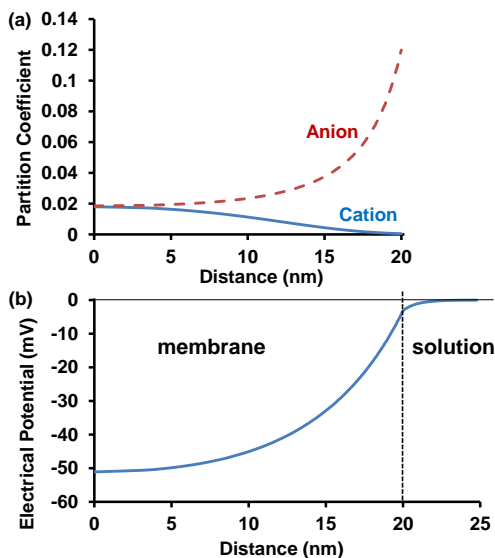


**Figure 4.** Simulated (a) ion-concentration profiles and (b) electrical potential for a membrane equilibrated on both sides with a solution containing 31 mM MA<sub>2</sub>. In figure (a), the partition coefficient is the ratio of the concentration at the location in the membrane to the feed concentration. The X-axis is the distance from the center of the membrane barrier, which has a total thickness of 40 nm. The concentration profile is symmetric about zero due to the assumption of a low concentration difference across the membrane. The simulation assumes intrinsic partition coefficients (in the absence of electrical potential) of 0.14 for the anion A<sup>-</sup> and  $3.4 \times 10^{-4}$  for the cation M<sup>2+</sup>.

An Analytical Solution to Ion Transport in Nanofiltration. In a second modeling study, we developed an analytical solution to the equations governing the solution-diffusion-electromigration transport of the ions from two salts that contain a common ion.<sup>3</sup> The analytical expressions, which rely on constant ion permeances throughout the membrane, enable simple spreadsheet computations of the permeate ion concentrations in NF. With such accessible calculations, we examined ion rejections as a function of transmembrane volume fluxes, feed solution compositions, and permeance values. For solutions containing dissolved MA and M<sub>2</sub>B, when the membrane permeance to B<sup>2-</sup> is much lower than that to A<sup>-</sup> and M<sup>+</sup>, plots of A<sup>-</sup> rejection versus transmembrane volume flux show a negative minimum. Additional calculations show that B<sup>2-</sup> rejection increases with increasing MA in the feed solution. Moreover, under some permeance conditions, rejection of A<sup>-</sup> decreases and then becomes negative as the ratio of A<sup>-</sup> to B<sup>2-</sup> decreases in the feed solution. This model is much simpler than those based on exclusion from nanopores and yet it effectively reveals trends in NF ion rejections and can help to identify the desired ion permeances or solution compositions for specific separations.

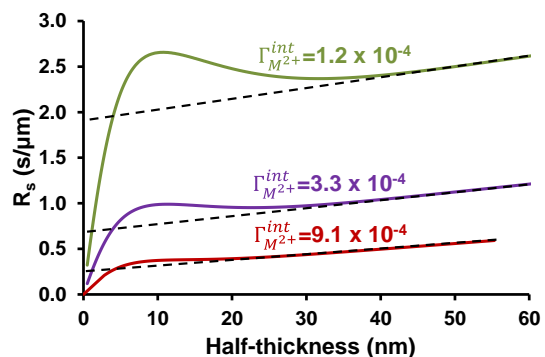


**Figure 5.** Resistances to salt transport,  $R_s$ , as a function of barrier-layer half-thickness for a layer equilibrated on both sides with a solution containing 31 mM MA<sub>2</sub>. The simulation assumes  $\Gamma_i^{int} = 0.14$  for A<sup>-</sup> and several values of  $\Gamma_{M^{2+}}^{int}$  for M<sup>2+</sup>, as noted on the plot. The calculations also employ barrier-layer diffusion coefficients of  $5 \times 10^{-12}$  m<sup>2</sup>/s for M<sup>2+</sup> and  $1 \times 10^{-11}$  m<sup>2</sup>/s for A<sup>-</sup>. Dashed lines show the linear relationship between thickness and resistance that occurs when the barrier layer is significantly thicker than the electrical double layer.

## Publications Acknowledging this Grant in 2015 – present

### (I) Exclusively funded by this grant;

1. Zhu, Y.; Ahmad, M.; Yang, L.; Misovich, M.; Yaroshchuk, A.; Bruening, M.L. Adsorption of Polyelectrolyte Multilayers Imparts High Monovalent/Divalent Cation Selectivity to Aliphatic Polyamide Cation-exchange Membranes *J. Membr. Sci.* **2017**, 537, 177–185.
2. White, N.; Misovich, M.; Alemayehu, E.; Yaroshchuk, A.; Bruening, M.L. Highly Selective Separations of Multivalent and Monovalent Cations in Electrodialysis Through Nafion Membranes Coated with Polyelectrolyte Multilayers *Polymer* **2016**, 103, 478–485.

### (II) Jointly funded by this grant and other grants with leading intellectual contribution from this grant;

3. Yaroshchuk, A.; Bruening, M.L. An Analytical Solution of the Solution-Diffusion-Electromigration Equations Reproduces Trends in Ion Rejections During Nanofiltration of Mixed Electrolytes *J. Membr. Sci.* **2017**, 523 361–372.
4. Yaroshchuk, A.; Zhu, Y.; Bondarenko, M.; Bruening, M.L. Deviations from Electroneutrality in Membrane Barrier Layers: A Possible Mechanism Underlying High Salt Rejections *Langmuir* **2016**, 32, 2644–2658.
5. White, N.; Misovich, M.; Yaroshchuk, A.; Bruening, M.L. Coating of Nafion Membranes with Polyelectrolyte Multilayers to Achieve High Monovalent/Divalent Cation Electrodialysis Selectivities *ACS Appl. Mater. & Interfaces* **2015**, 7, 6620–6628.

**Exploiting Insertion Processes for Continuous Membrane-free Ion Separations**  
Department of Chemistry, The University of Texas at Austin

**Presentation Abstract**

The ultimate goal of our DOE-sponsored research is to develop a fundamental understanding of how electrochemistry can be used to desalinate seawater. The basic-research approach to this technological goal is to develop methods for creating local ion concentration gradients. In the past, we have done this by electrochemically converting ions into neutral species using a metallic bipolar electrode (BPE). This resulted in a local decrease in ion concentration (e.g., ion concentration polarization, ICP) near the poles of the BPE, and this in turn led to a local electric field that could be used to steer secondary ions (like those in seawater, particularly  $\text{Na}^+$  and  $\text{Cl}^-$ ). This method was effective in that it provided a high degree of control over the way ion concentration gradients form and thus made it possible to partially desalinate seawater (though on a very small scale) without the need for a membrane. Even after these advances, however, problems remained having to do with the selectivity and the robustness of the electrode, which tended to either degrade or, worse, co-electrogenerate impurities that compromised the steepness of ion concentration gradients. Now we have found that ion insertion materials, of the type usually associated with batteries, can act as BPEs. Specifically, when properly configured, a Prussian blue (PB) BPE selectively inserts, transports, and deinserts small ions like  $\text{K}^+$ , and this leads to controlled ICP in the vicinity of the anodic and cathodic poles of the PB BPE. This finding seems to resolve most of the problems associated with the use of normal, metallic BPEs in that it leads to continuous transport of ions without electrogeneration of byproducts that compromise the degree of ICP. In this presentation we will briefly discuss our general approach for controlling ion motion, and then discuss preliminary findings related to the use of PB as a ion-conducting BPE.

**Grant or FWP Number: Electrochemically Mediated Membraneless Separations  
DE-FG02-06ER15758**

**Postdoc(s):** Jan Clausmeyer

**Student(s):** Eunsoo Yoon and Collin D. Davies

**Affiliations(s):** Dr. Dzmitry Hlushkou and Prof. Ulrich Tallarek, Department of  
Chemistry, Philipps-Universität Marburg

**RECENT PROGRESS**

*Continuous redirection and separation at a bipolar electrode.* The ultimate goal of our DOE-sponsored research is to develop a fundamental understanding of how electrochemistry can be used to desalinate seawater. The basic-research approach to this technological goal is to develop methods for creating local ion concentration gradients. In the past, we have done this by

electrochemically converting ions into neutral species. This results in a local decrease in ion concentration near an electrode, and this in turn leads to a local electric field that can be used to steer secondary ions (like those in seawater).

In the past we have used fluorescent tracers, like BODIPY<sup>2-</sup>, as a proxy to visualize the redistribution of ions near electrodes. It is, of course, impossible to track individual BODIPY<sup>2-</sup> molecules, and therefore many of the important details of ion motion were left unresolved. To address this issue, we began using charged microbeads as proxies for ion motion. Figure 1 shows the general approach for these microbead experiments. A bipolar electrode (BPE) is present within a microchannel (Figure 1a). Faradaic electrochemical reactions occurring at its poles result in

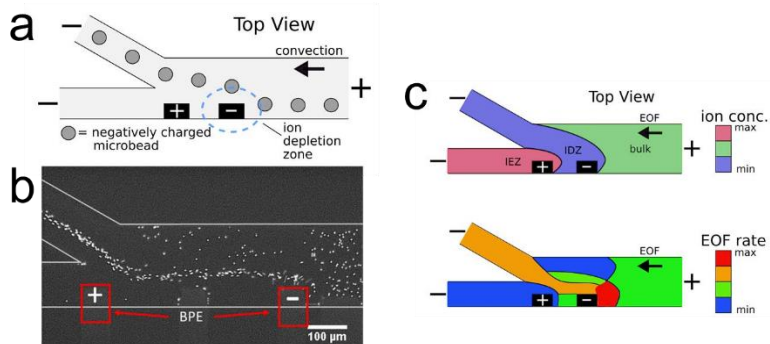


**Figure 1.** (a) Schematic illustration of continuous microbead redirection and separation at a bipolar electrode. (b) A fluorescent micrograph showing fluorescent microbead redirection and separation at a bipolar electrode. (c) Schematic illustration of local variations in ion concentration and the resulting local variations in EOF rate throughout the channel during bipolar electrochemistry.

formation of an ion depletion zone (IDZ) at the cathode and an ion enrichment zone (IEZ) at the anode. The IDZ and IEZ, in turn, lead to formation of an electric field gradient across a portion of the channel width that results in continuous redirection of negatively charged microbeads into the secondary channel (Figure 1b). By tracking discrete microbeads, regions of non-uniform electroosmotic flow (EOF), which have a significant impact on ion motion, can be visualized. These effects are summarized in Figure 1c.

### Light-driven ion

**separation.** During the present contract period, we developed a method to utilize a new class of materials, semiconductor photoelectrodes, for the membrane-free and light-driven separation of ions in water. In this method, electrochemical redox reactions at a TiO<sub>2</sub> photoanode and a Pt cathode within a microchannel lead to formation of an IDZ. Figure 2a is an illustration of the photoelectrochemical system. Here, the faradaic electrochemical reactions at the photoanode are coupled to reduction of water (to hydroxide) at the Pt cathode. Hydroxide

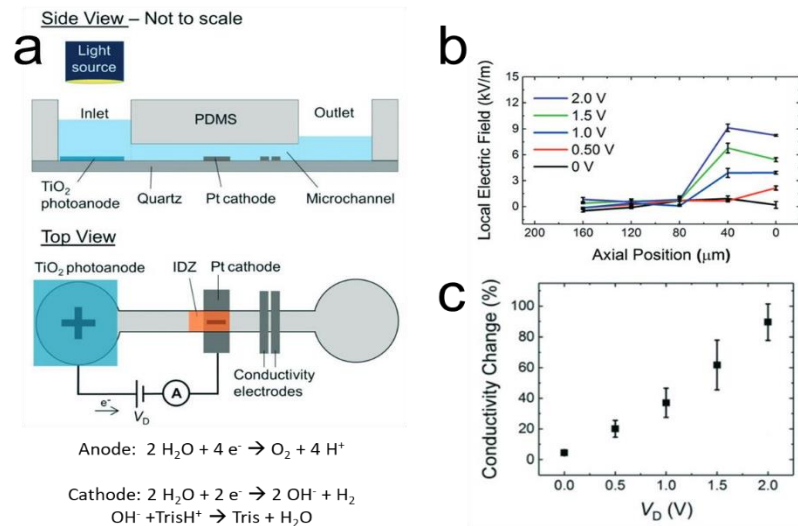


**Figure 2.** (a) Schematic illustration of photoelectrochemistry within a microfluidic system. (b) Local electric field measurements collected upstream of the Pt cathode (axial position 0 μm) as a function of the supplementary driving voltage (V<sub>D</sub>) applied between the photoanode and cathode. (c) Solution conductivity measured downstream of the Pt cathode as a function of V<sub>D</sub>. Solution conductivity is reported as the percent decrease in solution conductivity during photoelectrochemistry compared to bulk solution conductivity. The photoanode was illuminated by a Hg arc lamp during all experiments.

neutralizes  $\text{TrisH}^+$  present in solution, thereby leading to a region of low ionic strength (i.e., an IDZ) and a corresponding local electric field gradient (Figure 2b). This gradient results in accumulation of secondary charge carriers near the BPE, which in turn leads to a decrease in ion conductivity downstream of the BPE (Figure 2c). The main finding is that light can be used to control ion motion and, perhaps, to desalinate seawater.

**Ion separation by continuous ion insertion.** As discussed above, we have previously shown that electrochemical processes can lead to the formation of an IDZ and a corresponding local electric field gradient that can control the movement of charged species (microbeads and ions). We have now discovered that intercalation materials of the type used in batteries can also act as BPEs, and we have tested these materials to determine if they can generate an IDZ. The results show that when properly configured, a Prussian blue (PB) BPE selectively inserts, transports, and deinserts small ions like  $\text{K}^+$ , and this leads to an IDZ and hence a local electric field gradient that can be used to manipulate ion motion.

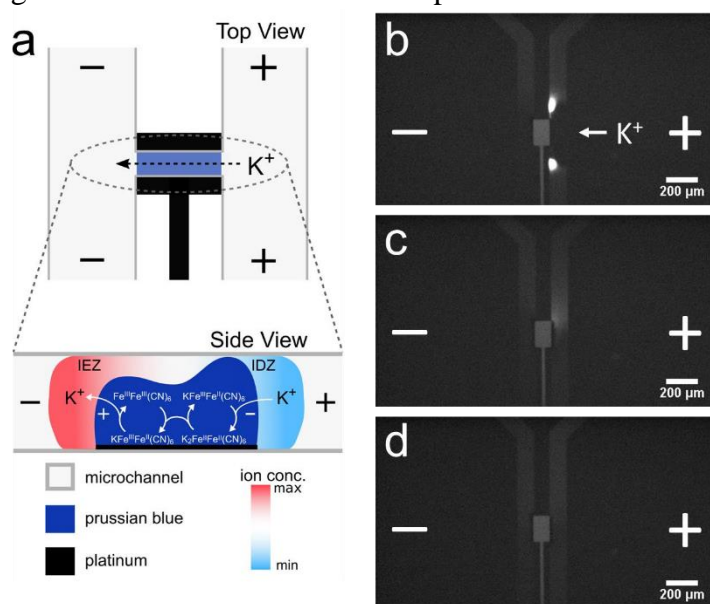


Figure 3. (a) Schematic illustration of  $\text{K}^+$  transport through PB electrodeposited in the connecting cross channel. (b-d) Fluorescence micrographs captured following application of a driving voltage of 35 V across the H-shaped microfluidic channel for 70 s. Electrolyte contains (b) 5.0 mM KCl, 10.0  $\mu\text{M}$  BODIPY<sup>2-</sup>, (c) 7.1 mM Tris-HCl, 10.0  $\mu\text{M}$  BODIPY<sup>2-</sup>, and (d) 10.0 mM TBAP, 10.0  $\mu\text{M}$  BODIPY<sup>2-</sup>. All solutions were prepared to have identical conductivity and pH value. The direction of electroosmotic flow and pressure-driven flow was right to left across the connecting cross channel.

Figure 3a is an illustration showing how a microfluidic device is configured so that PB acts as a BPE. Here, PB is electrodeposited in the connecting cross channel of an H-shaped microfluidic system. When a driving voltage is applied to reservoirs in the main channels,  $\text{K}^+$  is continuously transported through the PB, and this leads to an IDZ and an IEZ at the cathodic and anodic poles of the PB BPE, respectively.

The local electric field gradient associated with the IDZ can be used for enrichment and separation of charged ions via electric field gradient focusing. For example, Figure 3b shows enrichment of the tracer BODIPY<sup>2-</sup> in the vicinity of the cathodic pole of the PB BPE. However, if cations present in solution are too large to intercalate into the PB crystal lattice, no IDZ forms, as shown in Figures 3c and 3d.

These findings reveal that insertion processes result in the separation of ions by two distinct mechanisms. The first mechanism separates ions by selective transport via ionic conductance through an intercalation material operated as a BPE. The second mechanism separates and enriches secondary ions along the electric field gradient formed by ion insertion into the intercalation material. The findings in this project provide a first step toward the development of continuous ion separation strategies based on insertion processes.

## Publications Acknowledging this Grant in 2015 – present

Please classify your publications into three categories according to the source of support for the work published:

(I) *Exclusively funded by this grant\**

1. Davies, C. D.; Yoon, E.; Crooks, R. M. Continuous Redirection and Separation of Microbeads via Faradaic Ion Concentration Polarization. *ChemElectroChem* **2017**, (published on the Wiley website; DOI: 10.1002/celec.201700450).
2. Yoon, E.; Davies, C. D.; Hooper, T. A.; Crooks, R. M. Photoelectrochemical Ion Concentration Polarization: Membraneless Ion Filtration Based on Light-Driven Electrochemical Reactions. *Lab Chip* **2017**, *17*, 2491-2499 (DOI: 10.1039/C7LC00455A).
3. Hlushkou, D.; Knust, K. N.; Crooks, R. M.; Tallarek, U. Numerical Simulation of Electrochemical Desalination. *J. Phys.: Condens. Matter* **2016**, *28*, Art. No. 194001 (DOI: 10.1088/0953-8984/28/19/194001).

(II) *Jointly funded by this grant and other grants with leading intellectual contribution from this grant;*

n/a

(III) *Jointly funded by this grant and other grants with relatively minor intellectual contribution from this grant*

n/a

\*May include attribution to a collaborator's grant or to the Robert A. Welch Fdn., which provides sustaining support for our research program in the form of an endowment.

## Tailoring High Performance Carbon Molecular Sieve Membranes for Energy Intensive Separations

Bill Koros

Georgia Institute of Technology, School of Chemical & Biomolecular Engineering

### Presentation Abstract

This project pursues fundamental understanding of carbon molecular sieve (CMS) membranes, which can provide major reductions in separation costs and energy use. Pyrolyzed polymer precursor dense films and asymmetric fibers provide dramatically higher separation performance than achievable by state-of-the-art polymeric membranes for important O<sub>2</sub>/N<sub>2</sub>, C<sub>2</sub>H<sub>4</sub>/C<sub>2</sub>H<sub>6</sub>, N<sub>2</sub>/CH<sub>4</sub> and CO<sub>2</sub>/CH<sub>4</sub> pairs. The high performance results from ability to constrain diffusional translational, rotational and vibrational activated state degrees of freedom of the rejected component of gas pairs. Fortunately, such constraints reduce diffusion coefficients of the rejected component greatly, but can maintain high diffusion coefficients of the more compact member of each of the above pairs. Such so-called “entropic selectivity” also applies to even more complex C<sub>3</sub>H<sub>6</sub>/C<sub>3</sub>H<sub>8</sub> and n-C<sub>4</sub>H<sub>10</sub>/i-C<sub>4</sub>H<sub>10</sub> pairs. Broadly applying this fundamental principle can enable huge reductions in energy requirements versus current distillation approaches used for separations around the world. Equally important to the BES mission is identification of detailed transformational pathway from semi-flexible polyimide precursor structures, without entropic selectivity, to CMS forms with entropic selectivity. These insights, which our group is providing, will suggest advanced CMS structures with tailored properties for diverse challenging separations and will be discussed in this presentation.

**Grant or FWP Number: DE-FG02-04ER15510 – Tailoring High Performance Carbon Molecular Sieve Membranes for Energy Intensive Separations**

**PI:** Prof. William J. Koros

**Student(s):** Graham B. Wenz, PhD graduated December 15, 2017

**Student(s):** Samuel Hays

### RECENT PROGRESS

**1.0 Introduction and Overview:** Membrane-based separations offer the lowest energy-intensity separation option by using mechanical pressure sources of chemical potential rather than thermally-driven phase change processes. Replacement of energy-intensive separations is occurring rapidly for aqueous feeds, but gas feeds require much finer size discrimination versus aqueous feeds, thereby making this replacement more challenging. For instance in the most challenging aqueous reverse osmosis cases, a 6 Å hydrated salt ions must be rejected while permeating 3 Å water molecules. On the other hand, in gas separations as little as 0.1-0.5 Å

difference must be used to achieve the separations, thereby making absolute discrimination roughly an order of magnitude more difficult.

The “sorption-diffusion” mechanism describes permeation of component A (Eq 1) and permselection (Eq 2) of component A vs. B as a selective product of sorption selectivity and diffusion selectivity, viz.,

$$P_A = \frac{N_A \cdot l}{\Delta p_A} = D_A S_A \quad (1)$$

$$\alpha_{AB}^* = \frac{P_A}{P_B} = \frac{D_A S_A}{D_B S_B} \quad (2)$$

The permeability coefficient,  $P_A$ , of component A,  $N_A$ , the flux of A across the membrane of thickness,  $l$ , and the difference in partial pressure  $\Delta p_A$  (or fugacity difference) is *deceptively simple in appearance*. Indeed, ( $D_A$ ) the diffusion coefficient (kinetic factor), and ( $S_A$ ), the sorption coefficient (thermodynamic factor) of each penetrant in the polymer are actually complex fundamental parameters that must be tailored by molecular engineering for success. Permeability is usually reported in Barrers, with  $1 \text{ Barrer} = 10^{-10} \text{ cc(STP) \cdot cm \cdot cm}^{-2} \cdot \text{s}^{-1} \cdot \text{cmHg}^{-1}$ .

**2.0 Fundamental Advances:** In membranes, penetrants execute size-dependent diffusion-selective jumps moderated by the activation energy needed to execute the jump, and such an energetically based selection process can be called “energetic selectivity”. Experience tailoring activation energies of diffusion in typical materials suggests this tool is reaching a point of diminishing returns for polymers. Taking the next step to increase diffusion selectivity in Eq. 2 requires addressing the transition state theory of diffusion, which shows a detailed expression for this complex parameter in Eq (3). The transition state representation of diffusion selectivity includes a quadratic ratio of jump lengths of component A vs. B, multiplied by the exponential difference in free energies of activation:

$$\left( \frac{D_A}{D_B} \right) = \frac{\lambda_A^2}{\lambda_B^2} \exp\left(\frac{-\Delta G_{D,AB}^\ddagger}{RT}\right) = \frac{\lambda_A^2}{\lambda_B^2} \exp\left(\frac{-\Delta(H_{D,AB}^\ddagger - TS_{D,AB}^\ddagger)}{RT}\right) = \frac{\lambda_A^2}{\lambda_B^2} \underbrace{\exp\left(\frac{-\Delta(H_{D,AB}^\ddagger)}{RT}\right)}_{\text{Energetic selectivity}} \underbrace{\exp\left(\frac{+\Delta S_{D,AB}^\ddagger}{R}\right)}_{\text{Entropic selectivity}} \quad (3)$$

Jump lengths between sorption sites are effectively identical for A & B in molecular sieving matrices, so the diffusion selectivity essentially equals the product of the exponential energetic and entropic selectivity terms. The revolutionary aspect of CMS materials lies in their ability to exert entropic selectivity by constraining *translational, rotational and vibrational activated state degrees of freedom of the rejected component of similarly sized gas pairs*. Such constraints reduce diffusion coefficients of the rejected component greatly, while maintaining high diffusion coefficients of the slightly more compact member in the above-mentioned important penetrant pairs. We have used the above framework to identify important penetrant pairs, such as O<sub>2</sub>/N<sub>2</sub>, C<sub>2</sub>H<sub>4</sub>/C<sub>2</sub>H<sub>6</sub>, N<sub>2</sub>/CH<sub>4</sub> and CO<sub>2</sub>/CH<sub>4</sub> that are well-suited to separations with CMS.

**3.0 Experimental Advances:** Our recent work with various complex 6FDA-based polyimide precursors further highlighted the lack of a simple connection between precursor physical properties and resulting CMS materials. Specifically, this work highlighted the lack of a direct

connection between free volume and x-ray “d-spacings” for various *polymer precursors* and the corresponding properties of CMS derived from these precursors (28) such as that shown in Fig. 1.

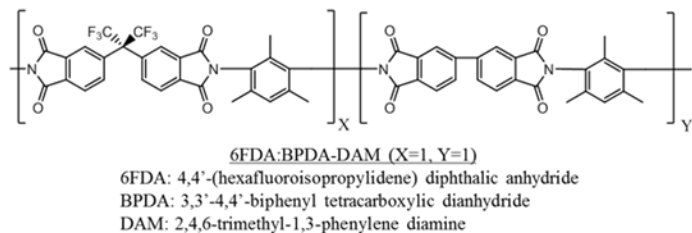


**Figure 1:** Chemical structure of semi-flexible 6FDA:BPDA-DAM 1:1: precursor

The above-mentioned lack of a simple connection between the random coil precursor and accepted slit-like structure of CMS, has motivated our DOE BES work in the current funding cycle. This work now provides a rational framework to develop a broad array of advanced CMS structures by tailoring properties for challenging separations. The general concepts presented here are relevant to most polyimide precursors. Much of our work has focused on the so-called 6FDA:BPDA-DAM (X=1:Y=1) (Fig. 1) discussed in our recent papers.

This material provides a useful comparison point for a family of relatives of 6FDA:BPDA-DAM also considered in our work in our current work cycle, for the important CO<sub>2</sub>/CH<sub>4</sub> gas pair in Fig. 2. Clearly the two materials containing the DABA diamine are especially attractive, and our work on them was enabled by an earlier BES funding cycle in which we discovered the ability to crosslink polyimide chains well below their glass transition temperatures. These DABA-derived CMS materials show either selectivities or permeabilities surpassing the 6FDA:BPDA-DAM base case—note the log axis in Fig. 2. Moreover, at higher pyrolysis temperatures, the selectivities are even higher—with still attractive permeabilities. The materials in Fig. 2 are stable in very aggressive feeds comprising of 800-1000 psia with high partial pressures of CO<sub>2</sub>. Unlike simple polymer precursors, d-spacings in the various CMS materials were only slightly different

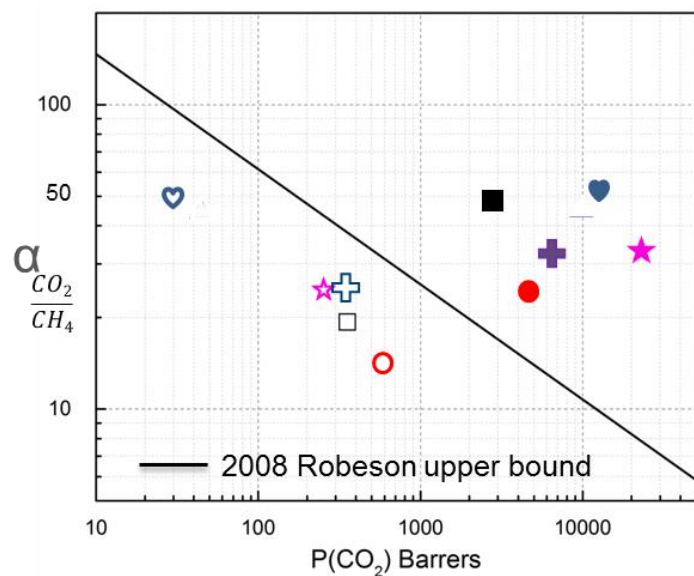
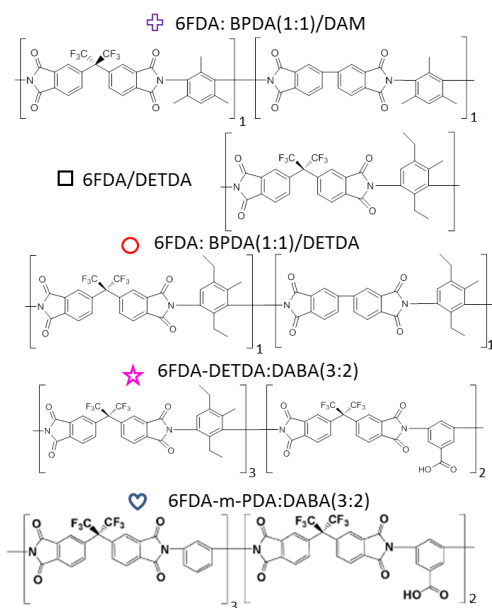


**Figure 2:** CO<sub>2</sub>/CH<sub>4</sub> performance summary for CMS materials (550 °C UHP Ar pyrolysis), relative to the well-known Robeson upper bound line soluble polymers. The open symbols are precursors and solid symbols are the CMS materials for the corresponding structures.



and provided no clear indicator of transport differences relative to the base case 6FDA:BPDA-DAM material. This observation is understandable, since the

key morphological features in rigid carbons are related to micropores and ultramicropores, which are not reflected well by average WAXD d-spacing or average fractional free volume results.

Moreover, both of these standard polymer characterizations are compromised by ill-defined WAXD peaks and incomplete knowledge of the free volume fraction of complex CMS materials. This realization in the past funding cycle led us to pursue alternate considerations of the nature of the CMS structure and its evolution from the glassy polymer precursors published in a recent paper. The various pyrolysis phases cause transformation from a random coil precursor into a disrupted plate molecular sieving structure. In this integrated process, chemical changes and evolution of gases comprising, for example,  $\text{CF}_3\text{H}$ ,  $\text{HF}$ ,  $\text{CO}_2$ ,  $\text{CO}$  &  $\text{CH}_4$  occurs. More aromatization occurs, with nitrogen remaining in the backbone until rather high temperatures, while  $\text{CO}$  and  $\text{CO}_2$  evolution at relatively low temperatures removes most, but not all, of the originally present oxygen atoms.

Pyrolysis of high molecular weight (150,000 g/mol) semi-flexible random coil polyimides result in ~40% weight loss at 800 °C. This process to produce a high molecular weight rigid structure clearly presents a *solid state packing problem*. An entangled semi-flexible precursor undergoing aromatization and linearization tends to create sufficiently large localized stresses to cause multiple scissions along its backbone. This process allows aromatization to proceed while producing shorter, more mobile structural strands; however, *a packing issue still exists* even for such shortened rigid strand oligomers. The impact of this issue regarding effects of strand composition is proposed for consideration in our current work using systematic copolymer composition studies. The rigid aromatized strands solve a “packing problem” similar to that found in rigid liquid crystalline polymers due to a high concentration of rigid strands—*by organizing into more packable entities such as plates and amorphous but molecularly sieving entities*.

Evolution to the many neighboring cells in such an idealized overall CMS structure is envisioned to occur during the final thermal soak and cooling phases after pyrolysis. During the soak and cooling phases, adjacent micropore “cells” can coalesce, and ultramicropore “walls” can be shared between “cells”, resulting in integrated cellular structures. In our current work, ramp rates and systematic variation of the **soak time and cooling rates** allow studying this mechanistic picture of structure development using gas transport. The amorphous CMS, with micropores separated by ultramicropores in the micropore plate walls possess molecular sieving properties. A spectrum of gases and vapors with well-defined critical sieving sizes such as  $\text{C}_2\text{H}_4$ ,  $\text{C}_2\text{H}_6$ ,  $\text{C}_3\text{H}_6$  and  $\text{C}_3\text{H}_8$  are used to characterize slit-like pores based on Corey-Pauling-Koltun space filling models. This spectrum of penetrants allows clarification of the permselectivity contributions from diffusion selectivity and sorption selectivity according to Eq (2).

This work is effort-intensive, since both temperature dependent, and pressure dependent sorption and permeation studies are needed to determine diffusion coefficients and their entropic vs. energetic components. This fact notwithstanding, such information is extremely well aligned with BES goals.

#### **4.0 Publications—Acknowledging this Grant in 2015 → present**

(I) *Exclusively funded by this grant;*

1. Koros, W.; Zhang, C. Materials for Next-Generation Molecularly Selective Synthetic Membranes, *Nature Materials*, **2017**, 16, 289-297.
2. Qiu W.; Liu, L.; Koros, W. Effect of Block Versus Random Copolyimide Structure on Hollow Fiber Membrane Spinnability. *J. Membr. Sci.*, **2017**, 529, 150-158.
3. Wenz, G.; Koros, W. Tuning Carbon Molecular Sieves for Natural Gas Separations: A Diamine Molecular Approach. *AICHE J*, **2017**, 63, 51-760.

4. Adams, J.; Bighane, N.; Koros, W. Pore Morphology and Temperature Dependence of Gas Transport Properties of Silica Membranes Derived from Oxidative Thermolysis of Polydimethylsiloxane. *J. Membr. Sci.*, **2017**, 524, 585-595.

(II) *Jointly funded by this grant and other grants with leading intellectual contribution from this grant;*

5. Kamath, M. G.; Fu, Shilu; Itta, Arun K.; Qiu, W. L.; Liu, G. P.; Swaidan, R.; Koros, W. J. 6FDA-DETDA: DABE Polyimide-Derived Carbon Molecular Sieve Hollow Fiber Membranes: Circumventing Unusual Aging Phenomena. *J. Membr. Sci.*, **2018**, 546, 197-205.
6. Fu, S.; Sanders, Edgar S.; Kulkarni, S.; Chu, Y. H; Wenz, GB; Koros, WJ. The Significance of Entropic Selectivity in Carbon Molecular Sieve Membranes Derived from 6FDA/DETDA:DABA(3:2) Polyimide. *J. Membr. Sci.*, **2017**, 329-343.
7. Zhang, C.; Wenz, G.B.; Williams, J.P.; Mayne, J. M.; Liu, G. P.; Koros W. J. Purification of Aggressive Supercritical Natural Gas Using Carbon Molecular Sieve Hollow Fiber Membranes. *Indus. & Engr. Chem. Res.*, **2017**, 56, 10482–10490.
8. Zhang, C.; Koros, W. J. Ultraselective Carbon Molecular Sieve Membranes with Tailored Synergistic Sorption Selective Properties, *Adv. Mater.* **2017**, 29, 1701631.
9. Rungta, M.; Wenz, G. B. Zhang, C.; Xu, L.; Qui, W. L.; Adams, J. S.; Koros, W. J. Carbon Molecular Sieve Structure Developments and Membrane Performance Relationships, *Carbon*, **2017**, 115, 237-248.
10. Liu, G.P.; Li, N.; Miller S.; Kim D. ; Yi, S.; Labreche, Y.; W. Koros. Molecularly Designed Stabilized Asymmetric Hollow Fiber Membranes for Aggressive Natural Gas Separation. *Angew. Chem.Int. Ed.* **2016**, 55, 13754-13758
11. Fu, S.; Wenz, G.B.; Sanders, S.; Kulkarni, S.; Qiu, W.; Ma, C.H.; Koros, W. J. Effects of Pyrolysis Conditions on Gas Separation Properties of 6FDA/DETDA:DABA(3:2) Derived Carbon Molecular Sieve Membranes. *J. Membr. Sci.*, **2016**, 520, 699-711
12. Fu, S.; Sanders, E.; Kulkarni, S.; Wenz, G. B. Koros, W. J. Temperature Dependence of Gas Transport and Sorption in Carbon Molecular Sieve Membranes Derived from Four 6FDA Based Polyimides: Entropic Selectivity Evaluation. *Carbon*, **2015**, 95, 995-1006.

(III) *Jointly funded by this grant and other grants with relatively minor intellectual contribution from this grant*

13. Zhang, C.; Koros, W. J. Tailoring the Transport Properties of Zeolitic Imidazolate Frameworks by Post-Synthetic Thermal Modification, *ACS Appl. Mater. Interfaces.* **2015**, 7, 23407-23411.
14. Zhang, C.; Koros, W. J. Zeolitic Imidazolate Frame work - Enabled Membranes: Challenges and Opportunities, *J. Phys. Chem. Lett.*, **2015**, 6, 3841–3849

**Influence of Pendant Group Basicity on the Facilitated Transport of CO<sub>2</sub>  
Across Hyperthin Polyelectrolyte Multilayers**

Steven L. Regen, Cen Lin and Erwin R. Stedronsky  
Department of Chemistry, Lehigh University, Bethlehem PA 18015

**Presentation Abstract**

Facilitated transport provides a means for enhancing the CO<sub>2</sub>/N<sub>2</sub> selectivity of polymeric membranes, which can have important practical consequences for the removal of CO<sub>2</sub> from flue gas-- the main source of man-made CO<sub>2</sub>. In the present study three basic science questions related to such transport have been addressed: (i) Can the facilitated transport of CO<sub>2</sub> be observed in a hyperthin (<100 nm thick) polymer membrane? (ii) Does such transport require the presence of strongly basic pendant groups? (iii) Is water vapor essential for such transport? Using hyperthin (20-30 nm thick) polyelectrolyte multilayers bearing pendant groups of varying basicity, the answers to these questions have been found to be yes, no and no, respectively.

**DE-FG02-05ER15720: Hyperthin Membranes For Gas Separations**

**Student(s):** Mr. Cen Lin

**RECENT PROGRESS**

***Three Basic Science Questions Related to the Facilitated Transport of CO<sub>2</sub> and a Design Strategy for Answering Them.***

The facilitated transport of CO<sub>2</sub> across polymer membranes provides a means for enhancing CO<sub>2</sub>/N<sub>2</sub> selectivity, which can have important practical consequences for the removal of CO<sub>2</sub> from flue gas-- the main source of man-made CO<sub>2</sub>. We have carried out a study that addresses three fundamental questions related to such transport: (i) Can the facilitated transport of CO<sub>2</sub> be observed in a hyperthin (<100 nm thick) polymer membrane? (ii) Does such transport require the presence of strongly basic pendant groups? (iii) Is water vapor essential for such transport?

To address these questions we used a design strategy that is shown in Figure 1. In brief, a series of hyperthin polyelectrolyte multilayers are formed *via* the layer-by-layer deposition method from poly(sodium 4-styrene sulfonate) (PSS) and poly(styrene)-based polycations bearing pendant groups of varying basicity. These membranes are then subjected to various feed pressures of CO<sub>2</sub> in the absence of water vapor, and their permeances (i.e., observed flux/pressure gradient) recorded. Since the facilitated transport of CO<sub>2</sub> contributes, significantly, to the total flux *only at low feed pressures* (i.e., at high feed pressures the active sites become saturated with CO<sub>2</sub> and the

total flux is dominated by solution-diffusion pathways), facilitated transport is revealed by plot of observed permeance versus feed pressure showing increased permeances at low feed pressures.

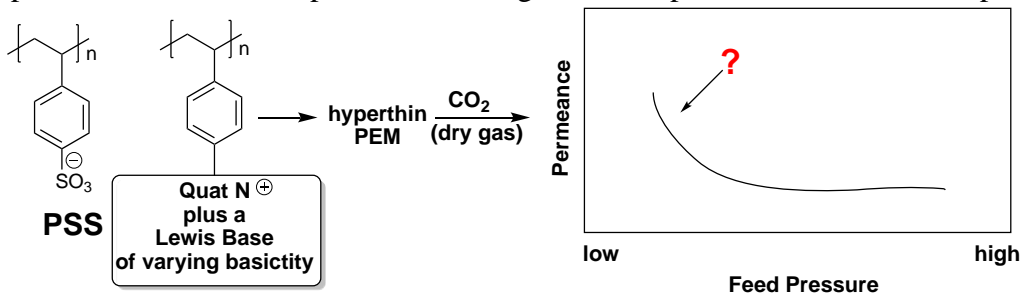


**Figure 1.** Design strategy used to address three basic science questions.

### Targeted Polycations

Specific polycations that have been synthesized and combined with PSS to form hyperthin polyelectrolyte multilayers (PEMs) *via* the layer-by-layer method are shown in Figure 2; the estimated pKa values of their pendant groups in their conjugate acid forms are also shown.

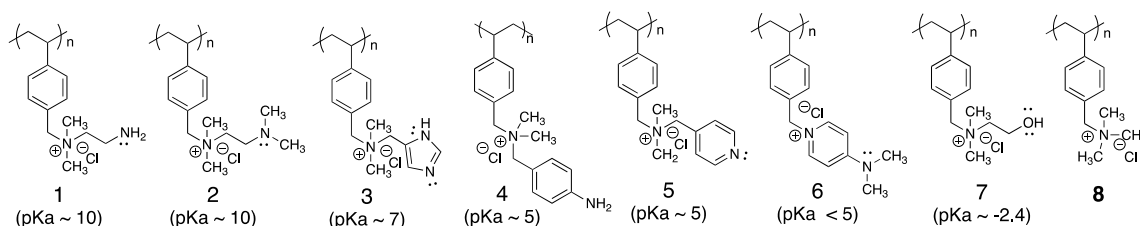


**Figure 2.** Poly(styrene)-based polycations.

### Evidence for Facilitated Transport of CO<sub>2</sub> Across 22 nm Thick PEMs of PSS/3.

In Figure 3 are shown plots of the permeance of dry CO<sub>2</sub>, H<sub>2</sub> and N<sub>2</sub> (inset) as a function of feed pressure. As is readily apparent, a significant increase in permeance is observed only for CO<sub>2</sub> at low feed pressures. These results provide strong support for the facilitated transport of CO<sub>2</sub> across such membranes.

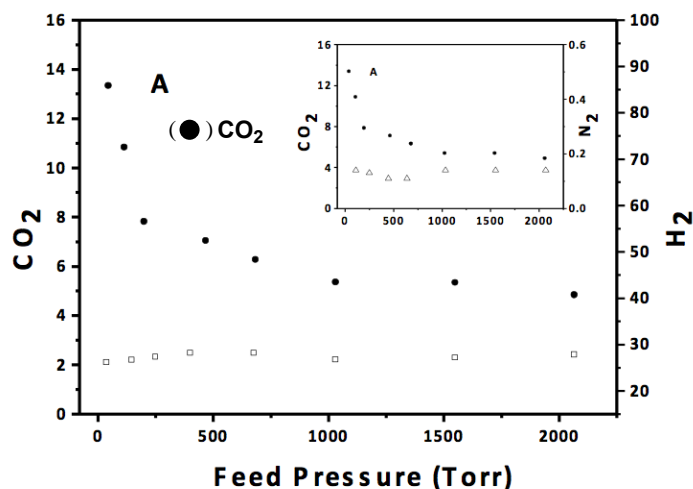


**Figure 3.** Plot of permeances for CO<sub>2</sub>, H<sub>2</sub> and N<sub>2</sub> across 22 nm PEMs of PSS/3. Permeance values are in GPU, where 1 GPU = 1 x 10<sup>-6</sup> cm<sup>3</sup> (STP)/cm<sup>2</sup>-s-cm Hg.

### ***Influence of Pendant Group Basicity.***

Table 1 summarizes the principal results obtained with all of the PEMs that were investigated. Specific permeance values listed were obtained using a pressure gradient of 2068 Torr. Also shown (in parentheses) are the CO<sub>2</sub>/N<sub>2</sub> selectivities observed when a pressure gradient of 50 Torr was employed. In all cases, H<sub>2</sub> and N<sub>2</sub> permeances were constant at both pressures. For some of these membranes, especially ones having pendant groups of intermediate basicity (i.e., estimated pKa values lying between 5 and 7), a significant increase in the permeance of CO<sub>2</sub> was found.

### ***Conclusions.***

These findings show that (i) the facilitated transport of CO<sub>2</sub> is possible in hyperthin membranes, (ii) strongly basic pendant groups are not essential for such transport, (i.e., an intermediate pKa of ca. 5-7 appears optimal), and (iii) water vapor is also not essential for the facilitated transport of CO<sub>2</sub>. A plausible explanation for the greater facilitated transport found with pendant groups of intermediate basicity is that such basicity allows for the fastest binding and release of CO<sub>2</sub>, and also an equilibrium constant that lies closest to 1.0; i.e., it has the most favorable kinetics and thermodynamics for facilitated transport.

**Table 1. Permeances in GPUs at 2068 Torr**

Polymer	<i>l</i> (nm)	H <sub>2</sub>	CO <sub>2</sub>	N <sub>2</sub>	H <sub>2</sub> /N <sub>2</sub>	CO <sub>2</sub> /N <sub>2</sub>
----	----	620	1400	260	2.4	5.4
<b>1 [10]</b>	27	15	1.9	.025	630	76(84)
		9.9	1.7	.018	550	95(100)
<b>2 [10]</b>	32	5.6	0.23	.016	400	14(17)
		4.3	0.20	.015	290	13(15)
<b>3 [7]</b>	22	28	4.8	0.14	200	34(100)
		25	3.1	0.13	190	24(78)
<b>4 [5]</b>	25	23	4.7	.056	400	84(160)
		19	5.1	.053	360	96(170)
<b>5 [5]</b>	27	28	4.5	.054	530	83(140)
		25	4.6	.051	490	90(150)
<b>6 [5]</b>	22	123	46	.47	260	100(140)
		125	52	.51	250	100(150)
<b>7 [-2]</b>	28	28	6.1	.066	420	92(92)
		28	5.7	.062	450	92(96)
<b>8 [--]</b>	21	115	42	0.44	260	95 (92)
		114	48	0.53	220	91(87)

[estimated pKa]

(selectivity at 50 Torr)

## Publications Acknowledging this Grant in 2015 – present

(I) Exclusively funded by this grant;

1. Lin, C.; Stedronsky, E.; Regen, S. L. pKa-Dependent Facilitated Transport of CO<sub>2</sub> Across Hyperthin Polyelectrolyte Multilayers. *ACS Appl. Mater. Interfaces*, **2017**, *9*, 19525-19528.
2. Yi, S.; Leon, W.; Vezenov, D.; Regen, S. L. Tightening Polyelectrolyte Multilayers With Oligo Pendant Ions. *ACS Macro Lett.*, **2016**, *5*, 915-918.
3. Yi, S.; Lin, C.; Leon, W.; Vezenov, D.; Regen, S. L. Gas Permeability of Hyperthin Polyelectrolyte Multilayers Having Matched and Mismatched Repeat Units. *Langmuir*, **2016**, *32*, 12332-12337.
4. Lin, C.; Yi, S.; Regen, S. L. Consequences of Tacticity on the Growth and Permeability of Hyperthin Polyelectrolyte Multilayers. *Langmuir*, **2016**, *32*, 375-379.
5. Yi, S.; Lin, C.; Regen, S. L. Splaying Hyperthin Polyelectrolyte Multilayers to Increase Their Gas Permeability. *Chem. Commun.*, **2015**, *51*, 1439-1441.

## **Design and Study of Hybrid Polyimide-Ionene Architectures for Membrane Separations**

Jason E. Bara, C. Heath Turner, Kathryn E. O’Harra, Grayson P. Dennis, Ashgar Abedini  
University of Alabama, Department of Chemical & Biological Engineering

### **Presentation Abstract**

Hybrid polyimide-ionene architectures represent a radically new way to integrate the structures of polyimide materials and ionic liquids (ILs) within the backbone of a condensation polymer. The combination of the desirable properties of each of class of material within a single, covalently-bonded structure offers vast possibilities to control polymer properties such as fractional free volume (FFV) which will influence the gas permeability and gas pair selectivity of membranes formed from these polyimide-ionene hybrids. The modular approach by which hybrid polyimide-ionene materials are constructed allows for the systematic variation of multiple structural variables in the polymer backbone and is also amenable to the inclusion of elements associated with polymers of intrinsic microporosity (PIMs) and thermally-rearranged (TR) polymers. This presentation will detail the progress made in the first few months of this project in the design, synthesis and study of hybrid polyimide-ionene architectures for membrane separations. Specifically, the new approaches we have taken in the design and synthesis of these polyimide-ionene hybrids from both experimental and computational approaches will be presented along with results of thermal properties, structural characterizations, processing techniques, membrane formation and transport/separation properties.

### **Design and Study of Hybrid Polyimide-Ionene Architectures for Membrane Separations (DE-SC001818)**

**PI:** Jason E. Bara (PI), C. Heath Turner (co-PI)

**Postdoc(s):** TBD – Interviews currently underway

**Student(s):** Kathryn E. O’Harra, Grayson P. Dennis, Ashgar Abedini

**Affiliations(s):** University of Alabama, Department of Chemical & Biological Engineering

### **RECENT PROGRESS**

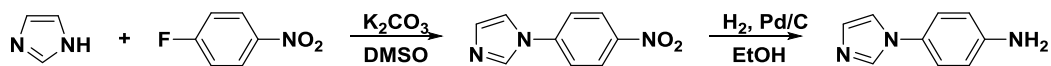
#### ***Synthesis of Advanced Monomers and Ionic Polyimide Materials***

Preliminary work in the design and synthesis of these hybrid polyimide-ionene materials relied on the use of commercially available compounds such as 1-(3-aminopropyl)imidazole, pyromellitic dianhydride (PMDA) and *p*-dichloroxylyene. This approach yielded materials with good film-forming ability but low gas permeability. However, in order to achieve materials with

increased aromatic character, greater MW and control over regiochemistry, entirely new monomers have been designed and synthesized from fundamental building blocks. As this project officially began on 8/15/2017, our progress primarily relates to success in achieving the proposed polymer architectures which are radically different from the conventional ionene concepts reported in the literature.

Our work has demonstrated that imidazole-aniline compounds can be successfully synthesized at scales of up to 200 g starting from imidazole and 4-fluoronitrobenzene, followed by catalytic reduction according to Scheme 1:

**Scheme 1:** Example synthesis of imidazole-aniline derivatives.



The approach displayed in Scheme 1 has also been applied to several other fluoronitrobenzene derivatives (Figure 1) which allows for control over the relative position of the amine group and the introduction of other substituents which increase steric bulk (e.g., -CH<sub>3</sub> and -CF<sub>3</sub>) and which may facilitate thermal rearrangement (i.e., -OCH<sub>3</sub>).

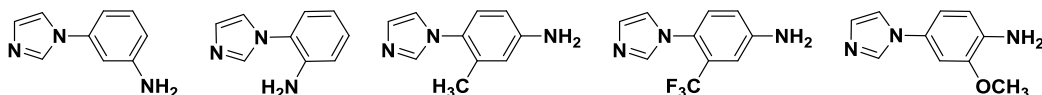
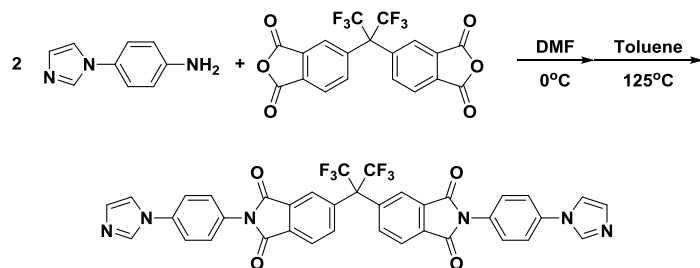


**Figure 1:** Other imidazole-aniline derivatives synthesized with different regiochemistry, steric bulk and thermally rearrangeable group.

The imidazole-aniline derivative (Scheme 1) was then combined with a bulky dianhydrides (e.g., 6-FDA) to form the di-imidazole di-imide monomer (Scheme 2).

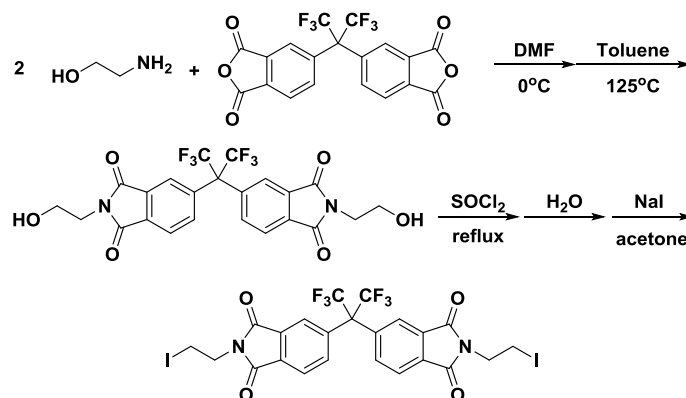
**Scheme 2:** Example synthesis of di-imidazole di-imide monomer.



In order to form a polyimide-ionene from the di-imidazole di-imide monomer shown in Scheme 2, a stoichiometric quantity of a difunctional monomer is required. Historically, these linking monomers are simple alkyl or aryl dihalides (e.g. 1,10-dibromodecane, *p*-dichloroxylylene). While we have experimented with the use of such compounds, the design of hybrid polyimide-ionene architectures for gas separation membranes with truly unique properties will require unique linking monomers which are also based on di-imide species. Scheme 3 details methods which we

have successfully applied to produce unprecedented dihalides derived from 6-FDA and monoethanolamine (MEA) (or other primary alkanolamines).

**Scheme 3:** Example synthesis of unprecedented di-imide diiodide compounds.



The combination of the di-imidazole di-imide compound in Scheme 2 with the di-imide diiodide yields results in a polyimide- based on 6-FDA with precisely spaced cationic imidazolium groups covalently attached within the backbone. These charges in the backbone facilitate the absorption of additional ionic liquid (IL) into the polymer matrix which have already observed through both x-ray diffractometry (XRD) and polarized optical microscopy (POM) to enhance organization and interactions between polymer chains. Excluding counterions, the MW of a single polymer repeat unit is over 1250 amu and exceeds 1800 amu when bistriflimide ( $\text{Tf}_2\text{N}^-$ ) anions are present as the counterions. Repeat units (including anions) as large as 3000 amu or greater are possible when even more sophisticated monomers are employed.

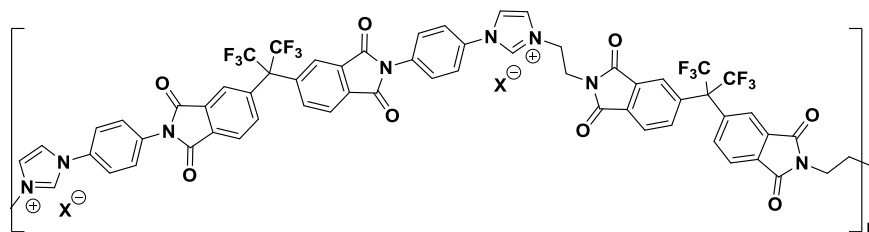


**Figure 2:** Structure of one hybrid polyimide-ionene material already produced.

In addition to being unprecedented polymer structures, these hybrid polyimide-ionenes are pushing new boundaries across all types of polymer materials in terms of the molecular weight (MW) of a discrete polymer repeat unit. These very large repeat units may strongly influence gas permeability and selectivity as they may present multiple types of void structures / free volume. We are currently in the process of characterizing the material in Figure 2 and forming membranes for gas permeation testing.

## ***Simulations and Computational Studies***

The goal of our simulations and computational studies is to develop a multi-scale simulation approach to predict experimentally-relevant membrane performance as a function of molecular-level structure/composition. There are four components to this aspect of the work:

- Quantum mechanical (QM): calculate partial charges on the sites of the polymer backbone.
- Molecular dynamics (MD): model the atomistic polymer structure and the short-time transport behavior of different gas molecules in the bulk polymer.
- Molecular dynamics (MD): estimate gas adsorption properties at the gas/polymer interfaces.
- Kinetic Monte Carlo (KMC): simulations of a comprehensive gas/polymer/gas system to predict penetrant permeability and selectivity for the gases: CO<sub>2</sub>/N<sub>2</sub>, CO<sub>2</sub>/CH<sub>4</sub>, H<sub>2</sub>/CO<sub>2</sub> and O<sub>2</sub>/N<sub>2</sub>.

The first step in the modeling work is developing realistic molecular models for the molecular dynamics simulations (MD). While intramolecular parameters can be adopted from standard forcefields, the partial charge assignments need to be estimated from electronic structure methods (using Gaussian09). Different polymer fragments have been constructed, followed by energy minimization and single-point energy calculation (MP2/6-311++g(3d,3p)//B3LYP/6-31g++(d,p)). Following these calculations, the partial charges are extracted using a natural bond order analysis (NBO). Currently, these calculations have been completed for the following polymer building blocks: 6-FDA, TRIPDA, and PIMDA.

We have also applied Gaussian09 to aid in the design of additional imidazole-aniline candidate compounds (cf. Scheme 1, Figure 1). The introduction of one or more methyl groups on both the imidazole and benzene rings will cause the rings to be non-coplanar, which may present further opportunities to tune void space and free volume.

### **Publications Acknowledging this Grant in 2015 – present**

*Jointly funded by this grant and other grants with relatively minor intellectual contribution from this grant:*

O’Harra, K. E.; Wagle, D.; Jackson, E.; Thomas, B.; Bara, J. E. Ionenes 2.0: Ultra-High Performance Polymers Meet Ionic Liquids, *Macromol. Chem. Phys.* (2018, Submitted).

Abedini, A.; Crabtree, E.; Bara, J. E.; Turner, C. H. Molecular Analysis of Gas Solubility within Ionic Polyimides and Composites with Ionic Liquids, *J. Phys. Chem. B* (2018, in preparation).

# **Poster Session Abstracts**

## Elucidating the Role of Spatial and Chemical Inhomogeneity in Separations Processes

Jared L. Anderson, Jacob W. Petrich, Emily A. Smith  
Ames Laboratory, Division of Chemical and Biological Sciences

### Presentation Abstract

Ionic liquids are salts with melting points below 100 °C that typically are comprised of an organic cation (*e.g.*, imidazolium, pyridinium, pyrrolidinium) and a variety of anions (*e.g.*, tetrafluoroborate, trifluoromethanesulfonate). Ionic liquid solvents have a multitude of unique physicochemical properties, including negligible vapor pressure and high thermal stability, as well as properties that are tunable based on the combination of their constituent anion and cation, including viscosity and solvation characteristics. Owing to vast synthetic tunability, there are up to  $10^{18}$  possible cation/anion combinations.<sup>1</sup> The synthetic flexibility can be exploited to customize the combinations and produce solvents with an extremely broad and diverse range of interactive capabilities. The ability to customize physicochemical properties of the solvent while imparting desired solvation interactions makes them very attractive in a variety of separation systems. For example, we have previously exploited these unique properties to develop separation systems based on liquid and gas chromatography in which the ionic liquid is a component of the mobile or stationary phase,<sup>2-6</sup> as well as liquid-liquid and solid-liquid extractions in which the ionic liquid constitutes one of the immiscible liquid phases.<sup>7-8</sup>

Ionic liquids exhibit more ordering than traditional solvents, including nanostructures of polar and nonpolar domains.<sup>9-11</sup> Our overarching hypothesis is that nanoscale spatial and chemical inhomogeneities are important to separation processes using ionic liquids and that these inhomogeneities can be tuned for more favorable separations. Important advancements in key areas of separation science will not be made without a molecular understanding of these inhomogeneities, but our understanding of their behavior in ionic liquids is in its infancy. We shall uncover the nature of these inhomogeneities and elucidate how they affect the macroscopic properties of the media and, ultimately, how they participate in the molecular mechanism of the separation processes (Figure 1).

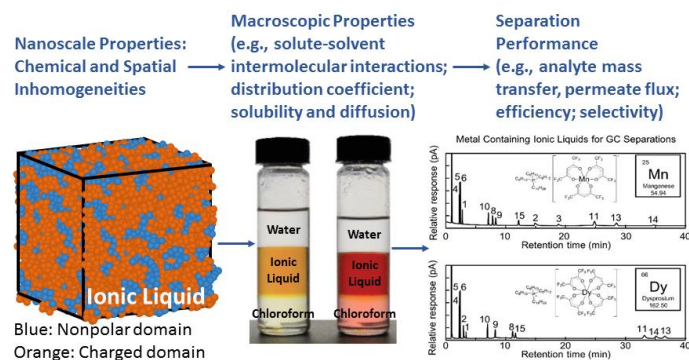


**Figure 1.** Schematic diagram outlining how the measured nanoscale properties and molecular interactions will be related to the macroscopic properties of the separations media and their performance in energy-relevant separations.

## References

1. Hallett, J. P.; Welton, T., Room-Temperature Ionic Liquids: Solvents for Synthesis and Catalysis. 2. *Chemical Reviews* **2011**, *111* (5), 3508-3576.
2. Baltazar, Q. Q.; Leininger, S. K.; Anderson, J. L., Binary ionic liquid mixtures as gas chromatography stationary phases for improving the separation selectivity of alcohols and aromatic compounds. *Journal of Chromatography A* **2008**, *1182* (1), 119-127.
3. Hantao, L. W.; Najafi, A.; Zhang, C.; Augusto, F.; Anderson, J. L., Tuning the Selectivity of Ionic Liquid Stationary Phases for Enhanced Separation of Nonpolar Analytes in Kerosene Using Multidimensional Gas Chromatography. *Analytical Chemistry* **2014**, *86* (8), 3717-3721.
4. Nan, H.; Zhang, C.; O'Brien, R. A.; Benchea, A.; Davis Jr, J. H.; Anderson, J. L., Lipidic ionic liquid stationary phases for the separation of aliphatic hydrocarbons by comprehensive two-dimensional gas chromatography. *Journal of Chromatography A* **2017**, *1481*, 127-136.
5. Zhang, C.; Ingram, I. C.; Hantao, L. W.; Anderson, J. L., Identifying important structural features of ionic liquid stationary phases for the selective separation of nonpolar analytes by comprehensive two-dimensional gas chromatography. *Journal of Chromatography A* **2015**, *1386*, 89-97.
6. Zhang, C.; Park, R. A.; Anderson, J. L., Crosslinked structurally-tuned polymeric ionic liquids as stationary phases for the analysis of hydrocarbons in kerosene and diesel fuels by comprehensive two-dimensional gas chromatography. *Journal of Chromatography A* **2016**, *1440*, 160-171.
7. Joshi, M. D.; Chalumot, G.; Kim, Y.-w.; Anderson, J. L., Synthesis of glucaminium-based ionic liquids and their application in the removal of boron from water. *Chemical Communications* **2012**, *48* (10), 1410-1412.
8. Yao, C.; Anderson, J. L., Dispersive liquid-liquid microextraction using an in situ metathesis reaction to form an ionic liquid extraction phase for the preconcentration of aromatic compounds from water. *Analytical and Bioanalytical Chemistry* **2009**, *395* (5), 1491.
9. Canongia Lopes, J. N. A.; Pádua, A. A. H., Nanostructural Organization in Ionic Liquids. *The Journal of Physical Chemistry B* **2006**, *110* (7), 3330-3335.
10. Pereiro, A. B.; Pastoriza-Gallego, M. J.; Shimizu, K.; Marrucho, I. M.; Lopes, J. N. C.; Piñeiro, M. M.; Rebelo, L. P. N., On the Formation of a Third, Nanostructured Domain in Ionic Liquids. *The Journal of Physical Chemistry B* **2013**, *117* (37), 10826-10833.
11. Paredes, X.; Fernández, J.; Pádua, A. A. H.; Malfreyt, P.; Malberg, F.; Kirchner, B.; Pensado, A. S., Bulk and Liquid-Vapor Interface of Pyrrolidinium-Based Ionic Liquids: A Molecular Simulation Study. *The Journal of Physical Chemistry B* **2014**, *118* (3), 731-742.

## **ARGET ATRP Grafting on Membranes: Predictive Tool and Characterization**

Georges Belfort, John J. Keating IV, Angelo Setaro,  
Mirco Sorci, Alexander Lee, Patrick Underhill

Howard P. Isermann Department of Chemical and Biological Engineering and Center for  
Biotechnology and Interdisciplinary Studies, Rensselaer Polytechnic Institute, Troy, New York  
12180, United States

### **Presentation Abstract**

The Activators Regenerated by Electron Transfer (ARGET) Atom Transfer Radical Polymerization (ATRP) reaction cascade is extremely complex with many adjustable species concentrations and reaction parameters. The effect of varying any of these parameters on the resulting temporal conversion trajectory of the polymerization is not straightforward. To optimize this reaction cascade for grafting uniform brushes on membranes, the reactions were implemented in MATLAB and used to compare conversion versus time behavior with published experimental results. The resulting model is shown to be very accurate, especially at conversions of 0.4 and lower. Sensitivity analysis was performed on the ARGET ATRP mechanism using MMA as a model monomer to identify key reaction parameters to ensure successful, controlled polymerization. Experiments and simulations were then used to graft alkyl methacrylate monomers from commercial poly(ether sulfone) (PES) nanofiltration membranes through a combination of helium and oxygen atmospheric pressure plasma (APP) treatment followed by ARGET ATRP. This technique allows enhanced synthesis of polymer grafted membranes using relatively green reaction solvents and enables “structure-by-design” surface morphology control with future applications in membrane separation processes such as organic solvent nanofiltration, gas separations, and desalination.

**DOE Grant #:** DE-FG02-09ER16005 – “Combinatorial Membrane Synthesis: Tailoring Membrane Surfaces to Separations”

**PI:** Dr. Georges Belfort; **Co-PI:** Dr. Patrick Underhill

**Postdoc:** Dr. Mirco Sorci

**Students:** John J. Keating IV (Grad. Student)); Angelo Setaro (Grad Student); Alexander Lee (Undergrad. student)

### **RECENT PROGRESS**

#### ***Model Verification[1]***

The experimental data [2] for the styrene (St) monomer with targeted degree of polymerization (DP) of 800 was modeled in MATLAB with our kinetic model. The experimental data and the

model fit (with  $\pm$  Root-Mean-Square-Error (RMSE) values) for St with DP = 800 and  $k_{red} = 2.4 \text{ M}^{-1}\text{s}^{-1}$  are shown in **Fig. 1A** with experimental conditions.

The RMSE = 0.036 for this fit. The model appears to fit the data well for the DP = 800 case. Experimental data [2] for the same ARGET ATRP reaction of St was then modeled with targeted DP = 400. The experimental data and model fit (with  $\pm$  RMSE values) with  $k_{red} = 2.4 \text{ M}^{-1}\text{s}^{-1}$  is plotted in **Fig. 1B**. The RMSE = 0.027 for this fit. The model fit is least accurate at the very beginning of the polymerization and all data are within  $\pm$  RMSE as the reaction proceeds. Through use of Arrhenius expressions for the various reaction rate constants, the kinetic model proved to be accurate for methacrylate-based monomers at different temperatures such as methyl methacrylate (MMA) and glycidyl methacrylate (GMA), extending the applicability of our model results.

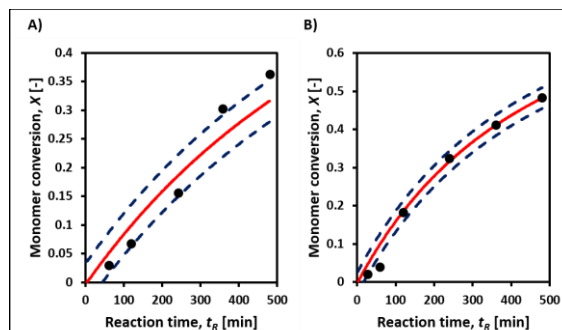


**FIG. 1. VARIATION OF DP FOR ST MONOMER.** ARGET ATRP polymerization of St in a constant volume batch reactor (20 mL) at 100°C in anisole solvent (50 w/w%). MATLAB model fit (—) to experimental data (●) and fit  $\pm$  RMSE (---) with  $k_{red} = 2.4 \text{ M}^{-1}\text{s}^{-1}$  for [St]:[EBIB]:[Cu(II)Br<sub>2</sub>] : [PMDETA]:[NaAsc] mola ratios of **A)** 800:1:0.1:1:1 and **B)** 400:1:0.1:1:1.

### Sensitivity Analysis[1]

Increasing the maximum attainable monomer conversion requires an increase in the ratio of the rate of propagation to termination,  $k_p:k_t$ . This can be accomplished through increasing the temperature of the ARGET ATRP reaction. For example the ratio of the propagation and termination rate constants at 363 K to the ratio at

$$303 \text{ K}, \left( \frac{k_p}{k_t} \Big|_{363 \text{ K}} \right) = 2.46 \text{ for MMA.}$$

The sensitivity of the monomer conversion profile on the ARGET ATRP reaction is shown in **Fig. 2**. As is evident from the conversion profiles, increasing the temperature yields a higher initial rate of polymerization while still allowing for much higher attainable conversions at longer reaction times. This is presumably due to the increase in relative importance of propagation rate constant over termination rate constant as temperature increases, preventing dead chains from accumulating to a greater extent due to irreversible termination events.

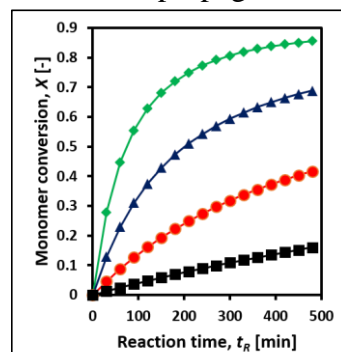


**FIG. 2. INCREASING REACTION TEMPERATURE.** Simulated effect on the conversion profile of reaction temperatures (K): 273 (■); 303 (●); 333 (▲); and 363 (◆) with molar ratios set to 800:1:0.1:1:1.

### APP-ARGET ATRP Grafting from PES[3]

A schematic of the proposed surface modification technique for grafting monomers from PES NF membranes is shown in **Fig. 3**. The atmospheric plasma polymerization (APP) jet impinging on the membrane surface causes scission of the PES chains, which results in the formation of radicals which subsequently react with the energetic oxygen radicals produced by the plasma.[4] The resulting activated membrane surface contains various oxygentaed functional groups, which may include hydroxyl groups.[5] Through the activation of the PES surface with reactive hydroxyl groups, ATRP

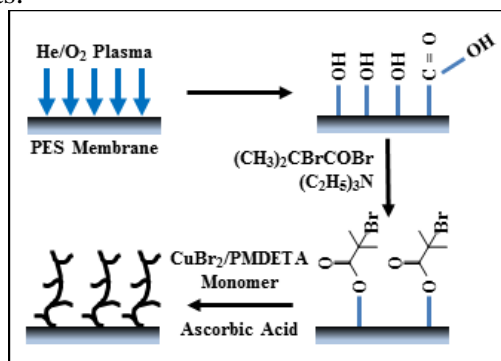
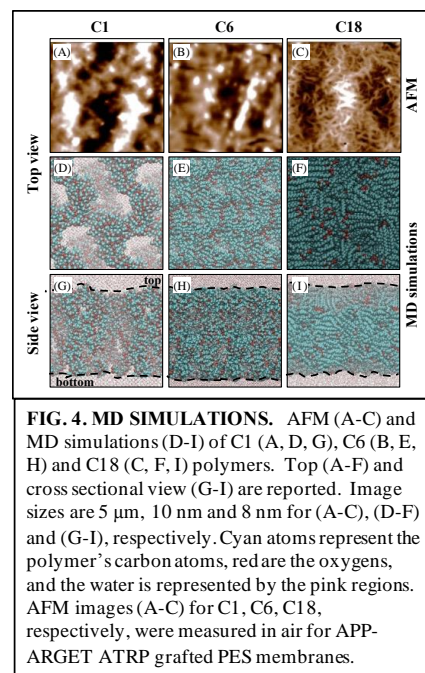


**FIGURE 3. SCHEMATIC OF THE COMBINED APP-ARGET ATRP METHOD.** Grafting of various monomers from the surface of PES NF membranes.

initiators can be covalently coupled to the surface. In this case,  $\alpha$ -bromoisobutyryl bromide was used which contains a reactive acid bromide functionality at one end of molecule and a tertiary bromine group at the other end. The acid bromide reacts with hydroxyl groups to form an ester linkage with the surface and HBr byproduct. Triethylamine was added to the reaction mixture to scavenge the HBr, forming triethylammonium bromide. Once the initiator-functionalized PES membrane was rinsed with acetonitrile and ethanol, the membrane was ready for the ARGET ATRP modification to graft suitable monomers such as C1 (methyl methacrylate), C6 (hexyl methacrylate), and C18 (stearyl methacrylate). **Fig. 4** shows MD simulations of the equilibrium morphology of grafted polymer layers composed of C1, C6, and C18 side chains in contact with water. The first atoms of the polymers are constrained as if they were attached to the support. Each simulation contained 16 polymers arranged in a 4 by 4 hexagonal lattice with grafting densities of 0.6, 0.6, and 0.27 polymers/nm<sup>2</sup>, respectively. The side views that the hydrophobic C6 or C18 side chains expel most of the water from the polymer layer. The top views (without showing the water for clarity) show the morphology of the polymer surface. Only the C18 side chains produce a structured surface in which the side chains line-up.



### References:

- [1] J.J.V. Keating, A. Lee, G. Belfort, Predictive Tool for Design and Analysis of ARGET-ATRP Grafting Reactions, *Macromolecules*, 50 (2017) 9.
- [2] S. Hansson, E. Ostmark, A. Carlmark, E. Malmström, ARGET ATRP for versatile grafting of cellulose using various monomers, *ACS Applied Materials & Interfaces*, 1 (2009) 2651-2659.
- [3] J.J.I. Keating, M. Sorci, I. Kocsis, A. Setaro, M. Barboiu, P. Underhill, G. Belfort, Atmospheric Pressure Plasma - ARGET ATRP Modification of Poly(ether sulfone) Membranes: A Combination Attack, *J. Membr. Sci.*, 546 (2017) 6.
- [4] E. Gonzalez, M.D. Barankin, P.C. Guschl, R.F. Hicks, Ring opening of aromatic polymers by remote atmospheric-pressure plasma, *Plasma Science, IEEE Transactions on*, 37 (2009) 823-831.
- [5] M.L. Steen, A.C. Jordan, E.R. Fisher, Hydrophilic modification of polymeric membranes by low temperature H<sub>2</sub>O plasma treatment, *Journal of Membrane Science*, 204 (2002) 341-357.

### Publications Acknowledging this Grant in 2015 – present:

(I) *Exclusively funded by this grant;*

1. Imbrogno, J.; Williams, M. D.; Belfort, G., A new combinatorial method for synthesizing, screening, and discovering antifouling surface chemistries. *ACS Appl Mater Interfaces* **2015**, *7* (4), 2385-92.
2. Li, Q.; Imbrogno, J.; Wang, X.-L., Making polymeric membranes antifouling via “grafting from” polymerization of zwitterions. *J. Applied Poly. Sci.* **2015**, *132* (21), 41782-41791.
3. Barrett, A.; Imbrogno, J.; Belfort, G.; Petersen, P. B., Phosphate Ions Affect the Water Structure at Functionalized Membrane Surfaces. *Langmuir* **2016**, *32* (35), 9074-82.
4. Keating, J. J.; Imbrogno, J.; Belfort, G., Polymer Brushes for Membrane Separations: A Review. *ACS Appl Mater Interfaces* **2016**, *8* (42), 28383-28399.
5. Keating, J. J. V.; Lee, A.; Belfort, G., Predictive Tool for Design and Analysis of ARGET-ATRP Grafting Reactions. *Macromolecules* **2017**, *50*, 9.
6. Keating, J. J. I.; Sorci, M.; Kocsis, I.; Setaro, A.; Barboiu, M.; Underhill, P.; Belfort, G., Atmospheric Pressure Plasma - ARGET ATRP Modification of Poly(ether sulfone) Membranes: A Combination Attack. *J. Membr. Sci.* **2017**, *546*, 6.

(II) *Jointly funded by this grant and other grants with relatively major intellectual contribution from this grant;*

7. Grimaldi, J.; Imbrogno, J.; Kilduff, J. E.; Belfort, G., New Class of Synthetic Membranes: Organophilic Pervaporation Brushes for Organics Recovery. *Chem Materials* **2015**, *27*, 4142-4148.
8. Tian, Y.; Zonca Jr., M. R.; Imbrogno, J.; Unser, A. M.; Sfakis, L.; Temple, S.; Belfort, G.; Xie, Y., Polarized, Cobblestone, Human Retinal Pigment Epithelial Cell Maturation on a Synthetic PEG Matrix. *ACS Biomater. Sci. & Eng.* **2017**, *3*, 890-902.

(III) *Jointly funded by this grant and other grants with relatively minor intellectual contribution from this grant;*

9. Imbrogno, J. and Belfort, G. (Invited Review) Membrane desalination: Where are we and what can we learn from fundamentals? *Annual Reviews of Chemical and Biomolecular Engineering*, **2016**, *7*: 29-64.
10. Imbrogno, J.; Keating IV, J. J.; Kilduff, J. E.; Belfort, G., Critical aspects of RO desalination: A combination strategy. *Desalination* **2017**, *401*, 68-87.

## Nanoscale Coupling of Transport and Chemical Reactivity

Paul W. Bohn

Department of Chemical and Biomolecular Engineering

Department of Chemistry and Biochemistry

University of Notre Dame

Notre Dame, IN 46556 USA

### Presentation Abstract

The ultimate goal of our program is to establish intelligent control of molecular transport in space and time at small length scales – enabling the construction of materials and structures that can sense molecular characteristics, *e.g.*, size, charge, molecular shape, *etc.*, and use the information to control other events even if the action occurs far away. A particular focus of these experiments is the coupling of transport to reactivity. Recently, we have been addressing this global objective in two ways. First, we have developed signal-actuated strategies, using bipolar electrodes, to effect action-at-a-distance for chemical analysis and chemical processing. The architectures constructed to accomplish this combine signal amplification strategies, such as self-induced redox cycling, with bipolar electrodes (BPEs) to translate an electronic (electrochemical) measurement to a distal readout event, such as luminescence, an electrochromic reaction, or a shift in a localized surface plasmon resonance (LSPR). These provide an ideal way to couple the events occurring in an inherently high-background separation medium to a low-noise, high-sensitivity readout. In addition, we are developing one-dimensional (1D) nanofluidic structures to control the chemical environment and achieve high efficiency vectorial flow-coupled catalytic reactions in nanofluidic environments. Nanosphere lithography and graphoepitaxy have been combined to create ultra-high density arrays of parallel, vertically-oriented nanopores, each containing a reactor capable of housing a single catalyst particle. Because of the small length scales involved, transport may be controlled to effectively “gate” the entry of desired particles while rejecting unwanted species.

### DE FG02 07ER15851: Molecular Aspects of Transport in Thin Films of Controlled Architecture

**PI:** Paul Bohn

**Students:** Erick Foster, Wei Xu (through 3/17), Arielle Lopez

### RECENT PROGRESS

#### Closed Bipolar Electrochemistry for Control of Chemical Separations and Processing

*Multiplexed Closed Bipolar Electrochromic Cells for Enzyme-Catalyzed Assays.* Sensors based on converting electrochemical signals into optical readouts are attractive candidates as low-cost, high-

throughput platforms due to the relative ease of photon detection. In this project period, we have exploited this principle by developing a closed bipolar electrode (CBE)-based two-cell electrochromic device for sensing multiple analytes. The system consists of a split-cell geometry in which an analytical cell is used for the recognition reaction. The CBE couples the reaction in the analytical cell to a physically separate reporter cell, containing an electrochromic reporter reaction – in our case the reduction of colorless  $MV^{2+}$  to highly absorbing (purple)  $MV^{+\bullet}$ - which is subsequently readout by acquiring an image of the reporter cell. Images can be acquired by platforms ranging from high-performance photodetectors all the way to portable personal cameras, *e.g.* a smartphones. The analytical cell is capable of addressing redox-active analytes directly and non-redox active analytes by including a mediator and enzymatically converting target analytes to redox-active products, thus producing the initial electrochemical signal.

*Coupling Electron Transfer Events to Responsive Materials.* Nanosphere lithography (NSL), is an efficient means of fabricating nanostructures arrays of highly polarizable metals, *e.g.* Au, Ag, on substrates. The surface confined nanostructures exhibit highly interesting and characteristic optical properties, such as localized surface plasmon resonances (LSPR), which can be characterized by measuring the extinction maximum ( $\lambda_{max}$ ) using an ultraviolet-visible (uv-vis) spectrometer. The LSPR of these nanostructure arrays can be tuned from visible to near infrared wavelength range by simply varying the size, shape, inter-particle distance, and dielectric properties of the material as well as the local environment. These properties of metal nanostructure arrays qualify them as good stimulus-response agents. For example, changing the shape and/or composition of the metals (by electrodeposition) can dramatically alter the LSPR response. Thus, metal nanostructure arrays not only can be used as optical sensors, but they can also be combined with electrochemical and mechanical manipulation to effect chemical action-at-a-distance.

### High Efficiency Nanofluidic Catalytic Reactors

*Capture and Manipulation of Single Catalytic Nanoparticles.* We have begun an effort to separate, characterize, and isolate single catalyst nanoparticles. In order to accomplish this, we have developed a capability to implement voltage-gated nanoparticle transport inside nanopore electrode arrays using what we term hierarchically organized transport control (HOTC), as shown schematically in **Figure 1**. In HOTC, there are two functional nanomaterials that operate on different length scales. These structures were achieved using a combination of NSL-templated graphoepitaxy of polystyrene-*b*-polydimethylsiloxane to produce highly ordered silica nanochannels (SNC) with areal densities approaching 1000 elements  $\mu\text{m}^{-2}$  and aspect ratios  $> 5:1$  on a large scale. The resulting ultra-high density SNC arrays were found to be competent to serve as ion gates to discriminate between cationic and anionic species, due to the permselective character of the SNC nanochannels. This surface charge-dominated behavior was demonstrated by suppression of current from anionic redox species while almost no change of current was observed for cationic redox species. Furthermore, the polarity of the permselective behavior can be flipped by chemically modifying the SNC nanochannels surfaces with positively charged amine groups, *i.e.* screening positively charged species and accumulating negatively charged redox analytes. Finally, the massively parallel fabrication strategy produces high density nanoscale SNC arrays over large scales, which can subsequently be transferred to another substrate without damaging the molecular sieving or ion gating properties. This proof-of-concept sets the stage for potential

applications in pre-concentration of target molecules and improved electrochemical selectivity for electrode materials not capable of supporting the SNC fabrication process directly.

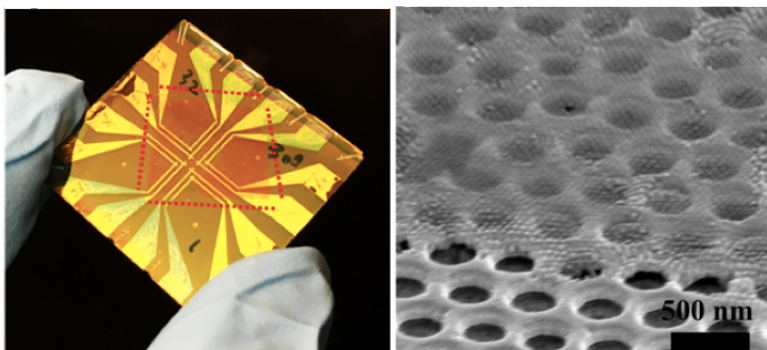


**Figure 1.** One realization of the hierarchically organized transport control concept. (Left) Photograph of a structure containing 8 unique HOTC regions with independent voltage controls. (Right) SEM image of a small portion of one HOTC region illustrating the  $\sim 250$  nm diameter nanopores covered with a  $\sim 20$  nm diameter nanopillar array.

Recently, we have used this concept to establish a voltage-gated single-particle electrochemical processing capability for the control and study of single catalyst particles. In this approach, the top layer serves as an actively-switchable particle gate to control the transport of nanoparticles within individual attoliter-volume nanopores, as shown by redox collisions of NPs at the bottom disk electrode. A voltage threshold is

observed above which NPs are able to access the bottom electrode of the nanopores, *i.e.* a minimum potential at the gate electrode is required to switch between few and many observed collision events on the collector electrode. We further show that this threshold voltage is strongly dependent on the applied voltage at both electrodes as well as the size of the NPs. We believe that the HOTC concept, as implemented here, represents a precise method of monitoring nanoparticle transport and controlling *in situ* redox reactions within nano-confined spaces at the single particle level.

### Publications Acknowledging this Grant in 2015 – present

- (I) Contento, N.M.; Bohn, P.W. “Electric Field Effects on Current-Voltage Relationships in Microfluidic Channels Presenting Multiple Working Electrodes in the Weak-Coupling Limit,” *Microfl. Nanofl.* **2015**, 18, 131-140. [DOI 10.1007/s10404-014-1424-9]
- (II) Ma, C.; Zaino, L.P. III; Bohn, P.W. “Self-Induced Redox Cycling Coupled Luminescence on Nanopore Recessed Disk-Multiscale Bipolar Electrodes,” *Chem. Sci.* **2015**, 6, 3173-3179. [DOI 10.1039/c5sc00433k]
- (III) Zaino, L.P. III; Grismer, D.A.; Han, D.; Crouch, G.M.; Bohn, P.W. “Single Molecule Spectroelectrochemistry of Freely Diffusing Flavin Mononucleotide in Zero-Dimensional Nanophotonic Structures,” *Faraday Disc.* **2015**, 184, 101-115. [DOI 10.1039/C5FD00072F; PMID: 26406924]
- (I) Wichert, R.A.W.; Han, D.; Bohn, P.W. “Effects of Molecular Confinement and Crowding on Horseradish Peroxidase Kinetics Using a Nanofluidic Gradient Mixer,” *Lab Chip* **2016**, 16, 877-883. [DOI 10.1039/C5LC01413A; PMID: 26792298]

- (II) Xu, W.; Ma, C.; Bohn, P.W. “Coupling of Independent Electrochemical Reactions and Fluorescence at Closed Bipolar Interdigitated Electrode Arrays,” *ChemElectrochem* **2016**, 3, 422-428. [DOI 10.1002/celec.201500366]
- (II) Xu, W.; Fu, K.; Ma, C.; Bohn, P.W. “Closed Bipolar Electrode-Enabled Dual-Cell Electrochromic Detectors for Chemical Sensing,” *Analyt* **2016**, 141, 6018-6024. [DOI 10.1039/C6AN01415A; PMID: 27704078]
- (II) Ma, C.; Xu, W.; Wichert, W.R.A.; Bohn, P.W. “Ion Accumulation and Migration Effects on Redox Cycling in Nanopore Electrode Arrays at Low Ionic Strength,” *ACS Nano* **2016**, 10, 3658-3664. [DOI 10.1021/acsnano.6b00049].
- (III) Zaino, L.P. III; Wichert, R.A.W.; Crouch, G.M.; Bohn, P.W. “Microchannel Voltammetry in the Presence of Large External Voltages and Electric Fields,” *Analyt. Chem.* **2016**, 88, 4200-4204. [DOI 10.1021/acs.analchem.6b00399; PMID: 27045936]
- (I) Xu, W.; Fu, K.; Bohn, P.W. “Electrochromic Sensor for Multiplex Detection of Metabolites Enabled by Closed Bipolar Electrode Coupling,” *ACS Sens.* **2017**, 2, 1010-1026. [DOI 10.1021/acssensors7b00292]
- (II) King, T.L.; Jin, X.; Nandigana, V.R.; Aluru, N.; Bohn, P.W. “Electrokinetic Transport and Fluidic Manipulation in Three Dimensional Integrated Nanofluidic Networks,” in *Nanofluidics*, 2nd Edition, A. de Mello and J. Edel, Eds., Royal Society of Chemistry, Cambridge, UK, Ch. 2, pp. 37-75, **2017**.
- (II) Xu, W.; Zaino, L.P. III; Bohn, P.W. “Electrochemically Modulated Luminescence in Nanophotonic Structures,” in *Combined Luminescence and Electrochemistry: Involvements and applications in analytical chemistry, physics and biology*. F. Miomandre, P. Audebert, Eds., **2017** Springer, pp. 79-104.
- (I) *Exclusively funded by this grant;*
- (II) *Jointly funded by this grant and other grants with leading intellectual contribution from this grant;*
- (III) *Jointly funded by this grant and other grants with relatively minor intellectual contribution from this grant;*

## Grant DE-FG02-98ER14888

### Self-Assembled Ionophores in Water: Supramolecular Hydrogels and Membrane Transporters

Jeffery T. Davis, Principal Investigator

Taylor Plank, Keith Sutyak and Songjun Xiao, Graduate Students Department of Chemistry and Biochemistry, University of Maryland, College Park, MD 20742

Email: [jdavis@umd.edu](mailto:jdavis@umd.edu)

Collaborators: Professor Srini Raghavan, Dept. Chemical and Biomolecular Engineering, University of Maryland, College Park, MD 20742, USA

Professor Stefano Masiero, Dept. of Chemistry, University of Bologna, Italy  
Professor Steven Brown, Dept. of Physics, University of Warwick, Coventry, UK

**Overall research goals:** This project's two major aims are: **Aim 1**) to synthesize supramolecular hydrogels from nucleoside derivatives that have new properties and functions. In particular, we seek to develop self-assembled hydrogels that can be used for the selective separations of cations (such as Pb(II), Ba(II), Cs(I)) and also for the selective separation of small organic molecules, such as dyes and reactive aldehydes; **Aim 2**) to develop new ways to transport ions and small molecules such as nucleosides and nucleotides across lipid membranes.

**Significant achievements during 2015-2017: Achievement 1)** The synthesis of supramolecular hydrogels from is a completely new area for us. The first key finding is that guanosine and potassium borate form a transparent and stable hydrogel, based on guanosine-borate (GB) linkages. This supramolecular GB hydrogel is formed by a hierarchical self-assembly process that involves formation of borate diesters,  $K^+$  templated formation of hydrogen bonded  $G_4$ -quartets, stacking of these  $G_4$ -quartets to give nanofibers, and bundling of the nanofibers to give the hydrogel (**Fig. 1**).

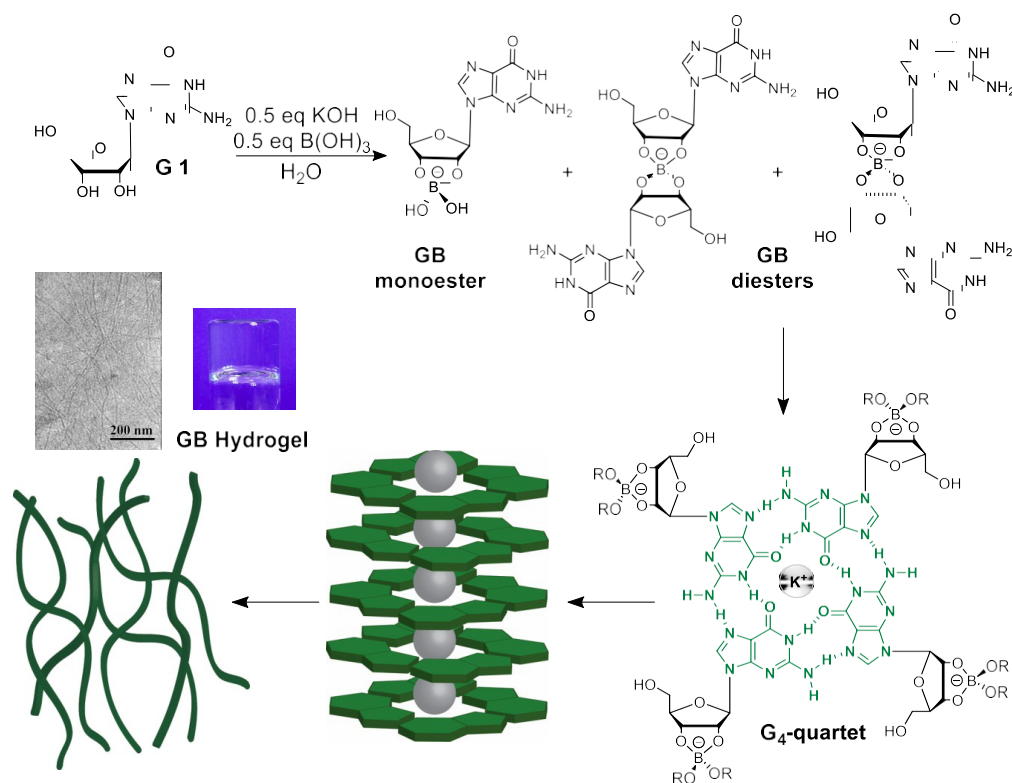


Fig. 1. Depiction of hierarchical self-assembly process that leads to formation of stable guanosine-borate (GB) hydrogels.

**Achievement 2)** *Cationic Dyes as Molecular Chaperones for GB gelation.* One major finding was that absorption of cationic dyes, such as thioflavin T (ThT), increased the strength of the anionic GB hydrogels. We hypothesized that the cationic dyes act as molecular chaperones by templating and stabilizing smaller G<sub>4</sub>-quartet fragments necessary for fiber formation and hydrogelation. The implications of this study, published in *J. Am. Chem. Soc.*, are significant. We provide fundamental insight into the nucleation-growth mechanism of these materials. For environmental remediation, the hydrogels can selectively separate cationic dyes from anionic dyes.

**Achievement 3)** *G<sub>4</sub>-Hydrogels for Separation and Remediation of Heavy Metals, Anionic Dyes and Reactive Aldehydes.* We discovered a new hydrogel made from KCl and the analog, 8-amino-guanosine (**8-AmG 2**), without the need for the borate salt. These **8-AmG** hydrogels are cationic, rather than anionic like the parent GB hydrogels made from guanosine **G 1** and borate. This charge difference is crucial for reversing the selectivity in separations of ionic dyes. Thus, hydrogels made from **8-AmG 2** extract and bind tightly to anionic dyes, such as naphthol blue black (NBB), a pollutant produced by the textile industry.

Science objectives for 2017-2019. We will focus on synthesis, characterization and application of new hydrogels. Our immediate goal in the first part of the next reporting period will be to finish up the projects on the Pb (II), anionic dye and aldehyde remediation applications. These studies should result in 2-3 papers in 2018. We will also initiate some new studies on the catalysis of the hydrogelation process. As always, we will be on the lookout for applications of new hydrogels in separations and analysis of toxic metals and organics.

Publications supported by this project 2015-2017:

1. "G<sub>4</sub>-Quartet·M<sup>+</sup> Borate Hydrogels." Gretchen M. Peters, Luke Skala, Taylor N. Plank, Hyuntaek Oh, G. N. Manjunatha Reddy, Andrew Marsh, Steven P. Brown, Srinivasa Raghavan and Jeffery T. Davis, *J. Am. Chem. Soc.* **2015**, *137*, 5819-5827. DOI: 10.1021/jacs.5b02753
2. "Interplay of Non-Covalent Interactions in Ribbon-Like Guanosine Self-Assembly: A NMR Crystallography Study." G. N. Manjunatha Reddy, Andrew Marsh, Jeffery T. Davis, Stefano Masiero and Steven P. Brown, *Crystal Growth and Design* **2015**, *15* (12), pp 5945–5954. DOI: 10.1021/acs.cgd.5b01440
3. "A Molecular Chaperone for G<sub>4</sub>-Quartet Hydrogels." Gretchen M. Peters, Luke Skala and Jeffery T. Davis, *J. Am. Chem. Soc.* **2016**, *138* (1), 134–139. DOI: 10.1021/jacs.5b08769 *J. Am. Chem. Soc.* **2016**, *138* (1), 134–139. DOI: 10.1021/jacs.5b08769
4. "A G<sub>4</sub>·K<sup>+</sup> Hydrogel that Self-Destructs." Taylor N. Plank and Jeffery T. Davis, *Chemical Communications*, **2016**, *52*, 5037-5041. DOI: 10.1039/C6CC01494A
5. "Supramolecular Gels made from Nucleobase, Nucleoside and Nucleotide Analogs." Gretchen M. Peters and Jeffery T. Davis, *Chemical Society Reviews*, **2016**, *45*, 3188-3206. DOI: 10.1039/C6CS00183A
6. "Controlling Molecularity and Stability of Hydrogen Bonded G-Quadruplexes by Modulating the Structure's Periphery." Keith B. Sutyak, Peter Y. Zavalij, Michael L. Robinson and Jeffery T. Davis, *Chemical Communications*, **2016**, *52*, 11112-11115. DOI: 10.1039/C6CC06271G
7. "Anion Transport and Supramolecular Medicinal Chemistry." Philip A. Gale, Jeffery T. Davis and Roberto Quesada, *Chem. Soc. Rev.* **2017**, *46*, 2417-2519. DOI: 10.1039/C7CS00159B (2 citations)
8. "Supramolecular Hydrogels for Environmental Remediation: G<sub>4</sub>-Quartet Gels that Selectively Absorb Anionic Dyes from Water." Taylor N. Plank, Luke P. Skala and Jeffery T. Davis, *Chem. Commun.* **2017**, *53*, 6235-6238. DOI: 10.1039/C7CC03118A
9. "G-Quartet Hydrogels for Effective Cell Growth Applications." Alexandru Rotaru, Gabriela Pricope, Taylor N. Plank, Lilia Clima, Laura Ursu, Dragos Peptanariu, Jeffery T. Davis and Mihail Barboiu, *Chem. Commun.* **2017**, *53*, 12668-12671. DOI: 10.1039/C7CC09900B
10. "A Self-Assembled Peroxidase from 5'-GMP and Heme." Deiaa M. Harraz and Jeffery T. Davis, *Chem. Commun.* **2018**, *in press*, DOI: 10.1039/c7cc07806d

## Atomic-level description of separations phenomena using multi-scale models

Vassiliki-Alexandra Glezakou, Grant E. Johnson, Alla Zelenyuk and Venky Prabhakaran  
Physical Sciences Division, Pacific Northwest National Laboratory, Richland, WA 99352  
Email: [Vanda.Glezakou@pnl.gov](mailto:Vanda.Glezakou@pnl.gov)

### Presentation Abstract

Our research is designed to interrogate the fundamental aspects of confinement, surface morphology, solvent effects and external stimuli on complexation, speciation, diffusion and reactivity of trace elements in complex liquids. While there is clearly a need for well-controlled experimental studies interrogating the atomistic level details, the latter are inherently accessible by theory and simulation. Theory acts as the cross-cutting and unifying element across the experimental efforts by providing molecular level insights on: (i) how confinement, functionalization, and double layer change the local structure of solvated ions providing insights regarding mechanistic steps (role of entropy); (ii) how does the interfacial morphology influence the structure and adsorption/ desorption of solvated ions; (iii) how hydrophobic domains and external fields may change the structure and transport between electrodes; (iv) extraction of structure-property correlations (kinetic or reduced order models).

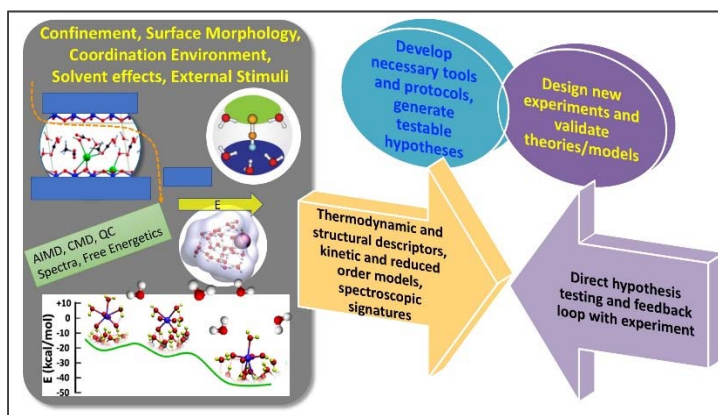


Figure 1. Integrated multi-scale modeling approach to study critical aspects of chemical separations at complex interfaces.

We will illustrate this approach with examples from previous work in CO<sub>2</sub> capture solvent systems<sup>1-2</sup>, carbon sequestration<sup>3-8</sup>, chemical conversions<sup>9-10</sup> and heavy element separation and storage<sup>11-12</sup>, as well as some preliminary results on the structure, energetics and dynamics of laminar, GO-supported Au-particles.

We will illustrate this approach with examples from previous work in CO<sub>2</sub> capture solvent systems<sup>1-2</sup>, carbon sequestration<sup>3-8</sup>, chemical conversions<sup>9-10</sup> and heavy element separation and storage<sup>11-12</sup>, as well as some preliminary results on the structure, energetics and dynamics of laminar, GO-supported Au-particles.

**Grant or FWP Number:** This abstract summarizes new theoretical work added to PNNL's legacy experimental analysis program (47327), as it is re-focused towards separations.

### References

1. Cantu, D. C.; Lee, J.; Lee, M.-S.; Heldebrant, D. J.; Koeh, P. K.; Freeman, C. J.; Rousseau, R.; Glezakou, V.-A. Dynamic Acid/Base Equilibrium in Single Component

- Switchable Ionic Liquids and Consequences on Viscosity. *The Journal of Physical Chemistry Letters* **2016**, *7*, 1646-1652.
2. Heldebrant, D. J.; Koech, P. K.; Glezakou, V.-A.; Rousseau, R.; Malhotra, D.; Cantu, D. C. Water-Lean Solvents for Post-Combustion CO<sub>2</sub> Capture: Fundamentals, Uncertainties, Opportunities, and Outlook. *Chemical Reviews* **2017**, *117*, 9594-9624.
  3. Lee, M.S.; McGrail, B. P.; Rousseau, R.; Glezakou, V.-A. A molecular level investigation of CH<sub>4</sub> and CO<sub>2</sub> adsorption in hydrated Ca-Montmorillonite. *J. Phys. Chem. C* **2017**, ASAP, DOI: 10.1021/acs.jpcc.7b05364.
  4. Lee, M.S.; McGrail, B. P.; Glezakou, V.-A. Microstructural Response of Variably Hydrated Ca-Rich Montmorillonite to Supercritical CO<sub>2</sub>. *Environ. Sci & Technol.* **2014**, *48*, 8612-8619.
  5. Lee, M.S.; McGrail, B. P.; Rousseau, R.; Glezakou, V.-A. **2015**. Structure, dynamics and stability of water/scCO<sub>2</sub>/orthoclase interfaces from first principles molecular dynamics simulations. *Sci. Rep. Nature* **2015**, *5*: 14857.
  6. Glezakou, V.-A.; McGrail, B. P.; Schaef, H. T. Molecular interactions of SO<sub>2</sub> with carbonate minerals under co-sequestration conditions: a combined experimental and theoretical study. *Geochim. et Cosmochim. Acta* **2012**, *92*, 265-274.
  7. Glezakou, V.-A.; McGrail, B. P. **2013**. "Density functional simulations as a tool to probe molecular interactions in wet supercritical CO<sub>2</sub>." Chapter 3 in *Application of Molecular Modeling to Challenges in Clean Energy. ACS Symposium Series*, vol. 1133, ed. G Fitzgerald and N Govind, pp. 31-49. American Chemical Society, Washington DC.
  8. Schaef, H.T.; Glezakou, V.-A.; Owen, A. T.; Ramprasad, S.; Martin, P. F.; McGrail, B. P. Surface Condensation of CO<sub>2</sub> onto Kaolinite. *Environ. Sci. & Technol. Lett.* **2014**, *1*, 142-145.
  9. Alexopoulos, K.; Lee, M.-S.; Liu, Y.; Zhi, Y.; Liu, Y.; Reyniers, M.-F.; Marin, G. B.; Glezakou, V.-A.; Rousseau, R.; Lercher, J. A. Anharmonicity and Confinement in Zeolites: Structure, Spectroscopy, and Adsorption Free Energy of Ethanol in H-ZSM-5. *J. Phys. Chem. C* **2016**, *120*, 7172-7182.
  10. Wang, Y.-G.; Mei, D.; Glezakou, V.-A.; Li, J.; Rousseau, R. Dynamic Formation of Single-Atom Catalytic Active Sites on Ceria-Supported Gold Nanoparticles. *Nature Comm.* **2015**, *6*, 6511.
  11. Glezakou, V.-A.; deJong, W. A. Cluster-models for uranyl (VI) adsorption on  $\alpha$ -alumina. *J. Phys. Chem. A* **2011**, *115*, 1257-1263.
  12. Lee, M.-A.; Um, W.; Wang, G.; Kruger, A. A.; Lukens, W. W.; Rousseau, R.; Glezakou, V.-A. Impeding <sup>99</sup>Tc (IV) mobility in novel waste forms. *Nature Comm.* **2016**, *7*, 12067.

**New Ionic Covalent Organic Framework (iCOF) for Selective Cr(VI) Removal**

Santa Jansone-Popova,\* Anthonin Moinel, Shannon M. Mahurin, Gabriel M. Veith, Ilja Popovs, Alexandr S. Ivanov, Bruce A. Moyer  
 Oak Ridge National Laboratory, Chemical Sciences Division

**Presentation Abstract**

Selective chromium(VI) oxoanion removal has been demonstrated using a novel ionic covalent organic framework (iCOF). Based on our hypothesis, we have synthesized a porous framework in which the ionic groups are symmetrically positioned on the edges of the hexagonal pores (Figure 1.). We further characterized the material by using FTIR, EA, CP MAS solid-state NMR, BET, and PXRD analyses. The monovalent anions in iCOF readily and quantitatively undergo exchange with the divalent oxoanions at close to neutral pH value, suggesting excellent accessibility of the cationic sites in the porous framework. Moreover, Cr(VI) oxoanions are selectively removed by iCOF in the presence of a variety of other tetrahedral oxoanions (e.g., sulfate and selenate). In a single treatment with iCOF, Cr(VI) concentration in aqueous solution is lowered from 1 ppm to 10 ppb level, which is an order of magnitude lower than the current US Environmental Protection Agency maximum contaminant level for total chromium of 100 ppb. The manuscript has been prepared for publication and will be submitted within 30 days.

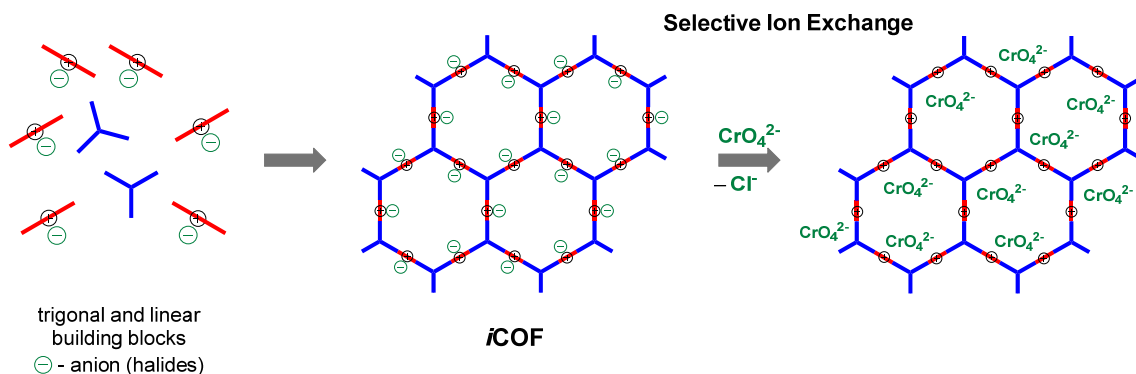


**Figure 1.** Schematic representation of the synthesis of iCOF and ion exchange process.

## Computational Insight into Novel Membranes and Sorbents for Gas Separations

Poster presented by: De-en Jiang, University of California, Riverside (UCR)

Part of ORNL FWP, “Fundamental Studies of Novel Separations”

Sheng Dai, Principal Investigator

Co-PIs: De-en Jiang and Shannon Mahurin

UCR team: Song Wang, Nicole Onishi (graduate students); Ziqi Tian (former postdoc);

Weihong Wu (visiting student)

Overall research goals: The overarching goal of this program is to investigate fundamental issues of chemical separations by nanostructured architectures and unconventional media that selectively bind and/or transport target molecular species via tailored interactions. The theory effort aims to provide guidance and predictive design of novel separation media for future chemical separations.

### Significant achievements in 2016-2018:

- We proposed a novel concept of **ion-gated gas separation**.<sup>1</sup> We demonstrated from molecular dynamics simulations that an ion-gated graphene membrane comprising a monolayer of ionic liquid coated porous graphene can dynamically modulate the pore size to achieve selective gas separation. This approach enables the otherwise non-selective large pores on the order of 1 nm in size to be selective for gases whose diameters range from three to four angstroms.
- We demonstrated that **site partition**<sup>2</sup> is the key reason for the great increase in gas uptake when guest molecules were introduced into flexible MOFs with open-metal sites. We showed that this concept can be generalized to double gas uptake in nanoporous materials, by designing a geometry-matching guest molecule for a covalent-framework material.
- We designed the calix-based cages for gas capture.<sup>3</sup> Our dispersion-corrected density functional theory calculations show convincingly that the designed **cage compounds** have both highly favorable and tunable thermodynamics and facile kinetics for gas separation.
- We found from simulations an **optimal size** for adsorbing CO<sub>2</sub> inside cylindrical pores,<sup>4</sup> due to the overlap of potential-energy surface. We found that a cylindrical pore size between 7 and 8 Å would be most beneficial for post-combustion CO<sub>2</sub> capture and the simulated CO<sub>2</sub> uptake and CO<sub>2</sub>/N<sub>2</sub> selectivity are competitive in comparison with popular porous materials.

### Science objectives for 2018-2019:

Simulate nanostructured membrane systems comprising ionic liquids inside porous materials for gas adsorption and permeation.

Design and simulate porous liquids based on cage compounds and deep eutectic solvents.

Test advanced pore-size control concepts in ultrathin membranes made of graphene layers.

References to work supported by this project 2016-2018:

1. Tian, Z.; Mahurin, S. M.; Dai, S.; Jiang, D.-e., Ion-Gated Gas Separation through Porous Graphene. *Nano Lett.* **2017**, *17*, 1802-1807.
2. Tian, Z.; Dai, S.; Jiang, D.-e., Site Partition: Turning One Site into Two for Adsorbing CO<sub>2</sub>. *J. Phys. Chem. Lett.* **2016**, *7*, 2568-2572.
3. Wu, W.; Tian, Z.; Wang, S.; Peng, C.; Liu, H.; Dai, S.; Jiang, D.-e., Design of Calix-Based Cages for CO<sub>2</sub> Capture. *Ind. Eng. Chem. Res.* **2017**, *56*, 4502-4507.
4. Wang, S.; Tian, Z.; Dai, S.; Jiang, D.-e., Optimal Size of a Cylindrical Pore for Post-Combustion CO<sub>2</sub> Capture. *J. Phys. Chem. C* **2017**, *121*, 22025-22030.
5. Tian, Z.; Dai, S.; Jiang, D.-e., What Can Molecular Simulation Do for Global Warming? *Wiley Interdisciplinary Reviews: Comput. Mol. Sci.* **2016**, *6*, 173-197.

**Grant E. Johnson**

## **Interfacial Structure and Dynamics in Ion Separations**

Grant E. Johnson, Venky Prabhakaran, Alla Zelenyuk and Vanda Glezakou  
Physical Sciences Division, Pacific Northwest National Laboratory, Richland, WA 99352

### **Presentation Abstract**

The analysis program at PNNL has developed a suite of unique tools for the preparation and characterization of extremely well-defined model systems and is now directing these capabilities toward separations research. Incorporating an additional theory task, the objective of this redefined program is to develop a predictive understanding of ion separation from liquids by systematically changing the solvation environment and dynamics through variation and control of interfacial double layers, nanoconfinement, surface morphology and functionality, hydrophobic domains and electric fields. Removal of trace contaminants from liquid waste streams and selective recovery of high-value elements constitute a critical use-inspired need in separation science with broad energy-related implications. The specific aims of the new program are to understand: 1) how does the solvation shell surrounding an ion change as it passes through a double layer and the ion adheres to a binding site of a functionalized interface? 2) how are the double layer structure at neutral interfaces, the structure of hydrated ions, and ion aggregation processes influenced by nanoconfinement? 3) how does ion adsorption depend on the morphology and curvature of nanoadsorbers functionalized with charged surface groups? and 4) how do hydrophobic domains and electric fields influence solvent ordering and transport between electrodes and ions to promote selective separations? Knowledge about how perturbations to interfacial solvent structure influence separations obtained from these studies will complement synchronous work in other research areas including desalination, interfacial science, and catalysis.

**Grant or FWP Number:** 47327

**PI:** Grant E. Johnson

**Postdoc(s):** Marshall Ligare, Don Gunaratne, David Bell and Kaitlyn Suski

**Affiliations(s):** Pacific Northwest National Laboratory

## RECENT PROGRESS

### Rational Understanding of Electrode-Electrolyte Interfaces

Achievements reported for the 2015-2018 funding period are related to the objectives of the previous chemical analysis program. For example, high-intensity ion soft landing (SL) using a new source enabled preparation of model redox super-capacitor electrodes, providing unprecedented insights into the role of anion-cation interactions and aggregate formation on the performance of energy storage devices. The model device was composed of two carbon nanotube (CNT)-coated paper electrodes separated by a porous ionic liquid-based electrolyte membrane. Multi-redox active polyoxometalate (POM) anions were deposited onto the CNT electrodes either using SL or electrospray deposition (ESD) of a  $\text{Na}_3[\text{PMo}_{12}\text{O}_{40}]$  solution. ESD was selected for comparison due to its superior performance in delivering both anions and counterions in solvent to the surface compared to other solution-based methods. In comparison, SL enables deposition of pure redox-active POM anions without counterions and solvent molecules. To understand the role of inactive counterions we acquired high-angle annular dark-field scanning

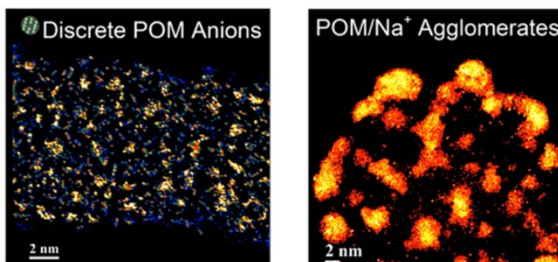


**Fig.1.** TEM images of  $\text{PMo}_{12}\text{O}_{40}^{3-}$  deposited onto CNT-electrodes using ion soft landing (left) and ambient electrospray (right). Note the difference in agglomeration due to elimination of cations, which influences capacitance and stability.

transmission electron microscopy (HAADF-STEM) images of the CNT electrodes. As shown in Figure 1, SL produced a uniform distribution of discrete  $\text{PMo}_{12}\text{O}_{40}$  clusters on the CNT electrode. In contrast, ESD resulted in formation of larger aggregates, which was attributed to agglomeration of POM in the presence of counterions. Agglomeration was shown to have a detrimental effect on the device's total specific capacitance. Furthermore, SL of POMs improved the long-term stability of the CNT electrodes. The maximum capacitance was observed with only  $\sim 50$  ng of  $\text{PMo}_{12}\text{O}_{40}$  on 25 ng of active CNT material, demonstrating the unexpectedly high contribution of nanogram quantities of pure POM to total capacitance. These results provide the first detailed insights into the effect of agglomeration and counterions on the stability and electron transfer efficiency at electrode-electrolyte interfaces and establish SL as a versatile tool for both model device fabrication and fundamental studies in energy storage. These achievements were published in *Nature Communications*.<sup>13</sup>

### Effect of Particle Shape on Dynamics and Physicochemical Properties

These reported achievements are also related to the objectives of the previous chemical analysis program. Due to the fact that microscopy is the most common offline particle-shape characterization method, it is essential to establish a relationship between particle properties determined with our unique single particle mass spectrometer (SPMS) and parameters commonly used to describe particle morphology based on their analysis by electron microscopy. In pursuit of this objective we used electron microscopy and helium

ion microscopy images of different particles to calculate critical parameters including aspect ratios, roundness, convexity, 2D fractal dimensions, aspect ratios, maximum lengths, area equivalent diameters, average number of monomers, and monomer mean diameter to connect with the particle attributes that we measure in our real-time analyses by SPMS. Importantly, these experiments were conducted, for the first time, on fully characterized, mass- and shape-selected particles. The first example of helium ion microscope images of two particles of the same mass separated by shape using this method is presented in Figure 2. The fact that the differences between the shapes of these two particles are clearly resolved suggests that separation based on shape is highly effective which opens up broad new opportunities to understand the role of morphology in determining particle dynamics and properties.

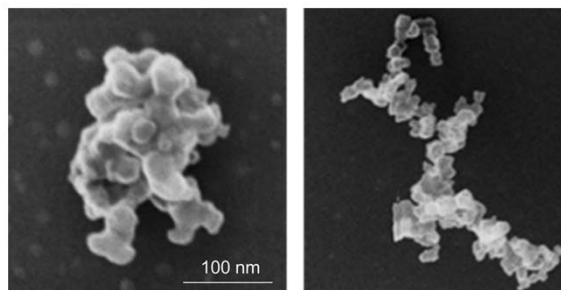


**Fig. 2.** Helium ion microscope images of two 1.97 fg particles separated by shape using our unique approach.

#### **Publications Acknowledging this Grant in 2015 – present<sup>1-42</sup>**

1. Ligare, M. R.; Johnson, G. E.; Laskin, J. Observing the real time formation of phosphine-ligated gold clusters by electrospray ionization mass spectrometry. *Phys Chem Chem Phys.* **2017**, *19*, 17187-17198. (I)
2. Ligare, M. R.; Baker, E. S.; Laskin, J.; Johnson, G. E. Ligand induced structural isomerism in phosphine coordinated gold clusters revealed by ion mobility mass spectrometry. *Chem Commun.* **2017**, *53*, 7389-7392. (I)
3. Laskin, J.; Hu, Q. C. Reactive Landing of Gramicidin S and Ubiquitin Ions onto Activated Self-Assembled Monolayer Surfaces. *J Am Soc Mass Spectr.* **2017**, *28*, 1304-1312. (I)
4. Bell, D. M.; Imre, D.; Martin, S. T.; Zelenyuk, A. The properties and behavior of alpha-pinene secondary organic aerosol particles exposed to ammonia under dry conditions. *Phys Chem Chem Phys.* **2017**, *19*, 6497-6507. (II)
5. Zelenyuk, A.; Wilson, J.; Imre, D.; Stewart, M.; Muntean, G.; Storey, J.; Prikhodko, V.; Lewis, S.; Eibl, M.; Parks, J. Detailed characterization of particulate matter emitted by lean-burn gasoline direct injection engine. *Int J Engine Res.* **2017**, *18*, 560-572. (III)
6. Shrivastava, M.; Lou, S. J.; Zelenyuk, A.; Easter, R. C.; Corley, R. A.; Thrall, B. D.; Rasch, P. J.; Fast, J. D.; Simonich, S. L. M.; Shen, H. Z.; Tao, S. Global long-range transport and lung cancer risk from polycyclic aromatic hydrocarbons shielded by coatings of organic aerosol (vol 114, pg 1246, 2017). *P Natl Acad Sci USA.* **2017**, *114*, 1246-1251. (II)
7. Zelenyuk, A.; Imre, D. G.; Wilson, J.; Bell, D. M.; Suski, K. J.; Shrivastava, M.; Beranek, J.; Alexander, M. L.; Kramer, A. L.; Simonich, S. L. M. The effect of gas-phase polycyclic aromatic hydrocarbons on the formation and properties of biogenic secondary organic aerosol particles. *Faraday Discuss.* **2017**, *200*, 143-164. (II)

8. Wang, J.; Zelenyuk, A.; Imre, D.; Mueller, K. Big Data Management with Incremental K-Means Trees–GPU-Accelerated Construction and Visualization. *Informatics*. **2017**, *4*, (I)
9. Viswanathan, S.; Rothamer, D. A.; Foster, D. E.; Fansler, T. D.; Zelenyuk, A.; Stewart, M. L.; Bell, D. M. Evolution of deep-bed filtration of engine exhaust particulates with trapped mass. *Int J Engine Res*. **2017**, *18*, 543-559. (III)
10. Viswanathan, S.; Rothamer, D.; Zelenyuk, A.; Stewart, M.; Bell, D. Experimental investigation of the effect of inlet particle properties on the capture efficiency in an exhaust particulate filter. *J. Aerosol Sci*. **2017**, *113*, 250-264. (II)
11. Shrivastava, M.; Lou, S.; Zelenyuk, A.; Easter, R. C.; Corley, R. A.; Thrall, B. D.; Rasch, P. J.; Fast, J. D.; Simonich, S. L. M.; Shen, H. Z.; Tao, S. Global long-range transport and lung cancer risk from polycyclic aromatic hydrocarbons shielded by coatings of organic aerosol. *P Natl Acad Sci USA*. **2017**, *114*, 1246-1251. (II)
12. Lin, P.; Bluvshstein, N.; Rudich, Y.; Nizkorodov, S. A.; Laskin, J.; Laskin, A. Molecular Chemistry of Atmospheric Brown Carbon Inferred from a Nationwide Biomass Burning Event. *Environ Sci Technol*. **2017**, *51*, 11561-11570. (II)
13. Prabhakaran, V.; Mehdi, B. L.; Ditto, J. J.; Engelhard, M. H.; Wang, B. B.; Gunaratne, K. D. D.; Johnson, D. C.; Browning, N. D.; Johnson, G. E.; Laskin, J. Rational design of efficient electrode-electrolyte interfaces for solid-state energy storage using ion soft landing. *Nat Commun*. **2016**, *7*, (I)
14. Pratihar, S.; Barnes, G. L.; Laskin, J.; Hase, W. L. Dynamics of Protonated Peptide Ion Collisions with Organic Surfaces: Consonance of Simulation and Experiment. *J Phys Chem Lett*. **2016**, *7*, 3142-3150. (III)
15. Riva, M.; Bell, D. M.; Hansen, A. M. K.; Drozd, G. T.; Zhang, Z. F.; Gold, A.; Imre, D.; Surratt, J. D.; Glasius, M.; Zelenyuk, A. Effect of Organic Coatings, Humidity and Aerosol Acidity on Multiphase Chemistry of Isoprene Epoxydiols. *Environ Sci Technol*. **2016**, *50*, 5580-5588. (II)
16. Wang, J.; Mueller, K. The Visual Causality Analyst: An Interactive Interface for Causal Reasoning. *Ieee T Vis Comput Gr*. **2016**, *22*, 230-239. (II)
17. Alexander, J. M.; Bell, D. M.; Imre, D.; Kleiber, P. D.; Grassian, V. H.; Zelenyuk, A. Measurement of size-dependent dynamic shape factors of quartz particles in two flow regimes. *Aerosol Sci Tech*. **2016**, *50*, 870-879. (II)
18. Gunaratne, K. D. D.; Prabhakaran, V.; Andersen, A.; Johnson, G. E.; Laskin, J. Charge retention of soft-landed phosphotungstate Keggin anions on self-assembled monolayers. *Phys Chem Chem Phys*. **2016**, *18*, 9021-9028. (I)
19. Hiranuma, N.; Mohler, O.; Kulkarni, G.; Schnaiter, M.; Vogt, S.; Vochezer, P.; Jarvinen, E.; Wagner, R.; Bell, D. M.; Wilson, J.; Zelenyuk, A.; Cziczo, D. J. Development and characterization of an ice-selecting pumped counterflow virtual impactor (IS-PCVI) to study ice crystal residuals. *Atmos Meas Tech*. **2016**, *9*, 3817-3836. (III)
20. Hu, Q. C.; Laskin, J. Secondary Structures of Ubiquitin Ions Soft-Landed onto Self Assembled Monolayer Surfaces. *J Phys Chem B*. **2016**, *120*, 4927-4936. (I)
21. Johnson, G. E.; Gunaratne, D.; Laskin, J. Soft- and reactive landing of ions onto surfaces: Concepts and applications. *Mass Spectrom Rev*. **2016**, *35*, 439-479. (I)
22. Johnson, G. E.; Laskin, J. Understanding ligand effects in gold clusters using mass spectrometry. *Analyst*. **2016**, *141*, 3573-3589. (I)

23. Johnson, G. E.; Moser, T.; Engelhard, M.; Browning, N. D.; Laskin, J. Fabrication of electrocatalytic Ta nanoparticles by reactive sputtering and ion soft landing. *J Chem Phys.* **2016**, *145*. (II)
24. Laskin, J.; Johnson, G. E.; Prabhakaran, V. Soft Landing of Complex Ions for Studies in Catalysis and Energy Storage. *J Phys Chem C.* **2016**, *120*, 23305-23322. (I)
25. Laskin, J.; Lanekoff, I. Ambient Mass Spectrometry Imaging Using Direct Liquid Extraction Techniques. *Anal Chem.* **2016**, *88*, 52-73. (II)
26. Prabhakaran, V.; Johnson, G. E.; Wang, B. B.; Laskin, J. In situ solid-state electrochemistry of mass-selected ions at well-defined electrode-electrolyte interfaces. *P Natl Acad Sci USA.* **2016**, *113*, 13324-13329. (I)
27. El-Khoury, P. Z.; Johnson, G. E.; Novikova, I. V.; Gong, Y.; Joly, A. G.; Evans, J. E.; Zamkov, M.; Laskin, J.; Hess, W. P. Enhanced Raman scattering from aromatic dithiols electrosprayed into plasmonic nanojunctions. *Faraday Discuss.* **2015**, *184*, 339-357. (III)
28. Fooshee, D. R.; Aiona, P. K.; Laskin, A.; Laskin, J.; Nizkorodov, S. A.; Baldi, P. F. Atmospheric Oxidation of Squalene: Molecular Study Using COBRA Modeling and High-Resolution Mass Spectrometry. *Environ Sci Technol.* **2015**, *49*, 13304-13313. (III)
29. Gunaratne, K. D. D.; Prabhakaran, V.; Ibrahim, Y. M.; Norheim, R. V.; Johnson, G. E.; Laskin, J. Design and performance of a high-flux electrospray ionization source for ion soft landing. *Analyst.* **2015**, *140*, 2957-2963. (I)
30. Gunaratne, K. D. D.; Prabhakaran, V.; Johnson, G. E.; Laskin, J. Gas-Phase Fragmentation Pathways of Mixed Addenda Keggin Anions: PMo<sub>12</sub>-nWnO<sub>40</sub> (3-) (n=0-12). *J Am Soc Mass Spectr.* **2015**, *26*, 1027-1035. (I)
31. Zelenyuk, A.; Imre, D.; Wilson, J.; Zhang, Z. Y.; Wang, J.; Mueller, K. Airborne Single Particle Mass Spectrometers (SPLAT II & miniSPLAT) and New Software for Data Visualization and Analysis in a Geo-Spatial Context. *J Am Soc Mass Spectr.* **2015**, *26*, 257-270. (I)
32. Wilson, J.; Imre, D.; Beranek, J.; Shrivastava, M.; Zelenyuk, A. Evaporation Kinetics of Laboratory-Generated Secondary Organic Aerosols at Elevated Relative Humidity. *Environ Sci Technol.* **2015**, *49*, 243-249. (II)
33. Romonosky, D. E.; Laskin, A.; Laskin, J.; Nizkorodov, S. A. High-Resolution Mass Spectrometry and Molecular Characterization of Aqueous Photochemistry Products of Common Types of Secondary Organic Aerosols. *J Phys Chem A.* **2015**, *119*, 2594-2606. (II)
34. Laskin, J.; Futrell, J. H. New approach for studying slow fragmentation kinetics in FT-ICR: Surface-induced dissociation combined with resonant ejection. *Int J Mass Spectrom.* **2015**, *378*, 160-168. (I)
35. Laskin, J. Ion-surface collisions in mass spectrometry: Where analytical chemistry meets surface science. *Int J Mass Spectrom.* **2015**, *377*, 188-200. (I)
36. Laskin, J. Surface-induced dissociation: a unique tool for studying energetics and kinetics of the gas-phase fragmentation of large ions. *Eur J Mass Spectrom.* **2015**, *21*, 377-389. (I)
37. Johnson, G. E.; Colby, R.; Laskin, J. Soft landing of bare nanoparticles with controlled size, composition, and morphology. *Nanoscale.* **2015**, *7*, 3491-3503. (II)

38. Laskin, J. Effect of basic residue on the kinetics of peptide fragmentation examined using surface-induced dissociation combined with resonant ejection. *Int J Mass Spectrom.* **2015**, *391*, 24-30. (I)
39. Laskin, A.; Laskin, J.; Nizkorodov, S. A. Chemistry of Atmospheric Brown Carbon. *Chem Rev.* **2015**, *115*, 4335-4382. (II)
40. Johnson, G. E.; Olivares, A.; Hill, D.; Laskin, J. Cationic gold clusters ligated with differently substituted phosphines: effect of substitution on ligand reactivity and binding. *Phys Chem Chem Phys.* **2015**, *17*, 14636-14646. (I)
41. Johnson, G. E.; Laskin, J. Soft landing of mass-selected gold clusters: Influence of ion and ligand on charge retention and reactivity. *Int J Mass Spectrom.* **2015**, *377*, 205-213. (I)
42. Johnson, G. E.; Colby, R.; Engelhard, M.; Moon, D.; Laskin, J. Soft landing of bare PtRu nanoparticles for electrochemical reduction of oxygen. *Nanoscale.* **2015**, *7*, 12379-12391. (II)

(I) *Exclusively funded by this grant;*

(II) *Jointly funded by this grant and other grants with leading intellectual contribution from this grant;*

(III) *Jointly funded by this grant and other grants with relatively minor intellectual contribution from this grant;*

## Investigations into the Gas Separation Performance of Siloxane-Substituted Polynorbornene Membranes

Brian K. Long,<sup>1</sup> Christopher R. Maroon,<sup>1</sup> Jacob Townsend,<sup>1</sup> Konstantinos D. Vogiatzis,<sup>1</sup>  
Shannon M. Mahurin,<sup>2</sup>

<sup>1</sup>University of Tennessee, Knoxville, Department of Chemistry

<sup>2</sup>Oak Ridge National Laboratory, Chemical Sciences Division

### Presentation Abstract

Gas separation membranes have been targeted for a variety of applications including the separation of light-hydrocarbons, natural gas purification, and even the separation of harmful greenhouse gases such as carbon dioxide (CO<sub>2</sub>). In this presentation, we will describe a series of siloxane-substituted polynorbornenes that were synthesized via vinyl-addition polymerization methodologies. Careful catalyst selection enabled access to these materials in high molecular weight and in good yield. Furthermore, they can be readily cast into large area, defect-free free-standing films that are both thermally and mechanically robust. Systematic investigations have provided useful insight into the effect that molecular structure at the monomeric and polymeric levels have on gas separation performance. These key structure-property relationships were used to inform subsequent polymer designs, some of which have shown performance near the CO<sub>2</sub>/N<sub>2</sub> upper bound. Lastly, these materials have also shown promise for the separation of heavier hydrocarbons from lighter hydrocarbons, such as butane from methane.

### DE-SC0018179: Advancing Polymeric Gas Separation Membranes through Molecular Engineering

**PI:** Brian K. Long

**Postdoc(s):** none

**Student(s):** Christopher R. Maroon, Jordan Kaiser, Morgan Higgins

**Affiliations(s):** University of Tennessee, Knoxville, Department of Chemistry

### RECENT PROGRESS

#### *Fundamental Structure-Property Relationships of Vinyl-added, Siloxane-substituted Polynorbornenes*

High molecular weight, siloxane-substituted polynorbornenes were previously thought to be inaccessible via vinyl-addition polymerization methods due to monomer-catalyst incompatibility. However, we recently reported that by using a unique Ni-based catalyst, *trans*-[Ni(C<sub>6</sub>F<sub>5</sub>)<sub>2</sub>(SbPh<sub>3</sub>)<sub>2</sub>], a variety of these polymers could be readily accessed.

Recent efforts to study these materials have focused extensively on Objective #1, which aims to enhance the gas separation performance of these materials by discerning key structure-property relationships and by tailoring polymer-penetrant gas interactions.

The targeted structure-property relationships were broken down into three fundamental sets of polymers. **Set 1** was selected to evaluate the effect that number of Si-O bonds have on gas separation performance. **Set 2** is intended to evaluate the effects that siloxane-substituent sterics have on chain packing, free volume, and ultimately gas separation performance. Lastly, **Set 3** is designed to determine how siloxane tether length and side-group flexibility perturbs gas permeability and selectivity. All monomers were prepared via Diels-Alder reaction between cyclopentadiene and their respective vinyl siloxane, which yields a mixture of *endo*- and *exo*-substituted monomers. Each polymer was synthesized via vinyl-addition polymerization using *trans*-[Ni(C<sub>6</sub>F<sub>5</sub>)<sub>2</sub>(SbPh<sub>3</sub>)<sub>2</sub>], which provided the desired materials in high yields (>50 %) and with high molecular weights (>100 kg/mol) for each polymer.

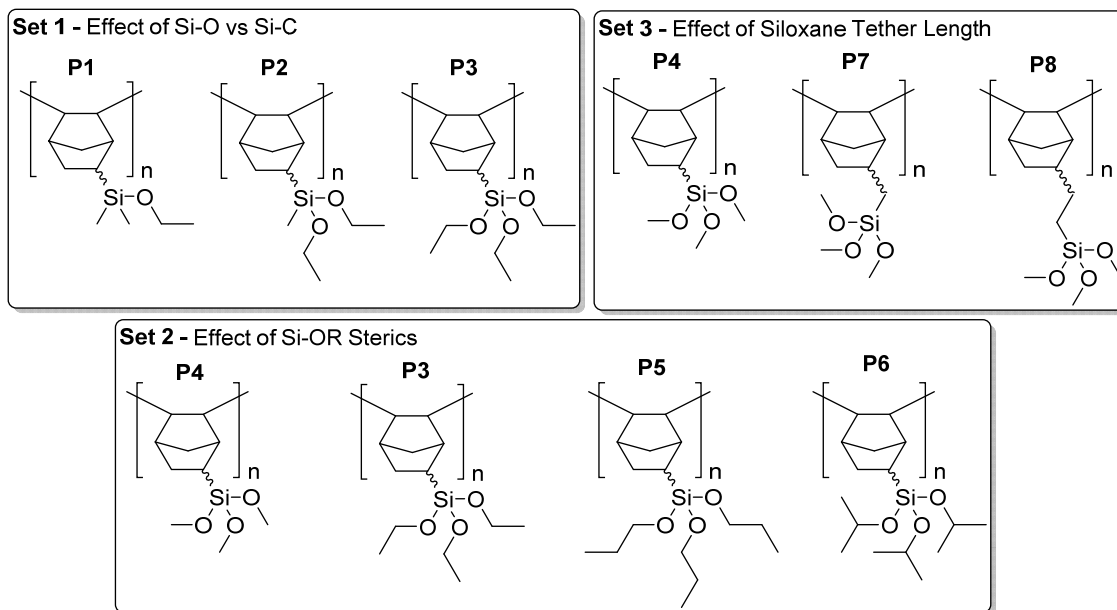


**Figure 1.** Synthesized polymers **P1-P8** that are designed to evaluate the structure property relationship between CO<sub>2</sub> separation performance and a) the number of Si-O linkages, b) siloxane sterics, and c) siloxane tether length.

As shown in Table 1, the CO<sub>2</sub> and N<sub>2</sub> permeabilities of polymers **P1-P8** were measured using the constant-volume variable-pressure gas flux method, and their corresponding ideal selectivities calculated. A plot of CO<sub>2</sub>/N<sub>2</sub> selectivity versus CO<sub>2</sub> permeability for these polymers (Figure 2) revealed clear trends within each polymer set. Specifically for polymer **Set 1** (**P1-P3**), it was noted that altering the number of Si-O bonds present resulted in behavior that follows the traditional permeability-selectivity trade-off relation. Polymer **Set 2** (**P3-P5**) revealed that both permeability and selectivity could be simultaneously increased as a function of decreasing siloxane-substituent sterics. Of note, **P4** nearly reached the 2008 upper bound. Lastly, polymer **Set 3** (**P4** and **P7-P8**) showed that increasing side-group tether length leads to higher selectivities, but at the cost of decreased permeability. We have preliminarily attributed this decrease in permeability to

tighter chain packing that is facilitated by the enhanced flexibility of the longer side-groups. Regardless, **P4**, **P7**, and **P8** all are promising candidates as they each lie remarkably close to the 2008 upper bound.

poly	$P$ (Barrer) <sup>a</sup>		$\alpha$ (CO <sub>2</sub> /N <sub>2</sub> ) <sup>b</sup>
	CO <sub>2</sub>	N <sub>2</sub>	
<b>P1</b>	471	25	18.9
<b>P2</b>	474	25	19.3
<b>P3</b>	937	57	16.4
<b>P4</b>	1428	52	27.6
<b>P5</b>	646	47	13.75
<b>P6</b>	1129	93	12.2
<b>P7</b>	775	23	34.4
<b>P8</b>	564	16	36.1

<sup>a</sup>Permeability values of free-standing polymer films were obtained using the constant-volume variable-pressure gas flux method. <sup>b</sup>Ideal selectivity calculated by a ratio of CO<sub>2</sub> and N<sub>2</sub> permeabilities.

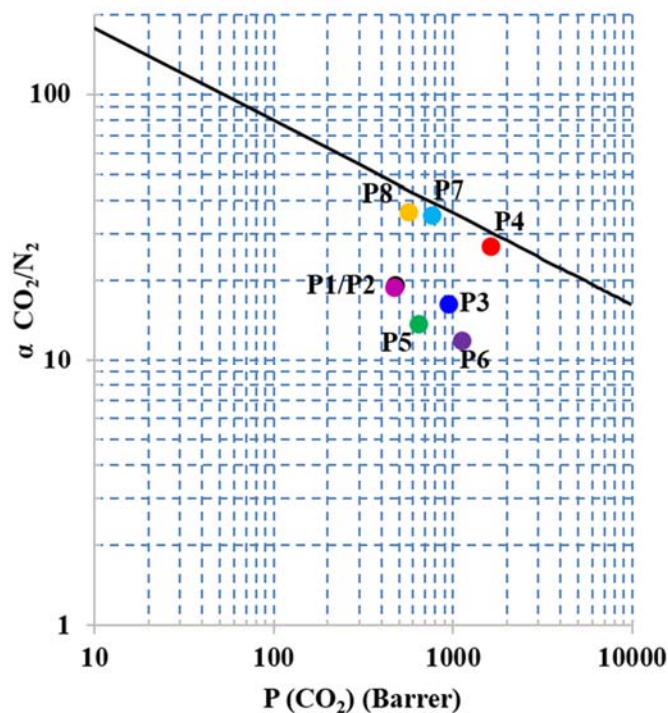


**Table 1.** Permeability and ideal selectivity of polymers **P1-P8**.

**Figure 2.** Robeson plot of polymers **P1-P8**. Note: all data points have error bars, but are simply not visible when plotted at this scale.

We have also recently discovered that incorporation of ethylene glycol-like units into the siloxane-substituted polymers (**P9-P13**, Figure 3) can result in significant enhancements in CO<sub>2</sub>/N<sub>2</sub> selectivity with minimal impact on CO<sub>2</sub> permeability. Table 2 shows the ideal permeability and selectivity for the homo- and copolymer series **P9-P13**. This data clearly shows that **P9** has an ideal selectivity that is  $\sim 2.3\times$  greater than the triethoxy substituted polymer **P13**, and that a nearly linear progression of CO<sub>2</sub> separation performance is obtained for random copolymers of the two monomers (**P10-P12**). This is more conveniently depicted in Figure 2 in which it is clear that these materials do not follow the traditional permeability-selectivity trade-off. Furthermore, it is intriguing that homopolymer **P9** nears the upper bound with a  $P_{\text{CO}_2} = 755$  and an  $\alpha_{\text{CO}_2/\text{N}_2} = 37$ .

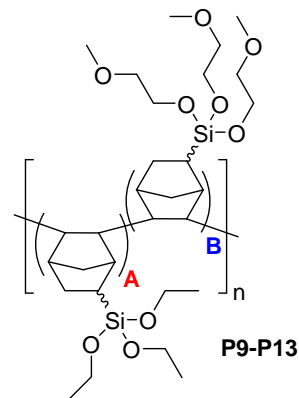


**Figure 3.** Structure of polymers **P9-P13**.

polymer	monomer incorporations		$P$ (Barrer) <sup>a</sup>		
	feed ratio A:B	Actual A:B	CO <sub>2</sub>	N <sub>2</sub>	$\alpha^b$ (CO <sub>2</sub> /N <sub>2</sub> )
<b>P9</b>	0:100	0:100	755	21	37
<b>P10</b>	25:75	34:66	700	20	34
<b>P11</b>	50:50	59:41	733	28	27
<b>P12</b>	75:25	79:21	869	41	22
<b>P13</b>	100:0	100:0	937	57	16

<sup>a</sup>Permeability values of free-standing polymer films were obtained using the constant-volume variable-pressure gas flux method, as detailed in the Experimental section. <sup>b</sup>Ideal selectivity calculated by a ratio of CO<sub>2</sub> and N<sub>2</sub> permeabilities.

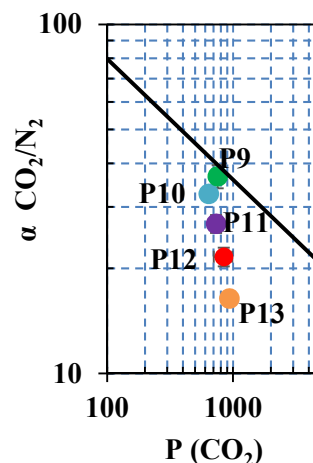


**Table 2.** Permeability and ideal selectivity of homo- and copolymers **P9-P13**.

**Figure 2.** Robeson plot of polymers **P9-P13**.

To better understand the origins of this enhanced performance, we are currently conducting a detailed investigation into the densities, fractional free-volumes, and individual diffusivity and solubility coefficients of polymers **P9-P13**. As was predicted, Table 3 demonstrates that the notable selectivity of **P9**, versus **P13**, can be almost entirely attributed to solubility selectivity, which we presume is due to the presence of the ethylene glycol-like side-chains. We hypothesize that these side-groups likely mimic the favorable CO<sub>2</sub>-polymer interactions found in poly(ethylene glycol) (PEG) based materials. Furthermore, computational investigations support this hypothesis through predicted electronic and enthalpic interaction energies.

polymer	density <sup>a</sup> (g/cm <sup>3</sup> )	FFV <sup>b</sup>	D <sup>c</sup> (x10 <sup>-6</sup> cm <sup>2</sup> /s)			S <sup>c</sup> (cm <sup>3</sup> ·[STP]/(cm <sup>3</sup> ·atm))		
			CO <sub>2</sub>	N <sub>2</sub>	(D <sub>CO<sub>2</sub>}/D<sub>N<sub>2</sub></sub>)</sub>	CO <sub>2</sub>	N <sub>2</sub>	(S <sub>CO<sub>2</sub>}/S<sub>N<sub>2</sub></sub>)</sub>
<b>P13</b>	1.088 (±0.017)	0.159 (±0.013)	2.14	1.33	1.61	5.30	0.49	10.82
<b>P11</b>	1.111 (±0.015)	0.164 (±0.012)	1.83	1.61	1.14	2.93	0.123	23.82
<b>P9</b>	1.155 (±0.015)	0.158 (±0.011)	1.9	1.84	1.03	2.83	0.076	37.24

<sup>a</sup>Determined using Archimedes Principle. <sup>b</sup>Estimated using the Bondi Method. <sup>c</sup>Estimated using Daynes-Barrer Lag-Time Method

**Table 3.** Understanding the enhanced CO<sub>2</sub>/N<sub>2</sub> selectivity of copolymers **P9-P13**.

### Publications Acknowledging this Grant in 2015 – present

None, Award start date – 09/01/2017

## The Eleven Ways to Use Host-Guest Chemistry to Extract Aqueous Ions

Bruce A. Moyer  
Oak Ridge National Laboratory, Chemical Sciences Division

### Presentation Abstract

Categorization of the different types of chemical schemes for extraction of ions has proven to be a useful tool in designing new selective separation systems and in identifying fertile areas for research. First articulated over a decade ago,<sup>1</sup> the eleven ways are divided into three groups: ion-pair extraction, cation exchange, and anion exchange, as shown in Figure 1. Indicated by rings in the figure, the hosts or receptors are confined to the organic phase by possessing sufficient lipophilicity; alternatively, the hosts could be tethered to a support. Early efforts in the field of host-guest chemistry, starting with the crown ethers, focused on many types of neutral macrocycles for cation extraction by Way #2, the anion being co-extracted for charge balance. Likewise, a neutral anion host such as a calixpyrrole can extract an anion (Way #3), though few examples have been reported. Since Ways #2 and #3 tend to be weak unless the co-extracted ion is lipophilic, researchers have mixed neutral hosts with straightforward results (Way #4) or designed elegant

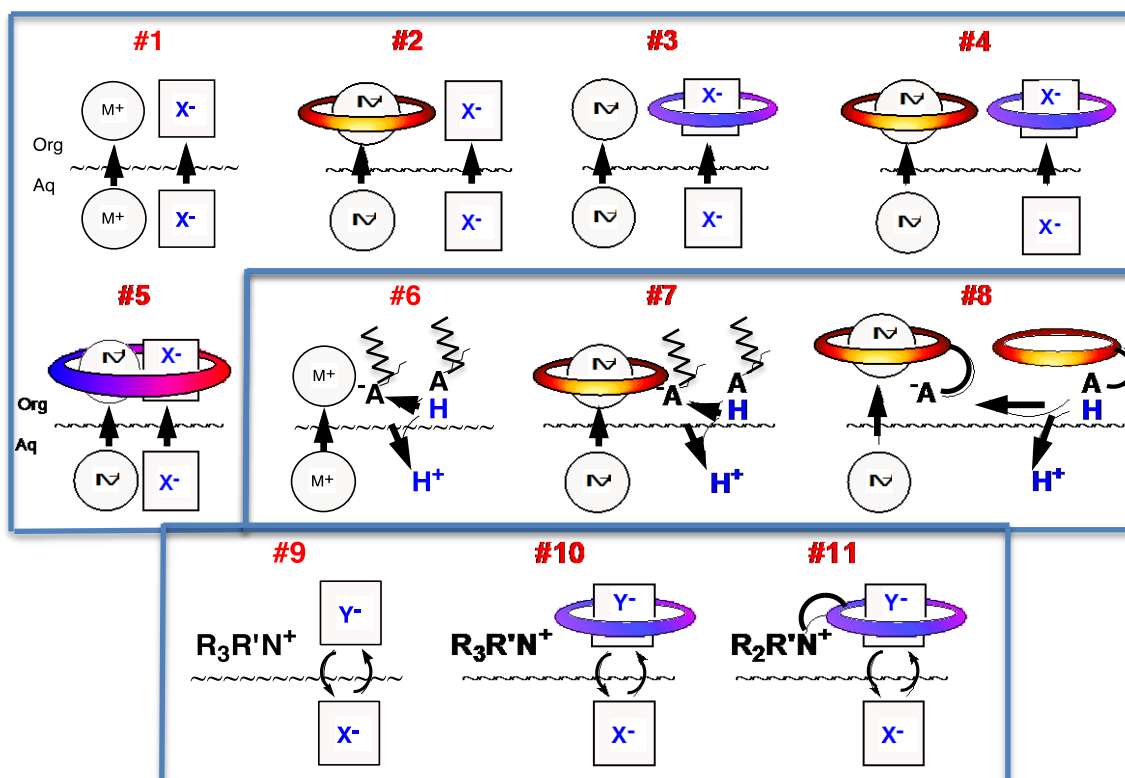


Figure 1. The "Eleven Ways" to use host-guest chemistry in extractive separations.

ion-pair hosts (Way #5).<sup>2</sup> The simple anion receptor calix[4]pyrrole surprised us by functioning as an ion-pair receptor in certain cases.<sup>3–5</sup> Alternatively, researchers have turned to cation- (Ways #6–8) or anion-exchange systems (Ways #9–11). Not yet well studied, the latter have attracted our recent attention,<sup>3</sup> particularly in examining the guanidinium functionality as a double hydrogen-bond donor exhibiting strong oxoanion selectivity.<sup>5,6</sup> In as-yet unpublished work, we have extended this theme to introduce iminoguanidiniums, micellar extractants exhibiting unprecedented oxoanion affinity.

## References

1. Moyer, B. A.; Bonnesen, P. V.; Custelcean, R.; Delmau, L. H.; Hay, B. P. Strategies for Using Host-Guest Chemistry in the Extractive Separations of Ionic Guests. *Kem. Ind.* **2005**, *54* (2), 65.
2. Kim, S. K.; Lee, J.; Williams, N. J.; Lynch, V. M.; Hay, B. P.; Moyer, B. A.; Sessler, J. L. Bipyrrrole-Strapped Calix[4]pyrroles: Strong Anion Receptors That Extract the Sulfate Anion. *J. Am. Chem. Soc.* **2014**, *136*, 15079.
3. Borman, C. J.; Bonnesen, P. V.; Moyer, B. A. Selectivity Control in Synergistic Liquid-Liquid Anion Exchange of Univalent Anions via Structure-Specific Cooperativity between Quaternary Ammonium Cations and Anion Receptors. *Anal. Chem.* **2012**, *84* (19), 8214.

## Principles of Chemical Recognition and Transport in Extractive Separations Field Work Proposal ERKCC08

**PI:** Bruce A. Moyer

**Co-PIs:** Vyacheslav Bryantsev, Radu Custelcean, Santa Jansone-Popova

## Publications Acknowledging this FWP in 2015–present

(I) *Exclusively funded by this grant;*

4. Ellis, R. J.; Reinhart, B.; Williams, N. J.; Moyer, B. A.; Bryantsev, V. S. Capping the Calix: How Toluene Completes Cesium(I) Coordination with Calix[4]pyrrole. *Chem. Commun.* **2017**, *53* (41), 5610.
5. Williams, N. J.; Bryantsev, V. S.; Custelcean, R.; Seipp, C. A.; Moyer, B. A.  $\alpha, \alpha', \alpha'', \alpha'''$ -meso-Tetrahexyltetramethyl-calix[4]Pyrrole: An Easy-to-Prepare, Isomerically Pure Anion Extractant with Enhanced Solubility in Organic Solvents. *Supramol. Chem.* **2016**, *28*, 176.
6. Seipp, C. A.; Williams, N. J.; Bryantsev, V. S.; Custelcean, R.; Moyer, B. A. A Conformationally Persistent Pseudo-bicyclic Guanidinium for Anion Coordination as Stabilized by Dual Intramolecular Hydrogen Bonds. *RSC Advances* **2015**, *5*, 107266–107269.
7. Seipp, C. A.; Williams, N. J.; Bryantsev, V. S.; Moyer, B. A. A Simple Guanidinium Motif for the Selective Binding and Extraction of Sulfate. *Sep. Sci. Technol.* **2017**, *Online Only*, DOI: 10.1080/01496395.2017.1318922.

(II) *Jointly funded by this grant and other grants with leading intellectual contribution from this grant;*

8. Brigham, D.; Ivanov, A.; Moyer, B. A.; Delmau, L.; Bryantsev, V. S.; Ellis, R. J. Trefoil-shaped outer-sphere ion clusters mediate lanthanide(III) ion transport with diglycolamide ligands. *J. Am. Chem. Soc.* **2017**, *139*, 17350–17358.

**Experimental and Theoretical Evaluation of the Thermodynamic Stability of True MOF Polymorphs Explains their Mechanochemical Interconversions**

Alexandra Navrotsky, Zamirbek Akimbekov, G. P. Nagabhushana  
Peter A Rock Thermochemistry Laboratory, UC Davis

**Presentation Abstract**

Mechanochemical synthesis overcomes kinetic barriers and allows transformations of metal organic frameworks (MOF) to new denser phases of increasing thermodynamic stability. Topologically different zeolitic imidazolate frameworks (ZIF) of the same composition (true polymorphs) were synthesized by mechanochemistry, including previously unknown phases. Their energetic stability was determined experimentally by solution calorimetry in 5M HCl and theoretically by periodic DFT calculations.

The thermodynamics follows molar volume trends discovered previously, with denser frameworks being more stable. An energy landscape of polymorphs of similar stability is accessed, with sequential transformations to more stable phases following Ostwald's rule of stages. Ethyl groups stabilize the frameworks more effectively than methyl substituents.

This advances the development of new porous frameworks potentially useful in separations and catalysis and provides means to control and improve MOF stability.

.....  
**DE-SC0016573: The Energetics and Dynamics of Confinement in Flexible Frameworks**

**Postdoc(s):** G. P. Nagabhushana

**Student(s):** Zamirbek Akimbekov, Novendra Novendra

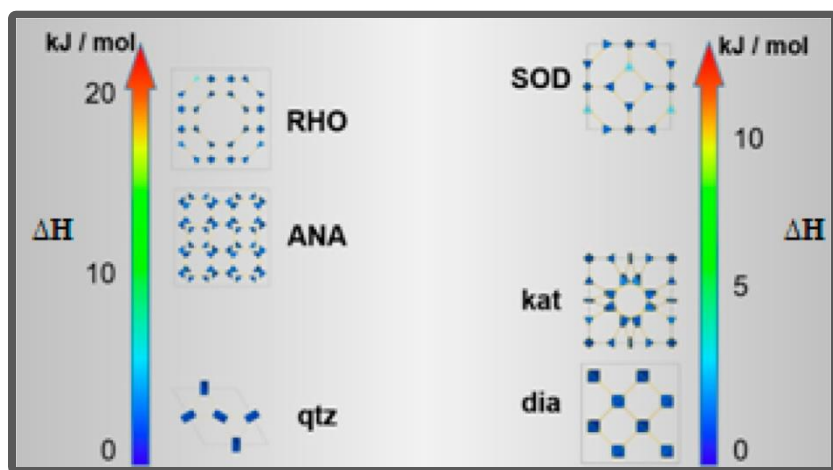
**RECENT PROGRESS**

As outlined in the proposal, Navrotsky's team has begun studying, by solution calorimetry, the energetics of a series of true ZIF polymorphs prepared by mechanochemical synthesis by Tomislav Friscic of McGill University. We provide the first combined experimental and theoretical evaluation of how differences in ligand structure and framework topology affect the relative stabilities of isocompositional (i.e. true polymorph) metal-organic frameworks (MOFs). We used solution calorimetry and periodic DFT calculations to analyze thermodynamics of two families of topologically-distinct polymorphs of zinc zeolitic imidazolate frameworks (ZIFs) based on 2-methyl- and 2-ethylimidazolate linkers, demonstrating a correlation between measured thermodynamic stability and density, and a pronounced effect of the ligand substituent on their stability. The results also show that thermodynamic stability of a given ZIF does not depend on the choice of synthetic method, and that mechanochemical syntheses and transformations of ZIFs

are consistent with Ostwald's rule of stages and proceed toward thermodynamically increasingly stable, more dense phases. Thus grinding, rather than creating more metastable phases by the added mechanical energy, enables the system to overcome kinetic barriers and form more stable denser MOF structures. Therefore a rich landscape of polymorphs closely spaced in energy becomes accessible. This work has been published in J. Am. Chem. Soc. We are extending these studies to ZIFs with modified linkers to separate out effects of porosity and chemistry. Zamirbek Akimbekov, Ph.D. student on this project, completed his dissertation in December. A second-year Ph.D. student, Novendra Novendra, is starting work on other selected MOFs and dense hybrid materials.

Woodfield's group has measured the low-temperature heat capacities of four of these ZIF polymorphs. The results show several interesting features. First, the heat capacities (and standard entropies at 298 K) are significantly different, indicating that the polymorphs differ substantially in lattice vibrations and/or defects. These differences are far more pronounced than those seen in earlier studies on silica zeotype polymorphs. Second, all of the samples exhibit gaps in the phonon spectra at low temperatures. This was expected as it is common for porous frameworks, e.g. zeolites, and is now confirmed for MOFs. Third, all the samples exhibit a broad  $C_p$  anomaly centered around 200 K. At first, it was thought this was a Schottky anomaly, but no suitable Schottky model was found that could fit the data. The data were also fit to other lattice models, but currently nothing has been found that is physically reasonable. We are now in the process of synthesizing, characterizing, and then measuring the heat capacity of a series of model imidazole and Zn-amine compounds that we can use as a non-framework model for the heat capacity of ZIFs. We will use the non-framework model as a baseline to subtract out the phonon modes unique to these MOF materials and then explore whether this behavior is unique or general. Neutron scattering studies by the Ross group will also shed light on the possible sources of these anomalies.

The Ross group is in the process of applying for neutron beam time.



Schematic of enthalpies of formation ZIF polymorphs.  
Higher energy means less thermodynamic stability.

left: HEtIm based ZIF polymorphs

right: HMeIm based ZIF polymorphs

## Publications Acknowledging this Grant

1. Akimbekov, Z., Katsenis, A., Nagabhushana, G., Ayoub, G., Arhangelkis, M., Morris, A., Friščic, T., Navrotsky, A., Experimental and Theoretical Evaluation of the Stability of True MOF Polymorphs Explains Their Mechanochemical Interconversions. *J. Am. Chem. Soc.* **2017**, *139*, 7952-7957.
2. J. Calvin, J., Asplund, M., Akimbekov, Z., Ayoub, G., Katsensis, A., Navrotsky, A., Friscic, T., Woodfield, B., Heat Capacity and Thermodynamic Functions of Crystalline and Amorphous Forms of the Metal Organic Framework Zinc 2-Ethylimidazolate, Zn(EtIm)<sub>2</sub>. *J. Chem. Thermo.* **2018**, *116*, 341-351.

**Developing Metal- and Ligand-Redox Properties in New Separations Methods for Rare Earth Elements**

Huayi Fang, Bren E. Cole, Yusen Qiao, Thibault Cheisson Joshua Nelson  
and Eric J. Schelter

*Chemistry Department, University of Pennsylvania*

**Presentation Abstract**

The Rare Earth Elements (REs) are critical materials due to their importance in clean energy and defense applications. It is not economically viable to produce pure REs in the U.S. given current separations technology and the domestic regulatory climate. To foster stable domestic RE production there is a critical need for fundamentally new REs chemistry that contributes to disruptive technologies in RE separations. Our *central hypothesis* for this proposal is that size-selective molecular apertures for RE<sup>3+</sup> cations can be formed using tridentate ligands and leveraged for solubility separations and that tailored coordination environments can enable separations based on (photo)redox chemistry. We are testing our central hypothesis of this project by 1) developing new separations systems based on oligomerization of RE coordination complexes using solubility differences between monomeric RE complexes and their oligomers, and 2) separating targeted RE complexes based on differences in their oxidative redox properties

**DE-SC0017259: Advancing Separations of Rare Earth Elements through Coordination and (Photo)Redox Chemistry**

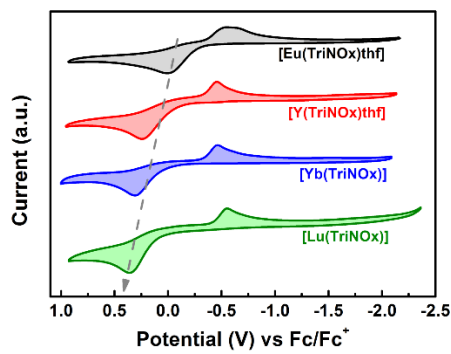
**Postdoctoral(s):** Dr. Huayi Fang, Dr. Thibault Cheisson

**Student(s):** Bren E. Cole, Joshua Nelson, Yusen Qiao

**RECENT PROGRESS**

***Electrokinetic Separations of Rare Earth Element Complexes.***

We demonstrated that complexes of redox active ligands with rare earth complexes could be separated using an oxidative, electrokinetic method. This is the first time that RE metals have been separated by kinetic means. The oxidation rates of the complexes [RE(TriNOx)thf] and [RE(TriNOx)] upon oxidation with [Fc][BAr<sup>F</sup>] were derived by their cyclic voltammogram measurements (see Figure, below). The oxidation rates for these compounds decreased with the atomic number increase from Eu to Lu ( $k_{0V}(\text{Eu}) > k_{0V}(\text{Y}) > k_{0V}(\text{Yb}) > k_{0V}(\text{Lu})$ ). And the derived oxidation rates were used to predict separation performance for mixtures of the ions based on simple rate equations. The predictions lead to a demonstration of an electro-kinetic separation method for REs based on a series of 50:50 molar ratio binary mixtures, including Eu/Y, Y/Yb, Y/Lu. Kinetic differences observed for the oxidation reactions of different RE-TriNOx compounds were consistent with predictions from the kinetic model. The separation factors for a single



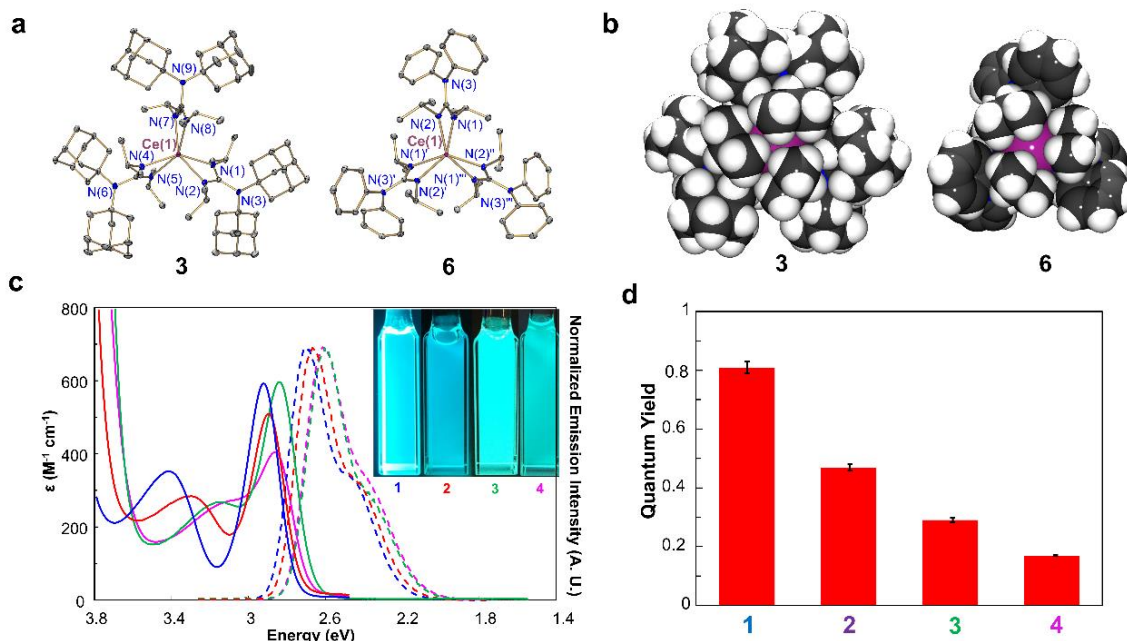
Scan rate (mV/s)	50	100	250
$k_{\text{ox}}(\text{Eu})$ ( $\times 10^{-4} \text{ cm s}^{-1}$ )	18.0	22.8	20.4
$k_{\text{ox}}(\text{Y})$ ( $\times 10^{-4} \text{ cm s}^{-1}$ )	1.86	2.82	2.07
$k_{\text{ox}}(\text{Yb})$ ( $\times 10^{-4} \text{ cm s}^{-1}$ )	0.193	0.239	0.195
$k_{\text{ox}}(\text{Lu})$ ( $\times 10^{-4} \text{ cm s}^{-1}$ )	0.130	0.356	0.198

Oxidation rates for RE-TriNOx compounds

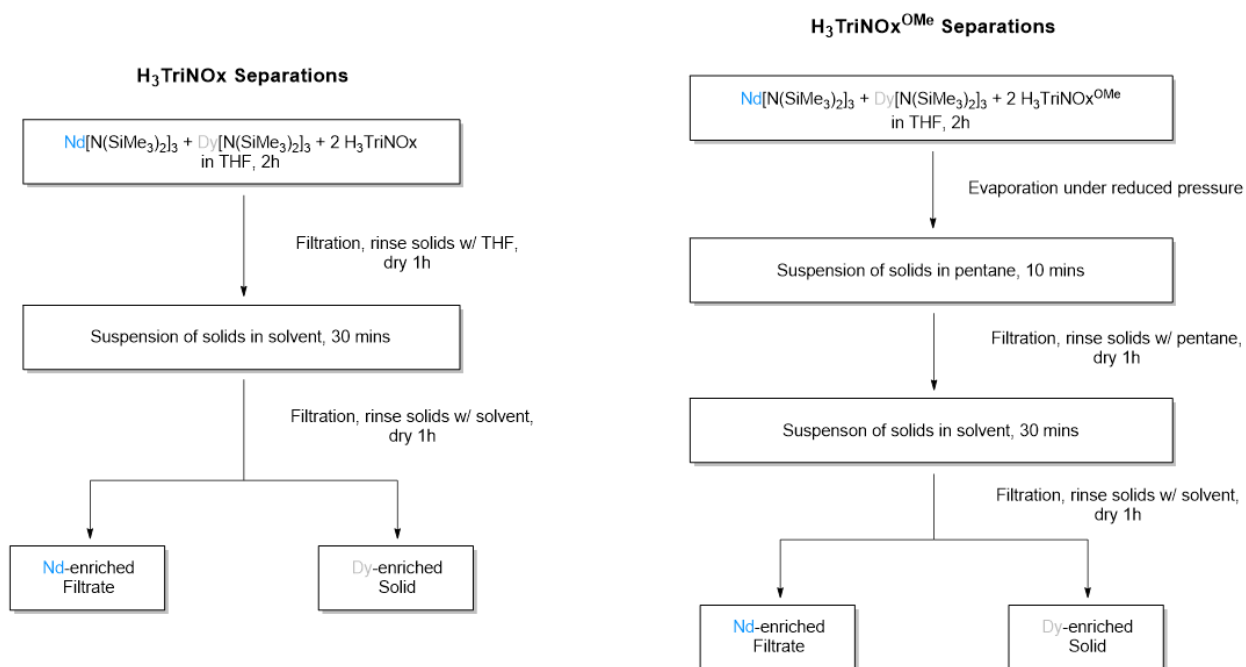
iteration were calculated based on the ICP-OES results as  $S_{\text{Y/Eu}} = 74.8$ ,  $S_{\text{Y/Yb}} = 55.6$  and  $S_{\text{Y/Lu}} = 261$ . These results were published in *Angewandte Chemie, International Edition*. We are currently optimizing the separation method using controlled potential electrolysis and modified ligand systems. This approach also holds promise for varied and challenging metals separation systems, using redox-active ligands to separate ions by kinetic control.

### Cerium Photoredox Chemistry – Physicochemical Characteristics.

In collaboration with Prof. Jochen Autschbach's group at Buffalo and locally with Prof. Jessica Anna's group at Penn, we developed a combined experimental and computational study, leveraging steric effects and ligand types can efficiently control the emission colors and brightness of cerium luminophores. The goals for this work were to understand how complex characteristics promote luminescence in lanthanide complexes that can be harnessed for photo-redox based separations. The results from a series of eight cerium(III) *tris*(guanidinate) complexes demonstrated that complexes with large ligand steric demand in  $C_3$  symmetry show tunable quantum yields, and therefore brightness. The key physical process at work here is the exclusion of exogenous solvent molecules from the coordination sphere, namely along the  $C_3$  axis, that provide quenching processes. Furthermore, our computational results included the first comprehensive computational analysis of molecular cerium(III) luminophores. We successfully



reproduced the experimental absorption and emission spectra and rationalized the Stokes shifts for two series of compounds. We conclude that by applying a rigid coordination sphere to the cerium center, the geometry relaxation is suppressed, yielding higher energy emitted light. NBO calculations support these observations by identifying relatively strong metal-ligand electronic coupling in those compounds with the largest Stokes shift. Finally, multi-configurational calculations further support the spectral assignments and optical band splitting due to SOC. We expect the results of this work can be applied to tailor optical properties to achieve new and specialized separations for complexes whose f-d electronic transitions can be exploited in the visible and UV range. cerium(III) *tris*(guanidinate) complexes demonstrated that complexes with large ligand steric demand in  $C_3$  symmetry show tunable quantum yields, and therefore brightness. The key physical process at work here is the exclusion of exogenous solvent molecules from the coordination sphere, namely along the  $C_3$  axis, that provide quenching processes. Furthermore, our computational results included the first comprehensive computational analysis of molecular cerium(III) luminophores. We successfully reproduced the experimental absorption and emission spectra and rationalized the Stokes shifts for two series of compounds. We conclude that by applying a rigid coordination sphere to the cerium center, the geometry relaxation is suppressed, yielding higher energy emitted light. NBO calculations support these observations by identifying relatively strong metal-ligand electronic coupling in those compounds with the largest Stokes shift. Finally, multi-configurational calculations further support the spectral assignments and optical band splitting due to SOC. We expect the results of this work can be applied to tailor optical properties to achieve new and specialized separations for complexes whose f-d electronic transitions can be exploited in the visible and UV range.



### ***Functionalization of the TriNOx System for Improved Separations***

We have demonstrated that substitution of our previously reported H<sub>3</sub>TriNOx aryl backbone with the electron-donating methoxy group caused pyramidalization of the nitrogen at the hydroxylamine moieties, which induced a subtle closing of the molecular aperture in

RE(TriNO<sub>x</sub>OMe) complexes. The nature of the molecular aperture was described by a number of metrics and compared to that of the parent complexes. Analysis of the structural metrics revealed that RE(TriNO<sub>x</sub>OMe)(THF) complexes contained longer hydroxylamine N-O bonds and RE-OTHF interactions than the parent RE(TriNO<sub>x</sub>)(THF) complexes, which is indicative of more electron-rich hydroxylamine arms and weaker RE-THF interactions in the methoxy-substituted complexes. Additionally, RE(TriNO<sub>x</sub>OMe)(THF) complexes exhibited slightly higher %V<sub>bur</sub>, suggesting that the RE cation is slightly less exposed in the methoxy-substituted complexes. Thermogravimetric analyses indicated that the RE-OTHF interaction in Dy(TriNO<sub>x</sub>OMe)(THF) was much weaker than that in the parent Dy(TriNO<sub>x</sub>)(THF) complex, and evaluation of the self-association equilibrium constant of Nd(TriNO<sub>x</sub>OMe)(THF) indicated that dimerization was more favorable by one order of magnitude, consistent with more electron-rich hydroxylamine groups at the molecular aperture. These phenomena all contribute to an increased solubility of [Nd(TriNO<sub>x</sub>OMe)]<sub>2</sub>, allowing for efficient Nd/Dy separations in a greener solvent (toluene) that was previously unavailable in the parent separations system. The results expand our capabilities to perform RE separations on a thermodynamic basis using tailored ligands with a size-sensitive molecular aperture.

#### **Publications Acknowledging this Grant in 2015 (2017) – present**

(I) *Exclusively funded by this grant;*

1. Fang, H.; Cole, B. E.; Bogart, J. A.; Cheisson, T.; Manor, B. C.; Carroll, P. J.; Schelter, E. J. *Angew. Chem., Int. Ed.* **2017**, *56*, 13450–13454. DOI: 10.1002/anie.201706894
2. Cole, B. E.; Falcones, I. B.; Cheisson, T.; Manor, B. C.; Carroll, P. J.; Schelter, E. J. **2018**, submitted.

(II) *Jointly funded by this grant and other grants with leading intellectual contribution from this grant;*

3. Qiao, Y.; Sergentu, D.-C.; Yin, H.; Zabula, A. V.; Cheisson, T.; McSkimming, A.; Manor, B. C.; Carroll, P. J.; Anna, J. M.; Autschbach, J.; Schelter, E. J. *J. Am. Chem. Soc.* **2018**, in revision.

(III) *Jointly funded by this grant and other grants with relatively minor intellectual contribution from this grant;*

4. Galley, S. S.; Pattenaude, S. A.; Gaggioli, C. A.; Qiao, Y.; Sperling, J. M.; Zeller, M.; Schelter, E. J.; Albrecht-Schmitt, T. E.; Gagliardi, L.; Bart, S. C. *Nature* **2018**, submitted.

**A nanoscale view of assisted ion transport across the liquid-liquid interface**

Mark L. Schlossman<sup>1</sup> and Ilan Benjamin<sup>2</sup>

<sup>1</sup> Department of Physics, University of Illinois at Chicago, Chicago, IL 60607, USA

<sup>2</sup> Department of Chemistry and Biochemistry, University of California at Santa Cruz, Santa Cruz 95064, USA

**Presentation Abstract**

During solvent extraction, amphiphilic extractants assist the transport of metal ions across the liquid-liquid interface between an aqueous ionic solution and an organic solvent. Investigations of the role of the interface in ion transport challenge our ability to probe fast molecular processes at liquid-liquid interfaces on nanometer length scales. Recent development of a thermal switch for solvent extraction has addressed this challenge, which has led to the characterization by X-ray surface scattering of interfacial intermediate states in the extraction process. Here, we review and extend these earlier results. We find that trivalent rare earth ions, Y(III) and Er(III), combine with DHDP extractants to form inverted bilayer structures at the interface; these appear to be condensed phases of small ion-extractant complexes. The stability of this unconventional interfacial structure is verified by molecular dynamics simulations. The ion-extractant complexes at the interface are an intermediate state in the extraction process, characterizing the moment at which ions have been transported across the aqueous-organic interface, but have not yet been dispersed in the organic phase. In contrast, divalent Sr(II) forms an ion-extractant complex with DHDP that leaves it exposed to the water phase; this result implies that a second process that transports Sr(II) across the interface has yet to be observed. Calculations demonstrate that the budding of reverse micelles formed from interfacial Sr(II) ion-extractant complexes could transport Sr(II) across the interface. Our results suggest a connection between the observed interfacial structures and the extraction mechanism, which ultimately affects the extraction selectivity and kinetics.

**DE-SC0018200: The Role of Molecular Ordering at the Liquid/Liquid Interface in Solvent Extraction**

**PI:** Mark Schlossman (PI), Ilan Benjamin (co-PI)

**Student(s):** Zhu Liang

**RECENT PROGRESS**

*A nanoscale view of assisted ion transport across the liquid-liquid interface*

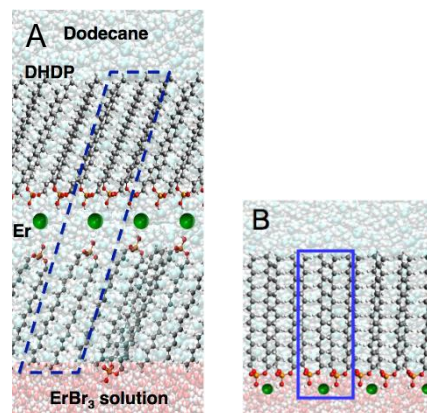
We use interface-sensitive X-ray scattering and fluorescence techniques to locate and identify interfacial species in model extraction systems. Our experimental system consists of a macroscopically flat liquid-liquid interface between a dilute, acidic aqueous solution of metal

chlorides (where the metal ion is Y(III), Er(III), or Sr(II)), and a dilute organic solution of the extractant DHDP ( $[\text{CH}_3(\text{CH}_2)_{15}\text{O}]_2\text{POOH}$ , bis(hexadecyl) phosphoric acid,  $10^{-4}$  M) in *n*-dodecane ( $\text{CH}_3(\text{CH}_2)_{10}\text{CH}_3$ ). The challenge of measuring fast ion transfer processes with slow X-ray techniques formerly led us to develop a thermal process that switches between fast and slow rates of extraction.<sup>1</sup> This allowed us to characterize intermediate states in the extraction process of a trivalent lanthanide Er(III) and a divalent main group ion Sr(II). One such state consisted of supramolecular erbium-extractant complexes condensed into an inverted bilayer structure in the form of a 2-dimensional layer of Er ions sandwiched between two layers of extractant (Fig. 1A). These Er-extractant complexes were formed at the dodecane-water interface within the time scale of minutes used to toggle the thermal switch, and possibly much faster.

Similar experiments with strontium ions revealed, instead, a conventional monolayer of extractants with bound Sr(II) ions located on the aqueous-side of the interface, with no obvious route to transfer ions into the organic phase (Fig. 1B).<sup>2</sup> Nevertheless, toggling the thermal switch led to extraction of both types of ions, though a larger fraction of erbium than strontium was extracted.

The unexpected structure of inverted bilayers at an organic solvent-water interface is confirmed by new X-ray studies of the same model solvent extraction system with Y(III) substituted for Er(III).<sup>3</sup> The inverted bilayer structure contains hydrophobic alkyl tailgroups in direct contact with water, instead of the conventional arrangement of amphiphiles in which polar headgroups are in contact with water (Fig. 1).

**Figure 1.** (A) Observation of ion-extractant complexes (as illustrated within the blue dashed box) condensed at the dodecane/water interface when an ongoing solvent extraction process is arrested. The bulk phases consist of  $5 \times 10^{-7}$  M  $\text{ErBr}_3$  in water (*pH* 2.5 adjusted with HBr) and  $10^{-4}$  M DHDP (dihexadecyl phosphate) in dodecane. The inverted bilayer structure was determined by X-ray reflectivity and fluorescence near total reflection measurements. New results for Y(III) revealed a similar inverted bilayer structure. (B) The conventional monolayer interfacial structure was not observed for Er(III) or Y(III), but was observed for Sr(II).



Our results demonstrate that Y(III) and Er(III) are more effective at coordinating with DHDP than Sr(II). For instance, the formation of inverted bilayers containing Y(III) and Er(III), as well as their extraction at temperatures above the adsorption transition  $T_o$ , were observed with *pH* 2.5 water for which 94% of the phosphoric acid headgroups would have been protonated and uncharged in the absence of metal ions. However, Sr(II) binding to the charge neutral DHDP monolayer under similar low *pH* conditions was not observed. Instead, Sr(II) binding was observed only at higher *pH*, with one Sr(II) for every two DHDP measured at *pH* 5.3 and higher *pH* values. Even under these conditions of Sr saturation of the interface, combined X-ray reflectivity and XFNTTR results show that approximately one third of the interfacial Sr(II) ions are not closely bound to the DHDP headgroups, but exist only in a diffuse electrical double layer near the interface.

Y(III) and Er(III) are also more efficiently extracted from the aqueous phase than Sr(II). Analysis of the metal content in the aqueous phase before and after extraction by inductively

coupled plasma atomic emission spectroscopy (ICP-AES) and ICP mass spectroscopy showed that 87(3)% of the Y(III) was extracted at 50 °C, more than 80% of the Er(III) was extracted at 55 °C, but only 45% of Sr(II) was extracted at 50 °C (pH 5.3).

The interfacial state of Y(III) and Er(III) sandwiched between layers of DHDP extractants suggests the prompt transfer of these cations from the aqueous side of the liquid-liquid interface to a coordinated ion-extractant environment on the organic side. These ion-extractant complexes represent an intermediate state in which ions have been transported across the aqueous-organic interface, but have not yet been dispersed in the organic phase. In contrast to this, the observation of a conventional monolayer of DHDP extractants with Sr(II) bound to DHDP headgroups, but remaining in contact with the water phase, suggests a slower kinetics of transfer of Sr(II) from water to dodecane, whose mechanism involves at least one additional step to transport the ion across the aqueous-organic interface.

We considered the possibility that reverse micelles form in our Sr(II)-DHDP extraction system. If so, then budding of the micelle at the interface could be the additional, unobserved step in the ion transfer across the aqueous-organic interface. A plausible mechanism for this process consists of 3 stages (see Figure 2): (1) DHDP adsorption onto the interface and binding to Sr(II) ions, (2) formation of interfacial domains of Sr(DHDP)<sub>2</sub> complexes, and (3) domain budding of reverse micelles into the organic phase. Within the context of a simple analytical model for domain budding, it can be shown that a minimum size  $L^0$  is required for the domain to form a complete bud. A domain can increase its size to this value by the aggregation of interfacial Sr(DHDP)<sub>2</sub> complexes. The larger domain size that results from this aggregation has a longer domain edge and, consequently, larger edge energy. This larger edge energy can be recovered: as the domain bends to form a more complete sphere, illustrated by progressing from Fig. 2B to Fig. 2C, the reduction in edge length reduces the edge energy. This reduction balances the cost in bending energy required to form a spherical bud.

Lipowsky showed that complete budding is energetically favorable for domain sizes  $L \geq L^0$ , where  $L^0 = 8k / \gamma \left[ 1 + (4k |C_{sp}| / \gamma)^{2/3} \right]^{3/2}$ .<sup>4</sup> Literature values for the bending rigidity  $k$ , the line tension  $\gamma$ , and the spontaneous curvature  $C_{sp}$  for compounds similar to our extractant DHDP yield a range of values for the ratio  $k / \gamma$ , given by  $4 \text{ nm} \leq k / \gamma \leq 20 \text{ nm}$ , and for  $C_{sp}$ , given by  $0.1 \text{ nm}^{-1} \leq C_{sp} \leq 0.3 \text{ nm}^{-1}$ . These values produce a range of limiting lengths,  $4 \text{ nm} \leq L^0 \leq 14 \text{ nm}$ , whose values describe buds that contain a similar number of extractants as the aggregation number of reverse micelles in organic phases that contain extracted metal ions.

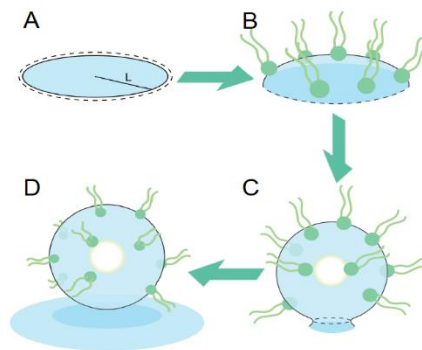


**Figure 2.** Domain budding mechanism. (A) A flat region of bare interface (dodecane above, water below) becomes (B) spontaneously curved due to the adsorption of extractants and their interactions with ions (not shown) at the interface. (C) The reduction in length of the domain edge (dashed line) reduces the line tension energy, which balances the bending energy required to form a spherical reverse micelle. (D) Separation of the micelle from the interface extracts ions in the interior of the reverse micelle into the bulk organic phase.

These calculations suggest that Sr-DHDP reverse micelles can be formed at the interface by spontaneous budding, though additional experiments are required to confirm this result.

According to this model, interfacial ion-extractant complexes that produce larger values of spontaneous curvature  $C_{sp}$  will require less bending energy to make a complete bud. Larger values of  $C_{sp}$  may result from the interaction of bulky extractants with ions at the interface – these include extractants that are commonly used in solvent extraction processes, like DEHP that has branched alkyl tailgroups, or malonamides and diglycolamides that have bulky headgroups. Bulky extractants form smaller complete buds since the spontaneous curvature is closer to the value of curvature  $C = 2/L$  required to make a complete spherical bud. Higher oxidation state ions that coordinate a larger number of extractants are expected to produce an even larger spontaneous curvature. This physical picture suggests the formation of small supramolecular complexes relevant to the extraction of Y(III) and Er(III). Further research is required to establish a quantitative relationship between the shape and chemical properties of the extractant molecule, the interfacial elastic properties –  $K$ ,  $l$ , and  $C_{sp}$  – and the extraction kinetics.

- (1) Bu, W.; ... Schlossman, M. L. Observation of a Rare Earth Ion-Extractant Complex Arrested at the Oil-Water Interface During Solvent Extraction. *J. Phys. Chem. B* **2014**, *118*, 10662-10674.
- (2) Bu, W.; ... Schlossman, M. L. X-Ray Studies of Interfacial Strontium-Extractant Complexes in a Model Solvent Extraction System. *J. Phys. Chem. B* **2014**, *118*, 12486-12500.
- (3) Liang, Z.; ... Benjamin, I.; Schlossman, M. L. A Nanoscale View of Assisted Ion Transport across the Liquid-Liquid Interface. *Proceedings of the National Academy of Sciences (USA)* **2018**, submitted.
- (4) Lipowsky, R. Budding of Membranes Induced by Intramembrane Domains. *J. de Physique II* **1992**, *2*, 1825-1840.

#### **Publications Acknowledging this Grant in 2015 – present**

- (II) Liang, Z.; Bu, W.; Schweighofer, K. J.; Jr., D. J. W.; Harvey, J. S.; Hanlon, G. R.; Amoanu, D.; Erol, C.; Benjamin, I.; Schlossman, M. L. A Nanoscale View of Assisted Ion Transport across the Liquid-Liquid Interface. *Proceedings of the National Academy of Sciences (USA)* **2018**, submitted.

- (I) *Exclusively funded by this grant;*
- (II) *Jointly funded by this grant and other grants with leading intellectual contribution from this grant;*
- (III) *Jointly funded by this grant and other grants with relatively minor intellectual contribution from this grant;*

## Ion Pair Receptors and Extractants

Jonathan L. Sessler, Qing He, and Xiaodong Chi  
Department of Chemistry, The University of Texas at Austin  
105 E. 24th Street - A5300, Austin, TX 78712-1224

### Presentation Abstract

A major goal of this research program has been to design and prepare so-called ion pair receptors, where both anion and cation are co-bound within a given molecular framework. The creation of ion pair receptors with unique binding characteristics permits to acquire higher control and target specific anion or cation binding in the presence of their corresponding counterion. By enforcing electroneutrality, the use of ion pair receptors allows the generation of selective extractants capable of recognizing highly solvated ions and remove them effectively from aqueous media. Over the years, we have created several generations of ditopic receptors based on the calixpyrrole framework and showed them capable of capturing cesium and potassium halide anion salts. This presentation will focus on newer systems that are capable of recognizing lithium cation salts, extracting CsOH from aqueous media, complexing more than one anion in a single framework, and controlling aggregation phenomena beyond the first coordination sphere.

**Grant or FWP Number: Functional Ion Pair Receptors Targeting Cesium, Lithium, Sulfate, and Uranyl (DE-FG02-01ER15186)**

**PI:** Lead PI(s) Name(s) (*include only if different from above*)

**Postdoc(s):** Qing He, Xiaodong Chi

**Student(s):** Juhoon Lee, James Brewster

**Affiliations(s):** (*include only if different from above*)

### RECENT PROGRESS

#### ***Calixpyrrole-based Ion Pair Receptors: LiX, CsOH, and Cs<sub>2</sub>CO<sub>3</sub> Extraction***

We have successfully targeted Li<sup>+</sup> salts by employing a calixpyrrole-hemispherand hybrid receptor. This system was found to be able to bind lithium chloride salt in the form of a water-bridged complex. It also allowed the extraction of certain lithium salts under aqueous-organic liquid-liquid and solid-liquid extraction conditions. Remarkable ion pair discrimination over other alkali salts (e.g., those of K<sup>+</sup> and Na<sup>+</sup>) was seen.

This same strapped hemispherand calixpyrrole-based receptor was also found to act as an extractant for the highly solvated basic anions, OH<sup>-</sup> and CO<sub>3</sub><sup>2-</sup>, in the form of their Cs<sup>+</sup> salts. These ions are found in high concentrations in radioactive tank waste (i.e., [OH<sup>-</sup>] = 0.02–8.1 M and [CO<sub>3</sub><sup>2-</sup>] = 0.005–1.4 M), which leads to highly basic radioactive aqueous solutions. Although

reductions in pH are generally made via the addition of a Brønsted acid, this is highly impractical when the central tenant is to reduce the amount of contaminated material that will be further treated. Our strapped hemispherand calixpyrrole receptor exhibited higher affinity for both cesium hydroxide (CsOH) and cesium carbonate ( $\text{Cs}_2\text{CO}_3$ ) over other cesium salts, such as CsF, CsCl, and CsBr, and other alkali hydroxide salts, such as LiOH, NaOH, and KOH. Liquid-liquid extraction efficacy calculated on the basis of mass transfer from an aqueous phase into chloroform using the calixpyrrole-hemispherand receptor (2 mM) was estimated to be  $\geq 50\%$  (using 4-6 M of CsOH and  $\text{C}_2\text{CO}_3$ ). U-tube transport experiments revealed a sharp increase in the pH and cesium concentrations in the receiving phase when the calixpyrrole-hemispherand receptor was used as carrier. While it is earlier days still, these extraction experiments may point the way to a new approach to adjusting (lowering) the pH via the removal of anions, rather than the addition of protons.

### ***Dicationic Calixpyrrole $\text{CO}_2/\text{HCO}_3^-$ Sensor***

The central role that carbon dioxide ( $\text{CO}_2$ ) and its hydrated forms, bicarbonate ( $\text{HCO}_3^-$ ), and carbonic acid ( $\text{H}_2\text{CO}_3$ ), play in nature resides in the participation of these molecules as building blocks for carbohydrate synthesis and as the end product of aerobic respiration. These are also involved in the equilibrium of  $\text{CO}_2/\text{HCO}_3^-$ , which is fundamental for optimal aquatic fauna. However,  $\text{CO}_2$  is also notorious as a greenhouse gas. Thus, there is an incentive to create easy-to-use sensors to monitor levels of  $\text{CO}_2$  and its hydrated forms. To target this problem, a dicationic *meso*-bis(benzilimidazolium) calixpyrrole system was synthesized. This macrocycle was found to capture  $\text{CO}_2$  by modulating the  $\text{HCO}_3^-/\text{CO}_2$  balance; it did so by acting as an effective  $\text{HCO}_3^-$  receptor. Under solution-phase indicator displacement assay conditions, this dicationic receptor functions as a selective sensor of bicarbonate anion at concentrations as low as 4 nM. In methanol solutions, the dicationic calixpyrrole receptor also promotes the conversion of hydrated  $\text{CO}_2$  into methyl carbonate ( $\text{CH}_3\text{OCO}_2^-$ ) under near-neutral conditions by stabilizing this normal unstable mono-ester species in bound form. To the best of our knowledge, this conversion is not possible to carry out under ambient, near-neutral conditions and the ability of our sensor to promote the formation of otherwise very unstable methyl carbonate species is unprecedented. Furthermore, it produces an organic product that may prove useful as a chemical feedstock, although that remains to be established. This chemistry appears to be generalizable in that related receptor systems appear to work.

### **Molecular Recognition Under Interfacial Conditions: Calix[4]pyrrole-Based Cross-linkable Micelles for Ion Pair Extraction**

An anthracene-functionalized, long-tailed calix[4]pyrrole, containing both an anion-recognition site and cation-recognition functionality, acts as an ion pair receptor for  $\text{FeF}_2$ . Upon complexation, self-assembly into multimicelles takes place in aqueous media. This aggregation process is ascribed to a change in polarity from nonpolar to amphiphilic induced upon concurrent anion and cation complexation and permits molecular recognition-based control over chemical morphology under interfacial conditions. Photoirradiation of the micelles serves to cross-link the anthracene units thus stabilizing the aggregates. The combination of ion pair recognition, micelle formation, and cross-linking can be used to extract  $\text{FeF}_2$  ion pairs from bulk aqueous solutions. The present work helps illustrate how molecular recognition and self-assembly may be used to control the chemistry of extractants at interfaces beyond the first coordination sphere.

## Publications Acknowledging this Grant in 2015 – present

### (I) Exclusively funded by this grant:

1. Sessler, J. L.; Vargas-Zúñiga, G. I.; Bähring, S. “Functionalized Calixpyrroles: Building Blocks for Self-Assembly,” in Neri, P.; Wang, M.-X.; Sessler, J. L., Eds. *Calixarenes and Beyond*, Springer, 2016.
2. Brewster, J. T. II; Qing He, Q.; Anguera, G.; Moore, M. D.; Ke, X.-S.; Lynch, V. M.; Sessler, J. L. “Synthesis and characterization of a dipyrriamethyrin-uranyl complex. *ChemComm*, **2017**, 53, 4981-4984. DOI: 10.1039/C7CC01674C
3. Deliomeroglu, M. K.; Lynch, V. M.; Sessler, J. L. “Schiff-base appended polymers for phosphate removal,” *Supramolecular Chemistry*, on line. DOI: [org/10.1080/10610278.2017.1372581](https://doi.org/10.1080/10610278.2017.1372581).

### (II) Jointly funded by this grant and other grants with leading intellectual contribution from this grant:

1. Kim, D. S.; Sessler, J. L. “Calix[4]pyrroles: Versatile molecular containers with ion transport, recognition, and molecular switching functions,” *Chem. Soc. Rev.* **2015**, 44, 532-546. DOI: 10.1039/C4CS00157E
2. Kim, S. K.; Lynch, V. M.; Hay, B. P.; Kim, J. S.; Sessler, J. L. “Ion Pair-Induced Conformational Motion in Calix[4]arene-Strapped Calix[4]pyrroles,” *Chem. Sci.* **2015**, 6, 1404-1413. DOI: 10.1039/C4SC03272A
3. Katayev, E. A.; Pantos P.; Karnas, E.; Kolesnikov, G. V.; Tananev, I. G.; Lynch, V. M.; Sessler, J. L. “Perrhenate and pertechnetate anion recognition properties of cyclo[8]pyrrole,” *Supramolecular Chem.* **2015**, 27, 346-356. DOI: 10.1080/10610278.2014.988628
4. Lee, J.; Waggoner, N. W.; Polanco, L.; You, G. R.; Lynch, V. M.; Kim, S. K.; Humphrey, S. M.; Sessler, J. L. “Ship in a breakable bottle: fluoride-induced release of an organic molecule from a Pr(III)-linked molecular cage,” *ChemComm.* **2016**, 52, 8514 – 8517 (cover). DOI: 10.1039/c6cc03471c
5. Sessler, J. L.; Vargas-Zúñiga, G. I.; Bähring, S. “Functionalized Calixpyrroles: Building Blocks for Self-Assembly,” in Neri, P.; Wang, M.-X.; Sessler, J. L., Eds. *Calixarenes and Beyond*, Springer, 2016.
6. He, Q.; Zhang, Z.; Brewster, J. T.; Lynch, V. M.; Kim, S. K.; Sessler, J. L. “Hemispherand-strapped Calix[4]pyrrole: An Ion-pair Receptor for the Recognition and Extraction of Lithium Nitrite,” *J. Am. Chem. Soc.* **2016**, 138, 9779–9782. DOI: 10.1021/jacs.6b05713. Highlighted in “Extracting inorganic ions organically,” Jyllian Kemsley, C & E News, 2016, 94(24), 18-19.
7. Yeon, Y.; Leem, S. J.; Wagen, C.; Lynch, V. M.; Kim, S. K.; Sessler, J. L. “A 3-(Dicyanomethylidene)indan-1-one Functionalized Calix[4]arene-Calix[4]pyrrole Hybrid: An Ion-Pair Sensor for Cesium Salts,” *Org. Lett.* **2016**, 18, 4396–4399. DOI: 10.1021/acs.orglett.6b02155
8. Kim, S. K.; Lee, H. G.; Vargas-Zúñiga, G. I.; Ju Hyun Oh, J. H.; Lynch, V. M.; Lee, M. H.; Sessler, J. L. “A fluorogenic calix[4]pyrrole with a small rigid strap showing different fluorescent responses to anions,” *Supramolec. Chem.* **2017**, 29, 651-657. DOI: [oi.org/10.1080/10610278.2017.1324624](https://doi.org/10.1080/10610278.2017.1324624)
9. Vargas-Zuniga, G.; Sessler, J. L. “Pyrrole N-H Anion Complexes,” *Coord. Chem. Rev.* **2017**, 345, 281–296. DOI: [10.1016/j.ccr.2017.04.004](https://doi.org/10.1016/j.ccr.2017.04.004)

10. Chi, X.; Peters, G. M.; Hammel, F.; Brockman, C.; Sessler, J. L. "Molecular Recognition Under Interfacial Conditions: Calix[4]pyrrole-based Cross-linkable Micelles for Ion Pair Extraction," *J. Am. Chem. Soc.* **2017**, *139*, 9124–9127. DOI: 10.1021/jacs.7b04529
11. Anguera, G.; Brewster, J. T. II; Moore, M.D.; Lee, J.; Vargas-Zúñiga, G. I.; Zafar, H.; Lynch, V. M.; Sessler, J. L.; Naphthylbipyrrole-Containing Amethyrin Analogue: A New Ligand for the Uranyl (UO<sub>2</sub><sup>2+</sup>) Cation," *Inorg. Chem.*, **2017**, *56*, 9409-9412. DOI: 10.1021/acs.inorgchem.7b01668
12. He, Q.; Peter, G. M.; Lynch, V. M.; Sessler, J. L. "Recognition and Extraction of Cesium Hydroxide and Carbonate by using a Neutral Multitopic Ion-Pair Receptor," *Angew. Chem. Int. Ed.* **2017**, *56*, 13396–13400. DOI: 10.1002/anie.201705788
13. Mulugeta, E.; He, Q.; Saren, D.; Hong, S. J.; Oh, J. H.; Lynch, V. M.; Sessler, J. L.; Kim, S. K.; Lee, C. H. "Recognition, Sensing, and Trapping of the Bicarbonate Anion using a Dicationic *meso*-bis(Benzimidazolium) Calix[4]pyrrole," *Chem*, **2017**, *3*, 1008–1020. DOI: <http://dx.doi.org/10.1016/j.chempr.2017.10.007>

(III) *Jointly funded by this grant and other grants with relatively minor intellectual contribution from this grant:*

1. Ho, I.-T.; Sessler, J. L.; Gambhir, S. S.; Jokerst, J. V. "Parts per billion detection of uranium with a porphyrinoid-containing nanoparticle and *in vivo* photoacoustic imaging," *Analyst*, **2015**, *140*, 3731-3737. DOI: 10.1039/c5an00207a
2. Park, S.-H.; Choi, Y. P.; Park, J.; Share, A.; Francesconi, O.; Nativi, C.; Namkung, W.; Sessler, J. L.; Roelens, Shin, I. "Synthetic aminopyrrolic receptors have apoptosis inducing activity," *Chem. Sci.* **2015**, *6*, 7284-7292. DOI: 10.1039/c5sc03200h
3. Mulugeta, E.; Dutta, R.; He, Q.; Lynch, V. M.; Sessler, J. L.; Lee, C. H. "Anion dependent binding mode switching in a benzimidazole-picket calix[4]pyrrole," *European J. Org. Chem.* **2017**, 4891–4895. DOI: 10.1002/ejoc.201700733

## Chemical Analysis of Nanodomains

Emily A. Smith, Jacob W. Petrich, Javier Vela  
Ames Laboratory, Division of Chemical and Biological Sciences

### Presentation Abstract

Many important phenomena occur on a spatial scale that is smaller than can be probed noninvasively by conventional optical techniques. Understanding these nanoscale phenomena is fundamental to the DOE mission of developing new and revolutionary technologies for clean energy. The Chemical Analysis of Nanodomain FWP develops and characterizes distinct and widely applicable strategies for preparing nanomaterials and films of nanomaterials having improved performance in energy capture and conversion devices. This is accomplished using state-of-the-art instrumentation, mostly developed by the Ames Laboratory team, without the use of vacuum or intrusive probes that can alter the properties being measured as well as skills in materials synthesis. The long-term goal is to develop an understanding of chemical phenomena to significantly improve the development of energy capture and conversion devices that will one day outperform existing commercial technologies in terms of efficiency, stability, and cost. The team works with a tight synergy between synthesis, structural characterization, and advanced optical characterization.

**Grant or FWP Number:** AL-01-380-009, Chemical Analysis of Nanodomains

**Postdoc(s):** Priyanka Bolel, Ujjal Bhattacharjee

**Student(s):** Himashi Andaraarachchi, Jonathan Bobbitt, Brett Boote, Long Men, Deyny Mendivelso, Charles Nyamekye, Kalyan Santra

### RECENT PROGRESS

*(1) Advances in instrumentation for the analysis of nanodomains.* The team has developed four new instruments for the *in situ* characterization of nanodomains and nanomaterials. A dual optical spectroscopy/x-ray diffraction instrument was set up for simultaneously illuminating samples while collecting their diffraction pattern to observe light-induced phase transitions. The second instrument is a visible-wavelength scanning angle Raman spectrometer for the analysis of thin films with 10-nm axial spatial resolution. Two instruments were developed that allow sensitive measurements of thin films using the phenomena of surface plasmons; one is an alternative to surface plasmon resonance (*i.e.*, SPR) with added monolayer chemical sensitivity and the other allows a multifrequency analysis of the reflected light intensity as a function of incident angle to simultaneously extract multiple sample parameters (e.g., thickness, index of refraction, absorption). Each experimental setup is briefly described below.

We have previously reported a variation of Raman spectroscopy termed scanning angle Raman spectroscopy. Scanning angle Raman instruments have a controlled and variable incident angle upon a prism/sample interface with an angular resolution of a tenth of a degree or less. The technique can be used to measure multilayer films to extract chemical identity and thickness of each layer with approximately 10-nm axial spatial resolution. Excitation wavelength is an important experimental parameter since the Raman intensity scales with the excitation frequency to the fourth power. Near-infrared excitation, however, is often used to reduce spectral background. In addition to these considerations, the excitation wavelength affects the predicted angular dependence of the scanning angle Raman signal. Visible excitation enables scanning a narrow angle range, and combined with the increased signal due to the short excitation wavelength and resonant enhancement, decreased experimental times are possible. We developed a 532-nm scanning angle Raman instrument (Figure 1) and demonstrated these benefits with measurements of thin polymer films of polystyrene or a diblock copolymer of polystyrene and poly(3-hexylthiophene-2,5-diyl).

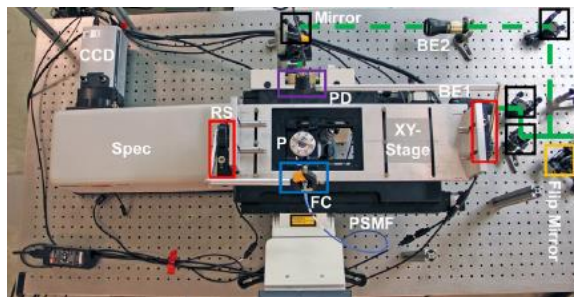
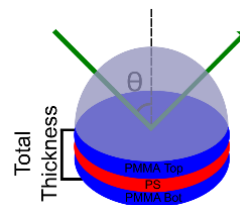


**Figure 1.** Schematic for 532-nm scanning angle Raman instrument built around a Leica microscope: beam expanders (BE1, BE2), polarization-maintaining single-mode fiber optic (PSMF), fiber collimator (FC), prism (P), photodiode (PD), rotational stages (red boxes), a spectrometer (Spec), and charged-coupled device (CCD).

The scanning angle Raman instrument was subsequently used to demonstrate that the interface between polymer layers in multilayer films of a few hundred nanometer total thickness could be quantified; each polymer layer thicknesses can be measured even when two of the layers are chemically identical (*i.e.*, a trilayer with two of the layers formed from the same chemical species as shown in Figure 2). Similar measurements were also demonstrated for block co-polymer films containing multiple chemical species. Other optical spectroscopy techniques cannot perform these analyses on intact thin polymer films.

**Figure 2.** Schematic of the sample setup for measuring interfaces in polymer multilayer films using scanning angle Raman spectroscopy.



Surface plasmon resonance (SPR) has been used extensively for a range of applications, including detecting and monitoring the kinetics, affinity, and selectivity of interactions between binding partners. A drawback to surface plasmon resonance is the encoded signal provides very little (if any) information about what is adsorbed at the surface. We have developed the technique directional surface-plasmon-coupled Raman scattering (directional Raman scattering) with the combined benefits of surface plasmon resonance and Raman spectroscopy, and the ability to measure adsorption and monolayer-sensitive chemical information. Directional Raman scattering is performed by optically coupling a thin gold film to a Weierstrass prism and scanning the angle of the incident laser under total internal reflection. The multi-parameter signal is collected on the prism side of the interface (Figure 3). An instrument for

performing directional Raman scattering has been developed and a quantitative study of the instrumental parameters has been performed. We demonstrated that the obtained signal can be easily modeled and is reproducible using self-assembled monolayers of alkanethiols and thin films. The technique has the possibility to outperform SPR in terms of sensitivity as well as provides chemical information for any species that produces a Raman signal.

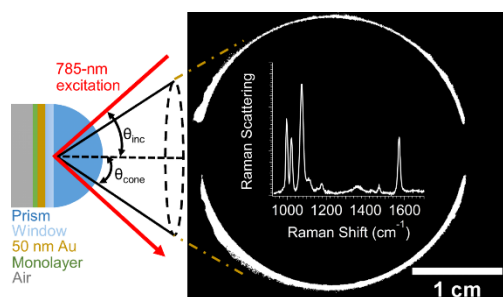


**Figure 3.** The signals in a directional Raman scattering experiment include a surface-plasmon-polariton cone (directional Rayleigh scattering) and directional Raman scattering (also produced within the cone) as a function of incident angle. The properties of the cone shift when adsorption takes place on the gold film. The Raman spectrum shows an excellent signal-to-noise ratio for a thiophenol monolayer.

We have developed an instrument for performing Fourier transform-plasmon waveguide resonance measurements to obtain the apparent anisotropic indices of refraction and thicknesses of a dielectric waveguide layer. High precision measurements have been demonstrated. We propose that Fourier transform-plasmon waveguide resonance can be used to quantify and detect anisotropic analytes at low concentrations when adsorbed to a waveguide interface and will be useful as a label free sensor.

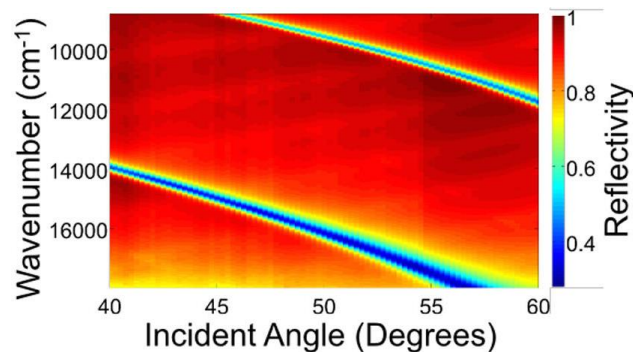


**Figure 4.** Multifrequency and multi-angle reflectivity plot of an  $\sim 700$ -nm polystyrene waveguide. We have shown that the reflectivity pattern encodes information about the sample's anisotropic index of refraction and thickness and can be well modelled with simple calculations.

Finally, the team observed that some of the novel photovoltaic nanomaterials that we have studied might be susceptible to structural changes upon illumination; and it became necessary for the team to develop methods of monitoring these changes. Consequently, we coupled easily accessible laser excitation with X-ray diffraction and studied the light-induced phase transitions of azobenzene as a reference. In the course of this work, fundamental aspects of light-induced, large-scale structural changes in solids were elucidated. The ability to produce large-scale, reversible structural changes in a variety of materials by photoexcitation of a wide variety of azobenzene derivatives has been recognized for almost two decades. Because photoexcitation of *trans*-azobenzene produces the *cis* isomer in solution, it has generally been inferred that the macroscopic structural changes occurring in materials are also initiated by a similar large-amplitude, *trans*-to-*cis* isomerization. The team's efforts in this arena have provided the first demonstration that a *trans*-to-*cis* photoisomerization occurs in polycrystalline azobenzene, and is consistent with the previously hypothesized nature of the trigger in the photoactuated mechanisms of the materials in question. It was also demonstrated that under

low irradiance, *trans*-to-*cis* isomerization occurs in the solid (not via a pre-melted phase); and the presence of the *cis*-isomer thus lowers the melting point of the sample, providing a liquid phase.

**(2) *Data analysis methods for subdiffraction luminescence lifetime imaging: application to sparse data sets.*** It is often convenient to know the minimum amount of data needed in order to obtain a result of desired accuracy and precision. It is a necessity in the case of subdiffraction-limited microscopies, such as stimulated emission depletion (STED) microscopy, owing to the limited sample volumes and the extreme sensitivity of the samples to photobleaching and photodamage. We have presented a detailed comparison of probability-based techniques (the maximum likelihood method and methods based on the binomial and the Poisson distributions) with residual minimization-based techniques for retrieving the fluorescence decay parameters for various two-fluorophore mixtures, as a function of the total number of photon counts, in time-correlated, single-photon counting experiments. The probability-based techniques proved to be the most robust (insensitive to initial values) in retrieving the target parameters and, in fact, performed equivalently to 2-3 significant figures. This is to be expected, as we demonstrate that the three methods are fundamentally related. Furthermore, methods based on the Poisson and binomial distributions have the desirable feature of providing a bin-by-bin analysis of a single fluorescence decay trace, which thus permits statistics to be acquired using only the one trace for not only the mean and median values of the fluorescence decay parameters but also for the associated standard deviations. These probability-based methods lend themselves well to the analysis of the sparse data sets that are encountered in subdiffraction-limited microscopies.

**(3) *Characterization of thin polymer films used in photovoltaic devices.*** Organic photovoltaic devices fabricated from polymer donors and fullerene-derivative acceptors are a promising portable and renewable source of electricity. Photostability measurements are important to understand how the light may affect the measured properties when using optical characterization techniques, and also to understand how the devices will perform when illuminated in real-world applications. Using resonance Raman spectroscopy and controlled laser irradiances, we showed upper limits for irradiances that do not affect the bulk heterojunction structure (i.e., nanostructure) of organic photovoltaic films containing a polymer donor and a fullerene-derivative acceptor. We also showed that the photostability was affected by the conditions used to prepare the photovoltaic films (e.g., thickness and solvent evaporation method), which has implications for how to manufacture the devices to achieve the best performance.

P3HT (poly (3-hexylthiophene)) has been widely used as a donor in the active layer in organic photovoltaic devices. Although moderately high-power conversion efficiencies have been achieved with P3HT-based devices, structural details, such as the orientation of polymer units and the extent of H- and J-aggregation are not yet fully understood; and different measures have been taken to control the ordering in the material. One such measure, which the team has exploited, is to apply an electric field from a Van de Graaff generator. The team used fluorescence (to measure *anisotropy* instead of *polarization*, which is more commonly measured) and Raman spectroscopy to characterize the order of P3HT molecules in thin films resulting from the field. We determined preferential orientations of the units in a thin film, consistent with observed hole mobility in thin-film-transistors, and observed that the apparent H-coupling strength changes when the films are exposed to oriented electrical fields during drying.

**(4) Unique optical properties of nanocrystals with applications in energy capture and conversion devices.** The team has studied the optical properties of two nanomaterials that have shown promise for energy-relevant applications and have also written a perspective and a review article on the topic. Organolead halide perovskites of general composition  $\text{CH}_3\text{NH}_3\text{PbX}_3$  ( $\text{X} = \text{Cl}^-, \text{Br}^-, \text{I}^-$ ) are attractive semiconductor materials owing to their low cost and outstanding photovoltaic performance. Germanium is particularly attractive for the development of near-infrared active quantum dot chromophores and for applications in energy conversion (photovoltaics, photocatalysis), telecommunications, high precision tracking, and bioimaging.

We demonstrated the controllable solution-phase synthesis of different low-dimensional lead halide perovskites. Our systematic study using a variety of solvents and capping agents was the first to show that it is possible to produce  $\text{CH}_3\text{NH}_3\text{PbI}_3$  and  $\text{CH}_3\text{NH}_3\text{PbBr}_3$  nanocrystals with different shapes (dot, rod, and plate or sheet morphologies). We also studied the optical properties of these differently shaped nanocrystals, and showed using single particle luminescence microscopy, that wire-, rod-, and dot-like  $\text{CH}_3\text{NH}_3\text{PbI}_3$  nanocrystals show coherent, shape-correlated photoluminescence across whole particles, with little photobleaching (or photobrightening) observed and very few off periods. Follow-up work showed that mixed halide compositions can be used to produce organolead mixed-halide perovskites with luminescence that is tunable across the visible to near-infrared region with very little photoblinking.

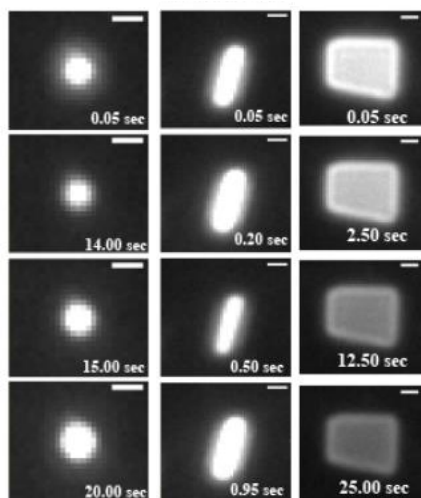


**Figure 5.** Single particle luminescence for dot (left) rod (middle) and plate-like (right)  $\text{CH}_3\text{NH}_3\text{PbI}_3$  nanocrystals over time (indicated in images). The images represented selected times over a 25 second measurement. The coherent nature of the luminescence is evident by the similar intensity across the entire nanoparticle over time. The scale bar is 1 micron in all images. The excitation wavelength is 540 nm, and the emission wavelength is 700 nm.

We demonstrated the solid-phase synthesis of organolead mixed-halide perovskites and used  $^{207}\text{Pb}$  solid state nuclear magnetic resonance to show that there are no semicrystalline phases in the nanocrystals, although dopants (nonstoichiometric impurities) were measured. This is in contrast to solution-phase synthesis methods where solid state nuclear magnetic resonance measured both semicrystalline phases and dopants in as-prepared and thermally annealed nanocrystals. The nonstoichiometric impurities measured in solid-phase and solution-phase nanocrystals are consistent with spinodal decomposition, which produces domains containing compositions that differ from the stoichiometric phase. Of note, this study revealed that x-ray diffraction does not explain the true microstructure or the amount of alloying that occurs between these mixed halide perovskites.

Germanium nanocrystals are less studied compared to perovskites. Germanium has an inherent indirect band gap, which decreases its absorption cross section and quantum yields and may seem to be a limitation for their use in many energy applications. We synthesized and characterized germanium nanocrystals with a direct band gap by exploiting tin doping of the germanium.

$\text{Ge}_{1-x}\text{Sn}_x$  alloy nanocrystals and  $\text{Ge}_{1-x}\text{Sn}_x$  core/shell nanocrystals were prepared via solution-phase synthesis. They were subsequently structurally and optically characterized. While the  $\text{Ge}_{1-x}\text{Sn}_x$  core nanocrystals did not exhibit enhanced luminescence compared to Ge nanocrystals, the  $\text{Ge}_{1-x}\text{Sn}_x$  core/shell nanocrystals exhibited up to 15-fold increased luminescence compared to the corresponding undoped germanium core/shell nanoparticles containing the same shell composition. Experimental evidence indicates that improved epitaxy between the lattice-expanded Sn-doped Ge cores and the structurally similar CdS shell, along with a reduced level of surface oxidation lead to the increased luminescence. The combination of scalability and improved PL intensities makes these  $\text{Ge}_{1-x}\text{Sn}_x$  core/shell nanocrystals promising alternatives to other near-infrared active materials for use as functional materials in solar cells and LEDs.

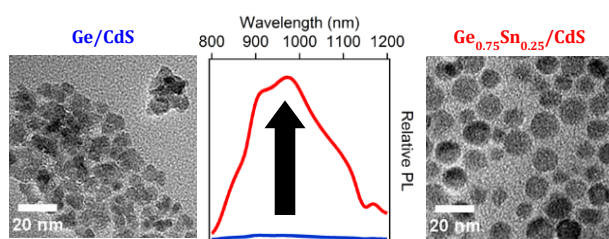


Figure 6. Ge/CdS nanocrystals have a relatively low luminescence intensity. Tin doping the core to produce  $\text{Ge}_{1-x}\text{Sn}_x$  core/shell nanocrystals results in an increase in luminescence as a result of improved epitaxy and surface passivation.

In addition to the team's studies on perovskite and germanium nanomaterials, we have been involved in studies of many other nanomaterials in collaboration with other FWPs at Ames Laboratory as well as scientists at Iowa State University. These studies are highlighted in the publication list.

## Publications Acknowledging this Grant in 2015 – present

### *Exclusively funded by this grant*

1. Nyamekye, C. K. A.; Weibel, S. C.; Bobbitt, J. M.; Smith, E. A., Combined measurement of directional Raman scattering and surface-plasmon-polariton cone from adsorbates on smooth planar gold surfaces. *Analyst* **2018**, *143*, 400-408.
2. Bobbitt, J. M.; Smith, E. A., Extracting interface locations in multilayer polymer waveguide films using scanning angle Raman spectroscopy. *J. Raman Spectrosc.* **2017**, *1-9*, DOI: 10.1002/jrs.5275.
3. Bhattacharjee, U.; Freppon, D.; Men, L.; Vela, J.; Smith, E. A.; Petrich, J. W., The photoinduced trans-to-cis phase transition of polycrystalline azobenzene at low irradiances occurs in the solid state. *Chem. Phys. Chem.* **2017**, *18*, 2526-2532.
4. Rosales, B. A.; Hanrahan, M. P.; Boote, B. W.; Rossini, A. J.; Smith, E. A.; Vela, J., Lead halide perovskites: Challenges and opportunities in advanced synthesis and spectroscopy. *ACS Energy Lett.* **2017**, *2*, 906-914.
5. Freppon, D. J.; Men, L.; Burkhow, S. J.; Petrich, J. W.; Vela, J.; Smith, E. A., Photophysical properties of wavelength-tunable methylammonium lead halide perovskite nanocrystals. *J. Mater. Chem. C* **2017**, *5*, 118-126.
6. Boote, B. W.; Men, L.; Andaraarachchi, H. P.; Bhattacharjee, U.; Petrich, J. W.; Vela, J.; Smith, E. A., Germanium-tin/cadmium sulfide core/shell nanocrystals with enhanced near-infrared photoluminescence. *Chem. Mater.* **2017**, *29*, 6012-6021.

7. Bhattacharjee, U.; Men, L.; Rosales, B. A.; Alvarado, S. R.; Vela, J.; Petrich, J. W., Using ATTO dyes to probe the photocatalytic activity of Au-CdS nanoparticles. *J. Phys. Chem. C* **2017**, *121*, 676-683.
8. Bobbitt, J. M.; Mendivelso-Perez, D.; Smith, E. A., Scanning angle Raman spectroscopy: A nondestructive method for simultaneously determining mixed polymer fractional composition and film thickness. *Polymer* **2016**, *107*, 82-88.
9. Rosales, B. A.; Men, L.; Cady, S. D.; Hanrahan, M. P.; Rossini, A. J.; Vela, J., Persistent dopants and phase segregation in organolead mixed-halide perovskites. *Chem. Mater.* **2016**, *28*, 6848-6859.
10. Damin, C. A.; Nguyen, V. H. T.; Niyibizi, A. S.; Smith, E. A., Application of scanning angle Raman spectroscopy for determining the location of buried polymer interfaces with tens of nanometer precision. *Analyst* **2015**, *140*, 1955-1964.
11. Chen, K. C.; Lin, C. C.; Vela, J.; Fang, N., Multishell Au/Ag/SiO<sub>2</sub> nanorods with tunable optical properties as single particle orientation and rotational tracking probes. *Anal. Chem.* **2015**, *87*, 4096-4099.
12. Lesoine, M. D.; Bobbitt, J. M.; Zhu, S. B.; Fang, N.; Smith, E. A., High angular-resolution automated visible-wavelength scanning angle Raman microscopy. *Anal. Chim. Acta* **2014**, *848*, 61-66.
13. Bobbitt, J. M.; Weibel, S. C.; Elshobaki, M.; Chaudhary, S.; Smith, E. A., Fourier transform-plasmon waveguide spectroscopy: A nondestructive multifrequency method for simultaneously determining polymer thickness and apparent index of refraction. *Anal. Chem.* **2014**, *86*, 11957-11961.

***Jointly funded by this grant and other grants with leading intellectual contribution from this grant***

14. Santra, K.; Smith, E. A.; Petrich, J. W.; Song, X. Y., Photon counting data analysis: Application of the maximum likelihood and related methods for the determination of lifetimes in mixtures of rose bengal and rhodamine b. *J. Phys. Chem. A* **2017**, *121*, 122-132.
15. Men, L.; White, M. A.; Andaraarachchi, H.; Rosales, B. A.; Vela, J., Synthetic development of low dimensional materials. *Chem. Mater.* **2017**, *29*, 168-175.
16. Santra, K.; Zhan, J. C.; Song, X. Y.; Smith, E. A.; Vaswani, N.; Petrich, J. W., What is the best method to fit time-resolved data? A comparison of the residual minimization and the maximum likelihood techniques as applied to experimental time-correlated, single-photon counting data. *J. Phys. Chem. B* **2016**, *120*, 2484-2490.
17. Bhattacharjee, U.; Elshobaki, M.; Santra, K.; Bobbitt, J. M.; Chaudhary, S.; Smith, E. A.; Petrich, J. W., Characterizing electric field exposed P3HT thin films using polarized-light spectroscopies. *Macromol. Chem. Phys.* **2016**, *217*, 1801-1809.
18. Zhu, F.; Men, L.; Guo, Y. J.; Zhu, Q. C.; Bhattacharjee, U.; Goodwin, P. M.; Petrich, J. W.; Smith, E. A.; Vela, J., Shape evolution and single particle luminescence of organometal halide perovskite nanocrystals. *ACS Nano* **2015**, *9*, 2948-2959.
19. Lesoine, M. D.; Bobbitt, J. M.; Carr, J. A.; Elshobaki, M.; Chaudhary, S.; Smith, E. A., Quantitative comparison of organic photovoltaic bulk heterojunction photostability under laser illumination. *J. Phys. Chem. C* **2014**, *118*, 30229-30237.

***Jointly funded by this grant and other grants with relatively minor intellectual contribution from this grant***

20. Mohapatra, P.; Shaw, S.; Mendivelso-Perez, D.; Bobbitt, J. M.; Silva, T. F.; Naab, F.; Yuan, B.; Tian, X.; Smith, E. A.; Cademartiri, L., Calcination does not remove all carbon from colloidal nanocrystal assemblies. *Nat. Commun.* **2017**, *8*(1), 2038.
21. Shaw, S.; Silva, T. F.; Bobbitt, J. M.; Naab, F.; Rodrigues, C. L.; Yuan, B.; Chang, J. J.; Tian, X.; Smith, E. A.; Cademartiri, L., Building materials from colloidal nanocrystal assemblies: Molecular control of solid/solid interfaces in nanostructured tetragonal ZrO<sub>2</sub>. *Chem. Mater.* **2017**, *29*, 7888-7900.
22. Nelson, N. C.; Boote, B. W.; Naik, P.; Rossini, A. J.; Smith, E. A.; Slowing, I. I., Transfer hydrogenation over sodium-modified ceria: Enrichment of redox sites active for alcohol dehydrogenation. *J. Catal.* **2017**, *346*, 180-187.
23. Lawrinenko, M.; Wang, Z.; Horton, R.; Mendivelso-Perez, D.; Smith, E. A.; Webster, T. E.; Laird, D. A.; van Leeuwen, J. H., Macroporous carbon supported zerovalent iron for remediation of trichloroethylene. *ACS Sustainable Chem. Eng.* **2017**, *5*, 1586-1593.
24. Elshobaki, M.; Gebhardt, R.; Carr, J.; Lindemann, W.; Wang, W. J.; Grieser, E.; Venkatesan, S.; Ngo, E.; Bhattacharjee, U.; Strzalla, J.; Jiang, Z.; Qiao, Q.; Petrich, J.; Vaknin, D.; Chaudhary, S., Tailoring nanoscale morphology of polymer: Fullerene blends using electrostatic field. *ACS Appl. Mater. Interfaces* **2017**, *9*, 2678-2685.
25. Luo, L.; Men, L.; Liu, Z. Y.; Mudryk, Y.; Zhao, X.; Yao, Y. X.; Park, J. M.; Shinar, R.; Shinar, J.; Ho, K. M.; Perakis, I. E.; Vela, J.; Wang, J. G., Ultrafast terahertz snapshots of excitonic rydberg states and electronic coherence in an organometal halide perovskite. *Nat. Commun.* **2017**, *8*, 15565.
26. Yagnik, G. B.; Hansen, R. L.; Korte, A. R.; Reichert, M. D.; Vela, J.; Lee, Y. J., Large scale nanoparticle screening for small molecule analysis in laser desorption ionization mass spectrometry. *Anal. Chem.* **2016**, *88*, 8926-8930.
27. Hamdeh, U. H.; Nelson, R. D.; Ryan, B. J.; Bhattacharjee, U.; Petrich, J. W.; Panthani, M. G., Solution-processed BiI<sub>3</sub> thin films for photovoltaic applications: Improved carrier collection via solvent annealing. *Chem. Mater.* **2016**, *28*, 6567-6574.
28. Klein, A. T.; Yagnik, G. B.; Hohenstein, J. D.; Ji, Z.; Zi, J.; Reichert, M. D.; MacIntosh, G. C.; Yang, B.; Peters, R. J.; Vela, J.; Lee, Y. J., Investigation of the chemical interface in the soybean-aphid and rice-bacteria interactions using MALDI-MASS spectrometry imaging. *Anal. Chem.* **2015**, *87*, 5294-5301.

## Heat Capacity and Thermodynamic Functions of Crystalline and Amorphous Forms of the MOF Zinc 2-Ethylimidazolate, Zn(EtIm)<sub>2</sub>

Brian F. Woodfield<sup>1</sup>, Jason J. Calvin<sup>1</sup>, Megan Asplund<sup>1</sup>, Zamirbek Akimbekov<sup>2</sup>, Ghada Ayoub<sup>3</sup>, Athanasios D. Katsenis<sup>3</sup>, Alexandra Navrotsky<sup>2</sup>, Tomislav Friščić<sup>3</sup>

<sup>1</sup>Department of Chemistry and Biochemistry, Brigham Young University, Provo, UT

<sup>2</sup>Peter A. Rock Thermochemistry Laboratory and NEAT ORU,  
University of California Davis, Davis CA

<sup>3</sup>Department of Chemistry, McGill University, Montreal H3A 0B8, Canada

### Presentation Abstract

Metal organic frameworks (MOFs) may be useful in a variety of applications, mostly related to their capacity to store gases and catalyze reactions. As several MOFs are mechanically milled, they transition through different structures, progressing toward denser and more energetically stable polymorphs. We have measured the constant pressure heat capacities of four zeolitic imidazolate frameworks (ZIFs) based on the 2-ethylimidazolate (EtIm) linker exhibiting identical chemical compositions and different framework structures. Specifically, the crystalline Zn(EtIm)<sub>2</sub> frameworks of zeolite rho (RHO), analcime (ANA), and  $\beta$ -quartz (*qtz*) topologies were compared to each other and to the amorphous form of the material prepared by milling. Molar heat capacities were measured from 1.8 to 300 K using a Quantum Design Physical Property Measurement System (PPMS), and the data were fit to a set of theoretical functions and orthogonal polynomials. These fits were then used to generate  $C_{p,m}^{\circ}$ ,  $\Delta_0^T S_m^{\circ}$ ,  $\Delta_0^T H_m^{\circ}$ , and  $\Phi_m^{\circ}$  values at smoothed temperatures from 0 to 300 K. While these MOFs have somewhat different heat capacities reflecting their varying structures, they share an unusual feature in the heat capacity around 100 K that is likely due to some common vibrational behavior related to their common linker and metal node and/or their open frameworks. Though the enthalpies of transition scale with molar volume or density, the entropies of transition show more complex behavior, and the free energies of the three energetically less stable polymorphs (RHO, *am*-RHO, and ANA) are very similar.

.....

### DE-SC0016446: The Energetics and Dynamics of Confinement in Flexible Frameworks

**Postdoc(s):** Baiyu Huang

**Student(s):** Jason Calvin (undergrad), Megan Asplund (undergrad), Peter Rosen (undergrad), Ying Zhang (graduate)

## RECENT PROGRESS

### *Heat Capacity Measurements on Loaded MOFs*

A major thrust of the project is to measure the heat capacities of MOFs at various levels of guest loading to reveal any changes in the lattice dynamics via fitting the data to theoretical functions. To accomplish this, we must load MOF samples in aluminum pans to pressures as high as 300 psi but also maintain the seal on those pans in the temperature range from 1.8 K to 300 K. The increased mass of the sample plus aluminum pans has necessitated that we also redesign the PPMS platforms used in the measurements which has, in turn, required validating the accuracy and precision of these new platforms. An unexpected and somewhat frustrating issue has been reliably sealing the pans and the operation of the crimper under vacuum and at 300 psi pressures. We believe we have identified the issues involved, and we are close to measuring our first MOF samples loaded with CO<sub>2</sub>. Given below is a figure showing measurements on standard benzoic acid with and without the use of a pan.

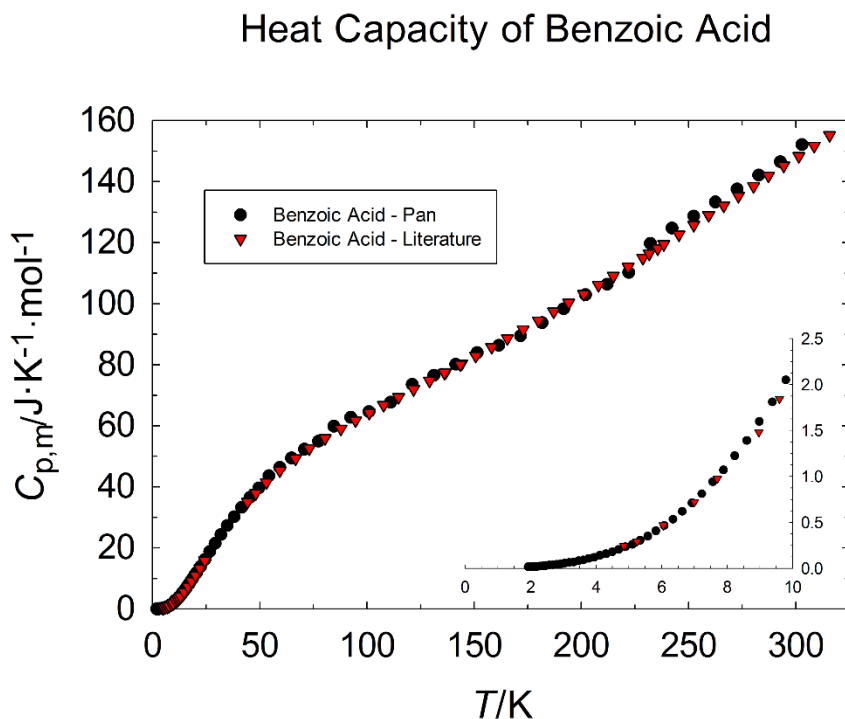


**Figure 1.** The heat capacity of standard benzoic acid compared against the measurements of benzoic acid under vacuum in a sealed pan.

### *Heat Capacity Measurements of Zeolite A*

To further explore confinement in other systems, we have also begun measurements on Zeolite A filled with H<sub>2</sub>O in equilibrium with the atmosphere and the empty zeolite. Contrary to the MOFs which require pressure to load with guest molecules, Zeolite A loads water freely. Some preliminary data is shown in Figure 2. Note that the heat capacity of the empty zeolite is higher

than that of the full zeolite. We need to investigate this observation further to determine if this is intrinsic or an error in our water content measurements.

### Heat Capacity of Zeolite Na-A

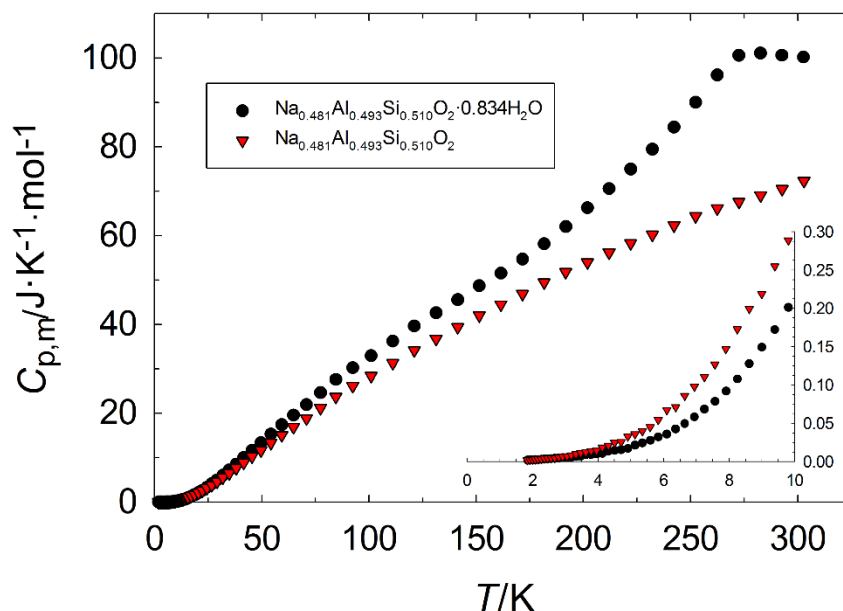


**Figure 2.** The heat capacity of empty and filled Zeolite A. Note the melting of the confined water in the filled zeolite.

### Publications Acknowledging this Grant in 2015 – present

#### *Exclusively Funded*

1. Calvin, J. J.; Asplund, M.; Akimbekov, Z.; Ayoub, G.; Katsenis, A. D.; Navrotsky, A.; Friscic, T.; Woodfield, B. F., Heat Capacity and Thermodynamic Functions of Crystalline and Amorphous Forms of the Metal Organic Framework Zinc 2-Ethylimidazolate,  $\text{Zn}(\text{EtIm})_2$ . *Journal of Chemical Thermodynamics* **2018**, *116*, 341-351.
2. Asplund, M.; Calvin, J. J.; Zhang, Y.; Huang, B.; Woodfield, B. F., Heat Capacity and Thermodynamic Functions of Silica-Doped  $\gamma\text{-Al}_2\text{O}_3$ . *Journal of Chemical Thermodynamics* **2018**, *118*, 165-174.
3. Calvin, J. J.; Asplund, M.; Zhang, Y.; Huang, B.; Woodfield, B. F., Heat Capacity and Thermodynamic Functions of Boehmite ( $\text{AlOOH}$ ) and Silica-doped Boehmite. *Journal of Chemical Thermodynamics* **2018**, *118*, 338-345.
4. Calvin, J. J.; Asplund, M.; Zhang, Y.; Huang, B.; Woodfield, B. F., Heat Capacity and Thermodynamic Functions of  $\gamma\text{-Al}_2\text{O}_3$ . *Journal of Chemical Thermodynamics* **2017**, *112*, 77-85.
5. Schliesser, J.; Lilova, K. I.; Pierce, E. M.; Wu, L.; Missimer, D. M.; Woodfield, B. F.; Navrotsky, A., Low temperature heat capacity and thermodynamic functions of anion bearing sodalities  $\text{Na}_8\text{Al}_6\text{Si}_6\text{O}_{24}\text{X}_2$  ( $\text{X} = \text{SO}_4, \text{ReO}_4, \text{Cl}, \text{I}$ ). *Journal of Chemical Thermodynamics* **2017**, *112*, 77-85.

**Alla Zelenyuk**

**Interfacial Structure and Dynamics in Ion Separations:  
Separation Phenomena in Nanostructured Materials**

Alla Zelenyuk, Grant E. Johnson, Venky Prabhakaran, and Vanda Glezakou  
Physical Sciences Division, Pacific Northwest National Laboratory, Richland, WA 99352

**Presentation Abstract**

Nanoparticles, i.e. nanoadsorbers, have the potential to revolutionize the efficiency and selectivity of separations by offering accelerated adsorption and reaction kinetics, increased sorption capacity, improved selectivity and size-, morphology- and composition-tunable properties. One promising class of nanoabsorbers for removal of contaminants from wastewater and recovery of high-value elements is nanoparticles with magnetic cores surrounded by shells conjugated with ion-specific chelators. These materials may be easily removed from solution, generating concentrated samples and minimizing secondary waste.

Their efficiency as separation media is affected by their physicochemical properties, environment, temperature, solvent and by the transformations that occur during the sorption process. We hypothesize that the morphology, surface area, curvature, and functionality of these nanoadsorbers determine their ion adsorption free energy for separation of solvated ions at complex interfaces.

To test this hypothesis and understand individual and synergistic role of competitive solvation and chelation between functional groups and ions we will conduct systematic studies aimed to quantify adsorption kinetics, sorption capacity, and selectivity of *segregated* nanoadsorbers with controlled physical properties and functionality. We will utilize one-of-a-kind tools and approaches for preparation, multimodal characterization, and separation of well-defined model nanoparticle systems with tailored properties and functionalities developed at PNNL as part of our chemical analysis program. These experimental studies will be coupled with cross-cutting theory and simulation effort that will provide molecular level insights into mechanisms, kinetics, and thermodynamics of chemical separations at complex interfaces.

**Grant or FWP Number:** 47327

# **PI MEETING PARTICIPANTS**

# BES Separation Science Research P.I. Meeting

February 6-7, 2018

## Participant List

Jared Anderson  
AMES Laboratory  
andersoj@iastate.edu

Mark Antonio  
Argonne National Laboratory  
mantonio@anl.gov

Jason Bara  
University of Alabama  
jbara@eng.ua.edu

Georges Belfort  
Rensselaer Polytechnic Institute  
belfog@rpi.edu

Paul Bohn  
University of Notre Dame  
pbohn@nd.edu

Kristin Bowman-James  
University of Kansas  
kbjames@ku.edu

Philip Britt  
Oak Ridge National Laboratory  
brittpf@ornl.gov

Merlin Bruening  
University of Notre Dame  
mbruenin@nd.edu

Vyacheslav Bryantsev  
Oak Ridge National Laboratory  
bryantsevv@ornl.gov

Jesse Carrick  
Tennessee Technological University  
jcarrick@tntech.edu

Aurora Clark  
Washington State University  
auclark@wsu.edu

Richard Crooks  
University of Texas, Austin  
crooks@cm.utexas.edu

Sheng Dai  
Oak Ridge National Laboratory  
dais@ornl.gov

Jeffrey Davis  
University of Maryland  
jdavis@umd.edu

Chris Fecko  
Department of Energy/BES  
Christopher.Fecko@science.doe.gov

Amar Flood  
Indiana University  
aflood@indiana.edu

Bruce Garrett  
U.S Department of Energy/BES  
bruce.garrett@science.doe.gov

Vassiliki-Alexandra Glezakou  
Pacific Northwest National Laboratory  
vanda.glezakou@pnnl.gov

Ruilan Guo  
University of Notre Dame  
rguo@nd.edu

Joel Harris  
University of Utah  
harrisj@chem.utah.edu

David Heldebrant  
Pacific Northwest National Laboratory  
david.heldebrant@pnnl.gov

Joseph Hupp  
Northwestern University  
j-hupp@northwestern.edu

# BES Separation Science Research P.I. Meeting

February 6-7, 2018

## Participant List

Takashi Ito  
Kansas State University  
ito@ksu.edu

Santa Jansone-Popova  
Oak Ridge National Laboratory  
jansonepopos@ornl.gov

Cynthia Jenks  
Argonne National Laboratory  
cjenks@anl.gov

De-en Jiang  
University of California, Riverside  
djiang@ucr.edu

Grant Johnson  
Pacific Northwest National Laboratory  
grant.johnson@pnnl.gov

William Koros  
Georgia Institute of Technology  
wjk@chbe.gatech.edu

Brian Long  
University of Tennessee  
Long@utk.edu

Shannon Mahurin  
Oak Ridge National Laboratory  
mahurinsm@ornl.gov

Raul Miranda  
U.S. Department of Energy/BES  
raul.miranda@science.doe.gov

Bruce Moyer  
Oak Ridge National Laboratory  
moyerba@ornl.gov

Karl Mueller  
Pacific Northwest National Laboratory  
karl.mueller@pnnl.gov

Alexandra Navrotsky  
University of California, Davis  
anavrotsky@ucdavis.edu

Charles Peden  
U.S. Department of Energy/BES  
charles.peden@science.doe.gov

Marek Pruski  
AMES Laboratory  
mpruski@iastate.edu

Steven Regen  
Lehigh University  
slr0@lehigh.edu

Nancy Ross  
Virginia Tech  
nross@vt.edu

Eric Schelter  
University of Pennsylvania  
schelter@sas.upenn.edu

Mark Schlossman  
University of Illinois, Chicago  
schloss@uic.edu

Daniel Schwartz  
University of Colorado  
daniel.schwartz@colorado.edu

Jonathan Sessler  
University of Texas, Austin  
sessler@cm.utexas.edu

David Sholl  
Georgia Institute of Technology  
david.sholl@chbe.gatech.edu

Emily Smith  
AMES Laboratory  
esmith1@iastate.edu

# **BES Separation Science Research P.I. Meeting**

**February 6-7, 2018**

## **Participant List**

Lynda Soderholm  
Argonne National Laboratory  
LS@anl.gov

Gregory Voth  
University of Chicago  
gavoth@uchicago.edu

Philip Wilk  
U.S. Department of Energy/BES  
philip.wilk@science.doe.gov

Brian Woodfield  
Brigham Young University  
brian\_woodfield@byu.edu

Alla Zelenyuk-Imre  
Pacific Northwest National Laboratory  
alla.zelenyuk-imre@pnnl.gov

Cover images courtesy of: Aurora Clark (Washington State University), Daniel Schwartz (University of Colorado), Eric Shelter (University of Pennsylvania), Sheng Dai (Oak Ridge National Laboratory), Jonathan Sessler (University of Texas, Austin), Amar Flood (Indiana University)



U.S. DEPARTMENT OF  
**ENERGY**

Office of  
Science